



Faro Landscape Hazards

Geoscience Mapping for Climate
Change Adaptation Planning



Northern Climate ExChange
YUKON RESEARCH CENTRE • Yukon College



Aboriginal Affairs and
Northern Development Canada

Affaires autochtones et
Développement du Nord Canada

This publication may be obtained from:

Northern Climate ExChange
Yukon Research Centre, Yukon College
500 College Drive
P.O. Box 2799
Whitehorse, Yukon
Y1A 5K4
867.668.8895
1.800.661.0504
yukoncollege.yk.ca/research

Recommended citation: Benkert, B.E., Fortier, D., Lipovsky, P., Lewkowicz, A., Roy, L.-P., de Grandpré, I., Grandmont, K., Turner, D., Laxton, S., and Moote, K., 2015. Faro Landscape Hazards: Geoscience Mapping for Climate Change Adaptation Planning. Northern Climate ExChange, Yukon Research Centre, Yukon College. 130 p. and 2 maps.

Front cover photograph: Aerial view of Faro looking southeast towards the Pelly River.

Photo credit: archbould.com

Disclaimer: The report including any associated maps, tables and figures (the “Information”) convey general observations only. The Information is based on an interpretation and extrapolation of discrete data points and is not necessarily indicative of actual conditions at any location. The Information cannot be used or relied upon for design or construction at any location without first conducting site-specific geotechnical investigations by a qualified geotechnical engineer to determine the actual conditions at a specific location (“Site-Specific Investigations”). The Information should only be used or relied upon as a guide to compare locations under consideration for such Site-Specific Investigations. Use of or reliance upon the Information for any other purpose is solely at the user’s own risk. Yukon College and the individual authors and contributors to the Information accept no liability for any loss or damage arising from the use of the Information.

LEAD AUTHORS

Bronwyn Benkert

Northern Climate ExChange, Yukon Research Centre,
Yukon College

Daniel Fortier

Université de Montréal

Panya Lipovsky

Yukon Geological Survey, Government of Yukon

Antoni Lewkowicz

University of Ottawa

CONTRIBUTING AUTHORS

Louis-Philippe Roy

Northern Climate ExChange, Yukon Research Centre,
Yukon College

Isabelle de Grandpré

Université de Montréal

Katerine Grandmont

Université de Montréal

Derek Turner

Yukon Geological Survey, Government of Yukon

Sarah Laxton

Yukon Geological Survey, Government of Yukon

Kelly Moote

Northern Climate Exchange, Yukon Research Centre,
Yukon College

TECHNICAL ADVISORS

Jeff Bond

Yukon Geological Survey, Government of Yukon

Lacia Kinnear

Northern Climate ExChange, Yukon Research Centre,
Yukon College

TECHNICAL EDITING AND PRODUCTION

Leyla Weston, private consultant, Whitehorse, Yukon

ACKNOWLEDGEMENTS

The project team would like to thank all the participants in this project for their enthusiasm and commitment. We would like to express our appreciation to the Yukon Geological Survey, Yukon Research Centre, Université de Montréal, University of Ottawa, Government of Yukon, and all those noted above for their support.

We would especially like to thank the community of Faro for supporting this project and welcoming us into their community. We appreciate the support and cooperation of community residents, which have led to fruitful conversations that enhanced the research presented here.

Thank you to the many field assistants involved in the project, including several of our contributing authors, as well as Derek Turner, Alexandre Bevington, Michel Sliger and Alex Brooker. Bob Sagar compiled the instrumental climate data that appears in this report, and Philip Bonnaventure prepared the air temperature and permafrost probability models. Cover design by Lalena Designs.

Funding for this project was provided by Aboriginal Affairs and Northern Development, Government of Canada, and in-kind contributions were made by project partners. Project management was conducted by the Northern Climate ExChange, part of the Yukon Research Centre at Yukon College.

TABLE OF CONTENTS

INTRODUCTION	1
Climate Change Adaptation Planning.....	1
What are Hazards Maps?.....	1
Hazards Maps and Decision-Making.....	1
HOW HAZARDS MAPS ARE CREATED	2
Community Consultation.....	2
Disturbance History.....	2
Surficial Geology Characterization.....	3
Permafrost Distribution and Characteristics.....	3
Hydrological Characterization.....	3
Projections of Future Environmental Conditions.....	4
Hazard Ranking.....	4
<i>Limitations and uncertainty</i>	4
THE FARO REGION	5
Physiography.....	7
Vegetation.....	7
Contemporary Climate.....	8
Past Climate Trends.....	9
Hydrology.....	10
<i>Surface water</i>	10
<i>Groundwater</i>	13
Environmental Disturbance History.....	13
Bedrock Geology.....	15
Landscape Evolution During the Pleistocene and Holocene Epochs.....	17
Surficial Materials.....	18
<i>Anthropogenic materials</i>	18
<i>Organic materials</i>	19
<i>Volcanic materials</i>	19
<i>Eolian materials</i>	19
<i>Colluvial materials</i>	20
<i>Fluvial materials</i>	20
<i>Glaciofluvial materials</i>	21
<i>Morainal materials</i>	22
<i>Glaciolacustrine materials</i>	24
<i>Bedrock</i>	25
Stratigraphy.....	25
Permafrost.....	26
<i>Organic cover</i>	26
<i>Forest cover</i>	27
<i>Surface sediment texture</i>	27
POTENTIAL HAZARDS RISKS FOR THE FARO REGION	28
Landslide Processes.....	28

Permafrost Processes.....	30
<i>Permafrost development</i>	30
<i>Geotechnical properties</i>	30
<i>Permafrost as a hazard risk</i>	33
Seismicity.....	35
ASSESSING CURRENT HAZARD RISKS FOR THE FARO REGION	36
Case Study Sites.....	36
Tintina Subdivision.....	37
Future Country Residential Subdivision.....	39
Sewage Lagoon.....	41
Douglas Drive/Yates Crescent.....	45
Del Van Gorder School and Baseball Diamond.....	49
Faro Ski Hill Landslide.....	51
HAZARD RISKS IN A CHANGING CLIMATE	55
Projected Climate Change for the Faro Region.....	55
<i>Global climate models</i>	55
<i>Climate change scenarios</i>	56
Landscape Sensitivity to Climate Change.....	57
<i>Sensitivity of local surface material types</i>	58
<i>Projected changes in permafrost distribution</i>	59
INTEGRATING RISK IN A LANDSCAPE HAZARDS MAP FOR THE FARO REGION	64
GENERATING ACTION FROM SCIENCE	68
REFERENCES	69
APPENDIX A - APPROACH AND METHODS	76
APPENDIX B - BOREHOLE LOGS	87
APPENDIX C - GRAIN SIZE ANALYSIS	95
APPENDIX D - CLIMATE PROJECTIONS	100
APPENDIX E - HAZARD RANKINGS	107
APPENDIX F - SAFE HOME CONSTRUCTION ON PERMAFROST	110

INTRODUCTION

Climate change is a significant challenge for northern communities, where the impacts of a warming climate are already having considerable effects (Huntington and Weller, 2005). Many people living in small, isolated communities in northern Yukon are concerned about climate-related risks in their regions. Because adverse impacts are a reality, it is important to implement measures to reduce or moderate the negative effects of climate change – in other words, to implement climate change adaptation strategies.

CLIMATE CHANGE ADAPTATION PLANNING

Community-based adaptation planning aims to incorporate the potential impacts of climate change into decision-making for community development. For example, the design of a new building that is resilient to permafrost thaw, or the selection of future development zones away from areas that may be prone to flooding during spring melt, are both decisions rooted in adaptation planning. Ultimately, adaptation planning anticipates future scenarios, reduces risk, increases resilience, and may even seek to reap the benefits of certain aspects of climate change.

In order to better prepare our communities to incorporate adaptation planning in the decision-making process, we must first identify the risks of, or vulnerabilities to, climate change, and then mitigate or reduce these risks so that we may adapt in a safe, sustainable manner.

Hazards maps help identify potential future risks associated with natural phenomena such as permafrost thaw, landslides and flooding. In order to adequately measure the potential risks associated with climate change, it is critical to gather scientific baseline data. These data, in conjunction with complementary research and future climate projections, strive to reduce vulnerability by increasing our knowledge base; this in turn will increase a community's adaptive capacity to climate change.

WHAT ARE HAZARDS MAPS?

A hazards map is a map that delineates or highlights areas on the land that are affected by, or are vulnerable to, a particular hazard. For example, in northern latitudes such as Yukon, thawing permafrost can be a significant climate change-related hazard. Flooding is another common hazard faced by Yukon communities, which may or may not be directly related to thawing permafrost. Hazards maps illustrate the risk associated with these and other hazards (ranked by risk severity), and are represented graphically in stoplight colours.

Hazards maps integrate complex environmental data into an easy-to-interpret, user-friendly tool for decision-making. The maps are created on a community-by-community basis and combine information about current and future landscape and climate conditions in order to rank the risk related to environmental change. As a result, they are tailored to each community's unique environment.

HAZARDS MAPS AND DECISION-MAKING

Hazard mapping, in conjunction with risk assessment, forms the basis of the risk management decision-making process by providing a community with baseline information that is necessary to understanding what risks may exist. One of the main objectives of the risk management process is to determine "what risks potentially interfere with the community's ability to meet the goals and objectives defining the community's vision for the future" (Noson, 2002). In this case, hazards

maps help address a community's goal of incorporating climate change adaptation planning into its approaches to decision making and community development.

The series of landscape hazards maps produced by Northern Climate Exchange (NCE) and its partners are prepared as guides; that is, they act as one of the first steps in community planning and development. They identify areas where there is low risk of hazards exposure, as well as areas requiring more advanced and detailed scientific and engineering studies, should development be desired. Because hazards maps depict risk using stoplight colours, they are accessible and easy to interpret; in addition to community planning, hazards maps are useful educational tools illustrating local environmental conditions. They may also be used by scientists studying hazard phenomena (Noson, 2002), or could be revisited several years in the future to assess landscape change over time.

While hazards maps are tailored to local conditions and provide more detail than most other existing map products, it is important to note that they do not capture fine-scale variability within a site. For example, a slope underlain by permafrost may be more susceptible to thaw slumps in some areas compared to others because of small-scale variations in ice content of the soil. However, the entire slope may be classified as moderate risk to encompass the highest possible degree of vulnerability. Because of this, it is important to recognize the limitations of hazards maps – they provide an initial guide to local conditions, but detailed site studies (e.g., geotechnical or engineering studies) may still be required.

HOW HAZARDS MAPS ARE CREATED

There are many different approaches to creating hazards maps. Different mapping projects from different jurisdictions around Canada's North, and globally, will incorporate different hazards elements and types of data. For this project, we developed an approach that incorporates local community concerns and infrastructure, disturbance history, permafrost distribution and characteristics, surficial geology conditions, hydrology, and projections of future climate. Approaches for each stage are briefly described below. Detailed descriptions of each approach, including equipment used, lab analyses conducted, and data processing specifics are included in Appendix A.

COMMUNITY CONSULTATION

Support from local community governments and First Nations is sought for each hazards mapping project when project funding proposals are developed. Upon project commencement, community consultations, meetings and interviews are held with members of the public and local decision-makers to identify areas of concern and sites for potential future development. These areas of interest then become case-study sites as part of the hazards project. Where local capacity exists, a community project liaison is hired to serve as a link between the research team and the community.

DISTURBANCE HISTORY

The research team gathers information about natural and human-caused disturbances that may affect current landscape conditions. For example, forest fires change vegetation cover and affect permafrost distribution, while regulating and re-routing waterways or clearing land for development can affect local hydrology and permafrost conditions. Old disturbances help explain why current landscape dynamics operate as they do, while newer disturbances offer insight into potential future landscape evolution.

SURFICIAL GEOLOGY CHARACTERIZATION

Surficial geology is the study of the unconsolidated material (i.e., the surficial material that overlies bedrock) on the Earth's surface, including all sediments and soils. Surficial geology mapping involves a combination of aerial photograph interpretation and fieldwork. Surficial geology maps provide information on the physical properties and characteristics of the surface sediments, the morphology (shape) of the landforms produced, and the genesis or origin of the landforms. In the process of mapping the surficial geology, the distribution of permafrost is also captured, making these maps an essential part of the hazards assessment process. The surficial geology maps become the basis for the final hazards maps produced through each project.

PERMAFROST DISTRIBUTION AND CHARACTERISTICS

Permafrost is defined as ground (including rock, soil and organic material) that remains at or below 0°C for a minimum of two consecutive years. For this project, the research team studied both the distribution and characteristics of permafrost as part of the hazards map development.

Permafrost distribution is studied via the application of two geophysical surveys: 1) ground-penetrating radar (GPR), and 2) electrical resistivity tomography (ERT). Ground-penetrating radar uses electromagnetic radiation to send a tiny pulse of energy into the ground, and then measures the speed and strength of that pulse's reflection back to the instrument. It produces an image that delineates boundaries created by changes in soil characteristics (e.g., the presence of frozen ground or stratigraphic layers). Electrical resistivity tomography is another type of non-invasive geophysical survey that measures the changes in the ability of the ground to conduct electricity along a transect. ERT profiling has been used extensively to investigate mountain permafrost in Europe (e.g. Kneisel et al., 2000, 2008; Hauck et al., 2004; Hilbich et al., 2008, 2009) and is growing in importance in North America as a technique for permafrost investigations in mountains and elsewhere (e.g., Lewkowicz et al., 2011). An electrical resistivity survey produces a two-dimensional image of the subsurface which can be used to identify frozen (high resistivity) versus unfrozen (low resistivity) soils, and can therefore be used to map permafrost distribution along a transect. A critical part of the interpretation is the threshold resistivity value that represents the boundary between frozen and thawed soils. This value is typically between 300 and 800 ohm m in southern Yukon (Lewkowicz et al., 2011), but is dependent on local ground temperatures and stratigraphy. The value used for most of the ERT profiles in this report is 400 ohm m which generally coincided with a gradient in resistivity indicative of phase change. A uniform shading scale has been used for all the resistivity profiles presented so that visual comparisons can be made between sites.

Permafrost characteristics are studied by extracting cores of permafrost from the ground and conducting a series of laboratory analyses on subsections of these cores. These analyses provide information about grain size, porosity, ice volume, and settlement potential, among other properties. These characteristics affect how different sediments will behave if permafrost thaws, and are also useful in verifying interpretations of the geophysical techniques described above.

HYDROLOGICAL CHARACTERIZATION

The study of the movement and distribution of water is critical in understanding responses to climate change. Having baseline knowledge of the hydrologic regime in an area is essential in defining potential future hazards that are related to climate change. To incorporate hydrological conditions and risk into hazards maps, data about river discharge, lake level and the groundwater table are gathered from monitoring stations. Flood histories are also compiled from existing records and anecdotal evidence. Historical patterns are analyzed, and current conditions are assessed on the context of projected future changes in climate.

PROJECTIONS OF FUTURE ENVIRONMENTAL CONDITIONS

An important component of the hazards mapping projects involves projections of future environmental conditions. These represent an important aspect of adaptation planning, which by definition requires a future focus; thus, incorporating future-oriented data is a key element of the development of hazards maps.

The future environmental conditions modelled through this project are done through permafrost probability projections and climate projections. Models of permafrost probability are developed using data from a series of meteorological and permafrost monitoring stations established by research partners throughout the territory. These models build on the existing knowledge of permafrost distribution to depict future changes in permafrost under different scenarios of annual air temperature increases as a result of climate change.

Climate projections for each community are developed by using a variety of Global Climate Models (GCMs) in combination with discrete scenarios, in order to make a range of projections for numerous climate variables (e.g., temperature and precipitation) on a local scale. Hazards projects typically incorporate a range of scenarios (reflecting escalating degrees of climate change) at several points in the future (e.g., 2020, 2050 and 2080).

HAZARD RANKING

Hazard mapping applies a variety of scientific data in order to arrive at a hazard risk ranking. The combination of surficial material type (glacial deposits and soils), landform shape and slope, permafrost nature and distribution, hydrological conditions, and present and future climate regime are used to rank hazard risk. For easy interpretation, a stop-light colour coding system is applied to each risk ranking.

The hazards ranking is tailored to suit the conditions in each of the communities mapped. For example, in communities where permafrost presence or absence largely determines risk, three risk categories are sufficient. In environments with more complex landscape conditions (e.g., where permafrost conditions are more nuanced), a fourth risk category is introduced. Tailoring risk ranking to community conditions makes hazards maps relevant and reflective of the local landscape. The hazards risk ranking matrix used in this project is discussed in more detail in the section “*Integrating risk in a landscape hazards map for the Faro region*”, p. 64 of this report.)

LIMITATIONS AND UNCERTAINTY

It is very important to note that this report is prepared as a guide for planning. It should not be used as the basis for final site selection for development, and it does not replace geotechnical and/or engineering assessments completed on a site level. Rather, it should be treated as a tool for use in identifying areas of interest with regards to future land use planning, which will then undergo subsequent site-specific investigations (which may include geotechnical or engineering assessments).

It is also important to note that the classification scheme applied here does contain a level of uncertainty. Because of the scale at which the study area was mapped, and the duration of the field programs for this project, researchers were unable to visit all the areas denoted by polygons in the map area. Therefore, results have been extrapolated to polygons beyond case study sites and areas visited by researchers. While we make our most informed assessment of hazards ranking for all polygons, this approach does introduce some uncertainty when making a determination of classification.

Finally, it is important to note that in some cases, a polygon may contain areas of both higher and lower risk. In such cases, we have taken a precautionary approach and applied a category of higher risk where we were not confident in lower categories. This is another reason why the hazards map should serve only as an initial guide for planning purposes, and should not replace site-specific investigations – the landscape within each polygon will vary naturally.

THE FARO REGION

The Town of Faro (62°N, 133°W) is located in the central-southeastern region of Yukon, in the Tintina Trench between the Hess and Pelly mountains (Figure 1). Road access to the community is via the Klondike and Campbell highways. Faro is situated just off the Robert Campbell Highway, approximately 356 km northeast of Whitehorse, and 423 km northwest of Watson Lake via the Campbell Highway.

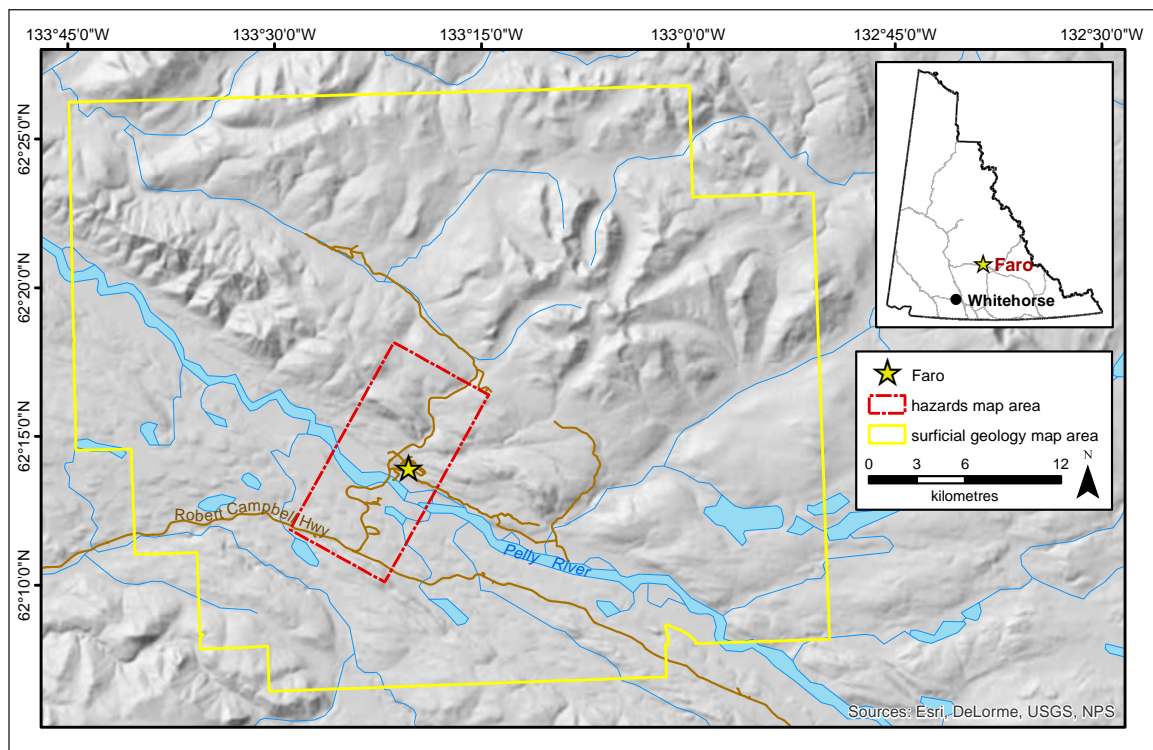


Figure 1. Location of study area, illustrating the surficial geology and hazards map footprints.

The history of what is now known as the Town of Faro began in 1953 when prospector Al Kulan, with the assistance of Kaska prospectors Jack Ladue, Robert Etzel, Joe Etzel, Art John and Jack Sterriah, staked the claim that would eventually become the Faro mine (Town of Faro, 2014). The claim was located in the traditional territory of the Kaska Dena (Yukon Environment Geomatics, 2012), 48 km downstream of the community of Ross River. At the time, the deposit was considered too small and too remote to be mined.

In 1960, Kulan and Aaro Aho formed the company Dynasty Explorations and began working the claims that Kulan had previously staked. In 1964, Dynasty commenced a detailed exploration program on several claim groups in the Faro area, and in 1965, discovered the Faro lead-zinc deposit (Faro Mine Remediation Project, 2011a). In that year, there were over 100 men working

in the area and Dynasty had built a rough road, a gravel airstrip, a large camp for employees, and helicopter facilities on the claim site (Weinstein, 1992). Additionally, the federal government installed a ferry at the Pelly River to support operations. In December 1965, the Cyprus Anvil Mining Corporation, a joint venture between Cyprus Mines and Dynasty Exploration, was formed to develop the Faro deposit.

In late 1969, open-pit mining operations commenced on the Faro lead-zinc deposit and the mine was officially opened on January 28, 1970 (Faro Mine Remediation Project, 2011a). Production at the Faro mine was halted in 1982 because of falling metal prices, low productivity, high operating costs, and the added burden of debt load that had been brought about by recent expansion efforts. Between June 1983 and December 1998 the mine was operated by various owners and re-opened and closed several times. On January 16, 1998 the Anvil Range Mining Company announced that it planned to file for court protection from creditors. On April 21, 1998, an interim receiver was appointed to handle the company's assets and maintain the mine site. At its peak production, the Faro mine produced approximately 15% of the world's zinc and lead output, and accounted for 20% of the Yukon's economy (Faro Mine Remediation Project, 2011a).

In 1968, prior to the official opening of the mine site, Cyprus Anvil and the federal government contributed to the development of a new town near the deposit that was capable of housing a work force of 1000 people (Weinstein, 1992). The town was called "Faro" after the gambling card game of the same name. By 1969, construction on approximately 50 houses had begun, but in June of that year a lightning fire spread down the slope of a nearby mountain and destroyed the new town. Due to the need for housing in the area, the town was quickly rebuilt and the first families had moved into Faro by September of that year.

While the mine was operating, the population of Faro fluctuated in parallel with the status of operations (Town of Faro, 2014). In 1970, the first year the mine operated, the population of Faro was approximately 800 people. As the mine expanded, the population grew until it reached its peak of just under 2000 in 1981. In both 1979 and 1981, Cyprus Anvil was forced to build more housing to ease housing shortages, and a second trailer court was established in order to support additional housing if needed. (This location, along Douglas Drive, is included as a case study site in the hazards mapping project described in this report.) In 1982, the prices of lead and zinc fell sharply, and by June of that year, production at the mine had ceased (Environmental Mining Council of British Columbia, 2001). In September the mine announced it would not be resuming operations that winter, causing many employees and their families to leave the area and Faro's population dropped to less than 900 (Environmental Mining Council of British Columbia, 2001). In 1984, Cyprus-Anvil announced that it was mothballing the mine causing the population to decrease once again. At this time Faro had only 90 residents, marking its lowest population level. In 2011, the population of Faro had increased to 380 (YBS, 2011), and it has been relatively stable at this level for several years. In 2011 there were 170 occupied private dwellings in the community (YBS, 2010).

Since a wide variety of community and recreational facilities were established when the mine was in operation, there is well-developed community and recreational infrastructure in Faro. There is a public school that provides education from kindergarten to Grade 12 and post-secondary education is available at Yukon College's Faro campus. Health care is provided through a Nursing Station and emergency care is available 24 hours a day. There is an RCMP detachment, a full-service postal outlet and banking services. Faro's recreation centre has a gymnasium, seasonal swimming pool, squash court, youth lounge and weight room, and an indoor ice arena is maintained in the winter months. Faro has a volunteer fire service, volunteer ambulance service, volunteer search-

and-rescue service, and the airport, which is open seven days a week, has a 1231-m gravel runway with lights.

PHYSIOGRAPHY

The town of Faro is located in the Yukon Plateau – North ecoregion (Smith et al., 2004) and is within the Tintina Trench physiographic region (Mathews, 1986). The Tintina Trench is a prominent linear valley that follows the trace of the Tintina fault, which extends in a northwesterly direction for almost 1000 km from the Northern Rocky Mountain Trench in British Columbia to central Alaska. Within the map area, the 5 to 10 km-wide trench separates the Ross Lowlands and MacMillan Highlands to the northeast from the Pelly Mountains to the southwest (Mathews, 1986). The MacMillan Highlands include the Anvil Range (elevations up to 2000 m in the map area) and several other small ranges and massifs separated by broad valleys. The Ross Lowlands in the region consist of rolling, rounded hills (less than 1500 m above sea level (a.s.l.), and wide, low elevation valleys. The rugged Pelly Mountains are a steeply rising range with local relief up to 1500 m a.s.l. in the map area. The Pelly River occupies the Tintina Trench valley floor, draining northwest towards the Yukon River and has an elevation of approximately 640 m a.s.l. near the town of Faro.

Jackson (1994) reports that throughout this ecoregion:

“Evidence of past glaciation is ubiquitous. Summits above 1800 meters typically feature arête ridges, cirques and horn peaks. Lower plateaus and the sides of larger valleys are marked by whaleback ridges and crag-and-tails, which indicate past ice flow directions. Valley bottoms contain complexes of glaciofluvial deposits or thick fills of glaciolacustrine sediments. Flights of gravelly benches are common on mountain sides and are nearly continuous from valley floor to mountain summit. The gravelly benches are the beds of former ice-walled channels.” (Page 6)

VEGETATION

Vegetation is determined by elevation, topography and microclimate. The vegetation of this ecoregion ranges from boreal to alpine. Northern boreal forest exists at elevations up to 1500 m. Higher elevations in this ecoregion are characterized by shrub and lichen tundra. In the subalpine environment, the dominant vegetation types include shrub birch, pine, white spruce, subalpine fir, and a lichen understory. Extensive shrublands exist at mid-elevations and on valley bottoms subject to cold air drainage. In the boreal zone, open black spruce with a moist moss or drier lichen understory is the dominant forest type. Black spruce dominates under poorly drained conditions and commonly indicates the presence of underlying permafrost (Jackson, 1994).

Mixed canopy forests are common due to frequent forest fires (Smith et al., 2004). The fires are caused by a high incidence of thunderstorms and lightning strikes along the Tintina Trench. Lodgepole pine frequently invades burned areas, occasionally forming extensive forests. Also common on disturbed sites are trembling aspen and balsam poplar. Paper birch is scattered throughout the ecoregion, usually occurring on cooler sites.

Low ericaceous shrubs, prostrate willows and lichens dominate the alpine. Talus slopes, common at high elevations, support communities of crustose lichens. Moister sites support more moss and graminoids than lichen.

Grasslands consisting of sagewort, juniper, kinnikinnick, forbs and aspen are common along the banks of large rivers and are often contiguous with unglaciated, high-elevation areas that would have supported similar vegetation during the last glacial period. These grassland plant communities are considered relicts of the glacial period.

The wetlands that exist on the margins of small lakes, marshes, and shallow, open water are dominated by willows, sedges and aquatic plants. Black spruce bogs, containing sedge tussocks and sphagnum moss and underlain by permafrost, occur in lowland areas throughout the ecoregion.

CONTEMPORARY CLIMATE

Faro is located in the Central Yukon Basin (Wahl et al., 1987). The St. Elias Mountains and the region’s distance from the Gulf of Alaska influences its climate, making it climatically different from areas to the south. Temperatures are highly variable – summers can be extremely warm, while winters can have very long cold periods. The record-low temperature for continental North America was recorded in this climate zone at Snag, Yukon (-62.8°C on February 3, 1947). Precipitation is moderate, winds tend to be light, and storm centers commonly skirt this region, especially in winter (Wahl et al., 1987).

Based on 30-year (1981-2010) climate normal data collected from the Faro Airport meteorological monitoring station (the closest station with a long-term monitoring record; 62°12’ N, 133°22’W; Environment Canada, 2014a), average January and July temperatures are -20.1°C and 15.0°C, respectively, while average precipitation is 319.7 mm (Environment Canada, 2014a). Of this, approximately one-third falls as snow during the winter season. Month-by-month climate normal temperature and precipitation data are summarized in Figure 2.

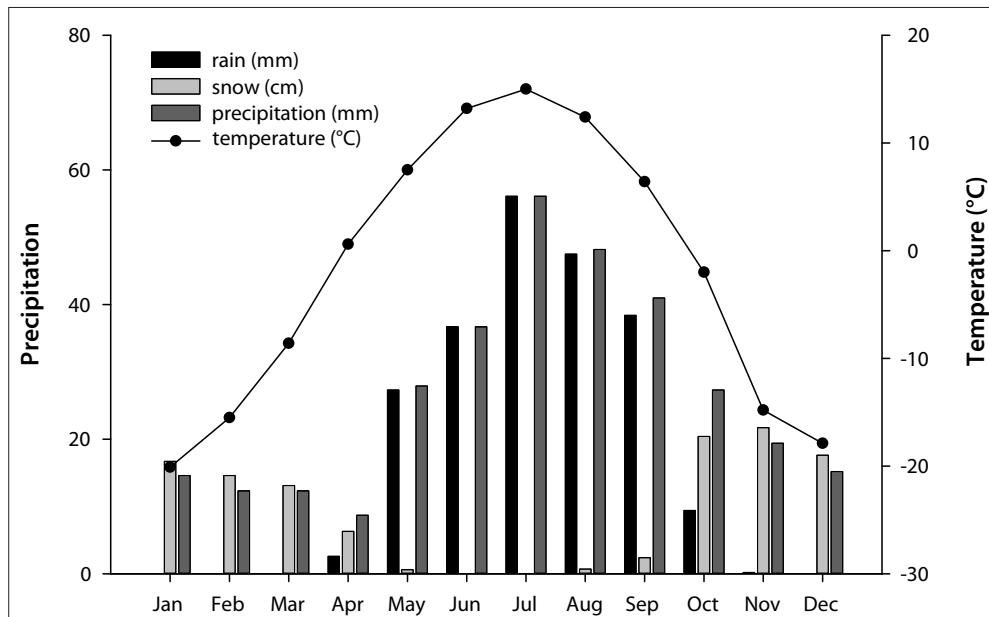


Figure 2. Climate normal (1981-2010) temperature and precipitation data for the Faro Airport meteorological monitoring station (Environment Canada, 2014a). To calculate total precipitation in millimetres, snowfall was converted to snow water equivalent (SWE) and summed with rainfall.

Mean annual air temperatures (MAAT) vary with elevation in the area. Measurements recorded around Faro between 2006 and 2008 show an average change in MAAT up to treeline of -2.3°C per 1000 m (Lewkowicz and Bonnaventure, 2011), which is a much slower rate of cooling than the global average of -6.5°C per 1000 m. This is due to the cold air pooling in the valley bottoms in winter, which offsets the more normal warmer conditions in the valley bottoms in summer.

PAST CLIMATE TRENDS

Environment Canada produces regional summaries of climate and precipitation data that provide a generalization of climate trends by integrating instrumental data from several stations (Environment Canada, 2014b). For this region, Environment Canada amalgamates data from northern British Columbia and Yukon stations, which has allowed them to develop a record of regional climate trends that spans the past 65 years. Data indicate that between ~1950 and 1975, the regional climate was generally cooler and drier than normal (based on 1961-1990 climate conditions), while between ~1975 and 2013 climate was generally warmer and wetter than normal (Figure 3).

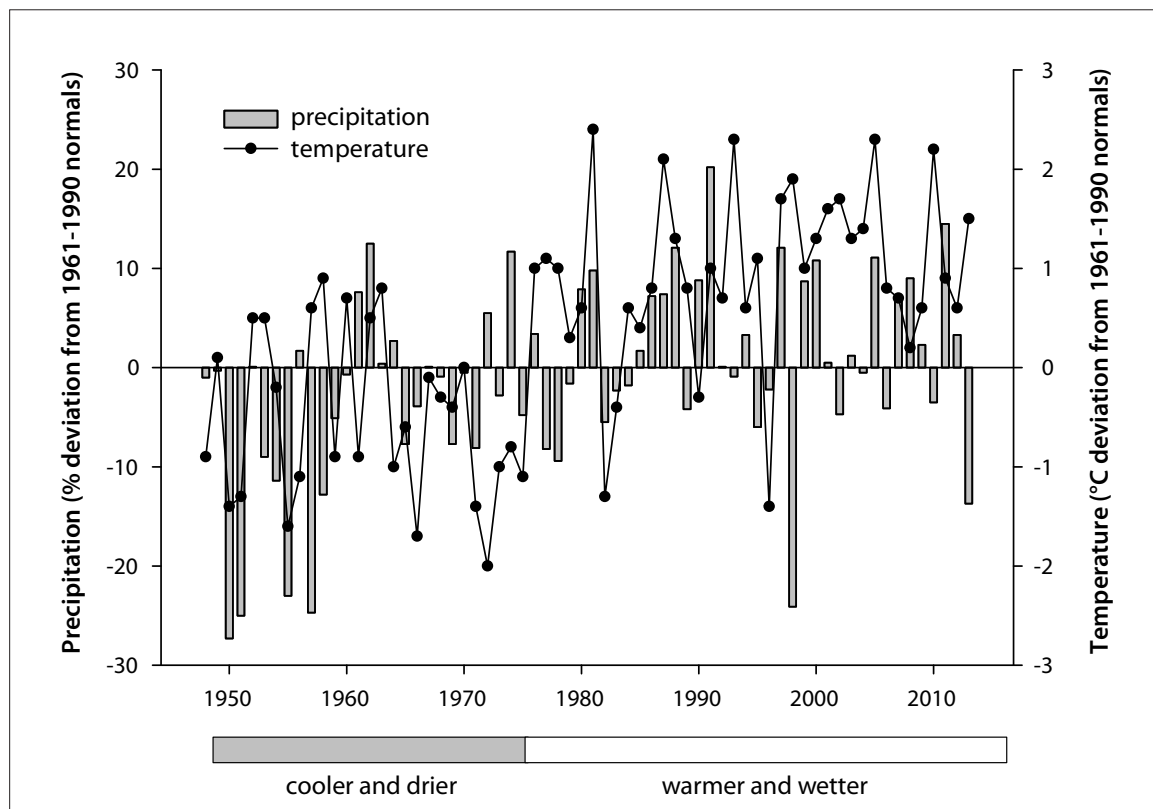


Figure 3. Regional climate trends for northern British Columbia and Yukon, developed using data amalgamated by Environment Canada (2014b). Data has been normalized to indicate deviation from 1961-1990 climate normal conditions. Negative values indicate precipitation amounts and temperatures below normal for the 1961-1990 period, while positive values indicate exceedance of normal conditions.

To examine local, past climate trends, the historical data record from the Faro Airport meteorological monitoring station was examined. Temperature data is available for the period 1979-2013 (Figure 4). The data were amalgamated by season for simplicity, and linear regressions were superimposed on seasonal data records. While the trends they represent are not statistically significant, the regression lines do provide a basis for identifying potential trends in temperature over the period of record.

The greatest range in seasonal temperature variability occurred in the winter, with a 14.8°C difference in the highest and lowest recorded temperatures over the period of record. In contrast, summer temperature variability was lowest (3.7°C). Temperature ranges in spring and fall are comparable (6.4°C and 8.1°C, respectively). Regression lines suggest winter temperatures are

increasing slightly over the period of record, which is consistent with modelling that predicts climate change-induced temperature increases will be greatest in winter (Warren and Lemmen, 2014). Interestingly, summer temperatures also appear to be increasing slightly over the period of record, while shoulder-season temperatures (spring and fall) remain relatively stable or decline slightly.

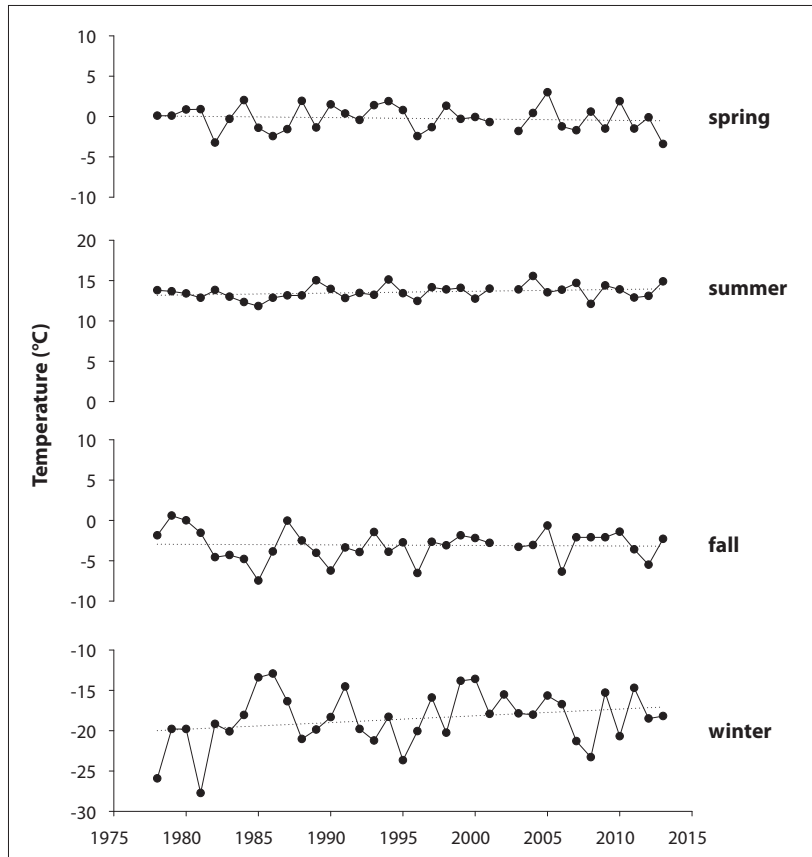


Figure 4. Past temperature records measured at the Faro Airport meteorological monitoring station (Environment Canada, 2014a). Seasonal average (spring = Mar-May; summer = Jun-Aug; fall = Sep-Nov; winter = Dec-Feb) and mean annual temperatures are shown. Dotted lines show linear regressions for each data series.

HYDROLOGY

SURFACE WATER

The subwatershed of the Faro region forms part of the Yukon River watershed, which covers 260 000 km² or 54% of Yukon Territory (Smith et al., 2004). The area is situated in the Interior Hydrologic Region of the Territory, where drainage from the southern foothills of the Selwyn Mountains flows west to the Yukon River. The first and second-order streams descending from the foothills are generally steep and relatively short, producing rapid, flashy streamflow responses during the spring melt and some of the highest peak flows in Yukon. Mean annual runoff in the region is moderately high compared with other regions of the Territory, at 236-385 mm (average 309 mm; Smith et al., 2004). Peak river flows in the Interior Hydrologic Region generally occur in May and June in response to snowmelt inputs during the spring freshet, while secondary discharge

peaks in response to late summer and autumn rainfall are also possible. Lowest flows are typically exhibited in this region in March and April, when groundwater contributions to streamflow, the only inputs to river discharge at this time, are minimal (Janowicz, 2008).

The town of Faro is situated between 671 and 732 m a.s.l., above the floodplain of the Pelly River (which has an elevation of approximately 641 m a.s.l.; see Figure 1). From its headwaters in the Mackenzie Mountains, the Pelly River flows 530 km generally west to its confluence with the Yukon River at Fort Selkirk, 25 km downstream of Pelly Crossing. By the time it reaches the community of Pelly Crossing, the Pelly River has drained an area of approximately 49 000 km² (Water Survey of Canada, 2015).

The Water Survey of Canada (WSC) has maintained several gauging stations in the region over the past several decades, some of which provide real-time hydrometric data. (See Table 1 for a summary of station information.) The WSC reports daily average, monthly average, and peak yearly discharge for each station (Water Survey of Canada, 2015). A hydrograph of monthly average discharge for the Pelly River at Vangorda Creek (the station closest to Faro with the most complete recent record; Figure 5) demonstrates the typical seasonal pattern of a river in Yukon's Interior Hydrologic Region, with rapid increases in discharge in April, May and June, followed by a recession through summer and autumn. Average monthly discharge is low through the winter months, when groundwater is the only input to the river, and the lowest flows occur in March, prior to the spring freshet. Figure 5 also illustrates monthly average discharge for 1980 and 1992, the years on record with the lowest and highest June peak discharge, respectively.

Table 1. Summary of Water Survey of Canada's (WSC) stations in the Ross River and Faro region (Water Survey of Canada, 2015). Stations are listed roughly in order they appear from headwaters to mouth.

Station name	Station ID	Latitude	Longitude	Gross drainage area (km ²)	Parameter	Period of record*
Ross River at Ross River	09BA001	61.989	-132.408	7250	flow, level	1960-2013
Pelly River below Fortin Creek	09BA002	62.031	-130.603	5020	flow	1986-1994
Pelly River at Pelly Crossing	09BC001	62.830	-136.581	49000	flow, level	1960-2013
Pelly River at Ross River	09BC002	61.987	-132.448	18400	flow, level	1954-2013
Rose Creek below Faro Creek	09BC003	62.342	-133.408	208	flow	1966-1969
Pelly River below Vangorda Creek	09BC004	62.222	-133.378	22100	flow, level	1972-2013

* Periods of record do not always contain complete datasets.

Peak yearly discharge also provides a basis for assessing the dynamics of surface water hydrology of the Faro region. Figure 6 presents peak yearly discharge for all WSC stations with year-long data in the vicinity of Ross River (see Table 1 for details of WSC station locations; Rose Creek has been excluded because of its short duration, seasonal record). As described, peak discharge usually takes place during the spring freshet, when snowmelt inputs are high. Figure 6 clearly

demonstrates that peak discharge events measured at headwater stations are mirrored in the discharge records of downstream stations, highlighting the importance of headwater snowmelt inputs to the Pelly River system (see NCE, 2011 for more details). It is also possible that those years in which headwater snowpacks are deep (producing high volumes of snowmelt and high, peak spring discharge events), downstream snowpacks are also deep. Thus, snowmelt contributions may continue to be significant along all reaches of the Pelly River and its tributaries, and act as a key input to discharge along the river system.

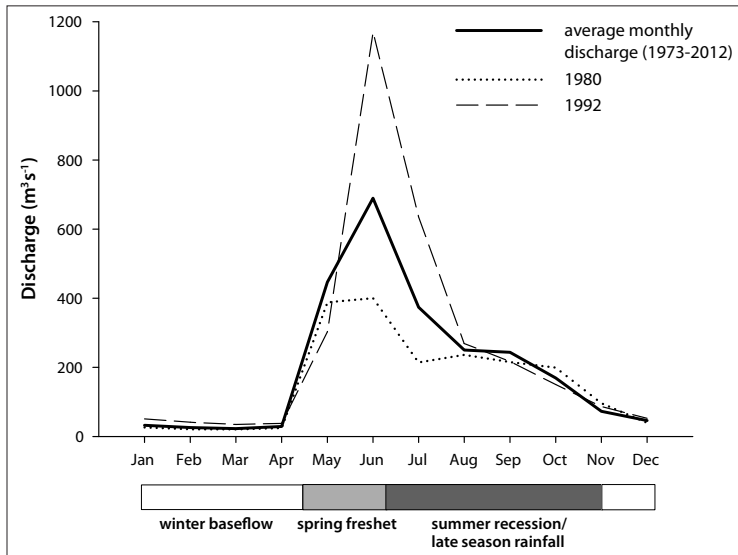


Figure 5. Average monthly discharge hydrograph for the Pelly River below Vangorda Creek (heavy solid line). Also shown are hydrographs for the years 1980 (dotted line) and 1992 (long-dashed line), demonstrating lowest and highest measured peak June discharge, respectively (Water Survey of Canada, 2015).

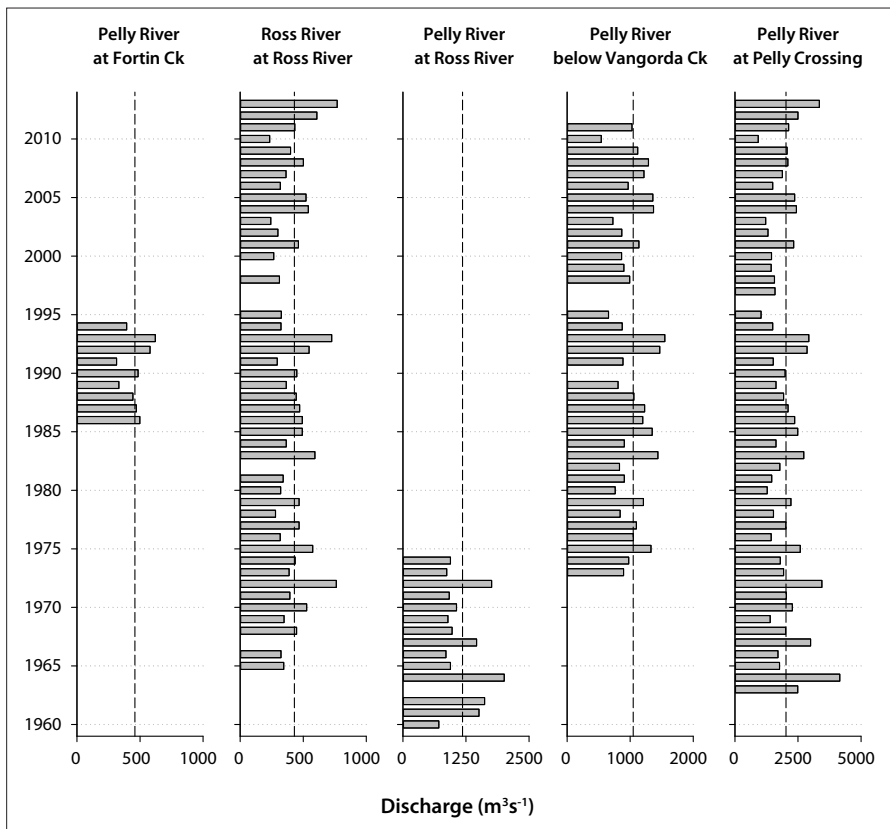


Figure 6. Peak discharge at WSC stations with full-year records, arranged generally upstream (left) to downstream (right). Vertical, long-dashed lines indicate average peak discharge for each station for its period of record (Water Survey of Canada, 2015).

GROUNDWATER

Relatively little information is available regarding groundwater in the Faro area. There are three municipal wells, all within shallow, unconfined aquifers in unconsolidated deposits of sand and gravel on a low terrace of the Pelly River. The wells are approximately 15 m deep (Gartner Lee Limited, 2003). It is expected that other shallow, unconfined aquifers exist in the region, with recharge stemming from the nearby Anvil Range and flowing generally towards the Pelly River. Gartner Lee Limited (2003) suggests that during times of high flow on the Pelly River, the river may serve as a groundwater recharge area for hydraulically connected aquifers. A water well database maintained by Yukon government lists several wells in the Faro area, all to depths of between 4 and 14 m. Additionally, depths of campground wells at Fisheye Lake and Johnson Lake are recorded at 13 m and 24 m, respectively (Water Resources Branch, 2010).

ENVIRONMENTAL DISTURBANCE HISTORY

Historically, the environmental disturbances that impacted the Faro region have been the result of mining-related development. These disturbances began around 1965 when Dynasty Explorations was actively pursuing its exploration program for what would eventually become the Faro mine. In the same year, in order to support economic activity in the Territory, the federal government also began to invest in infrastructure in the area - most notably initiating construction of an all-weather gravel road between Carmacks and Ross River (Weinstein, 1992). Between 1967 and 1969,

“6.5 million cubic yards of waste rock were removed from the deposit; and a winter water supply dam, a concentrator and associated facilities, a 1200 person town, a 540 foot bridge on the Pelly, a 30 kilometre access road, a 160 kilometre road between Carmacks and Ross River, increased hydro-generating capacity at Whitehorse, a 230 mile transmission line, multichannel VHF communications, bulk loading facilities at Skagway and new facilities for the White Pass Railway were all constructed” (Weinstein, 1992, p. 41).

Of course the largest source of environmental disturbance in the area was the development and operation of the Faro Mine Complex, which today has a footprint of over 25 km². The Faro Mine Complex consists of three distinct areas that cover an extensive portion of the region: the Faro Mine area, the Rose Creek tailings area, and the Vangorda/Grum Mine area (Faro Mine Remediation Project, 2011b).

The Faro Mine area includes the Faro Pit, which is approximately 1675 m long and 975 m wide, and covers an area of 1.06 km². Its maximum depth is 335 m below the highest point on the pit wall. Surrounding the pit are piles of waste rock, amounting to over 260 million tonnes of material that covers approximately 106 ha. The disused mill and associated buildings are also located at this site.

The Rose Creek tailings area stores over 55 million tonnes of tailings within an unlined containment system. The tailings area is approximately 4 km long and 1 km wide. A series of three dams hold the tailings in place, and a fourth dam holds contaminated water. Tailings were deposited between 1969 and 1992, and for many years the tailings impoundment was a source of leaks and large spills. Between 1969 and 1975 at least six leaks in the impoundment system were being monitored; additionally, there were a number of major failures resulting in large releases of effluent into nearby Rose Creek (MiningWatch Canada, 2001). In 1975, two dikes failed and 54 million gallons of contaminated tailings water were released into Rose Creek depositing tailings downstream for a distance of 15 km; large spills also occurred in 1976 and 1979.

The Vangorda/Grum mine area, also called the Vangorda Plateau, is made up of two large open pits - the Vangorda Pit and the Grum Pit. The Vangorda Pit is approximately 1150 m long, 350 m wide, and has a maximum depth of 150 m. It is surrounded by over 16 million tonnes of waste rock that is approximately 40 ha in size. The Grum Pit was designed to be approximately 1100 m long, 700 m wide, and up to 200 m deep. Mining operations stopped before the pit reached its design dimensions. The Grum Pit is surrounded by over 110 million tonnes of waste rock, covering approximately 148 ha.

Forest fire disturbance has also impacted the Faro area. As indicated in Figure 7, major fires passed through this area in the last several decades, including large fires in 1958 and 1969 that both affected the hazards map area footprint. Environmental disturbance as a result of forest fires includes changes in vegetation and re-establishment of early successional species. However, subsequent impacts on permafrost are also possible. Because the organic mat on the forest floor acts as an insulator for permafrost, its disturbance can result in deepening of the active layer, alterations to surface albedo, and accelerated permafrost thaw or the development of taliks (an unfrozen layer between the seasonally thawed active layer and the permafrost) (Yoshikawa et al., 2003). Forest fire impacts on permafrost in the Faro region will be discussed in more detail later in this report.

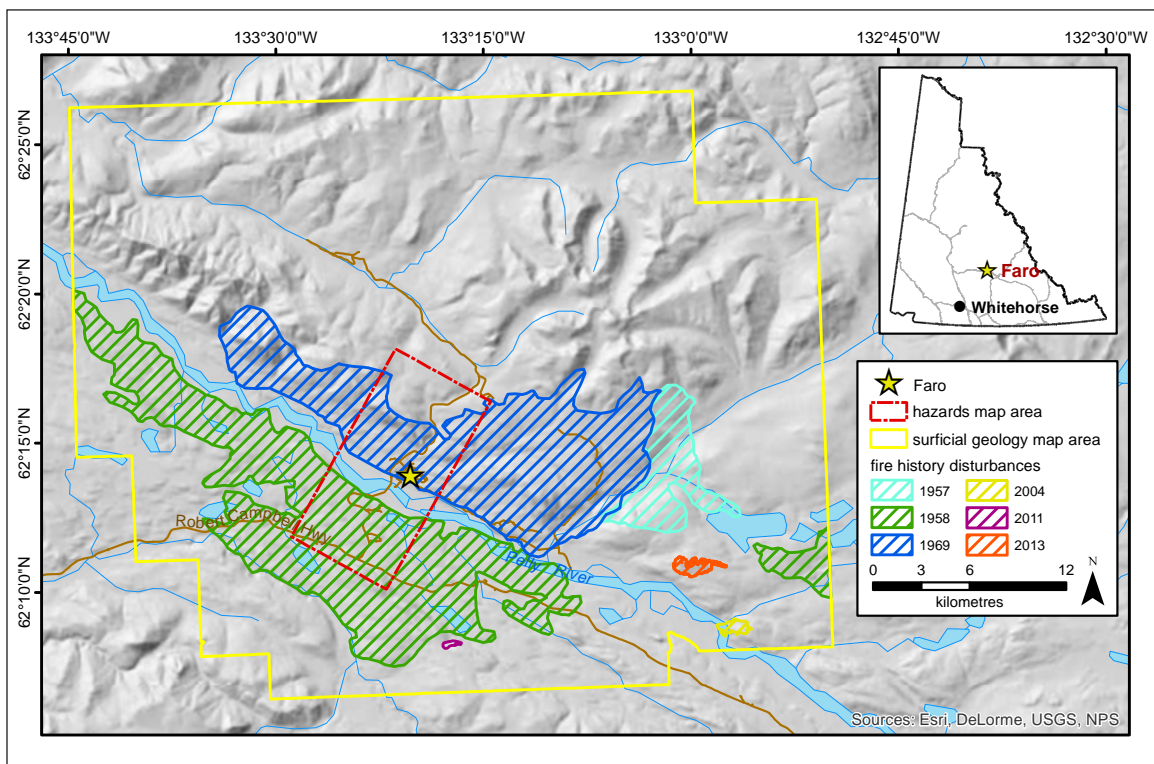


Figure 7. Fire history for the Faro region, based on fire history records provided by Yukon government (Government of Yukon, unpublished data).

BEDROCK GEOLOGY

Figure 8 displays regional bedrock geology for the map area as compiled by Colpron (2015). Map units southwest of the Tintina fault are almost entirely based on 1:250 000-scale mapping originally completed by Gordey and Irwin (1987), whereas those units spanning the portion of the Tintina Trench between the Tintina fault and Pelly River are based on 1:250 000-scale mapping completed by Gordey (2013a,b). Map units northeast of the Pelly River are derived from Pigage's (2004a) 1:100 000-scale Anvil District compilation map, which was based on his earlier (1999-2001) series of fifteen 1:25 000-scale geological maps for the area.

The Tintina fault is the most striking bedrock geological feature of the study area, forming the approximate southwest boundary of Tintina Trench (Figure 8). The fault has not been active since the early Tertiary (over 50 million years ago), when approximately 430-490 km of dextral strike-slip displacement occurred (Roddick, 1967; Tempelman-Kluit, 1980; Gabrielse et al., 2006). The fault juxtaposes widely different geological domains on either side: rocks of the Cassiar terrane, a displaced fragment of the North American passive continental margin, are to the southwest, whereas rocks of the Yukon-Tanana and Slide Mountain terranes, which evolved largely in the Paleo-Pacific Ocean, were mapped to the northeast. Cretaceous and Tertiary igneous rocks are noted locally on both sides of the fault.

In the southwestern corner of the map area, the Pelly Mountains are underlain by Cambrian to Devonian (approximately 360-540 Ma) rocks of the Cassiar terrane, St. Cyr assemblage, which primarily consist of marine shale, slate and limestone (CDS1, 3 and 5 on Figure 8). Early Tertiary (55-65 Ma) sedimentary rocks (ITR3 and 4) occur immediately southwest of the Tintina fault, and a belt of mid-Cretaceous (~97-109 Ma), Cassiar Suite granitic and dioritic plutonic rocks (mKGC) are found at the foot of the Pelly Mountains.

Carboniferous (290-360 Ma) cherty tuff (a fragmental volcanic rock; CK3), and a prominent light grey limestone (CK2) are found immediately northeast of Tintina fault. In the middle of the Tintina Trench, Tertiary (55-65 Ma) sedimentary rocks (ITR3) are faulted against older metamorphosed Yukon-Tanana terrane rocks (e.g., quartzite and schist; PDS3 and 5) of the Snowcap assemblage, which underlie the northeastern side of the Tintina Trench and the town of Faro. These formed in a marine basin that was subducted deep into the crust in the Late Permian (~260 Ma). Jurassic (145-200 Ma) Faro Peak formation sedimentary rocks, primarily composed of conglomerate (JFP1), are found just north of the town of Faro and are visible in outcrop at the "Fingers" recreation site.

North of the Vangorda fault, the southwestern portion of the Ross Lowlands are primarily underlain by mafic volcanic rocks (e.g., basalt, gabbro and greenstone (CPSM1), chert (CPSM2) and lesser ultramafic rocks (pieces of the earth's mantle; CPSM4) of the accreted Slide Mountain terrane. These rocks formed in an oceanic setting offshore of the ancient North American continental margin during the Carboniferous and Permian periods (250-360 Ma).

Further to the north, the Ross Lowlands are underlain by a complex of highly faulted and folded ancient North American (Laurentian) rocks which formed largely in the early to middle Paleozoic era (~400-520 Ma). In order from oldest to youngest, these ancient rocks include: the Mt. Mye formation shale, phyllite and schist (ICG1), and marble (ICG3); Vangorda formation phyllite (COR1); Menzie Creek formation basalt (CSM 8); and the Road River Group limestone, shale and chert. The Anvil district zinc-lead massive sulphide ore deposits occur at the stratigraphic contact between the Mount Mye and Vangorda formations (Pigage, 2004b). Mining of these deposits occurred between 1969 and 1997.

In the northeast part of the map area, the mid-Cretaceous (109 Ma) Anvil batholith comprises granitic rocks (mKgA; Pigage, 2004b).

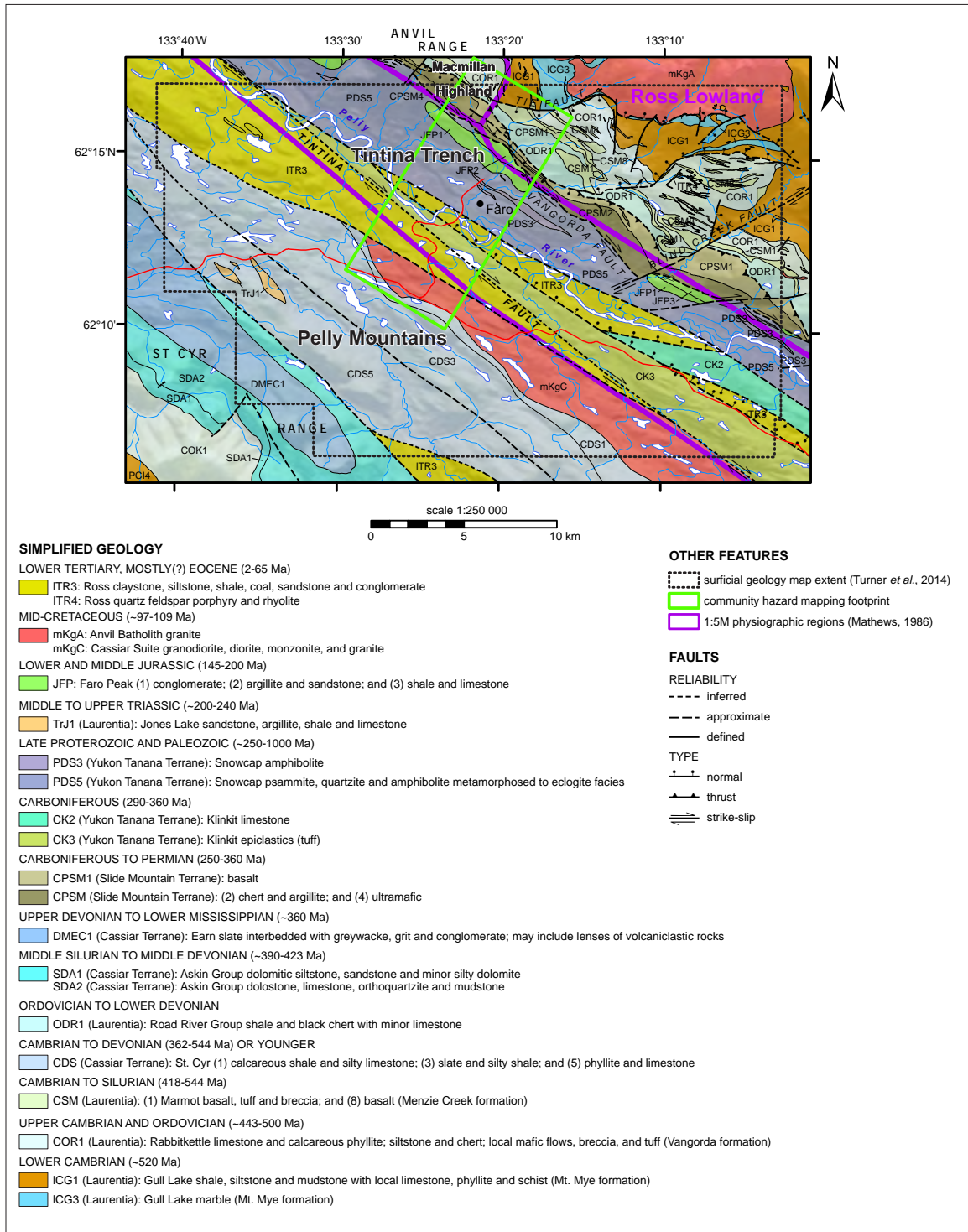


Figure 8. Simplified bedrock geology of the Faro area based on Colpron's (2015) 1:250 000-scale compilation. Physiographic region boundaries are approximated based on Mathews (1986) 1:5 000 000-scale map.

LANDSCAPE EVOLUTION DURING THE PLEISTOCENE AND HOLOCENE EPOCHS

Following millions of years of tectonic activity (discussed in the previous section), the present-day landscape configuration of the study area is largely a product of glacial activity during the Pleistocene (2.6 million years to 10 thousand years (ka)), combined with more recent Holocene (10 ka to present) modification by fluvial (stream) erosion and deposition, as well as colluvial (gravity) and cryogenic (ground freezing) processes.

The study area was repeatedly glaciated during the Pleistocene. To the northwest, closer to Dawson, at least seven advances of the Cordilleran Ice Sheet and local, montane ice from the Ogilvie Mountains, filled Tintina Trench with glacial sediment (Duk-Rodkin et al., 2010). The oldest of these occurred 2.64 million years ago in the Late Pliocene (Froese et al., 2000; Hidy et al., 2013). In the study area, however, most of the material deposited by these earlier glaciations has been eroded or buried, and all of the surficial materials and glacial landforms that currently exist in the study area were deposited in the most recent, late Wisconsinan McConnell glaciation (ca. 25-10 ka).

During the onset of the McConnell glaciation, ice flowed from well-developed alpine cirques in the Pelly Mountains and down the Lapie River valley into the Tintina Trench (Plouffe, 1989). The influx of meltwater into the trench from these accumulating glaciers caused the Pelly River to develop a braided and rapidly aggrading 'advance outwash' floodplain (Ward and Jackson, 2000). This initial phase of glaciation was followed by the advance of the Selwyn lobe of the Cordilleran Ice Sheet from its source region in the Selwyn Mountains (Jackson et al., 1991). During glacial maximum, an ice divide formed east of Finlayson Lake. Ice from this divide flowed southeast towards the Liard Lowland, and northwest down Tintina Trench across the study area.

At its maximum, the Cordilleran Ice Sheet reached elevations between 1550 and 1900 m a.s.l. over Faro and Ross River (Jackson, 1994), covering all but the highest peaks. Despite its thickness, the ice sheet was never topographically independent in this area. Instead, it was composed of numerous ice streams that diverged and coalesced around, and out of, large topographic obstacles such as the Anvil Range (Jackson, 1989; Bond, 1999a). A radiocarbon date on a *Bison priscus* bone fragment at a site along the Ketz River, 30 km southeast of Ross River, yielded an age of $26,350 \pm 280$ BP (TO-393; Jackson and Harington, 1991). This provides a maximum age for the start of the McConnell glaciation in this area.

Deglaciation in the study area was likely a combination of active frontal retreat with re-advances and final stagnation of the ice sheet. Jackson (1994) used high-elevation stagnation features (e.g., ice-contact or kame features) in the Pelly Mountains, thick and highly disturbed supraglacial sediments infilling valleys, and progressively lower lake elevations blocked by melting ice in the valley floor, as evidence for a rapid rise in the equilibrium line and widespread stagnation and down wasting of the ice sheet. However, others have found evidence that ice was still dynamically retreating during deglaciation, with multiple short re-advances of trunk ice flowing up-slope from Tintina Trench into the Pelly Mountains to the south (Bond and Kennedy, 2005; Plouffe, 1989) and the Anvil Range to the north (Bond, 1999a, 2001). One possible scenario is that the ice sheet initially actively retreated, before the equilibrium line rose above the ice elevation, causing wholesale starvation and stagnation of the remaining ice.

The timing of deglaciation is not well known and is the focus of research currently being undertaken by the Yukon Geological Survey and Simon Fraser University (J.D. Bond, pers. comm., 2015). Ward (1989) radiocarbon dated a *Pisidium* sp. shell in the Glenlyon Range to the west of the study area, yielding an age of $12,590 \pm 120$ BP (TO-931). However, this date is likely too old due to hard water effects. Other ages from willow wood at the confluence of the MacMillan and Pelly rivers

(9,140 ± 540 BP; AECV-484C), and seeds from northeast of Faro (10,550 ± 40 BP; Beta-128239) provide a minimum age for the establishment of upland vegetation across the study areas (Ward, 1989; Bond, 2001; Beierle and Bond, 2002). Immediately following McConnell ice retreat, a large glacial lake formed in the Tintina Trench (Bond, 2001; Jackson, 1994), depositing the thick glaciolacustrine sediments that are exposed in steep escarpments below the town of Faro and in many places along the banks of the Pelly River.

During the Holocene, a number of geomorphic adjustments occurred as the landscape transitioned from a glacial to a non-glacial regime. At the beginning of the Holocene, freshly exposed and unstable glacial deposits provided increased sediment loads for braided streams, causing the rapid building or aggradation of fluvial fans and the Pelly River floodplain. Organic deposits began to accumulate at the surface as warmer and wetter climatic conditions returned, and vegetation and soil processes were re-established. As the rate of upland erosion and sediment supply gradually declined, streams transitioned from braided to meandering systems. Terraces were formed as streams incised into the former fans, floodplains and glacial sediments. Based on radiocarbon dating, incision by the Pelly River approximately 100 km east of Ross River began by at least 8000 years BP (Jackson, 1994). Incision continued until sometime before 1200 years BP, as indicated by the presence of White River tephra (volcanic ash) within modern floodplain deposits (Jackson, 1994).

Changes in climate through the Holocene must have impacted the development and degradation of permafrost. In general, permafrost may take decades to centuries to form, and equally long periods to degrade, although degradation can accelerate if surface ponding occurs, or if ice within the ground is exposed. The surface organic mat can help preserve the permafrost for some decades during a warming phase, leading to what is termed ecosystem-protected permafrost (Shur and Jorgenson, 2007). Forest fires, which destroy the organic mat, may lead to the permanent loss of permafrost. The evolution of permafrost conditions in the Faro area has not been studied in detail, but it can be inferred that permafrost existed beneath any exposed land during the last glacial period, and formed in newly exposed land during deglaciation. During the Holocene, it may have aggraded and degraded several times in response to a cooling and warming climate, respectively. The latest phases of such changes are the cooler period of the Little Ice Age which lasted for several centuries up to the end of the 19th century, and the 20th century climatic warming which has continued through to the present. Given that there exists time lags in the response of permafrost degradation or aggradation, permafrost in the area is undoubtedly in a degrading phase.

SURFICIAL MATERIALS

Surficial materials in the Faro area are depicted in an accompanying 1:25 000-scale map by Turner et al. (2014; YGS Open File 2014-14). These materials are broadly classified into a variety of genetic types, based on the physical processes they are derived from, including: anthropogenic (human activity); volcanic; eolian (wind); organic (soil development); colluvial (downslope movement or creep); fluvial (rivers and streams); glacial (ice, glacial streams and lakes); and bedrock. Each of these material types are described below based on their texture or grain size (e.g., gravel, sand, silt or clay); sorting (variety of grain sizes); structure (e.g., layering or bedding); association with permafrost; and the general distribution of the material.

ANTHROPOGENIC MATERIALS

Anthropogenic materials are produced or significantly modified by human activity, such as landfills, mine tailings, and open-pit mines. The only significant anthropogenic materials identified in the map area are the Grum and Vangorda waste rock and mine pits, however these materials were not characterized in any further detail.

ORGANIC MATERIALS

Organic materials are produced by the accumulation of decomposing vegetative matter and contain at least 30% organic matter by weight (Figure 9a). They are generally found at the surface in low or flat-lying areas and in poorly drained depressions (especially in the swales between streamlined till and bedrock landforms within the Tintina Trench; Figure 9b). Poor drainage associated with these deposits inhibits decomposition of organic material and results in fibric or peaty textures, although mesic and humic textures were also observed. Shallow permafrost is commonly encountered in or beneath these materials due to their insulating capacity.

A shallow pocket of peat has been excavated and stockpiled within the Faro town limits near the start of Blind Creek Road.

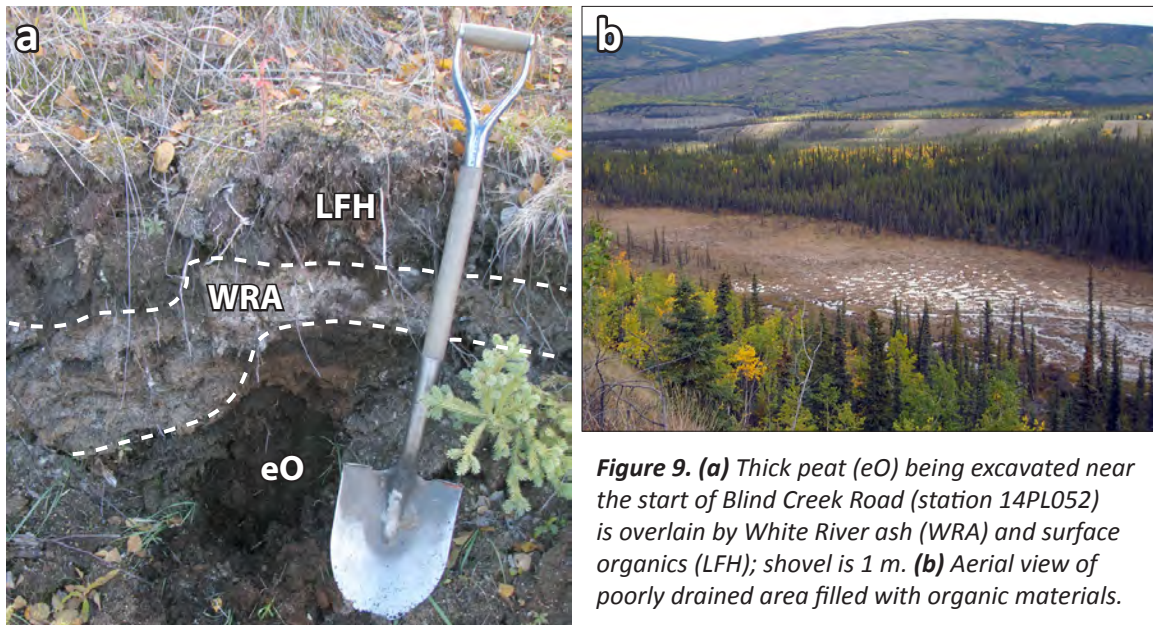


Figure 9. (a) Thick peat (eO) being excavated near the start of Blind Creek Road (station 14PL052) is overlain by White River ash (WRA) and surface organics (LFH); shovel is 1 m. (b) Aerial view of poorly drained area filled with organic materials.

VOLCANIC MATERIALS

A distinctive, white layer of volcanic ash known as the White River tephra is preserved near the ground surface in most areas (Figure 10; also visible in Fig. 9a, and Fig. 14c,d below), often immediately below the surface organic mat. It is generally not mapped because it is so thin (typically 5-15 cm thick), but an exposure with a layer of White River tephra up to 30 cm thick was observed just north of the airstrip. When Doal Lake was excavated during construction of the Grum open-pit, 25 cm of White River tephra was exposed above 90 cm of Holocene lacustrine gyttja (Beierle and Bond, 2002). The source of the volcanic ash was near Mt. Bona-Churchill in the St. Elias Mountains, about 25 km west of the Yukon-Alaska border. The most recent eruption occurred approximately 1200 years ago (Lerbekmo and Campbell, 1969; Clague et al., 1995; Lerbekmo, 2008; Jensen et al., 2014).

EOLIAN MATERIALS

Eolian materials are transported and deposited by wind. The dominant eolian sediment in the map area is loess, which is characterized by its reddish brown colour and well-sorted, silty, fine-grained sand texture. Loess is commonly found as a thin veneer immediately underlying the White River ash throughout the map area (e.g., Fig. 10; also visible in Fig. 39 below) and generally

varies in thickness between 10 cm and 50 cm, although pockets have been observed that exceed 1 m in thickness. The original source of the loess was derived from exposed glaciofluvial and glaciolacustrine surfaces during deglaciation.

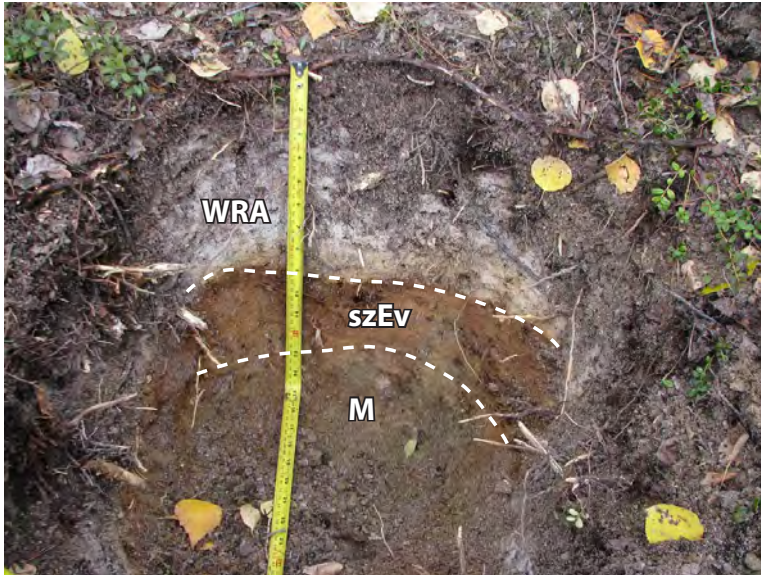


Figure 10. Thin basal till (M; olive-brown colour) overlain by 7 cm of silty, fine-grained sand loess (szEv; red-brown layer) and 22 cm of White River ash (WRA; white layer near surface) on a streamlined ridge crest approximately 1 km east of Faro (station 14PL035).

COLLUVIAL MATERIALS

Colluvium is sediment transported and deposited on, or at the foot of slopes by gravity-driven processes such as creep, solifluction, landslides, and snow avalanches. Colluvium is common on moderately steep to steep slopes, and in areas of high relief such as the Pelly Mountains. It typically comprises poorly sorted sediment ranging in size from clay to boulders. The texture of colluvium is directly related to the texture of the parent material that is entrained by the slope processes (e.g., morainal materials versus weathered bedrock). On gentle to moderate north-facing slopes, colluvium is commonly composed of fine-grained material and is deposited by periglacial processes such as sheetwash and active layer detachment slides. Coarse-grained colluvium with angular clasts is more typical on steeper slopes where larger landslides are the primary transport mechanism (e.g., Figure 11a,b). Colluvial fans, cones and aprons are also found at the base of slopes where they have been deposited by hazardous mass movement processes such as rockfall, rockslides, slumps, debris slides and debris flows. Permafrost presence in colluvium is highly variable and dependent on surface sediment texture, topographic position, and surface expression.

FLUVIAL MATERIALS

Fluvial sediments are transported by streams and rivers and deposited as floodplains, fluvial fans and terraces. They typically consist of well-sorted, stratified sand and rounded gravel with varying amounts of silt and organic materials (Figure 12a). Silt, sand and organic deposits make up thinly laminated or massive overbank deposits that are commonly interbedded with coarser, gravel deposits. Floodplain sediments are widespread adjacent to the Pelly River (Figure 12b). Fans are common where streams enter broad valleys. Higher elevation, narrow floodplains typically contain coarser-grained deposits compared to large, lower elevation floodplains where finer-grained sediments tend to accumulate. Steep bedrock canyons have also been cut along Vangorda Creek and its tributaries. Permafrost is uncommon in active fluvial deposits that have recently flooded or are subject to regular flooding, but may be found at depth in inactive floodplain areas.

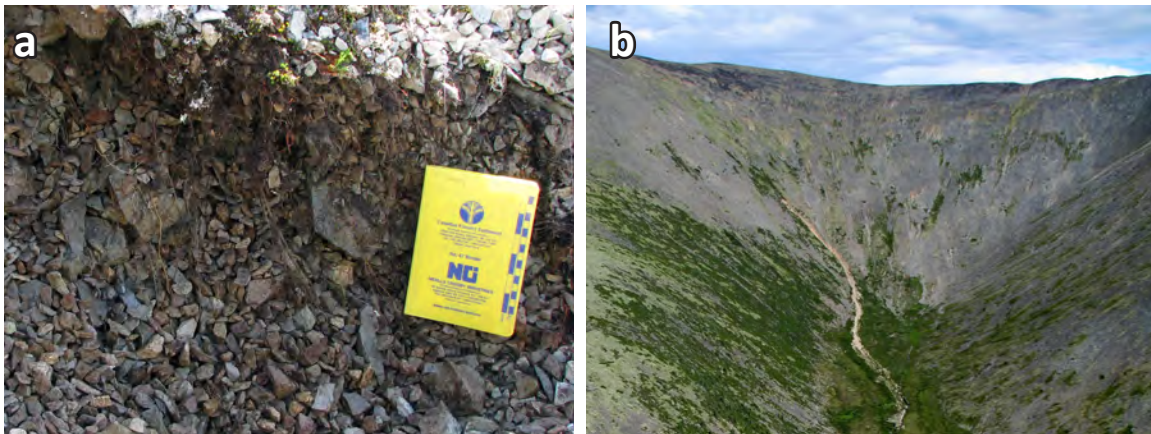


Figure 11. (a) Typical coarse, angular colluvium derived from weathered bedrock. **(b)** Steep alpine slopes mantled with colluvial veneer derived from weathered bedrock. Debris flows (note fresh track in centre of photo) are a common transport mechanism in this environment. (This example is from outside the study area on Mt. Cockfield in the Dawson Range).

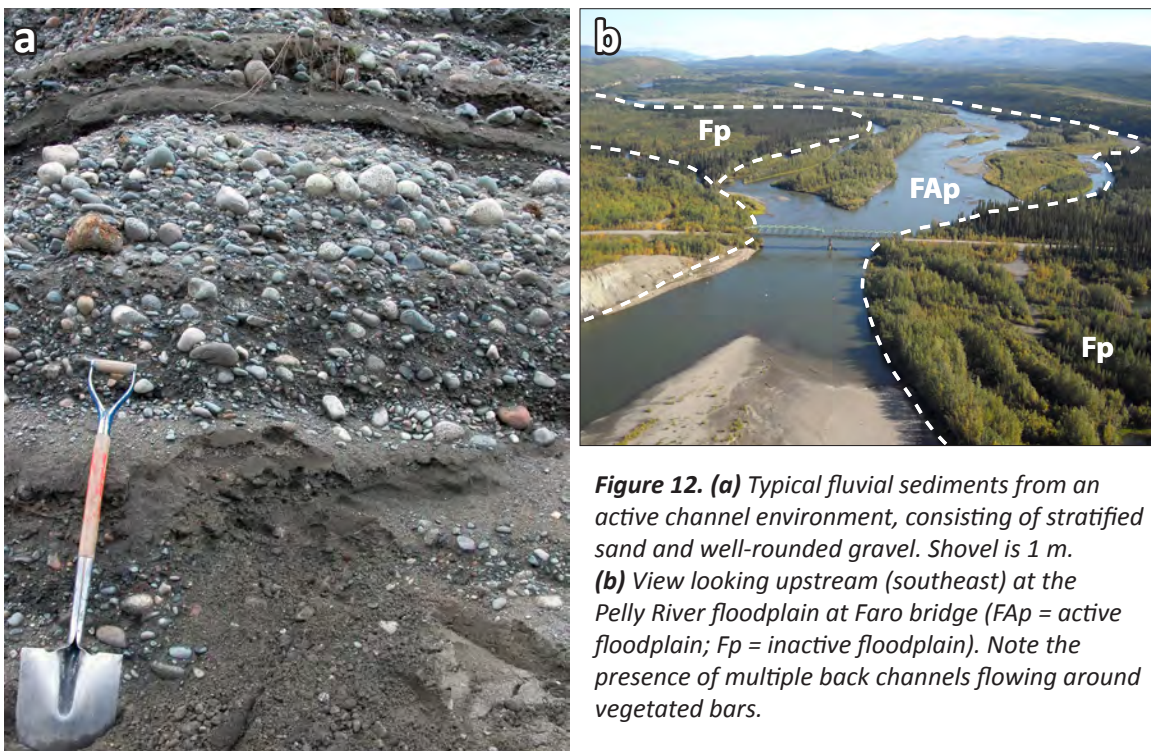


Figure 12. (a) Typical fluvial sediments from an active channel environment, consisting of stratified sand and well-rounded gravel. Shovel is 1 m. **(b)** View looking upstream (southeast) at the Pelly River floodplain at Faro bridge (FAp = active floodplain; Fp = inactive floodplain). Note the presence of multiple back channels flowing around vegetated bars.

GLACIOFLUVIAL MATERIALS

Glaciofluvial sediment exposed in the study area was deposited by glacial meltwater either directly in front of, or in contact with, late Wisconsin McConnell glacial ice. The sediment is typically poorly to well-sorted, rounded, and stratified gravel and sand (Figure 13a,b). Glaciofluvial materials in the study area were deposited as hummocky, ice marginal sediment, sub- and englacial eskers, and kettled outwash plains that were subsequently eroded into terraces in valley bottoms. The high porosity of glaciofluvial materials results in largely ice-free deposits or deep active layers. Sediments may be more ice-rich in areas with discontinuous, fine-grained sand and silt interbeds.

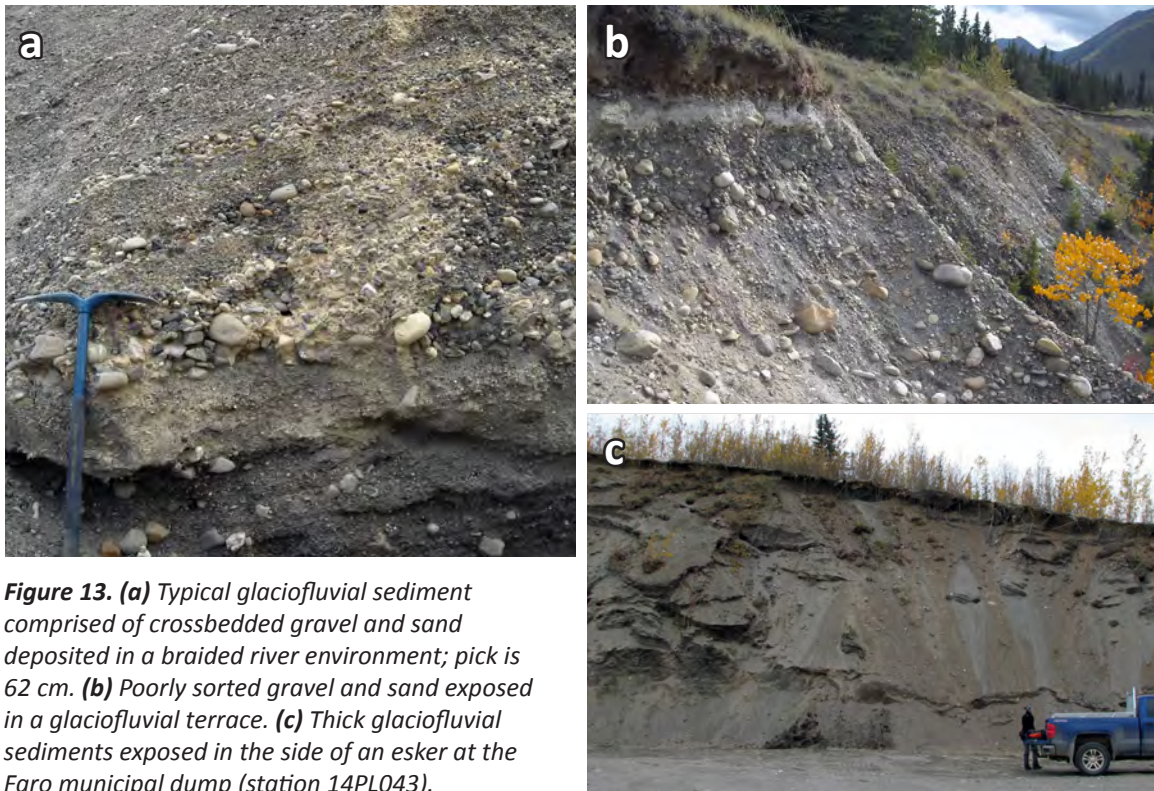


Figure 13. (a) Typical glaciofluvial sediment comprised of crossbedded gravel and sand deposited in a braided river environment; pick is 62 cm. (b) Poorly sorted gravel and sand exposed in a glaciofluvial terrace. (c) Thick glaciofluvial sediments exposed in the side of an esker at the Faro municipal dump (station 14PL043).

Glaciofluvial deposits and erosional landforms are abundant in and around the town of Faro and provide an excellent local source for gravel. Most of the town is situated on a relatively thin glaciofluvial blanket (<5 m thick; Environment Yukon, 1976) mostly comprising well-sorted sand and some gravel. A large unit of thicker hummocky glaciofluvial material is also found immediately west of Vangorda Creek in the vicinity of the municipal dump, where prominent esker ridges and kettle holes are mapped (Figure 13c; see above). The eskers formed as sediment was deposited in meltwater streams that flowed northwest down Tintina Trench in, or beneath glacial ice. The kettle holes formed when large blocks of ice stranded during glacial retreat eventually melted out. The first 4 km of the Blind Creek Road are also underlain by extensive, hummocky, ice-marginal glaciofluvial material. Northwestern flowing glaciofluvial meltwater channels are also commonly found carved into till units throughout Tintina Trench and in the vicinity of Faro.

MORAINAL MATERIALS

Morainal deposits in the study area (also referred to as till) were deposited directly by late Wisconsin McConnell glacial ice without modification by any other transportation agent. These deposits are widespread, both in valley bottoms and across gentle to moderate slopes across the map area. Till is typically a poorly sorted and consolidated mixture of silt, sand, and clasts that are rounded to angular, and pebble to boulder-sized (Figure 14a). Many of these clasts are heavily striated and have keels, lee-end fractures, and other evidence of glacial erosion. Morainal deposits are typically found as veneers or blankets that follow the underlying topography. Streamlined drumlins, flutings, and crag and tails (Figure 14b) composed of heavily compacted basal till are abundant across Tintina Trench, which is attributed to rapid, unobstructed ice flow through the trench during glacial maximum (Bond, 2001). The streamlined features were formed from sediment deformation at the ice-bed interface below the ice sheet and are typically composed of till greater than 5 m thick. Till may be thin (less than 15 cm) in high elevation areas

but reaches thicknesses of up to 20 m at Vangorda mine pit (Bond, 1999b), and up to 50 m near Tintina Subdivision (Environment Yukon, 1990). Several exposures of thick till are visible near the town of Faro along Vangorda Creek near Vangorda Falls (Figure 14c) and across from the lower bench (Figure 14d). Morainal deposits also form undulating and hummocky topography. Till is generally colluviated when found on slopes, and is commonly associated with permafrost with varying amounts of ice.

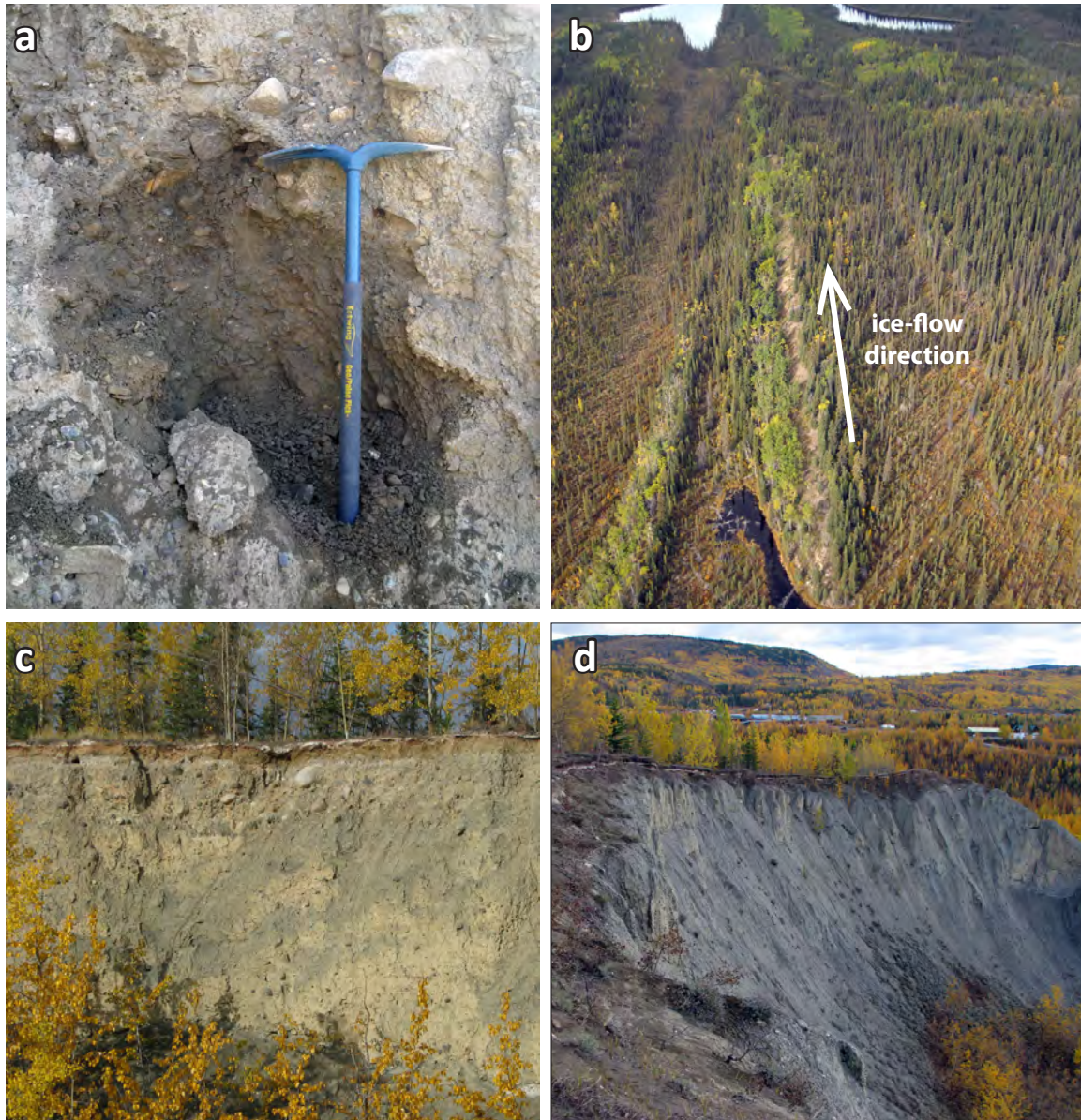


Figure 14. (a) Typical morainal sediments (basal till), containing a wide range of clast sizes embedded in a very dense, fine-grained matrix; pick is 62 cm (station 13DT019). (b) Streamlined drumlin in Tintina Trench, indicating that ice flow was in a northwesterly direction. (c) Eight metre-high exposure of till along the south side of Vangorda Creek, just downstream of Vangorda Falls (near station 14PL030). Exposure demonstrates the typical, chaotic, unsorted nature of basal till. Note thin layer of White River ash near surface. (d) Thirty metre-high exposure of till along Vangorda Creek, directly across from station 14PL047. Basal till is typically very dense and cohesive, and often becomes heavily gullied, as demonstrated near the top of the exposure. Note the thin layer of White River ash near surface.

The presence of two distinct till units exposed in the headscarp of the Faro ski hill landslide (see case study section on page 51) suggests that following glacial maximum, ice re-advanced up-slope from Tintina Trench into the Anvil Range as depicted by Bond (1999a; Pelly re-advance). The lower till unit is darker grey in colour, likely due to the incorporation of phyllite clasts of the local Vangorda formation, while the upper unit is a light brown colour with more granitic clasts which likely originated from a more distal source in the Tintina Trench. A similar configuration of till deposits were noted to the east in Swim Basin by Bond (2001), who interpreted the lower till as a glacial maximum deposit, and the upper till as a re-advance deposit.

GLACIOLACUSTRINE MATERIALS

Glaciolacustrine materials primarily consist of interbedded and interlaminated clay, silt, and sand deposited in glacial lakes during late Wisconsin McConnell deglaciation (Figure 15a,b). Glaciolacustrine deposits are widespread in Tintina Trench, and reach thicknesses up to 40 m above the Faro sewage lagoon. Many of these deposits are covered by glaciofluvial, colluvial, lacustrine and organic sediment. A notable exception to this is the presence of large glaciolacustrine terraces on the southwest side of the Pelly River. These terraces are ~30 m above the Pelly River floodplain and have a plain to undulating expression. Glaciolacustrine terraces of similar thickness also exist on the northeast side of the river, but they have been covered by 5-10 m of glaciofluvial sediment. The fine-grained texture of glaciolacustrine deposits promotes the growth of ice-rich permafrost and thermokarst lakes, and segregated ice lenses are common within these deposits. Furthermore, Glaciolacustrine materials are commonly unstable and associated with landslide activity when saturated, although no specific examples of this are documented in the study area.

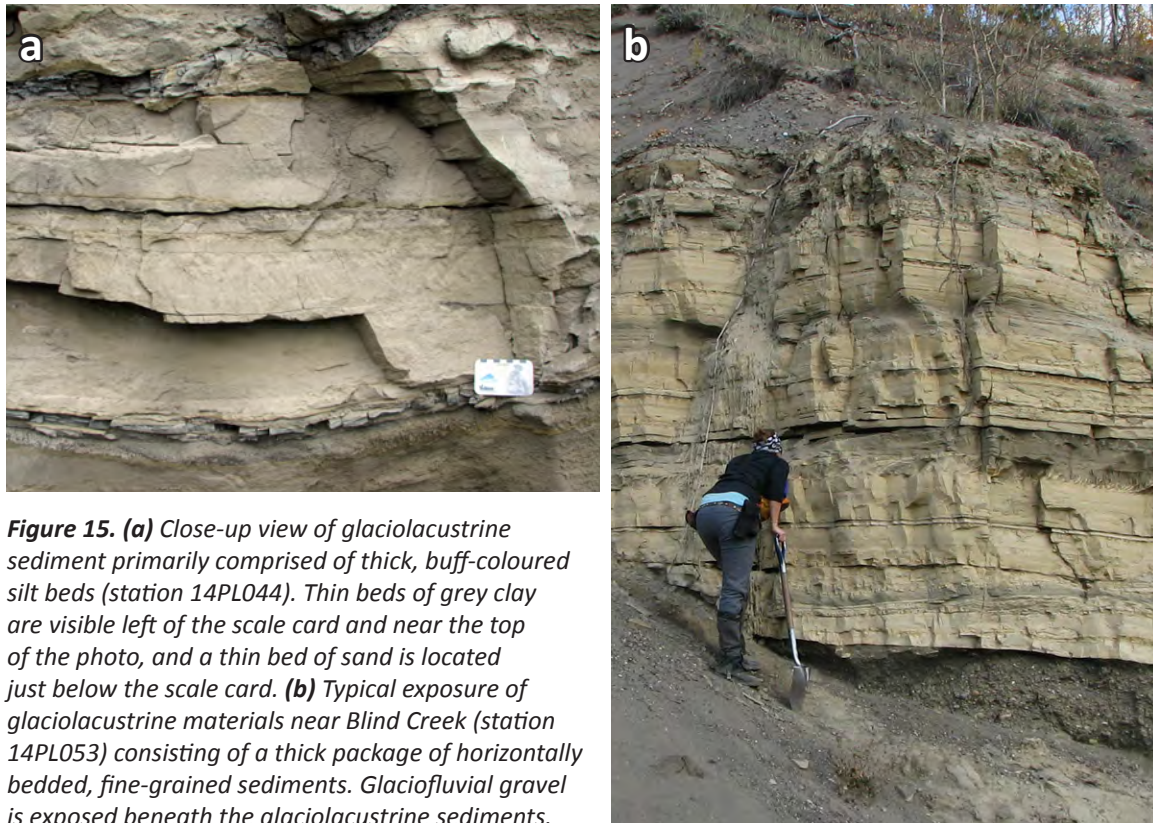


Figure 15. (a) Close-up view of glaciolacustrine sediment primarily comprised of thick, buff-coloured silt beds (station 14PL044). Thin beds of grey clay are visible left of the scale card and near the top of the photo, and a thin bed of sand is located just below the scale card. (b) Typical exposure of glaciolacustrine materials near Blind Creek (station 14PL053) consisting of a thick package of horizontally bedded, fine-grained sediments. Glaciofluvial gravel is exposed beneath the glaciolacustrine sediments.

BEDROCK

Bedrock is mostly exposed on alpine summits, ridges and spur crests, and on steep valley sides (Figure 16a). Lower elevation exposures in the Tintina Trench are streamlined to the northwest (Figure 16b), in the down-ice flow direction. Bedrock is also exposed in valley bottoms where streams have incised canyons (e.g., at Vangorda Falls; Figure 16c) and eroded through valley-bottom sediments. Bedrock is commonly associated with colluvial deposits and may be a source of rockfall and rockslide deposits.

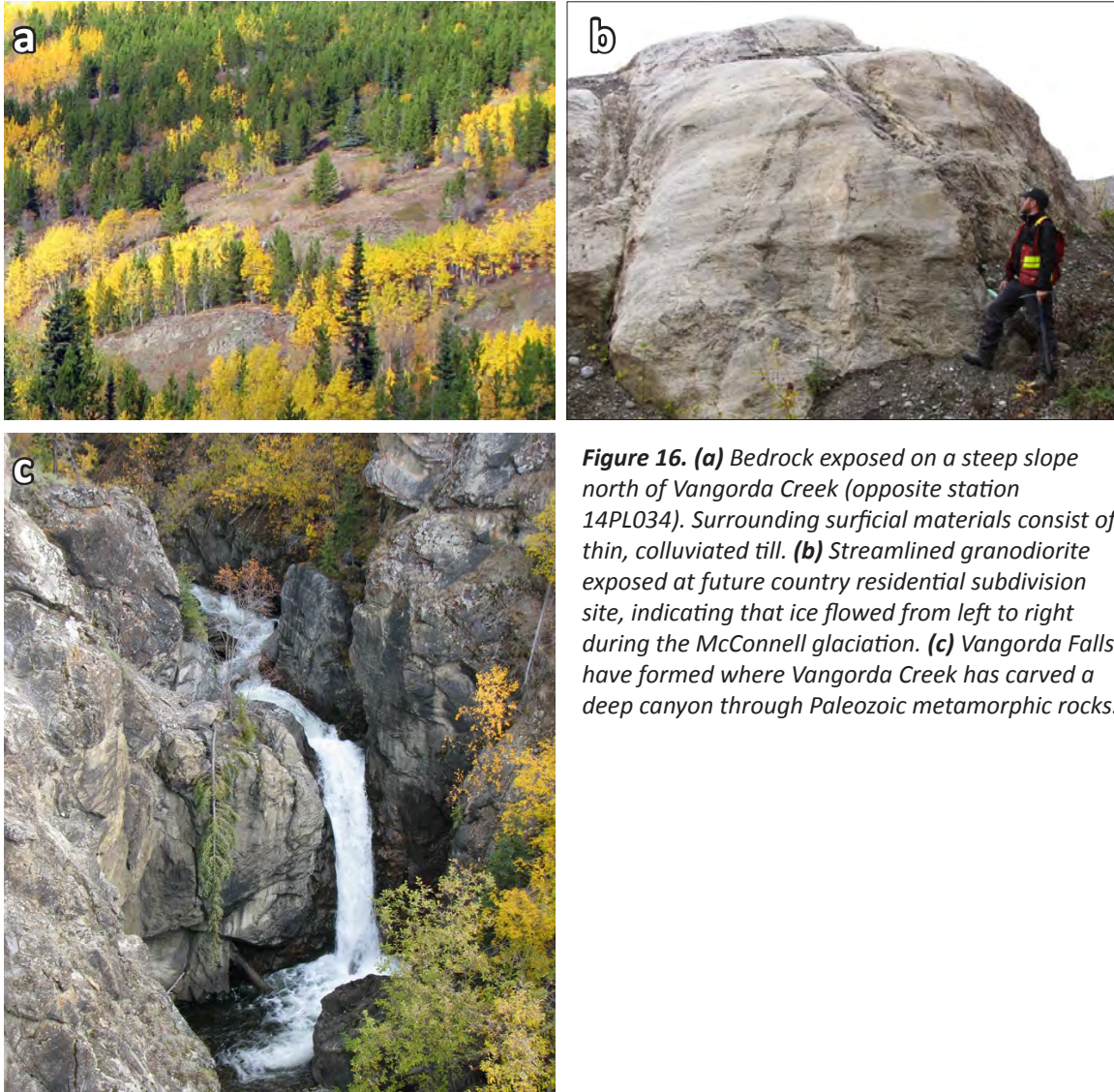


Figure 16. (a) Bedrock exposed on a steep slope north of Vangorda Creek (opposite station 14PL034). Surrounding surficial materials consist of thin, colluviated till. (b) Streamlined granodiorite exposed at future country residential subdivision site, indicating that ice flowed from left to right during the McConnell glaciation. (c) Vangorda Falls have formed where Vangorda Creek has carved a deep canyon through Paleozoic metamorphic rocks.

STRATIGRAPHY

The stratigraphy of the Faro area is complex having large lateral variability, but generally reflects the glacial history and subsequent Holocene fluvial and colluvial activity previously described (Figure 17). Much of the study area is blanketed by McConnell till up to 50 m thick (Environment Yukon, 1990) that has colluviated on slopes and escarpments. Generally the McConnell till is less than 20 m thick. In many cases, the till is interbedded with glaciofluvial and/or glaciolacustrine

sediments as a result of complex deglaciation processes and active ice retreat. During McConnell deglaciation, a large glacial lake formed in Tintina Trench, depositing the thick glaciolacustrine sediments that are exposed in steep escarpments below the town of Faro and in terraces along the Pelly River (Bond, 2001); extensive glaciofluvial sediments were also deposited in surrounding areas. After the lake drained, Pelly River incised into these sediments, forming the prominent escarpments and terraces that are found along the modern floodplain margin.

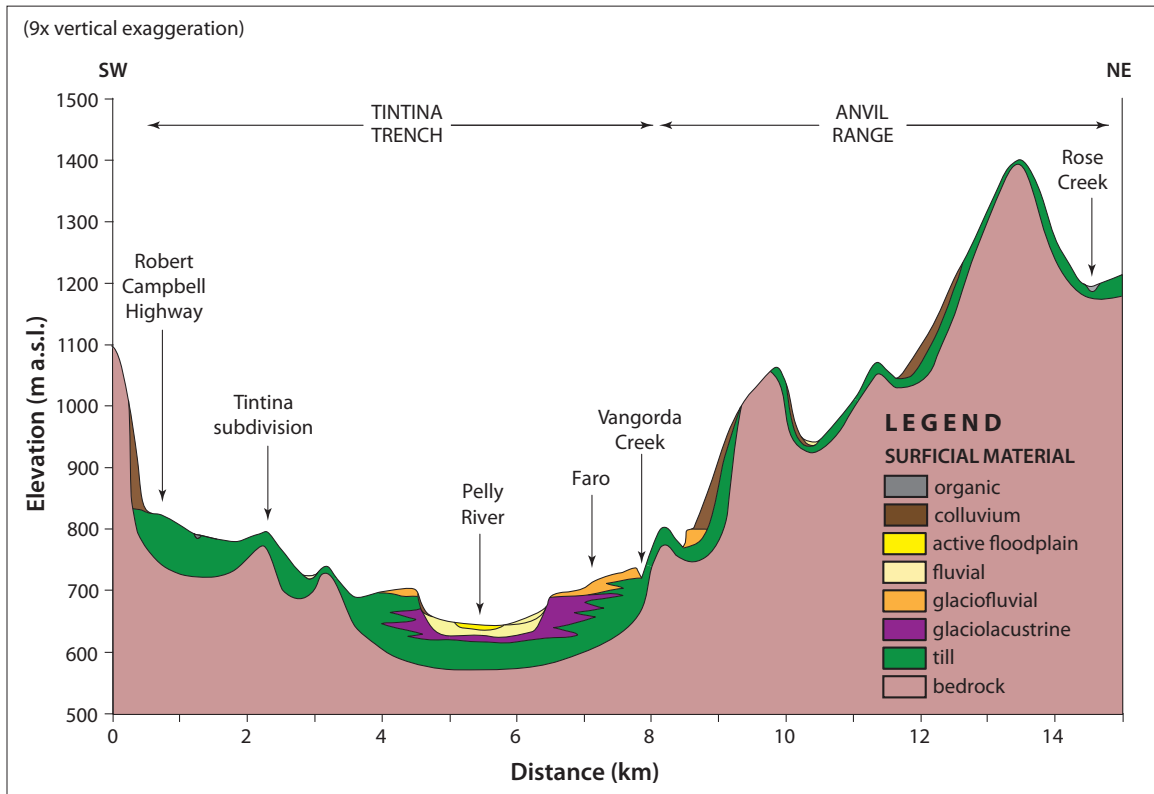


Figure 17. Hypothetical stratigraphy along a northeast-southwest transect perpendicular to Tintina Trench in the vicinity of Faro. Unit thicknesses are exaggerated for visual clarity. Relative thicknesses are estimated based on aerial photo interpretation, borehole logs, and observation of stratigraphic exposures.

PERMAFROST

In the study region, the permafrost profile is made up of several different components which must be considered collectively in order to accurately characterize local permafrost conditions. These components, and comments about their relevance to the Faro region, are described in the following section.

ORGANIC COVER

The organic cover (i.e., peaty materials) is generally found at the top of the soil column; it has a very low thermal conductivity when dry, which reduces atmospheric heat transfer to lower, underlying sediment beds. Therefore, the thicker the organic cover, the cooler the ground. Under a thick organic mat, the active layer is thin and colder permafrost may develop. The high porosity of peat allows it to retain a significant amount of water or pore ice. Regardless of the presence of a visible cryostructure, peat is solid when frozen, but becomes highly compressible when thawed. If compression is applied, porosity and hydraulic conductivity decrease while thermal conductivity increases. Since it is one of the most significant drivers for ground ice sustainability,

removing or compacting the organic cover can initiate degradation of the underlying permafrost by affecting its thermal regime. Additionally, high hydraulic conductivity in areas of groundwater flow can lead to preferential flow paths and discharge areas. When a flow pattern is disturbed by removal or compaction of the organic cover and degradation of the underlying permafrost, water accumulation may trigger further localized permafrost degradation by heat advection through groundwater and subsequent freeze-back.

FOREST COVER

The forest cover keeps the ground cool by providing shade, increasing the soil moisture (increase in heat capacity), and increasing energy diffusion before it hits the ground surface. In the winter, trees retain snow, which locally reduces snow cover on the ground that is acting as an insulating layer between the atmosphere and the ground (Brown, 1963; Brown and Péwé, 1973). Clearing of the forest cover by machinery or forest fire often leads to a deepening of the active layer. When the low-lying vegetation (e.g., bryophytes, herbs) is also removed, the effects are much more pronounced.

SURFACE SEDIMENT TEXTURE

Six different sediment types were identified in the Faro area based on the geotechnical characteristics of samples gathered during the permafrost drilling program. They were classified using the Unified Soil Classification System (USCS): sand, silty sand, silty sand with gravel, sandy organic silt, silt and peat.

Sand

Sand layers are generally well drained and do not contain excess ice when frozen. However, fine and very fine sand may be frost susceptible and can contain excess ice in the form of alternating ice lenses. Upon thawing, sediments with excess ice will undergo thaw settlement and will drain more slowly than coarser sand (medium to very coarse sand).

Silty sand

Coarse silt and fine sand may contain a considerable amount of excess ice in various forms under many surficial hydrologic and thermal conditions, because these two materials have important ice segregation potential (Darrow et al., 2008).

Silty sand with gravel

This type of deposit was present at all sites, except in the floodplain of the Pelly River (Sewage Lagoon site). Because of the presence of fine-grained material in the gravel, this type of deposit has high ice-segregation potential. In permafrost, if saturated with water, this deposit may develop layers with ice-rich cryostructures and be affected by strong differential thaw settlement. However, if present in under-saturated conditions, these sediments would not contain excess ice and would be mechanically stable upon thawing.

Sandy organic silt

Organic matter in a sandy-silty matrix increases the water retention capacity of a soil, which could lead to the development of excess ice in permafrost and an increase in settlement potential under a load, due to the highly compressible nature of peat.

Silt

This fine-grained material is usually highly frost-susceptible. If the silt is located in the active layer and water is available, annual frost heaving and settlement of the ground will occur. If the silty layer is located at or below the permafrost table, the upper part of the permafrost will be typically

ice-rich and mechanically unstable upon thawing. Where permafrost has degraded, these areas are characterized by poor drainage.

Peat

Peat deposits have high porosity and can retain water; they are highly compressible. In permafrost, peat is usually ice-rich. Upon thawing, the water is drained and the ground is susceptible to significant settlement, especially under a load (e.g., building, road, etc.).

POTENTIAL HAZARDS RISKS FOR THE FARO REGION**LANDSLIDE PROCESSES**

Landslides are created by the downslope movement (i.e., mass wasting) of surficial materials and/or bedrock fragments, often mixed with vegetative debris. They are generally triggered on moderate to steep slopes by a variety of factors including intense rainfall or snowmelt events, permafrost degradation, forest fires, river erosion, groundwater flow, and/or earthquakes. In many cases, several of these triggering forces act in combination.

Landslides range in size from metres to hundreds of metres. They may be restricted to very shallow surface layers, or they may be deep-seated and extend into thick sediments or bedrock. They may be rapid events that occur in seconds to minutes, or they may gradually creep or rotate over years to centuries. Depending on slope geometry and sediment water content, debris may free fall, slide, rotate and/or flow.

Large landslides are uncommon in the Faro area, and extensive gully erosion along steep escarpments throughout the map area is the most prominent form of mass wasting in the region. South-facing, steep slopes are particularly susceptible to gullying because they have very sparse vegetation cover which provides limited protection from erosion due to surface runoff.

The most common landslides mapped in the Faro region are debris flows, which are concentrated in steep gullies along the front ranges of the Pelly Mountains (e.g., Figure 18a) and in alluvial fans entering the Tintina Trench and the Pelly River floodplain. Debris flows occur when saturated, loose sediment flows rapidly downslope in a slurry, and often occupies a pre-existing stream channel or gully. They are generally triggered by excessive runoff from intense rainfall and/or snowmelt events, especially where drainage is restricted by shallow bedrock. Debris flows can be destructive and may be capable of entraining large trees and boulders. They are also one of the primary mechanisms by which colluvial and alluvial fans are built in valley bottoms.

Other types of landslides in the area include: small slides and slumps along river cutbanks, particularly along the Pelly River (e.g., Figure 18b); and scattered rockslides and rockfalls along the front ranges of the Pelly Mountains, and from the cliffs along the south shore of Fisheye Lake.

Permafrost-related landslides such as active-layer detachments and retrogressive thaw flows are also found in the region (see this study and Lipovsky and Huscroft, 2007). Permafrost influences slope stability by strongly affecting drainage (which is restricted by the permafrost table), soil moisture (which may increase in response to rapid thaw of ground ice), and strength (through bonding of frozen soil particles).

Active-layer detachments are triggered by the rapid thaw of the active layer, which is often caused by forest fires or exceptionally warm summers, especially on north-facing slopes (e.g., Figure 18 c,d,e). These landslides are generally relatively small (a few hundred metres long and tens of m wide) and shallow (<1 m deep), but they are capable of transporting mature trees and often occur on very gentle slopes and in large numbers, which may affect local sedimentation rates

(Lipovsky et al., 2006). Because they are so shallow, their scars revegetate quickly and their former presence is only indicated by subtle changes in vegetation (e.g., Figure 18d). A prominent active layer detachment failure recently occurred west of the Faro mine access road, approximately 1.5 km just southwest of the former ski hill (Figure 18e; see also Figure 19a below).

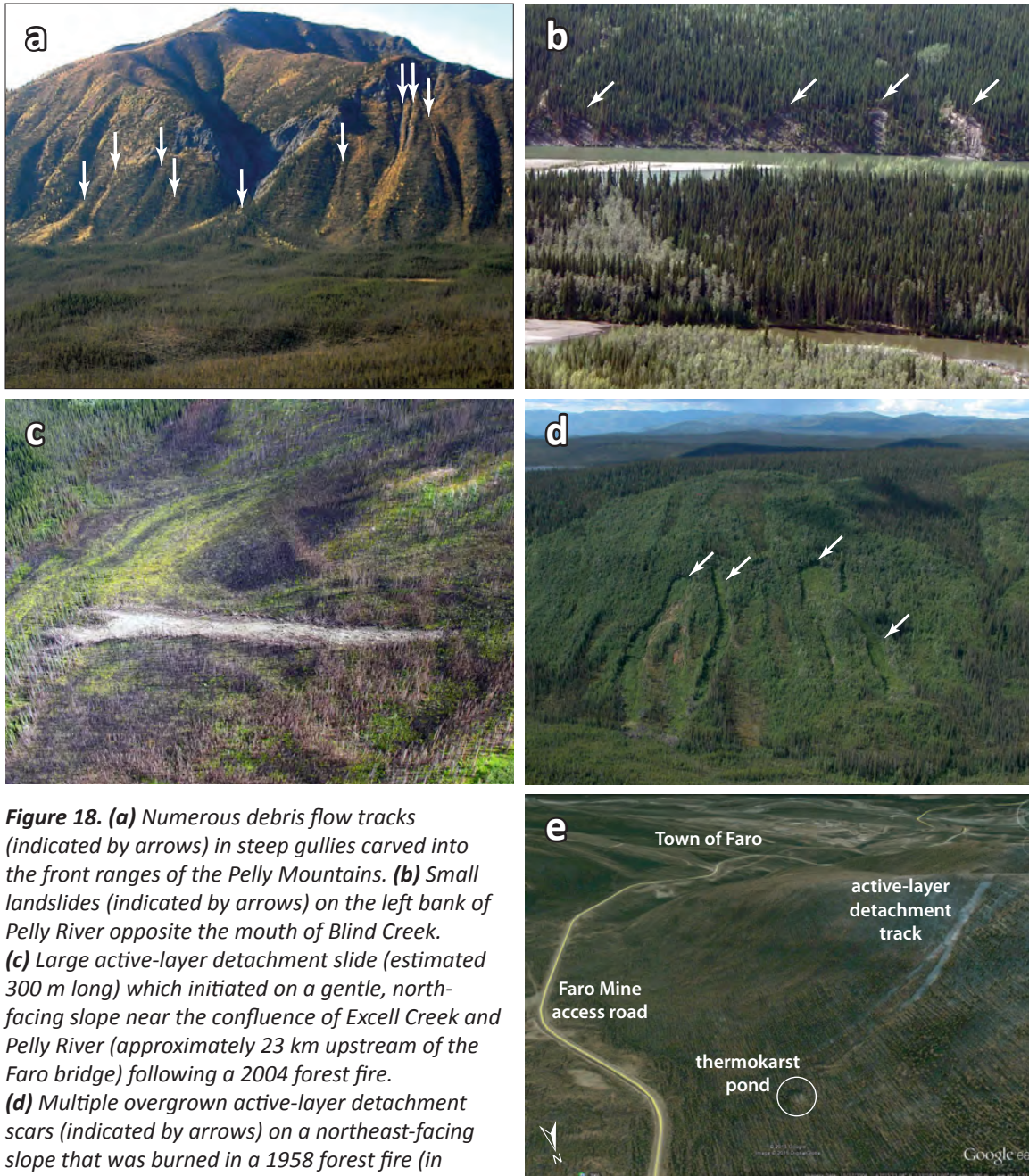


Figure 18. (a) Numerous debris flow tracks (indicated by arrows) in steep gullies carved into the front ranges of the Pelly Mountains. (b) Small landslides (indicated by arrows) on the left bank of Pelly River opposite the mouth of Blind Creek. (c) Large active-layer detachment slide (estimated 300 m long) which initiated on a gentle, north-facing slope near the confluence of Excell Creek and Pelly River (approximately 23 km upstream of the Faro bridge) following a 2004 forest fire. (d) Multiple overgrown active-layer detachment scars (indicated by arrows) on a northeast-facing slope that was burned in a 1958 forest fire (in Tintina Trench, 15 km northwest of Faro bridge). (e) Scar of large (600 m-long) active layer detachment slide on a steep, northeast-facing slope near Faro's former ski hill. (Image: Google Earth, 2004.) Note the thermokarst pond at the toe of the slide, and the town of Faro in the background. Based on air photo analysis, the slide occurred sometime between 1993 and 2004.

Retrogressive thaw slumps occur where thawing material continually flows away from a steep exposure of ice-rich permafrost. These slides gradually grow in size for years to decades as new ice-rich sediment is exposed and subsequently thaws. Retrogressive thaw slumps are especially common where river erosion exposes ice-rich glaciolacustrine sediments along cutbanks. An active retrogressive thaw slump is located at the former Faro ski hill and is described in more detail in the related case study section below. With climate change and warming, retrogressive thaw slumps could become more frequent, especially in areas where water comes in contact with exposed or buried glaciolacustrine material that contains segregated ice lenses. Examples of this are found on the south side of the Pelly River near Faro.

PERMAFROST PROCESSES

Hazards related to permafrost have the potential to impact several elements such as ground stability, hydrology, and infrastructure integrity. The following section provides a general description of permafrost structure and characteristics, in order to present a more comprehensive picture of the risks associated with permafrost thaw.

PERMAFROST DEVELOPMENT

In permafrost regions, the distribution of ice in surface sediments (cryostratigraphy) is related to the manner in which permafrost has aggraded and degraded through time. The understanding of permafrost genesis at a given site is important because permafrost structure and composition is directly related to the type of permafrost development. Permafrost genesis can be divided into four main types: epigenetic, syngenetic, quasi-syngenetic, para-syngenetic and polygenetic (French and Shur, 2010; O'Donnell et al., 2012). Epigenetic permafrost forms in bedrock or in sediments following deposition. The ice content of epigenetic permafrost usually increases with depth, and the soil layers in between ice features are usually ice-poor and over-consolidated or stiff (Stephani et al., 2010). The syngenetic growth of permafrost occurs when material is deposited at the surface while freezing is in progress. Thus, the permafrost is approximately the same age as the sediment in which it is found. The ice content of syngenetic permafrost is more likely to be uniform and ice-rich throughout the soil column. Quasi-syngenetic permafrost forms when the permafrost table shifts upward in response to vegetation growth at the surface, leading to the formation of an intermediate, ice-rich layer at depth. Para-syngenetic permafrost is defined by multidirectional refreezing of a talik zone (e.g., those areas of unfrozen ground under drained lakes). The ice content of para-syngenetic permafrost relates to the degree of saturation of the material prior to refreezing. If the permafrost has more than one origin it can be defined as polygenetic (Lunardini, 1994; French and Shur, 2010).

GEOTECHNICAL PROPERTIES

The cryostratigraphy and geotechnical properties of the ground are important characteristics as they influence permafrost dynamics and the thermal and mechanical sensitivity of frozen ground. Cryostratigraphy is defined as the study of frozen layers in the Earth's crust and is used to reconstruct the deposition history of a given site, define the type of permafrost present, determine how ice developed, and how the ice is distributed within the permafrost. It is useful to predict the rheology of surface and sub-surface terrains in the context of permafrost thaw (French and Shur, 2010). Cryostratigraphy is defined by cryofacies (e.g., ice-rich or ice-poor sediments), which are characterized by typical cryostructures.

Cryostructures are determined by the amount and distribution of ice within the pore structure, and by ice in excess of the porosity (e.g., lenses, layers of segregated ice; French and Shur, 2010). Table 2 presents typical cryostructures that may be observed in permafrost. Layered, lenticular,

and microlenticular cryostructures are present in ice-rich permafrost. They are the result of ice segregation in the sediment and are typical of fine-grained syngenetic permafrost. When permafrost thaws, the water from the melting of excess ice is drained, leading to settlement of the ground. Porous visible and porous invisible cryostructures are ice-poor and result from in-situ freezing of water trapped in the soil pores with little to no migration of water to the freezing front (cryosuction) within the freezing soil. These types of cryostructures are common in coarse-grained sediments, but can also develop in fine-grained sediments that were originally ice-rich, thawed, drained, and subsequently refrozen (Stephani et al., 2010). Because there is no excess ice present, no significant subsidence of the ground is expected upon thawing.

Table 2. Cyrostructure classification, from Stephani et al. (2014) and based on Murton and French (1994).


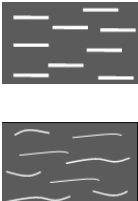


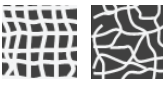




Name	Equivalent	Description	Sediment type	Illustration*
Lenticular	Lenticular ¹	<ul style="list-style-type: none"> • lens-shaped ice in sediment • generally continuously shaped • generally horizontal (parallel to freezing front) • may be straight, wavy, inclined, interlaced • may contain air bubbles • thickness: ≥1 mm: Syngenetic permafrost: mm to cm thick Epigenetic permafrost: cm to dm thick • usually ice-rich sediment	silt to fine sand; silty clay	see Fig. 3.1A 
Microlenticular	Lenticular ^{1,2}	<ul style="list-style-type: none"> • lens-shaped ice in sediment • generally discontinuously shaped • generally horizontal (parallel to freezing front) • may be straight, wavy, inclined, interlaced • very few air bubbles • thickness: <1 mm • usually ice-rich sediment: Syngenetic permafrost: >50% volume Epigenetic permafrost: 30-50% volume	silt to fine sand; peat	see Fig. 3.1A 
Layered/belt-like structure	Layered ¹	<ul style="list-style-type: none"> • assemblage of lenticular cryostructures • thickness: centimetre to decimetre • usually ice-rich sediment 	silt to fine sand; peat	see Fig. 3.1C 
Ice veins		<ul style="list-style-type: none"> • ice-filled crack or fissure in sediment • thickness variable (millimetre to centimetre) Frost crack: 1-5 mm thick Dilation/extension cracks: cm-dm thick	all types	

Table 2. Cryostructure classification, from Stephani et al. (2014) and based on Murton and French (1994), *continued*.

Name	Equivalent	Description	Sediment type	Illustration*
Reticulate	Reticulate ^{1,2}	<ul style="list-style-type: none"> • net-like cryostructure of interconnected sub-horizontal ice lenses and sub-vertical ice veins • usually ice-rich to very ice-rich sediment (~35-95% volume) 	silt to fine sand	see Fig. 3.1F 
Suspended	Suspended ¹ ; Ataxitic ²	<ul style="list-style-type: none"> • suspended aggregates in ice • usually very ice-rich sediment (up to 90-95% volume) • common in upper part of permafrost 	silt to fine sand; occasionally peat; silty clay	see Fig. 3.1E 
Crustal	Crustal ^{1,2}	<ul style="list-style-type: none"> • ice-coating around rock fragments, aggregates or wood fragments • usually partial coating, occasionally total • common just beneath permafrost table • thickness: few millimetres to centimetre thick coating 	gravel/rock fragments; diamicton	see Fig. 3.1D 
Porous visible	Ice cement ¹ ; Massive ²	<ul style="list-style-type: none"> • pore ice that is visible to the unaided eye • usually ice-poor sediment (<30% volume) 	gravel/rock fragments; diamicton	see Fig. 3.1F 
Porous invisible	Ice cement ¹ ; Massive ²	<ul style="list-style-type: none"> • pore ice not visible to the unaided eye • usually very ice-poor sediment (<10-30% volume) 	all types	see Fig. 3.1F 

*Illustrations modified from Murton and French, 1994

¹ Murton and French (1994); ² Kudryavtsev (1979)

Legend: grey = sediment; dark grey = aggregate or wood fragments; white = ice.

Generally, dry or unsaturated frozen sediments do not present a high risk upon thawing, as the water will remain in the soil porosity, or will drain away. In contrast, when saturated sediments thaw, it presents a much higher risk of settlement, mass movement, or ponding in response to poor drainage. Hazards related to the thawing of ice-rich deposits is affected by factors such as stratigraphy and the grain size distribution of the stratigraphic layers, as well as external factors such as slope, surface roughness, and vegetation.

For thaw-settlement hazard assessments, cryostratigraphy is used to locate ice-rich and ice-poor layers, and determine the geometry and distribution of massive ice (e.g., patterns of ice wedges). Generally speaking, the presence of ice-rich deposits raises concern in terms of hazard potential. Where ice-rich deposits overlie ice-poor layers, the thaw-settlement hazard is high in the short term, and the rate of change is fast. Conversely, where ice-poor deposits overlie ice-rich sediment, the thawing of the upper layer is rapid but with minimal thaw settlement and will be followed by the slow, but constant thawing of the underlying ice-rich layer resulting in differential thaw settlement.

The grain-size distribution of sediments determines the porosity and hydraulic conductivity of the ground. Coarse material (medium sand and coarser) has a high hydraulic conductivity and readily drains as ice melts, whereas fine-grained material drains poorly once it thaws due to its low hydraulic conductivity. Furthermore, fine-grained sediments often contain excess ice (i.e., the volume of ice in excess of the total pore volume of the ground when unfrozen) and may form ice lenses or layers by ice segregation. On flat terrain, ground with excess ice will undergo severe thaw settlement; likewise, on slopes, silt and clay deposits may experience mass movement when the pore water pressure created by melting ice is high. For slope deposits, the plastic and liquid limits of the material are used to evaluate the potential of ground failure.

PERMAFROST AS A HAZARD RISK

The ground thermal regime of permafrost is influenced by climate, surface conditions, and the complex interactions of geophysical factors such as hydrography, topography, vegetation, soil texture and ground-ice content (Jorgensen and Osterkamp, 2005). As a result, variations in climate or terrain conditions (e.g., environmental changes or human interventions) can both have a great impact on permafrost stability. Higher surface temperatures, variation in snow cover depth, active-layer hydrology variations, infrastructure, and fire disturbances are good examples of changes that can play, at various scales, a major role in permafrost degradation (Stephani et al., 2014). Additionally, since it is closely linked to local factors, permafrost response to environmental change can be spatially and temporally heterogeneous and can respond differently to geomorphological processes due to different terrain conditions. Therefore, permafrost landscapes will have a dynamic response to environmental change and must be considered holistically, at diverse spatio-temporal scales.

Because permafrost stability is essentially maintained by the bonding between ice and the ground particles, when ice melts, cohesion is lost and soil stability is diminished (French, 2007). Following an increase in air temperature, the active layer is expected to deepen as the ice contained in the upper part of the permafrost (right below the bottom of the active layer) melts. If the volumetric water content of the ground is lower than the volume of soil pores, the ground is not saturated. Thawing of this type of ice-poor soil results in moderate surface settlement and is essentially due to the loss of volume upon ground ice melting and subsequent soil consolidation. If the volumetric water content of the ground is equal to, or slightly above the volume of soil pores when unfrozen, the soil is saturated. Thawing of this type of ice-rich soil results in poorly drained surface conditions, and the soil will be unable to consolidate due to the high pore water pressure. If the volumetric water content of the ground is higher than the volume of soil pores, the ground is super-saturated and contains excess ice in its frozen state. Thawing of this type of ground results in severe surface settlement, and is essentially due to the loss of volume upon ground ice melting and soil drainage (Nelson et al., 2002). In gently sloping areas, water ponding is frequent; on steep slopes, the release of water builds excess pore water pressure in the soil pores, which is conducive to rapid mass movements (e.g., slides, slumps and debris flows). When the material is coarse-grained, soil water is drained according to the hydraulic conductivity of the material and there is minimal settling or movement of the sediment. When the material is fine-grained, the drainage is slow and pore water pressure may trigger slow mass movement (e.g., solifluction). Depending on the nature of the soil material and the amount of ground ice present, significant hazards may develop. Permafrost-related hazards represent some of the principal challenges for planning and development in northern environments.

Thermokarst collapse features, generally occupied by small ponds or lakes, occur in scattered locations around the map area, particularly within the glaciolacustrine terraces on the south side of the Pelly River, and on both sides of the Faro mine access road, just south of the former ski

hill (Figure 19a,b). Thermokarst depressions result from the thaw of ground ice and subsequent settlement of the ground surface. Ice-rich lacustrine sediments are most susceptible to thermokarst collapse following some kind of surface disturbance that exposes ground ice. Thermokarst depressions may grow in size for decades until the supply of ground ice is exhausted.

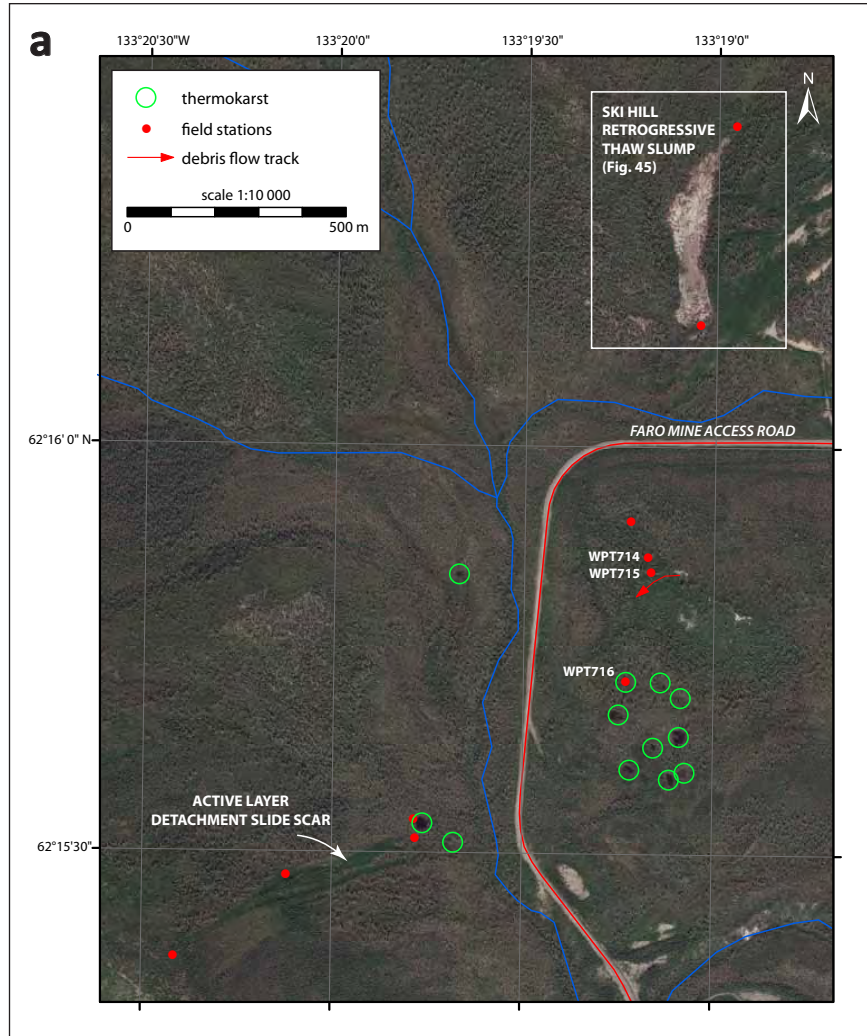


Figure 19. (a) Map illustrating thermokarst and landslide locations in the vicinity of the former Faro ski hill. GeoEye (2009/07/05) satellite image displayed in background. **(b)** Typical thermokarst collapse feature with pond surrounded by a low circular rim (station WPT716 on (a)).

Sheetwash or slope wash occurs where surface water flows in sheets along a shallow, impermeable permafrost table. It is recognized by a very distinctive surface pattern, where subtle vegetation differences give the land surface a strong, flowing appearance when viewed from the air (Figure 20). The process is most common on gentle to moderate north-facing slopes and contributes to the gradual downhill transport of fine-grained sediment to valley bottoms.



Figure 20. Typical surface expression indicating the presence of sheetwash on a north-facing slope underlain by permafrost.

Where the active layer is thin, surface soils are commonly saturated because the permafrost table is impermeable. Slopes with thin active layers are susceptible to creep through the processes of solifluction (i.e., gradual downhill flow of saturated soil) and frost creep (i.e., development of needle ice and subsequent heaving of freezing ground). The combined effects of sheetwash, solifluction and frost creep may produce subdued topography and generate ongoing sedimentation at the base of affected slopes.

SEISMICITY

Seismic hazards in the Faro region are relatively low (Figure 21), although minor earthquakes do occasionally occur. Fifty-one earthquakes have been recorded within 50 km of Faro since 1977 (Natural Resources Canada, 2010). Of these, the largest was magnitude 4.6, and the remaining earthquakes were all below magnitude 4. While the town is situated close to Tintina fault, which is a major structural feature, the fault has not been active since the early Tertiary, over 50 million years ago (Tempelman-Kluit, 1980).

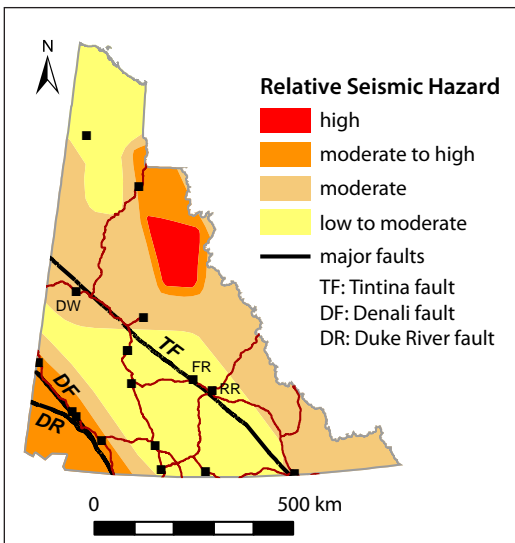


Figure 21. Simplified version of the National Building Code of Canada's 2010 seismic hazard map (for spectral acceleration at a 0.2 second period (5 cycles per second)), illustrating the relative likelihood of experiencing earthquakes strong enough to potentially damage some, but not all, single family (one and two-storey) dwellings (Natural Resources Canada, 2010). Faro (FR) is located in the low to moderate hazard zone, where there is a 1-5% chance that significant damage will occur every 50 years. DW = Dawson; RR = Ross River.

ASSESSING CURRENT HAZARD RISKS FOR THE FARO REGION

CASE STUDY SITES

To assess the risk of the hazards described above for the Faro region, the research team focused on several case study sites. Findings from case study sites were then used to assess risk on a regional scale.

The case study sites for Faro were determined in consultation with the community – they reflect areas where there are hazards-related concerns, or where future development may take place. Case study sites were also chosen to cover a variety of landscape types. Case study sites are: 1) the Tintina Subdivision; 2) a future Country Residential Subdivision; 3) the area around the sewage lagoon; 4) the Douglas Drive/Yates Crescent area; 5) Del Van Gorder School and baseball diamond; and 6) the slope failure near the Faro ski hill. The locations of case study sites are shown in Figure 22. At each site, researchers used geophysical approaches (ERT and GPR), permafrost borehole and soil pit observations, and examined exposed surficial material where possible. Results from each case study site are described below.

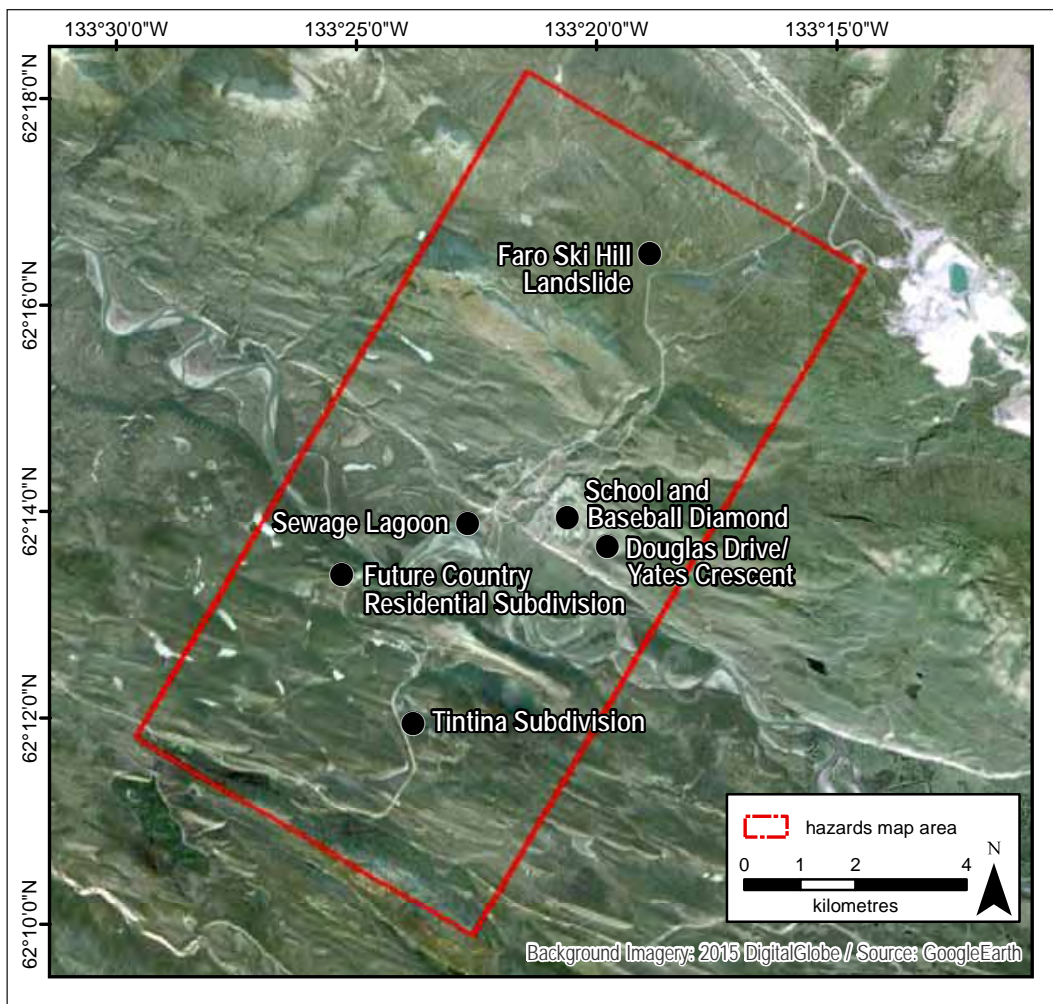


Figure 22. Map illustrating locations of all case study sites for the Faro project area.

TINTINA SUBDIVISION

Tintina Subdivision is located on the southwestern side of the Tintina Trench on a blanket of consolidated basal till. While till is variable in thickness in the surrounding undulating, streamlined terrain, it was observed to be 52 m thick above bedrock in a nearby water well (Environment Yukon, 1990). A two metre-high road cut (station 13DT048) exposed 10-15 cm of White River ash overlying till. This till unit is characterized as a dark grey diamict with 80-85% sandy silt matrix and 15-20% pebble to boulder-sized subangular clasts. The slopes to the north and east of the subdivision are subject to sheetwash processes and impede drainage.

Permafrost boreholes were drilled in the Tintina Subdivision in two locations to examine permafrost characteristics (Figure 23). The first study site is located on top of glacial, streamlined deposits. This particular flute-type landform has an area of about 0.45 km² with an east-west orientation. Soil pit *FARO_PIT02* is located at 235 m along the ERT profile *FARO_ERT05*, in black spruce forest 30 m from the road. The area is vegetated with a thick organic cover (15 cm) composed mainly of moss and sphagnum and scattered shrubs (*Salix* sp., *Vaccinium oxycoccos*). The surface layer is composed of tephra mixed with organic matter (22 cm thick), covering a layer of silty sand with gravel extending from a depth of 22 cm to the bottom of the borehole (at 110 cm). The water table was encountered at a depth of 95 cm. No permafrost was encountered. A stratigraphic cut (*FARO_CUT01*), located approximately 370 m west of soil pit *FARO_PIT02*, exposed a thick diamict deposit composed of coarse sand, gravel and subrounded to subangular cobbles from a depth of 30 cm to 250 cm.

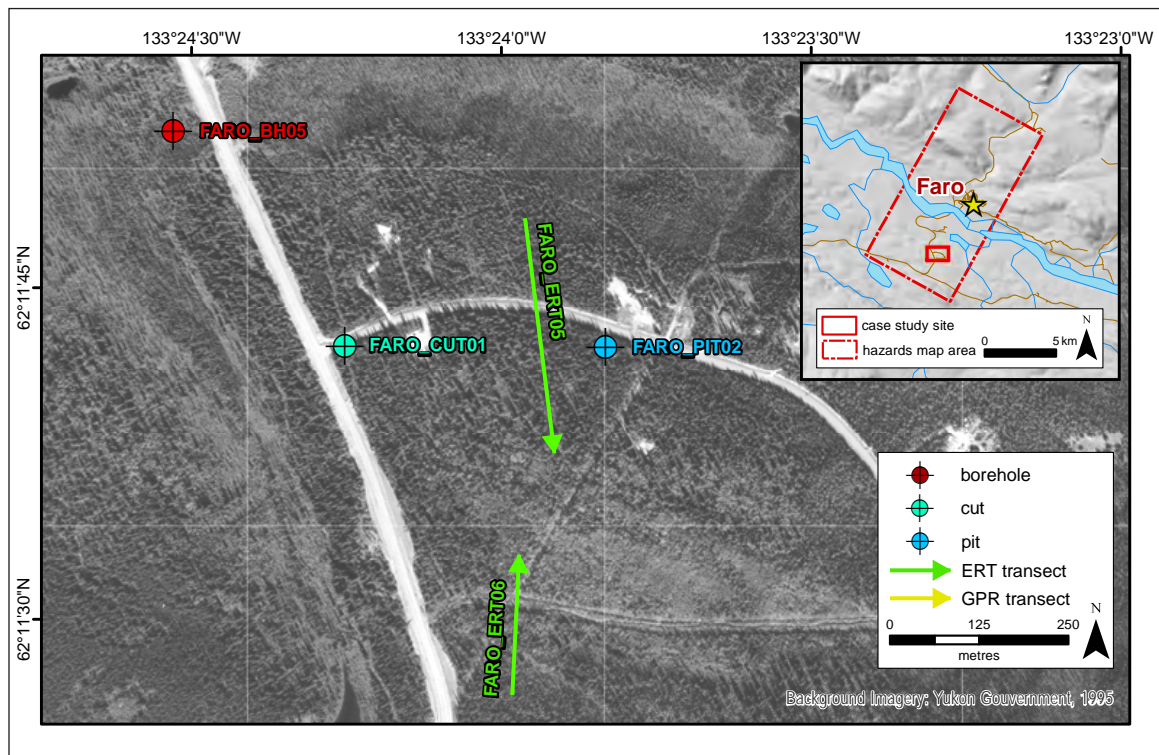


Figure 23. Map illustrating locations of detailed site investigations for the Tintina Subdivision. Refer to Figure 22 for all other case study locations within the study area boundary.

Borehole *FARO_BH05* was drilled between two profiled glacial landforms in an open forest of black spruce (about 7 m high) with scattered shrubs (*Salix* sp., *Rhododendron groenlandicum*) and a thick moss cover (40 cm; see Figure 23). The ground was saturated near the surface due to its location at the bottom of a depression. The frozen permafrost cores collected from the borehole were consistent throughout and made up of undecomposed peat (from a depth of 40 cm to 245 cm). The samples had a porous visible ice cryostructure and very high excess ice volume content (40%). The thaw settlement and consolidation test results were also high, having 24% total settlement under a stress load of 25 kPa, and 49% total settlement under a stress load of 150 kPa. At the bottom of the borehole, a small section of core composed of diamicton with silt (28%), sand (41%) and angular gravel (31%) was recovered (245-265 cm). This section of core had significantly lower excess ice content (8%) and a porous invisible cryostructure. The complete borehole log is shown in Appendix B, and grain size analysis and ice content results are shown in Appendix C.

Two ERT surveys were performed in the Tintina subdivision in late September 2013. The first (*FARO_ERT06*) is 200 m long, and was run from south to north, beginning in an area with open-forest cover and ending in a disturbed area reserved for future development. As is illustrated in Figure 24, the first 50 m of the profile (on a gentle, north-facing slope) is believed to be underlain by permafrost to a depth of up to 10 m. Using a threshold value of 400 ohm m as the boundary between unfrozen and frozen sediment, the remainder of the ERT profile is inferred to be permafrost free. If a slightly lower threshold is used, patches of degrading permafrost may exist, but this is viewed as improbable because similar values are associated with the location of the road and ditch which are very unlikely to be underlain by permafrost. Physical resistance was encountered when probing in the first part of the profile and was interpreted in some locations as the top of the frost table. However, the presence of clasts in the soil, and/or very stiff soils, renders these observations unreliable. The interpretation of the profile as being largely permafrost-free is also supported by the absence of permafrost in a soil pit excavated in the vicinity (*FARO_PIT02*). The 1958 forest fire which impacted this site may have affected permafrost distribution.

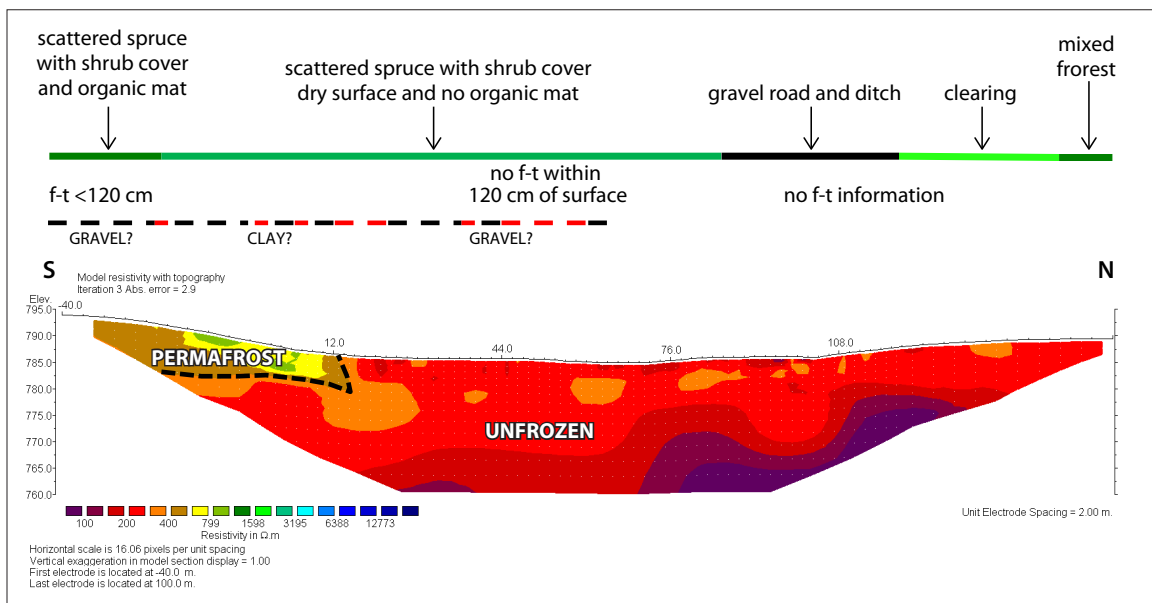


Figure 24. ERT profile *FARO_ERT06*, which is 200 m long (see Figure 23 for location). The profile has a maximum penetration depth of about 30 m. A likely area of permafrost is outlined by a black dashed line; f-t = frost table.

The second profile (*FARO_ERT05*) was located about 100 m to the north of the first and was also run along a gentle north-facing slope. The electrode spacing and length (400 m) permits imaging to a depth of more than 60 m (Figure 25). The majority of the profile area was covered by open spruce forest with the exception of a cleared area in the centre, where the survey crosses a subdivision road. Resistivities are generally low, as at the *FARO_ERT06* profile, with higher values in the northernmost segment. Frost tables less than 120 cm deep were measured from 0-70 m along the profile but measurements became unreliable after that point due to presence of clasts in the soil. Frost table measurements were impossible to obtain in the vicinity of the road; however, just south of the road, where measurements were possible, no frost table was encountered within 120 cm of the surface. The first part of the profile is interpreted as a patch of permafrost that is 5-10 m thick, whereas the remainder is believed to be permafrost free. Both the *FARO_ERT05* and *FARO_ERT06* profiles suggest that permafrost is absent in most of the area but that a few isolated patches exist on north-facing slopes.

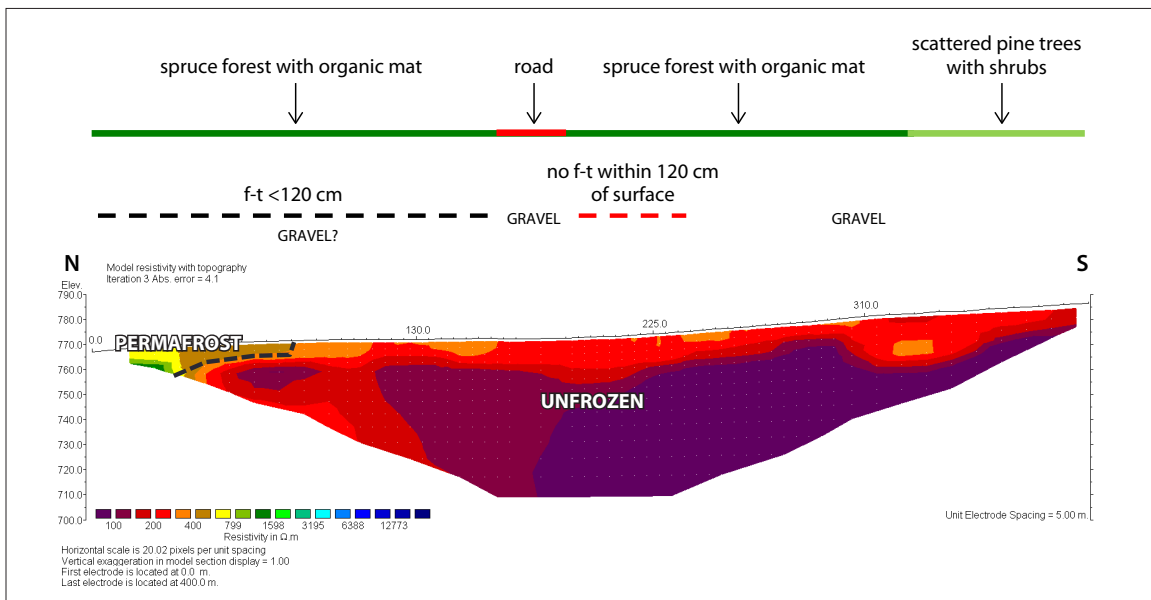


Figure 25. ERT profile *FARO_ERT05*, which is 400 m long (see Figure 23 for location). The profile has a maximum penetration depth of about 60 m. A likely area of permafrost is outlined by a black dashed line; *f-t* = frost table.

FUTURE COUNTRY RESIDENTIAL SUBDIVISION

A gravel pit currently exists at the site of this potential future country residential subdivision (station 13DT050). At this location, hummocky glaciofluvial gravel with discontinuous layers of thin (<15 cm thick) light brown till overlies striated and grooved hummocky bedrock (see Figure 16b, p. 25). The gravel is supported by a coarse-grained sand matrix with no observed structures; the well-rounded clasts are pebble-sized on average, but also include cobbles and boulders. Revegetated landslide scars and debris flow gullies are present a few hundred metres north of this site, on a glaciolacustrine escarpment on the left bank (facing downstream) of the Pelly River. Thermokarst collapse ponds are also present in the low-lying ground immediately southwest of the gravel pit, less than 1 km away.

To investigate permafrost characteristics at this site, borehole *FARO_BH01* was drilled near the toe of a steep slope at the bottom of a forested depression, northwest of an abandoned gravel pit (Figure 26). The borehole is located 120 m along the ERT profile *FARO_ERT01* in an open black spruce forest. The black spruce at this site had an average height of 6 m and the ground was moist and covered by a layer of moss and lichen (5-10 cm thick). The borehole was drilled to a depth of 268 cm, and the permafrost table was encountered at a depth of 35 cm, immediately beneath a thick organic cover. The active layer consisted of undecomposed fibric peat (0-15 cm), slightly decomposed humus (15-25 cm), and a tephra layer 10 cm thick. The collected frozen permafrost cores were homogeneous and composed of marbled (brown and black), frozen peat and layers of slightly decomposed wood and roots. The samples collected had a porous visible ice cryostructure because of the peat’s intrinsic porosity and its capacity to absorb large quantities of water. The excess ice content values varied depending on depth. Near the surface (70-132 cm), the samples had an average excess ice content of 12%, whereas at greater depths, the values varied from 53% to 64%. Because of these high values, results from thaw-settlement and consolidation tests were also very high, having 35% total settlement under a stress load of 25 kPa, and 59% total settlement under a stress load of 150 kPa. The complete borehole log is shown in Appendix B. Grain size analysis and ice content results are shown in Appendix C.

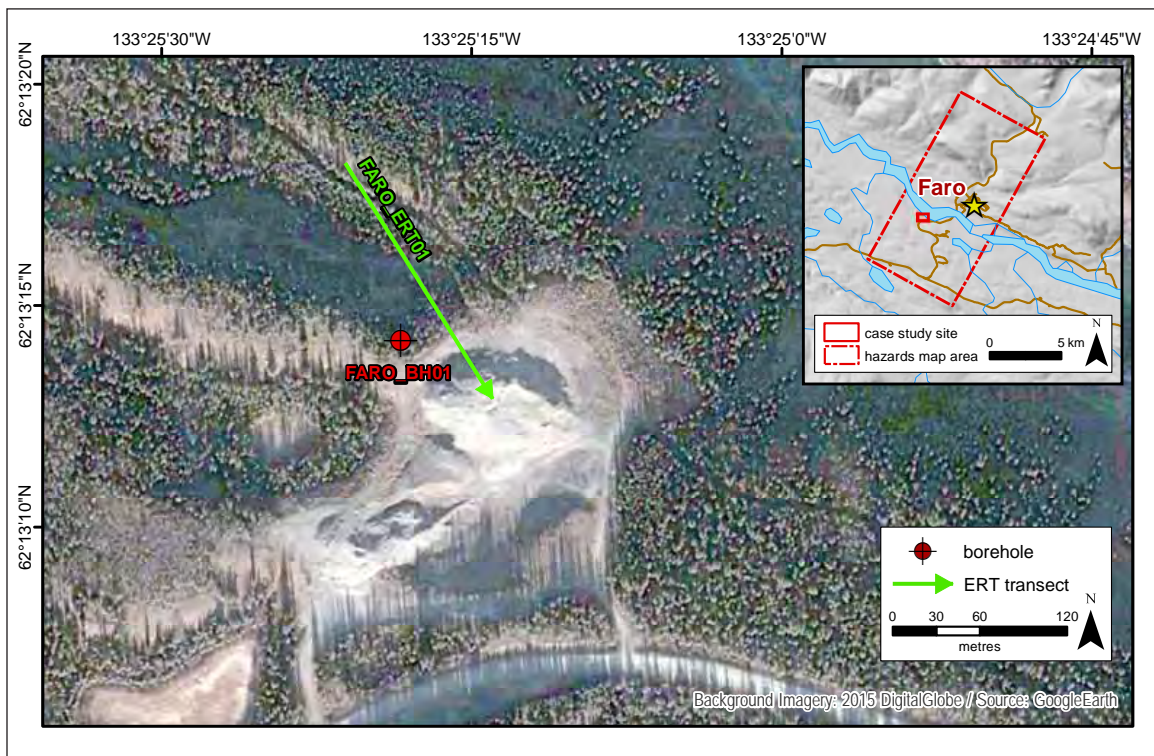


Figure 26. Map illustrating locations of detailed site investigations for the area of the future country residential subdivision. Refer to Figure 22 for all other case study locations within the study area boundary.

Additional ground truthing was done by digging a shallow (~10 cm deep) pit on top of a ridge approximately 130 m northeast of *FARO_BH01*. (Because this pit was so shallow, a log of the pit was not completed, and it is not included on Figure 26.) The pit exposed a thin forest litter (3 cm) on top of a mixed deposit of sub-rounded gravel and silty sand (3-10 cm). The surrounding open forest was composed of black spruce (4-5 m high) and short poplars (2 m). The ground

was significantly drier than the forested depression at the location of borehole *FARO_BH01*. No permafrost was reached.

The 160 m ERT profile at the site (*FARO_ERT01*) was run northeast to southwest from undisturbed forest across a partially vegetated gravel ridge and a gravel pit (Figure 27). The terrain and the permafrost are relatively complex based on the ERT profile and there is some uncertainty in the interpretation of the geophysical measurements because of a lack of ground truthing in the second half of the profile. Permafrost is clearly present in the northern segment of the profile, extending at least to the base of the section at a depth of 15-20 m. In this area, frost tables with an average depth of 62 cm (n=18) were measured. Borehole *FARO_BH01* also revealed ice-rich permafrost in this area. Further along the profile, resistivity values were high (up to 3000 ohm m) and assumed to represent frozen ground conditions. No frost tables could be probed in this area due to the presence of surface gravel. The higher resistivities in these sections of the profile are believed to be due to the presence of dry gravel or bedrock, whereas those areas with lower resistivities (such as near surface at 94 m along the profile) are due to wetter surface deposits. An alternative explanation is that the coarse-grained soils are in fact frozen, but if this is the case, they would be expected to have a low ice content.

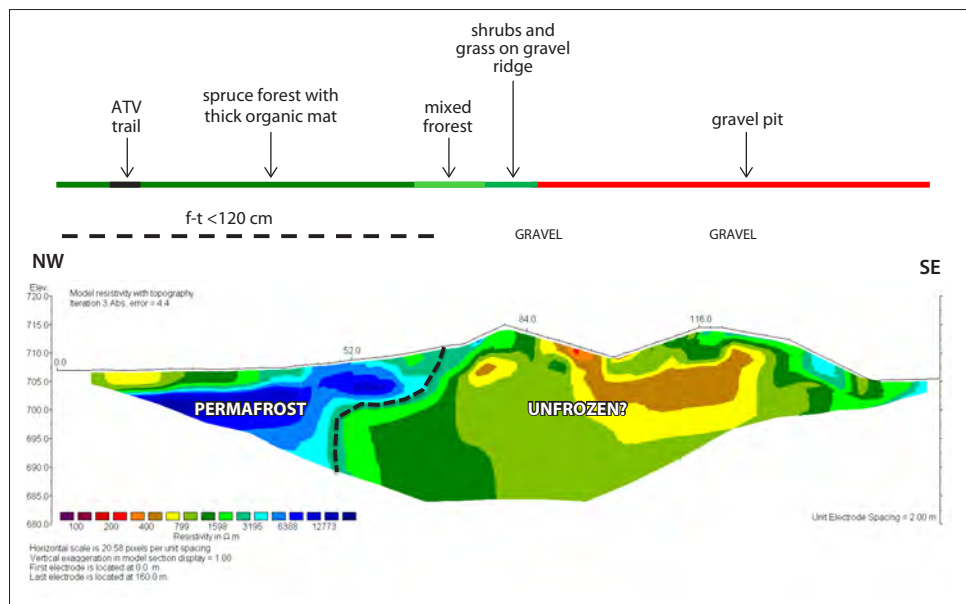


Figure 27. ERT profile *FARO_ERT01*, which is 160 m long and runs northwest to southeast from an undisturbed forest to a gravel pit (see Figure 26 for location). The profile has a maximum penetration depth of about 25 m. A likely area of permafrost is outlined by a black dashed line; *f-t* = frost table.

SEWAGE LAGOON

Faro's sewage lagoon (Figure 28) is situated on an abandoned section of the Pelly River floodplain which is only a few metres above the present-day level of the main river channel. The site is bounded to the north by a steep, gullied escarpment approximately 50 m high that exposes a thick sequence of glaciolacustrine sediments. The lowermost 10 m of these sediments are exposed in a pit on the northeast side of the sewage lagoon (station 14PL044). The deposits consist of thick-bedded silt and fine-grained sand, with occasional thin beds of clay and coarse-grained sand (see Figure 15a, p. 24).



Figure 28. Aerial view of Faro's sewage lagoon, looking to the north. Pelly River flows from right to left in the foreground.

To characterize permafrost in this area, a test pit was dug and a borehole was drilled, and four geophysical surveys were run (Figure 29). The pit (*FARO_PIT01*) is located about 60 m south of a colluvium cliff, west of the settling ponds of the sewage lagoon, and about 380 m from the Pelly River (100 m along ERT transect *FARO_ERT03*). Vegetation at the site consisted of a black spruce forest (up to 15 m high), shrubs (*Salix sp.*, *Rhododendron groenlandicum*) ranging from 30 cm to 200 cm high, and a thick moss cover (30 cm). Probing was completed to a depth of 407 cm and no permafrost was encountered; the water table was reached at 66 cm. Here, the soil stratigraphy is composed of black, silty and decomposed organic humus layers (29-66 cm) interlaced with a tephra layer (42-57 cm). A clayey silt deposit (66-180 cm) covers a grey silt unit and a thick layer of fine sand (351-407 cm) with iron oxide staining (351-360 cm).

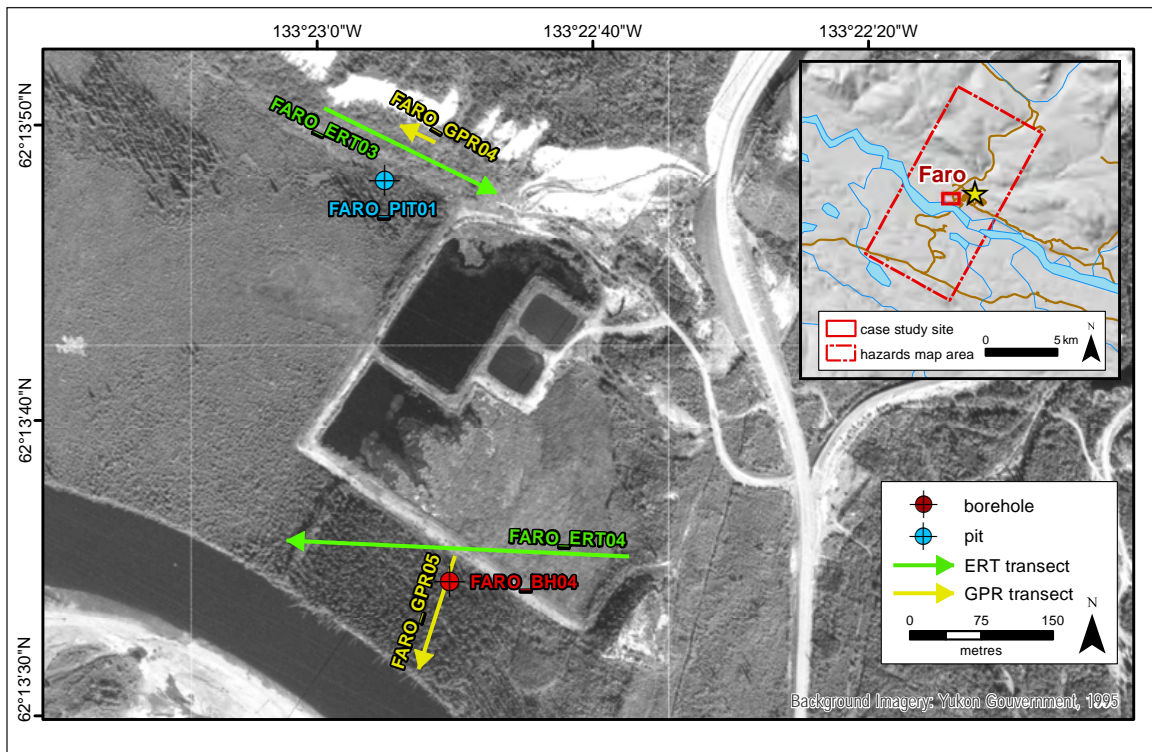


Figure 29. Map illustrating locations of detailed site investigations for the sewage lagoon area. Refer to Figure 22 for all other case study locations within the study area boundary.

The first ERT profile (*FARO_ERT03*), located in the northwest part of the sewage lagoon area, traverses 160 m from forest into a drained part of the lagoon area. The resistivities are uniformly low, and maximum values are all less than 300 ohm m (Figure 30). No confirmed frost tables were encountered, although the probe did reach resistance in a number of locations where gravel or stiff clay was present. At the end of the transect, the full probe length was able to penetrate the soil, and no frost was encountered. Given the uniform low-resistivity results and the absence of permafrost in the borehole at 100 m along the profile, it is concluded that permafrost is absent both beneath the forest and the sewage lagoon itself.

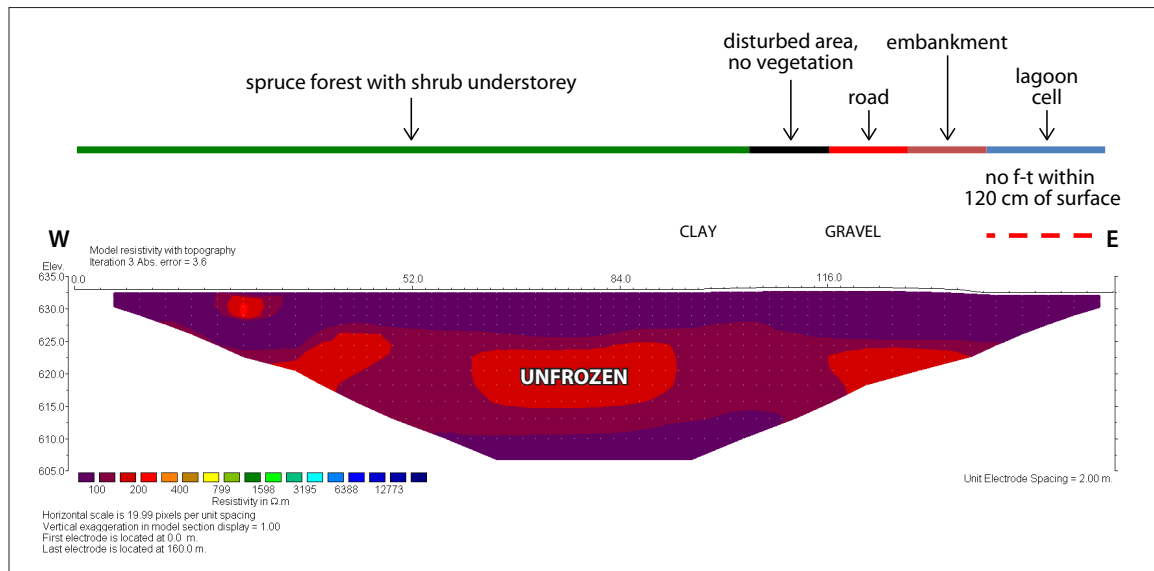


Figure 30. ERT profile *FARO_ERT03*, which is 160 m long and runs west to east towards the northwest corner of the sewage lagoon (see Figure 29 for location). The profile has a maximum penetration depth of about 25 m; f-t = frost table.

The second borehole, *FARO_BH04*, is located between the sewage lagoon and the Pelly River. The vegetation at this site was composed of black spruce (3-20 m high), shrubs (*Salix* sp., *Rhododendron groenlandicum*), and a thick moss cover (35 cm). The permafrost table was encountered at 45 cm, below a tephra layer (35-41 cm) and a sandy, organic silt layer (41-46 cm). At the top of the permafrost table, where the material is finer and composed mainly of well-decomposed, sandy, organic silt (46-50 cm) marbled with iron oxide (50-122 cm), the cryostratigraphic profile revealed both microlenticular and lenticular cryostructures. Excess ice content decreased from 34% to 15% by volume below 148 cm in coarser, sandy deposits. Samples extracted from the borehole below 214 cm were frozen but not consolidated, likely due to the coarse gravel found at the bottom of the borehole (at 240 cm). The complete borehole log is shown in Appendix B. Grain size analysis and ice content results are shown in Appendix C.

Two GPR surveys (*FARO_GPR04* and *FARO_GPR05*) were also carried out in this area. For *FARO_GPR04* the signal reached a depth of ~3.6 m, and exhibited a strong reflective horizon at a depth of ~1.5 m (Figure 31). This is approximately the same depth as the grey silt and blue clay unit identified in *FARO_BH04*, drilled in the spruce forest south of the GPR transect (see Figure 29). GPR transect *FARO_GPR05* (Figure 32) was run for 56 m starting near a trail, and ending near the Pelly River. The depth of signal penetration was ~6 m. An irregular layer was noted near surface at a depth of 0.5-1 m. According to borehole *FARO_BH04*, this contact corresponds to the permafrost

table. A second, mostly regular layer was documented at a depth of ~ 2 m, corresponding to a gravel layer. Finally, a weaker signal was identified at ~ 4 m, although this is likely an echo and not a real subsurface horizon.

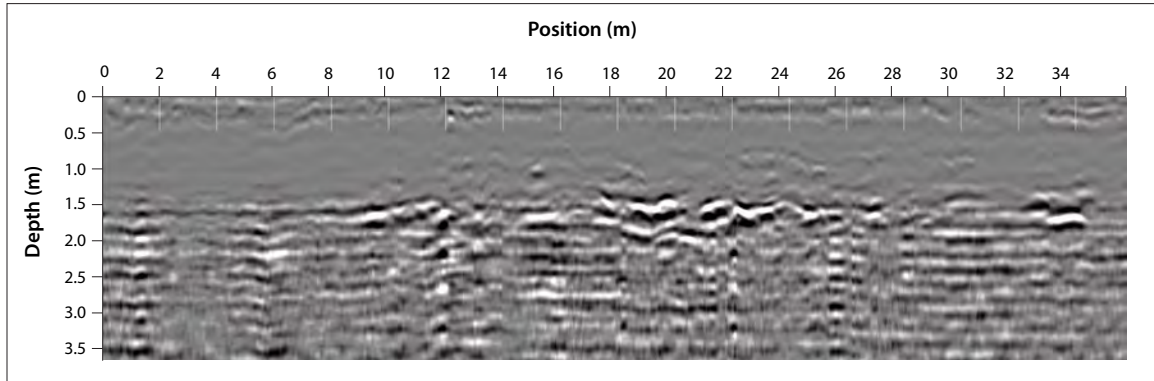


Figure 31. GPR profile FARO_GPR04, near the Faro sewage lagoon, illustrating a strong horizontal reflection at ~ 1.5 m, likely corresponding to a silt/clay layer that was identified in a nearby borehole.

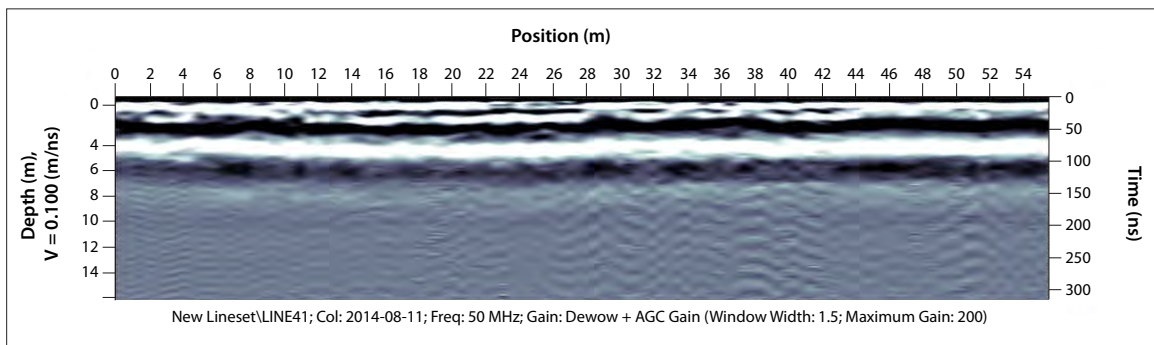


Figure 32. GPR profile FARO_GPR05, which runs from the south end of the Faro sewage lagoon towards the river, showing an irregular layer at a depth of 0.5-1 m, which likely corresponds to the top of the permafrost table.

A 400 m-long ERT profile (FARO_ERT04) was run from east to west, traversing the southeastern portion of the sewage lagoon area, across a section of undisturbed forest, and ending close to the bank of the Pelly River (Figure 33; see also Fig. 29). Surface conditions varied from disturbed sections of terrain at the start of the transect, to undisturbed forest at the end of the transect close to the river. Frost tables were measurable beneath the undisturbed spruce forest and the mixed forest at the end of the profile, both segments averaging a depth of 53 cm (n=12 and n=9, respectively). Elsewhere, frost tables were not detected within 120 cm of the surface, or probing was prevented by the presence of gravel or fine, cohesive deposits.

The inferred permafrost pattern is complex at this site. At the eastern end of the profile, which includes a portion of an unused sewage lagoon cell, the upper 10 m of soil appears unfrozen (i.e., a supra-permafrost talik is present) but there appears to be permafrost underlying the bottom of the profile (>60 m). It is possible, however, that this is bedrock rather than permafrost. In the central part of the profile, permafrost is present beneath the undisturbed spruce forest to a depth of 10-15 m, but there appears to be an intra-permafrost talik that partially extends under this part of the landscape that is connected to the talik beneath the sewage lagoon cell. The permafrost in

the top 10 m of the profile has much higher apparent resistivities than the permafrost beneath it, and is likely due to colder temperatures or higher ice contents, as indicated by the results from the nearby borehole (see above discussion on *FARO_BH04*). A climate station that measured air and ground temperatures was located in the spruce forest from 2006 to 2008 and recorded a mean temperature of -1.3°C at the top of permafrost (A. Lewkowicz, unpublished field data); this temperature value corresponds well with the observed thickness of permafrost (>60 m) in parts of this section of the profile. Finally, relatively thin (>10 m thick) permafrost is present beneath mixed forest at the western end of the profile. This area appears to undergo seasonal flooding as shown by surface deposits of fines. Furthermore, the permafrost in this part of the profile has lower resistivities, probably because it is warmer than that in the centre of the ERT profile.

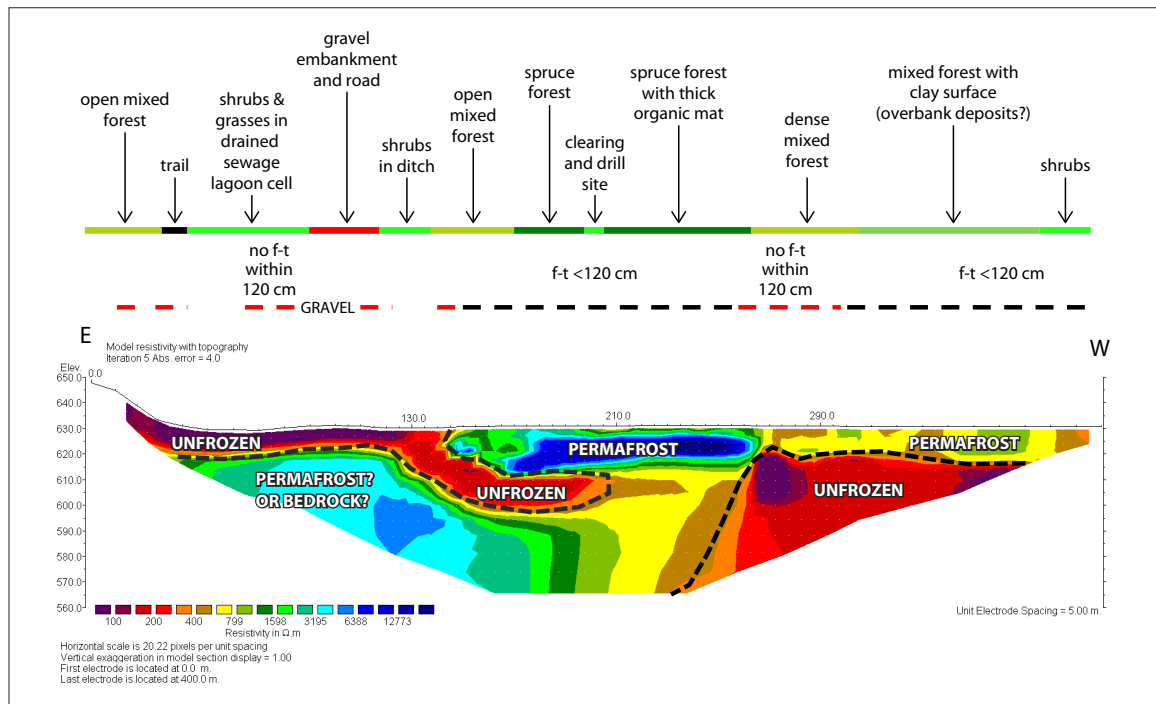


Figure 33. ERT profile *FARO_ERT04*, which is 400 m long and runs east to west along the bottom of the lagoons towards the Pelly River (see Figure 29 for location). The profile has a maximum penetration depth of about 60 m. Black dashed lines delineate areas where there is likely to be permafrost; *f-t* = frost table.

Thaw beneath the zone cleared for the sewage lagoon appears to have progressed to a depth of 10 m or more, and a talik is believed to extend beneath the permafrost to the south and towards the river; however, further drilling or additional ERT surveys would be needed to confirm this interpretation. At the southwest end of the profile, permafrost appears to be present directly beneath the active layer but is much thinner and warmer, presumably because of the regular flooding of the ground surface during spring melt.

DOUGLAS DRIVE/YATES CRESCENT

Douglas Drive and Yates Crescent are located on a low knob of till that is bounded by former meltwater channels to the north and south. Discontinuous patches of glaciofluvial sand and gravel are also present at the surface.

A shallow (50 cm) pit immediately south of the neighbourhood playground (station 14PL055) exposed 12 cm of White River ash overlying 8 cm of loess, on top of 30 cm of moderately dense

till. The till comprises 40% subangular to subrounded clasts (primarily pebble-sized) in a matrix (60%) of silty, fine-grained sand. A road cut just north of Yates Crescent (station 13DT021) exposed 15 cm of White River ash overlying 1.1 m of consolidated till characterized as a light grey diamict with 25% subangular clasts in a matrix of sandy silt (75%). A discontinuous veneer of reddish-brown, silty, fine-grained sand (loess) up to 25 cm thick is between the deposits of till and White River ash in nearby areas. Unpublished logs from geotechnical boreholes drilled on the north side of the subdivision indicate that till is between 2 and 6 m thick in the area, and bedrock is documented at depths between 2.1 m and 9.9 m (pers. comm., R. Trimble, Tetra Tech EBA).

Permafrost occurs close to the surface within fine-grained sediments in the nearby low-lying meltwater channels due to thick accumulations of surface organic material and peat. Active layer thicknesses of 70 and 90 cm were measured at stations 14PL054 and 14PL052, respectively. Long-term permafrost temperatures are being monitored by Yukon Geological Survey at station 14PL052 (Lipovsky and Yoshikawa, 2009), where mean annual ground temperatures at 1 m, 3 m and 3.9 m depths were -0.6°C for the 2008-2013 period (Lipovsky, 2015).

To characterize permafrost at this site, borehole *FARO_BH02* was drilled on the southern side of Douglas Drive on a site with slightly inclined terrain (Figure 34). This site is located 110 m along the ERT profile *FARO_ERT02* in an open black spruce (up to 10 m high) and poplar (average height of 10 m) forest. The ground was covered by shrubs (*Salix* sp., *Rhododendron groenlandicum*) ranging from 10-80 cm high and a litter composed mainly of leaves, branches and moss (6 cm thick). The active layer is composed of a fibric humus unit (0-5 cm) and grey silty sand (5-11 cm), overlying layers of silty, black, and decomposed organic matter (37-65 cm); the latter including a layer of undecomposed organic matter (at 11-37 cm), and tephra (at 44-55 cm). The permafrost table was encountered at a depth of 65 cm. The permafrost is mainly composed of layers of black, silty, decomposed peat (10-30 cm thick) overlying thin, grey, sandy silt layers (about 5 cm thick). The bottom of the core contains coarser fractions with 87% sand and 10% gravel. The borehole was drilled to a depth of 135 cm, at which point pebbles (10 cm in diameter) prevented further drilling. The finer deposits have a porous-invisible cryostructure with an excess ice content of 40%. At 115 cm, thaw settlement and consolidation test results revealed 23% total settlement under a stress load of 150 kPa. The complete borehole log is shown in Appendix B. Grain size analysis and ice content results are shown in Appendix C.

Additional drilling was done approximately 90 m from *FARO_BH02* on the northern side of Douglas Drive. Borehole *FARO_BH03* is located in an open poplar forest (average height of 8 m) with little to no litter on the ground. This site was entirely disturbed when the subdivision was built in the 1980s. The ground at this site was significantly drier and composed of sand and sub-angular gravel. No permafrost was reached at the maximum depth of the borehole (135 cm), and drilling was ceased due to large rocks at the bottom of the borehole.

Three GPR profiles were carried out at this site (see Figure 34). Along *FARO_GPR03*, which was carried out along a gravel road, there is a strong horizontal reflection at a depth of ~1.6 m, which may represent the contact between the base of the active layer and the top of permafrost (Figure 35). This is deeper than the top of permafrost in borehole *FARO_BH02*, which was documented at a depth of 65 cm. The discrepancy in the depth to permafrost in the GPR profile compared with the Yates Crescent borehole may be related to the differences in site locations; this GPR profile was carried out on a disturbed site where there was removal of vegetation, whereas borehole *FARO_BH02* is situated at a less disturbed site with insulating, vegetative cover (see Figure 34).

At GPR transects *FARO_GPR02* and *FARO_GPR01* (Figures 36 and 37, respectively), the GPR signal reached a depth of ~3.6 m and results exhibit a moderately dipping bed that may correspond to the silty sand layers identified in the Yates Crescent borehole *FARO_BH02*. GPR transects *FARO_*

GPR01 and _GPR02 were carried out approximately 100 m and 150 m, respectively, northwest of borehole FARO_BH02 (see Figure 34).

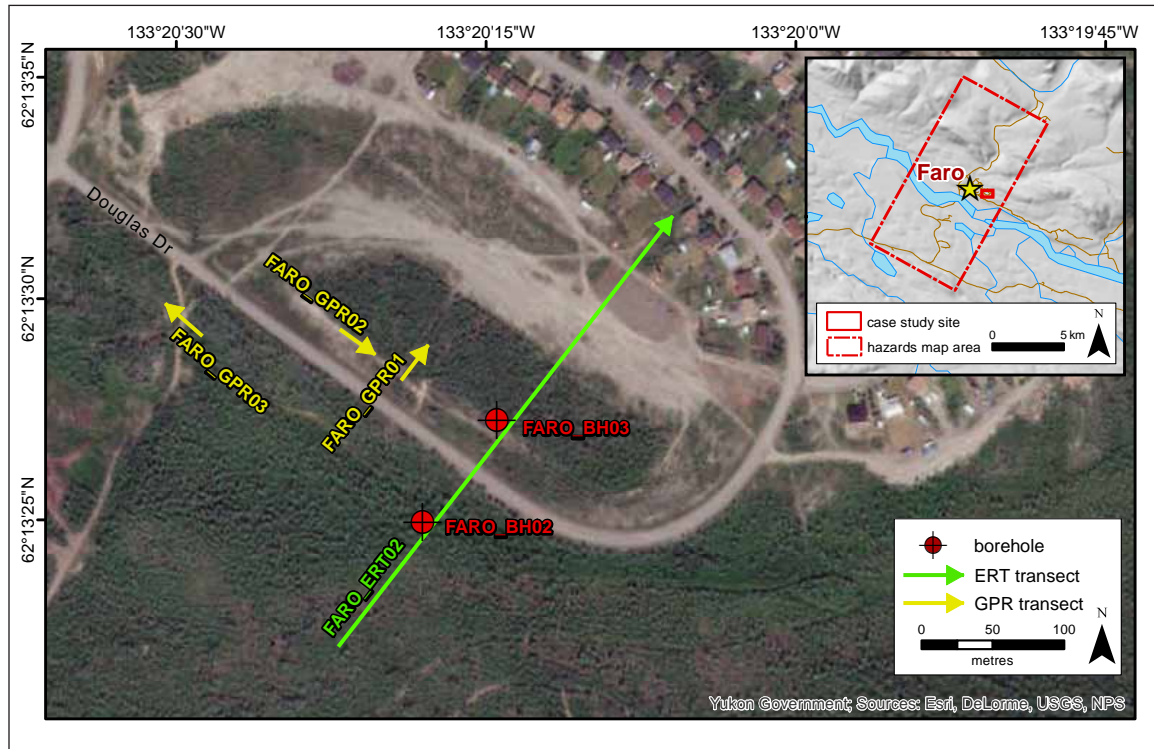


Figure 34. Map illustrating locations of detailed site investigations for the Douglas Drive/Yates Crescent area. Refer to Figure 22 for all other case study locations within the study area boundary.

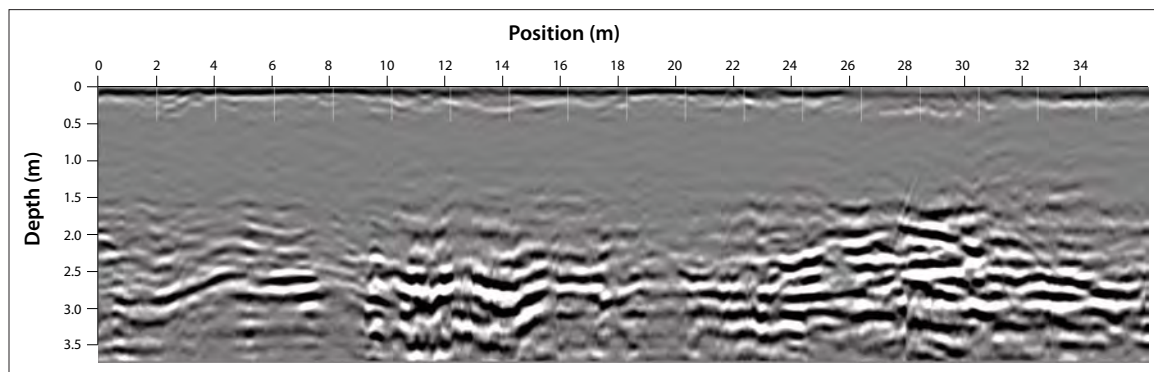


Figure 35. GPR transect FARO_GPR03, in the Douglas Drive area, depicting a strong horizontal reflection at ~1.6 m, likely corresponding to the top of permafrost.

The 400-m ERT profile at this site (FARO_ERT02) was run southwest to northeast from the mixed forest described above, across Douglas Drive, into areas which were previously cleared for development (Figure 38). Frost tables were documented at depths of less than 120 cm in some parts of the first section of the profile, but exceeded 120 cm elsewhere in the profile. The ERT values indicate that there is permafrost in this area (extending to depths of about 20 m), and is confirmed by observations made in borehole FARO_BH02. Although the resistivities are relatively low, they still suggest the possibility of frozen ground to a depth of 8 m from 130 m to 190 m along the profile. This could not be confirmed because probing was not possible due to the presence of

gravel, but the GPR profile along the road (*FARO_GPR03*) also suggests the presence of permafrost. An alternate explanation is that the readings represent dry gravel associated with the road and embankment. From 190 m along the profile to the end of the survey, the low resistivities suggest the absence of permafrost; this corresponds well with the nearby borehole *FARO_BH03* which encountered no permafrost.

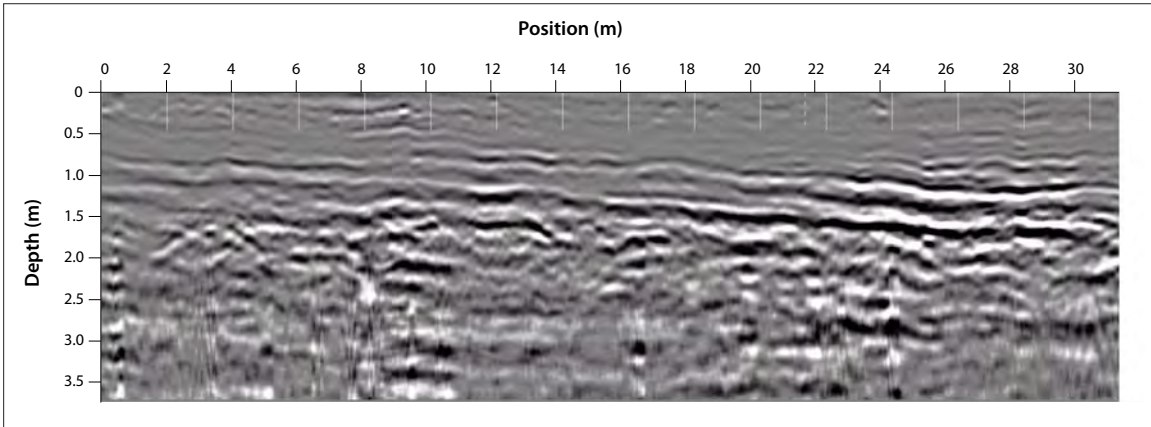


Figure 36. GPR transect *FARO_GPR02*, in the Douglas Drive area, denoting a moderately dipping bed, likely corresponding to sand layers that were identified in a nearby borehole.

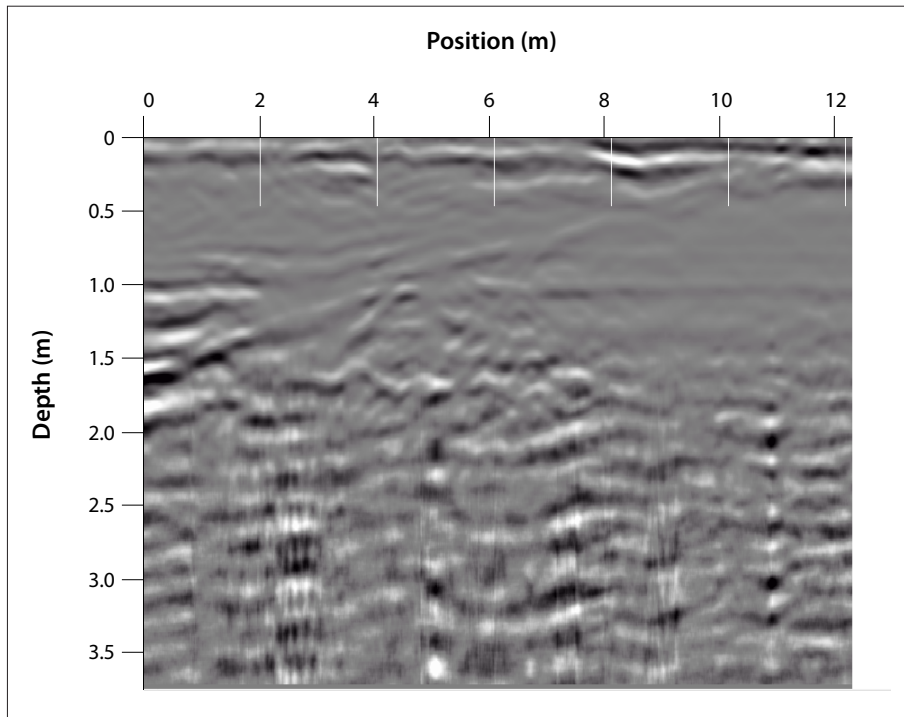


Figure 37. GPR transect *FARO_GPR01*, in the Douglas Drive area, showing a gently dipping bed, likely corresponding to sand layers that were identified in a nearby borehole.

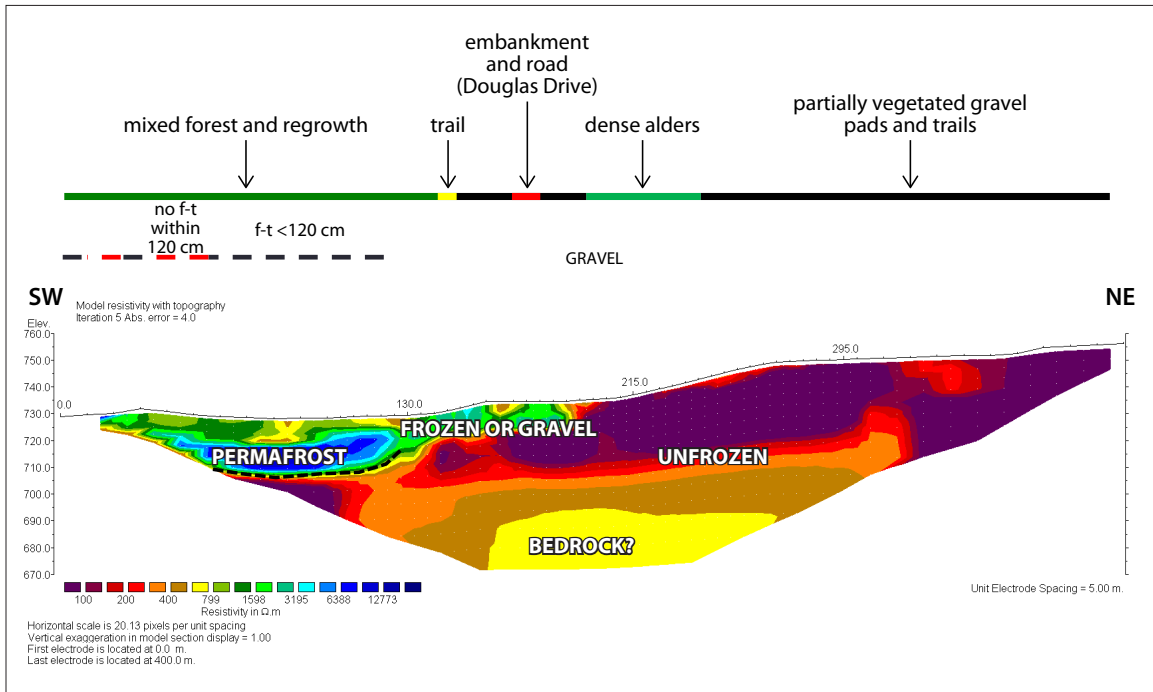


Figure 38. ERT profile FARO_ERT02, a 400 m-long profile that runs southwest to northeast across Douglas Drive towards Yates Crescent (see Figure 34 for location). The profile has a maximum penetration depth of about 60 m. Black dashed lines delineate areas where there is likely to be permafrost; *f-t* = frost table.

DEL VAN GORDER SCHOOL AND BASEBALL DIAMOND

Del Van Gorder School and the centre of the Faro townsite are built on a bench of glaciofluvial sediment (Figure 39) overlying thick glaciolacustrine silt. Up to 15 m of interbedded sand, silt and occasional gravel have been documented in multiple borehole logs drilled in the vicinity of the school (Environment Yukon, 1976; pers. comm., R. Trimble, Tetra Tech EBA).



The depth to the base of the permafrost in the Faro area is reported to be approximately 10 m (EBA, 1981). Permafrost degradation has caused settlement problems beneath Del Van Gorder School gymnasium, particularly in the late 1980s, as well as near the baseball diamond (Figure 40). The baseball diamond is located in a low-lying area that drains a large meltwater channel to the northeast; surface sediments are therefore likely finer-grained, wetter, and more organic-rich than in the surrounding areas. These ground conditions may have contributed to the growth of ice-rich permafrost in the immediate area. Permafrost degradation at the site has probably

Figure 39. Soil pit located at the top of the escarpment behind the radio tower, approximately 200 m west of Del Van Gorder School (station 14PL049). Over 1 m of glaciofluvial sand (*sFG*) underlies 7 cm of White River ash (*WRA*) and 5 cm of red-brown loess (*szEv*).

been accelerated by the disturbance associated with the development of the school and the removal of natural vegetation and organic cover.



Figure 40. Surface settlement (indicated by white arrow pointing to a dip in the fence line and adjacent ponding) at the Faro baseball diamond is likely caused by permafrost degradation. Photo: Kenji Yoshikawa, 2007.

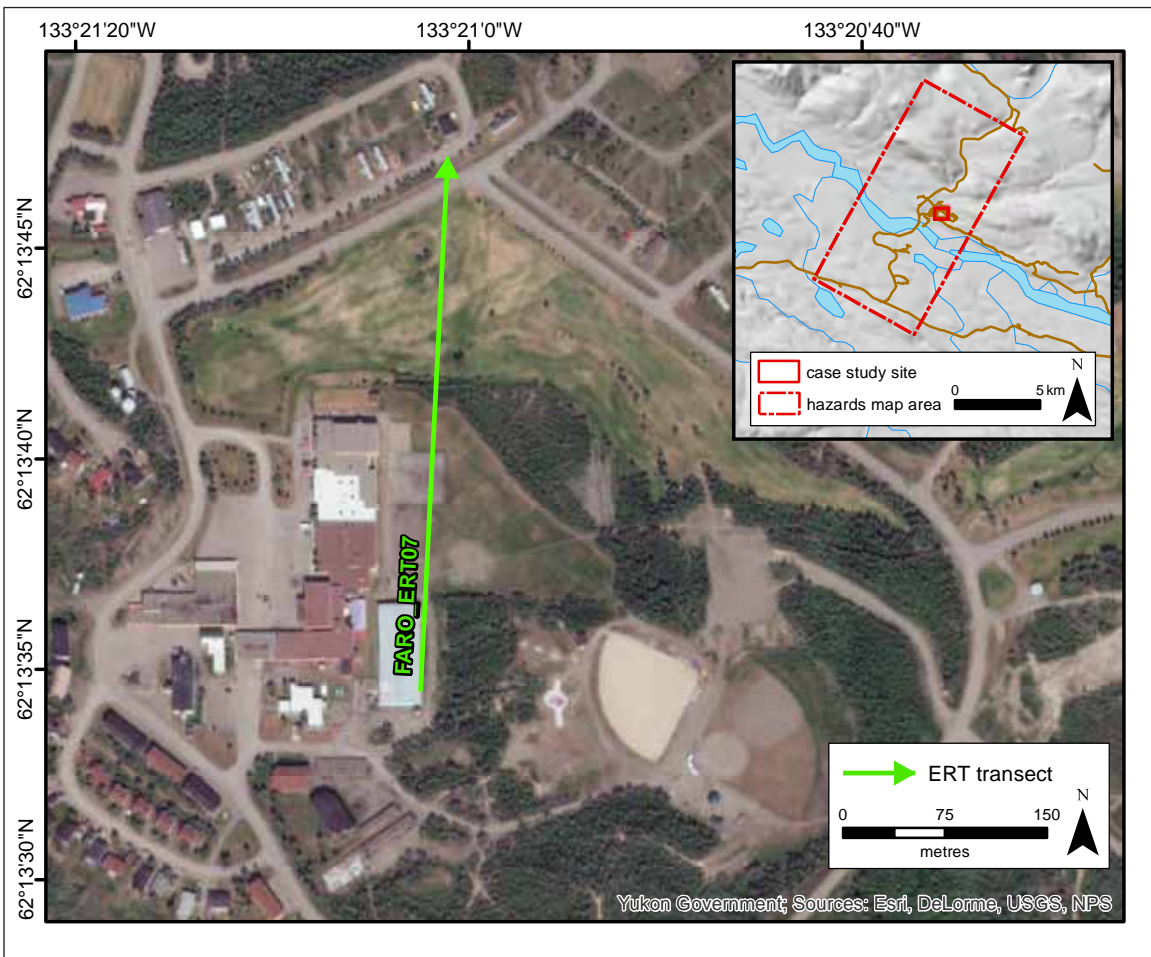


Figure 41. Map illustrating locations of detailed site investigations for the Del Van Gorder School and ball diamond area. Refer to Figure 22 for all other case study locations within the study area boundary.

A 400-m ERT profile (*FARO_ERT07*) was run from south to north, traversing the area between the school and the baseball diamond, and then across the golf course (see Figure 41, previous page). The terrain is almost flat and is mainly covered by grass. No frost tables were noted due to the presence of gravel in the first part of the transect and the presence of stiff fines beneath the golf course area. The ERT profile (Figure 42) indicates the presence of taliks from 40-160 m, and from 220-330 m along the profile, which overlie degrading permafrost 30-40 m thick. These results suggest that the base of permafrost is much deeper than 10 m as was noted in other ERT profiles in the Faro area. The top of the permafrost is interpreted to be at a depth of 10-15 m along the first 160 m of the profile, and 15-25 m in the latter part of the profile (~250 m onwards). Using a value of 400 ohm m as the boundary between frozen and thawed soils, the middle section of the profile appears to be unfrozen, but a lower threshold value would result in an interpretation of degrading permafrost in this part of the profile. Regardless of the value used, it is clear that surface disturbance at this site has resulted in significant and long-term permafrost thaw, and it appears to be ongoing in at least some parts of the profile. Given the considerable pre-existing permafrost thickness (30-40 m), this degradation can be expected to continue for decades.

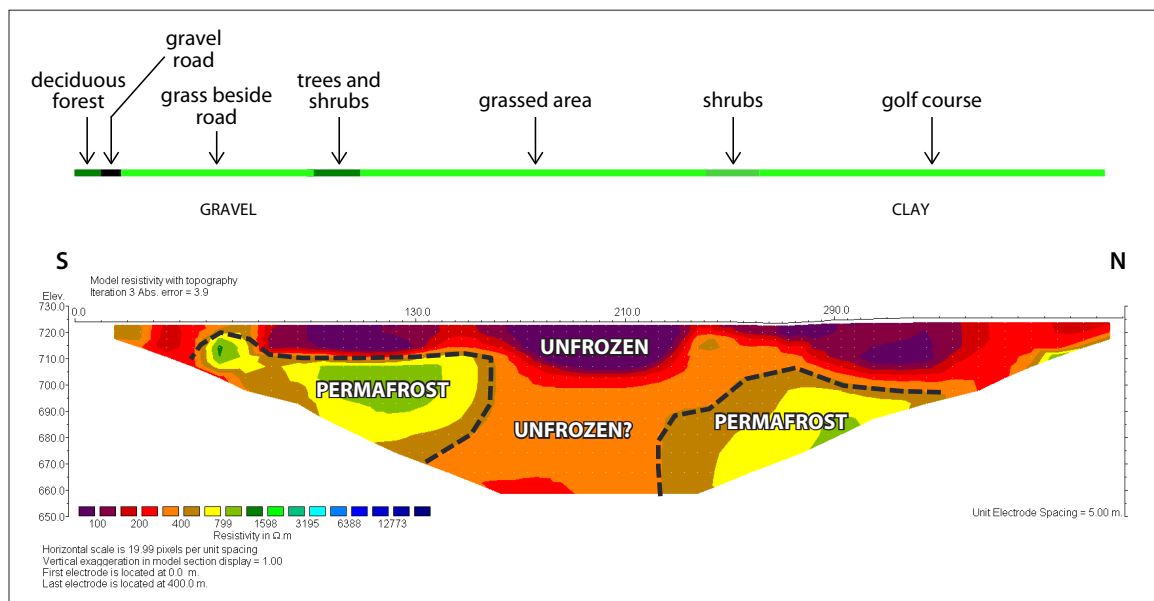


Figure 42. ERT profile *FARO_ERT07* is 400 m long and runs south to north across the golf course, and behind the school towards the baseball diamond (see Figure 41 for location). The profile has a maximum penetration depth of about 60 m. Black dashed lines delineate areas where there is likely to be permafrost.

FARO SKI HILL LANDSLIDE

A large landslide scar (480 m long and up to 90 m wide), exists at the former ski hill, approximately 5.5 km up the mine access road from Faro (Figure 43a; see also Figure 19a). The slide initiated on a moderate (15-20°), south-facing slope blanketed in till. Two distinct deposits of till were exposed in the initiation zone in September 2014 (Figure 43b). The lower till consists of an extremely dense, sticky, dark grey diamict with 30% dominantly pebble-sized phyllitic clasts in 70% sandy clay matrix. The upper till is brown in colour, with 40% largely granitic clasts in 60% sandy silt matrix.

The initiation zone is up to 100 m wide and approximately 270 m long. It is bounded by several steep scarps, including an upper headscarp up to 25 m high, and sidewall scarps which range in

height from 10-19 m. Several of the scarps have started to restabilize, but the upper headscarp is still freshly exposed and actively retreating. Below the initiation zone is a narrower transportation zone, approximately 30-40 m wide and 80 m long, where partly fluidized debris flows downslope and scours the underlying material. The deposition zone consists of a tongue of debris on the valley floor, approximately 130 m long and 80 m wide at the toe. Significant amounts of large woody debris and tree trunks are incorporated into debris piles at the toe of the landslide.

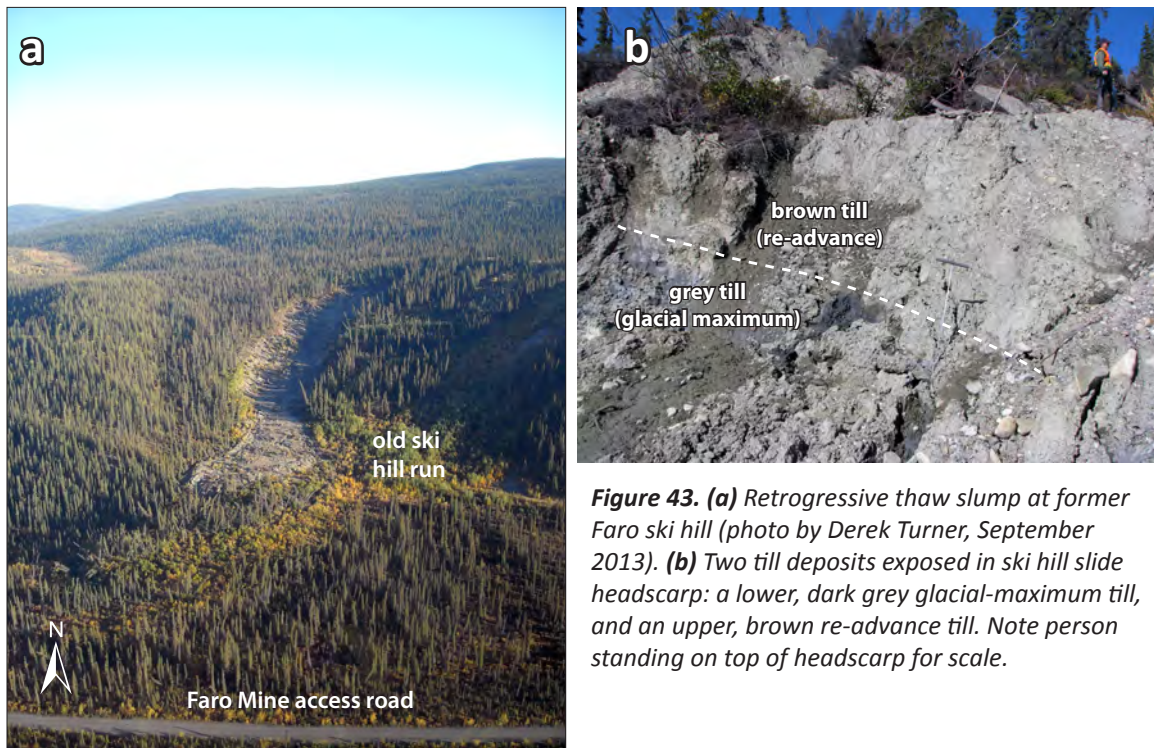


Figure 43. (a) Retrogressive thaw slump at former Faro ski hill (photo by Derek Turner, September 2013). **(b)** Two till deposits exposed in ski hill slide headscarp: a lower, dark grey glacial-maximum till, and an upper, brown re-advance till. Note person standing on top of headscarp for scale.

An ERT survey was conducted in September 2013 across the lower portion of the slide, near the bottom of the transportation zone (see Figures 44-46). The 160 m-long array penetrated to a depth of 25 m (Figure 45). While no permafrost was detected beneath the slide scar itself, the results suggest that permafrost 5-7 m thick remains below undisturbed ground on the west flank, and is about 10 m thick on the east flank. Similar permafrost conditions likely exist on the undisturbed slopes surrounding the initiation zone. There is generally a good correlation between these high, near-surface resistivities, and frost tables <120 cm deep that were identified by probing. Two higher resistivity bodies at depth from 120-136 m and 148-160 m along the profile may represent degrading permafrost, but this cannot be confirmed. Values obtained near the ends of ERT surveys should be treated with caution as the degree of detail is less in these areas due to a wider spacing of electrodes.

Based on air photo analysis, the landslide appears to have initiated after 1993 and before 2004 near an access road leading to the top of the ski hill; one local resident recalled that it initiated in “mid-summer of the mid-1990s” (Chris Wilkinson, pers. comm., 2014) Given its considerable depth (up to 8 m in places), failure likely occurred through the permafrost which may have progressively thinned as alder grew on the ski run, warming the ground by increasing snow accumulation. Berms present on either side of the slide track in May 2006 suggest that movement involved sliding of intact blocks, as was also indicated by upright displaced trees on transported blocks in the depositional zone (A. Lewkowicz, unpublished field observations). Downslope of the transported

blocks, surface folds showed that a stable portion of the slope had been impacted by moving material, while active thawing of the sidewalls resulted in a large viscous mudflow deposit upslope of the transported blocks. Two icings present in the headscarp also indicated active groundwater flow.

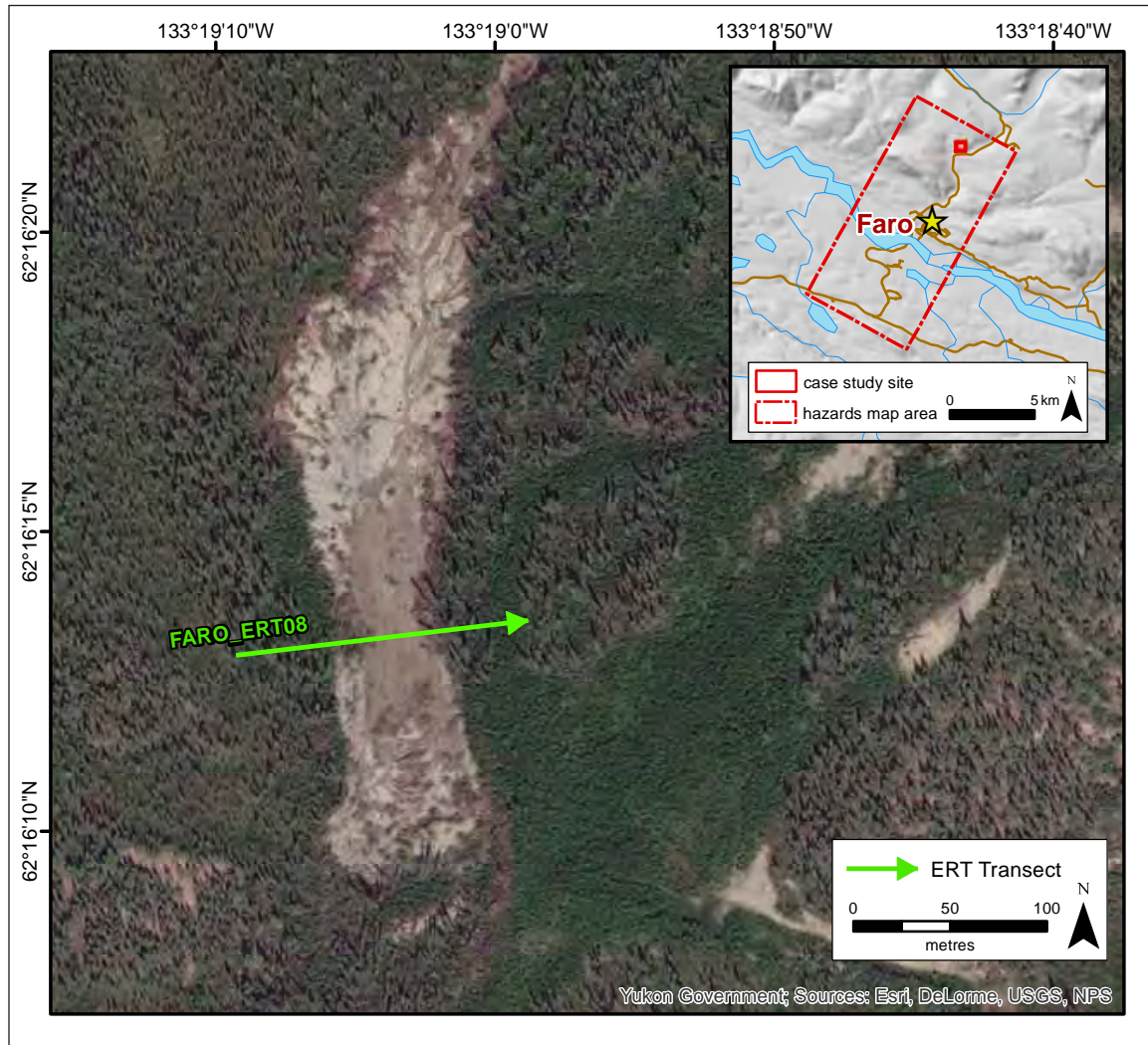


Figure 44. Map illustrating locations of detailed site investigations of the landslide near the Faro ski hill. Refer to Figure 22 for all other case study locations within the study area boundary.

The slide has grown considerably in size since its initiation (Figure 46). On August 9, 2004, the slide was approximately 0.7 ha in area, while on May 31, 2006, it was estimated to be 250 m long and 50 m wide (A. Lewkowicz, unpublished field observations). By August 10, 2008, the headscarp had retreated upslope about 60 m, and the slide occupied an area of 2.5 ha. By July 5, 2009, the headscarp had retreated a further 60 m and the slide occupied an area of 2.6 ha. By September, 2014, the headscarp had retreated a further 35 m and evidence of ongoing instability was observed in the field, including exposed sediment, disturbed vegetation, tension cracks and hummocky topography. A natural spring was also observed draining out of the headscarp; wet material was actively flowing from the headscarp zone in a thick, viscous slurry, suggesting the continued significance of groundwater. Based on the presence of permafrost on surrounding

undisturbed slopes, the steep headscarp drained by active debris flows, and the ongoing expansion in size, the landslide is currently classified as a retrogressive thaw slump.

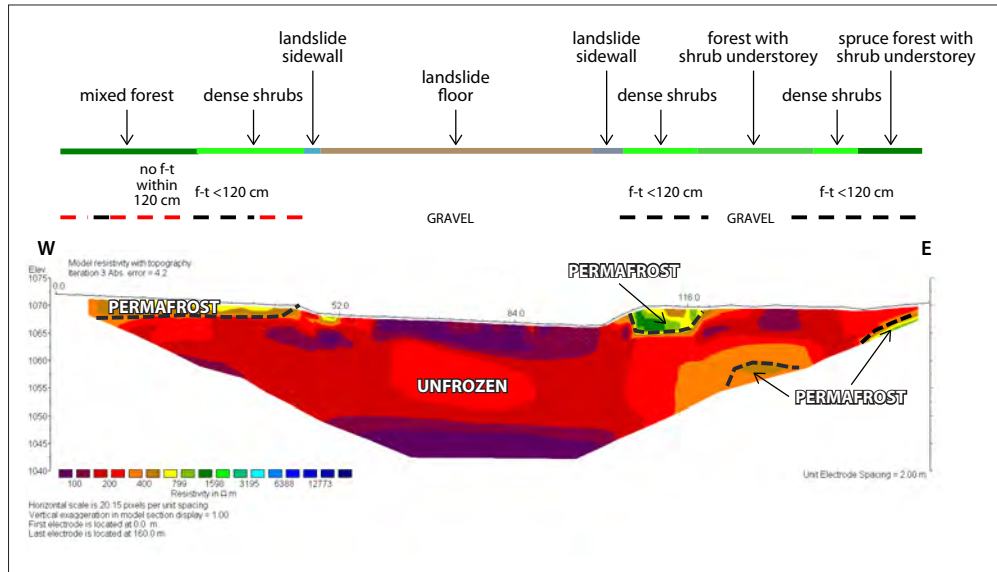


Figure 45. ERT profile FARO_ERT08 is 160 m long and runs west to east across the landslide face (see Figure 44 for location). The profile has a maximum penetration depth of about 25 m. Black dashed lines delineate areas where there is likely to be permafrost; f-t = frost table.

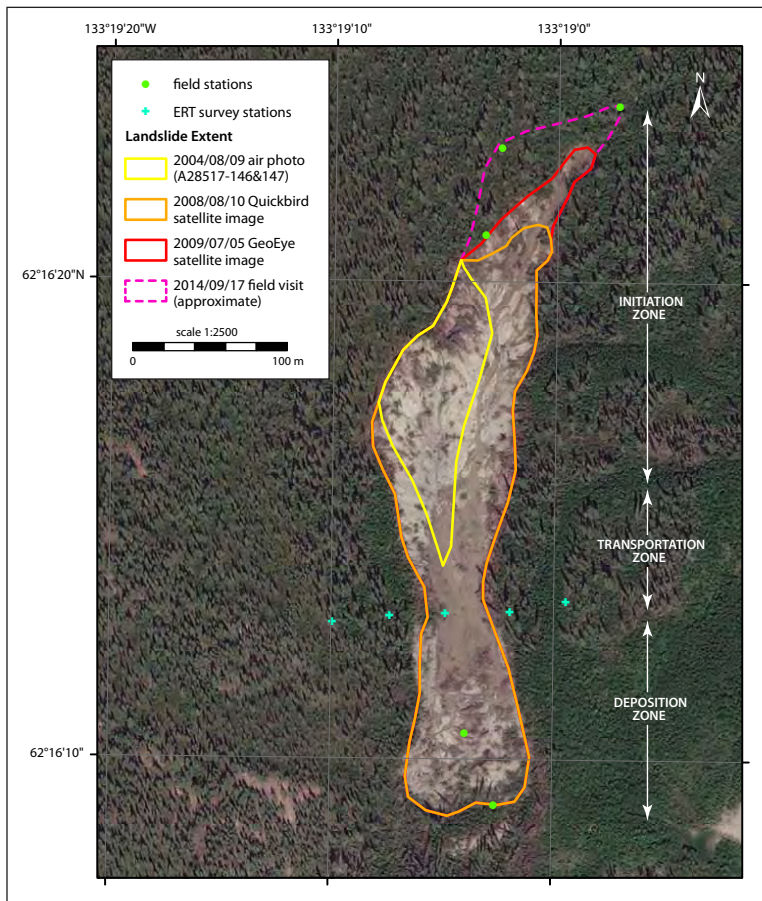


Figure 46. Map illustrating progressive growth of ski hill retrogressive thaw slump and location of ERT survey (FARO_ERT08). GeoEye (2009/07/05) satellite image displayed in background.

Additional signs of active instability were noted on a similar southwest-facing, till-blanketed slope, less than 1 km to the south that included split trees (Figure 47a; station WPT714) and fresh tension cracks in the surface organic mat (Figure 47b; see Figure 19a for station locations). At least eight thermokarst ponds exist at the base of this slope, and a large active layer detachment flow (see Figure 18e) also occurs immediately across the valley from this site, highlighting that the immediate region is extremely susceptible to a variety of permafrost and landslide hazards.



Figure 47. (a) Split tree (station WPT714 on Fig. 19a) and (b) fresh tension cracks emphasized by pulled roots (station WPT715 on Fig. 19a) indicate active instability on the southwest-facing slope immediately south of the ski hill.

HAZARD RISKS IN A CHANGING CLIMATE

PROJECTED CLIMATE CHANGE FOR THE FARO REGION

Climate projections for the Faro area were integrated into this project in order to evaluate how current environmental conditions may pose risk in the future as a result of changes in climate. Predicting future climate change around the globe has become a critical component in climate change science and adaptation. Scientists use a variety of Global Climate Models in combination with discrete scenarios in order to make a range of projections for numerous climate variables (e.g., temperature and precipitation).

GLOBAL CLIMATE MODELS

Global Climate Models (GCMs) – also referred to as Atmosphere-Ocean General Circulation Models – are mathematical representations of atmospheric and oceanic circulation in the world. There are several types of GCMs; however, three-dimensional global atmosphere and ocean models are most commonly used to generate future climate projections. GCMs are complex mathematical models that incorporate a wide range of climate variables including radiation, energy transfer by winds, cloud formation, evaporation and precipitation of water, and transport of heat by ocean currents (CCRUN, 2011). The model calculations are based on a complex grid system that covers the globe in both a horizontal and vertical dimension on the order of 200-500 km. Data for each grid box is input into the model equations to solve for atmosphere, land surface and oceans (CCRUN, 2011).

CLIMATE CHANGE SCENARIOS

In order to generate future climate projections, the Intergovernmental Panel on Climate Change – the leading international body for the assessment of climate change – developed several scenarios that outline a range of possible emission futures. There are a total of six scenario groups, each making different assumptions about the release of greenhouse gases (e.g., carbon dioxide (CO₂), methane (CH₄), nitrous oxide (N₂O) etc.; see Nebojša et al., 2000 for details). Projections used for Faro were derived from regionally downscaled climate data provided by the Scenarios Network for Alaska Planning (SNAP) at the University of Alaska Fairbanks (see SNAP, 2013). For the purpose of this project, SNAP applied three scenarios that best represented the possible shifts in climate for Yukon communities. The three scenarios used are defined as follows (SNAP, 2013):

The B1 scenario – low to moderate degrees of climate change

- rapid economic growth (as in A1B), but with rapid changes towards a service and information economy
- population rising to 9 billion in 2050 and then declining as in A1 (see Nebojša et al., 2000)
- reductions in material intensity and the introduction of clean and resource-efficient technologies
- an emphasis on global solutions to economic, social and environmental stability

The A1B scenario – medium to high degrees of climate change

- rapid economic growth
- a global population that reaches 9 billion in 2050 and then gradually declines
- the quick spread of new and efficient technologies
- a convergent world, i.e., income and way of life converge between regions
- extensive social and cultural interactions worldwide
- a balanced emphasis on all energy sources

The A2 scenario – high degree of climate change

- a world of independently operating, self-reliant nations
- continuously increasing population
- regionally oriented economic development
- slower and more fragmented technological changes and improvements to per-capita income

The climate projections developed by SNAP were then enhanced to reflect local landscape heterogeneity (like mountainous terrain, which can create local temperature inversions that are not typically captured in models; see Appendix D for more details). Climate projections for three time periods (the 2020s, 2050s and 2080s) were produced, and maps of all projections are included in Appendix D.

Based on climate normal data measured at the Faro Airport meteorological monitoring station for the period 1980-2010 (Environment Canada, 2014a), mean annual air temperature for the region is -2.8°C (Table 3). Interestingly, back-cast temperatures, were hindcasted for the period 1950-1979 using the modelling approaches described above, and indicate that mean annual air

temperature for this period was -4.0°C . This suggests a warming of 1.2°C has already taken place over the region in the past ~ 50 years.

Table 3. Mean, minimum and maximum air temperatures for the Faro region under current and backcast climate conditions, as well as for the 2020s, 2050s and 2080s, using the B1, A1B and A2 climate scenarios.

Projection	Air Temperature ($^{\circ}\text{C}$)		
	Mean	Minimum	Maximum
Current MAAT	-2.8	-3.5	-2.5
1950 - 1979	-4.0	-4.6	-3.7
B1 2020s	-2.7	-3.4	-2.4
B1 2050s	-2.1	-2.8	-1.8
B1 2080s	-1.1	-1.8	-0.8
A1B 2020s	-2.7	-3.4	-2.4
A1B 2050s	-1.5	-2.2	-1.2
A1B 2080s	-0.1	-0.8	0.2
A2 2020s	-2.8	-3.5	-2.5
A2 2050s	-1.8	-2.5	-1.5
A2 2080s	0.2	-0.5	0.5

Projections of mean annual air temperatures in the Faro region show continued warming will take place over the next several decades. All three scenarios predict temperatures in the 2020s that are comparable to climate normal conditions. By the 2050s, the B1 scenario predicts the lowest mean annual air temperature (-2.1°C), while A2 predicts the highest (-1.8°C). However, by the decade of the 2080s, A2 predicts a mean annual air temperature that exceeds 0°C , while the A1B scenario predicts -0.1°C . Even B1, the most conservative scenario applied, predicts a mean annual air temperature of -1.1°C by the 2080s, which is 1.7°C warmer than present. However, as discussed in earlier sections of this report, warming in the region will not be uniform – lapse rates (i.e., decreases in temperature with elevation gain) are variable and different from the global average (Lewkowicz and Bonnaventure, 2011). Regardless of scenario, continued increase in mean annual air temperature has the potential to exacerbate hazards in the Faro region in ways that are described below.

LANDSCAPE SENSITIVITY TO CLIMATE CHANGE

Under the projected climate scenarios presented in this report, risks associated with surficial materials and terrain stability are variable and primarily related to the effects of changing soil moisture and surface runoff. In general, terrain stability declines with increased soil moisture and/or surface runoff, both of which can be caused by thawing of ice-rich permafrost, and changing hydrological regimes (including streamflow, flooding, groundwater flow, seasonal precipitation patterns and extreme snowmelt and rainfall events).

Changes in permafrost strongly affect surface and groundwater drainage and can cause near-surface soils to become either wetter or drier depending on site conditions. In ice-rich permafrost, active layer thickening may increase soil moisture and decrease slope stability, whereas in ice-poor permafrost, deepening of the active layer may actually improve local drainage capacity and increase surface slope stability. Increases in regional moisture delivery could also raise stream

and lake levels which, in turn, may enhance incision or aggradation rates, and erosion on stream banks and lake shores. Changes in the amount or seasonal timing of precipitation, snowmelt and sediment supply may also increase stream channel instability and migration, undercutting and oversteepening of cutbanks and initiation of landslides. Extreme rainfall and snowmelt events will also trigger landslides by rapidly saturating soils, especially in areas where groundwater concentrates, such as in gullies or depressions, or where drainage is limited by shallow permafrost or bedrock. With climate amelioration, retrogressive thaw slumps could become more frequent, especially in areas where water comes in contact with ice-rich glaciolacustrine material. The projected degradation of near-surface permafrost will also increase hazards associated with periglacial processes, including active layer detachment slides, sheetwash, and thermokarst erosion. Most of these processes occur on north-facing slopes, but can also occur on other aspects.

SENSITIVITY OF LOCAL SURFACE MATERIAL TYPES

To assess permafrost stability for land-planning purposes, an estimation of the maximum thaw depth that could be reached under the changing climatic conditions is essential, mainly to evaluate the potential deformation that the soil may undergo in the future (Instanes, 2003). The rate and type of deformation is closely linked to the type of surficial deposits present, the ground ice content and how it is distributed in the ground, the ground temperature, and the soil hydrological regime. Recognizing the importance of understanding soil dynamics when evaluating permafrost sensitivity to environmental change, the characteristics and vulnerabilities of the major soil types identified in the study area have been characterized below.

Two typical stratigraphies are exhibited in the Faro region. On floodplains (e.g., the sewage lagoon case study site), the stratigraphy is mainly composed of fine silt over sand near the outer margin of the floodplain, and a mix of silt and sand layers near the main river channel. For the rest of the study area, the typical stratigraphy presented was a peat layer overlying silty sand with gravel. To evaluate the stability of a specific location in the area, it is recommended that deep boreholes be drilled to determine the complete stratigraphy. If a fine-grained layer was to be encountered, appropriate mitigation techniques would be required. In the absence of a fine-grained layer, risks of permafrost settlement are low and constructed infrastructure is most likely to remain stable. Nonetheless, the superposition of different soil layers can change the behaviour of a given soil (e.g., frost susceptibility, hydraulic response, etc.), and typical expressions are described below.

Silt on sand

Silt is a frost-susceptible, thaw-sensitive sediment that should be avoided for land-use planning involving buildings and transportation infrastructure. The impact of a layer of silt over a layer of sand depends on the thickness of the silt layer. When the active layer is entirely composed of silt, significant frost heaving and thaw settlement of the surface will occur, especially if the active layer is poorly drained. When the bottom of the active layer is composed of sand and the silts are drained or under-saturated when the freezing occurs, the material can be expected to remain stable. Active layer deepening in sand without fines does not create significant thaw settlement. This stratigraphy is present at the sewage lagoon case study site.

Peat on silty sand with gravel

This stratigraphy implies a high porosity layer (peat) over a relatively lower porosity layer (silty sand with gravel). The latter has a low hydraulic conductivity and can retain, for a period of time, the water in the layer above, leading to a high volumetric ice-content in the peat layer. During annual freezing of the active layer, this induces segregation of ice in the peat. Upon thawing, settlement due to melting of excess ice is expected, and the water will be drained down to the gravelly layer where infiltration will be slow. If the boundary between the organic and the mineral

layers is located in the transient layer (zone within which the permafrost table moves in response to decadal climatic changes), the water could refreeze, creating an ice-rich zone with a high settlement potential near the permafrost table.

PROJECTED CHANGES IN PERMAFROST DISTRIBUTION

Increases in mean annual air temperature will affect permafrost distribution in the Faro area. To assess potential future permafrost distribution in the study area, contemporary permafrost distribution must first be examined. A detailed assessment of the spatial pattern of current permafrost conditions in the Faro region can be extracted from a model of permafrost probability developed for the southern half of Yukon (Bonnaventure et al., 2012). This model is essentially climatically based, taking into account the impacts of air temperature trends with elevation (Lewkowicz and Bonnaventure, 2011) and solar radiation, but not accounting for site-specific factors such as snow depth or surficial materials. The calculated probabilities are for typical snow cover conditions and there can be considerable sub-grid cell variability where sites are locally blown clear of snow, resulting in a higher probability of permafrost, or at sites that accumulate early and deep snow covers, resulting in a lower probability of permafrost (Lewkowicz and Ednie, 2004). Results portray the broad spatial trends in permafrost conditions across the landscape but cannot be used for site-specific predictions. For example, if an area is shown as having a probability of 0.5 to 0.6, this means that 50-60% of the grid cells are predicted to be underlain by permafrost, but it does not indicate which of the cells may have permafrost and which may not.

Model results for the Faro region were extracted from the regional model (Figure 48). Results indicate that permafrost distribution in the area is largely consistent. Most of the terrain in the region exhibits permafrost probabilities of 60-70%. Permafrost probability on many south-facing slopes is lower (50-60%), while north-facing slopes exhibit values in the 70-80% range. This indicates that in the Faro region, permafrost distribution is largely influenced by aspect.

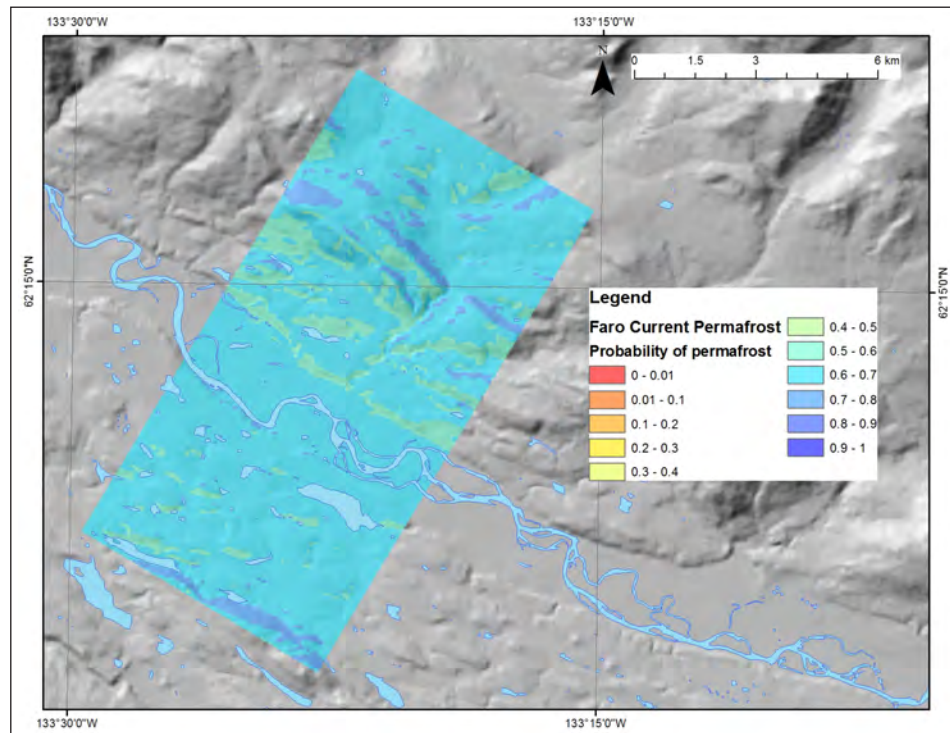


Figure 48. Permafrost probability for the Faro region under current climate conditions.

To map future permafrost distribution, the contemporary permafrost probability model is perturbed by altering the input variable of equivalent elevation which represents mean annual air temperature. This effectively simulates a uniform regional temperature change, which is used to predict the probability of permafrost occurrence in the study area under differing degrees of warming. A range of mean annual air temperature increases from +1°C to +5°C were imposed, based on widely accepted projections of change for the next several decades (e.g., see IPCC, 2015). A scenario approach was favoured over applying global or regional climate model predictions, because these tend to provide inadequate representations from the effects of topography in the Yukon (see Burn, 1994).

The goal of imposing climate change scenarios on the regional permafrost probability model is to examine the sensitivity of permafrost to changes in mean annual air temperature over time. It is important to note that modelling is done for equilibrium conditions and therefore does not take into account the rate at which the change in climate might occur, nor the lag times associated with permafrost thaw. Still, it is a useful indication of potential changes in the spatial distribution of permafrost regionally, under a changing climate.

Increases in mean annual air temperature were simulated in the spatial model by uniformly decreasing the values of equivalent elevation in the transformed digital elevation model (Janke, 2005; Lewkowicz and Bonnaventure, 2011; Bonnaventure et al., 2012), and then running the model to produce an altered basal temperature of snow surface. This affects the predicted permafrost probabilities that are calibrated with the non-linear logistic regression coefficients determined for 1971-2000 climate normal conditions. An increase of 1°C is represented by a decrease in the equivalent elevation surface of 154 m. Even though the change is uniformly applied across the region, it results in differential responses that depend on the surface lapse rates below treeline. This methodology has the advantage of preserving all elements of the spatial model for a given area such as aspect, shading and slope, as well as the specific relationships that exist between changes in elevation and basal temperature of snow values. Although other environmental factors, such as snow and vegetation, significantly influence permafrost distribution in the discontinuous zones (e.g., Smith and Riseborough, 2002) and are expected to change in the future (e.g., IPCC, 2015), the model cannot take such changes into account, as they are not part of the input variables.

As with contemporary permafrost probability modelling presented in Figure 48, results show probabilities on a scale of 0 to 1. If an area has a probability value of 0.6, this means that 60% of the grid cells in the area are likely to be underlain by permafrost. However, the model is not capable of distinguishing which grid cells in the area have permafrost; rather, it identifies local probabilities given local conditions.

The results of the perturbed permafrost probability modelling (see Figures 49-53) show that a relatively small increase in air temperature (1-2°C) is likely to have an impact on permafrost probability in the Faro region. Under current conditions, the probability of permafrost occurring at any point in the region (defined by the boundaries of the hazards map; see Figure 1 for map area) is 60%. With a mean annual air temperature increase of +1°C, the probability of permafrost declines to 50%. With subsequent increases, permafrost probability continues to decline, so that with a mean annual air temperature increase of +5°C, the probability of permafrost in the map area is 20% (Table 4). Potential declines in permafrost extent under increases in mean annual air temperature should be factored into adaptive planning decisions, as permafrost thaw poses a hazard risk for infrastructure during its degradation.

Table 4. Mean, minimum and maximum probability of permafrost occurrence in the Faro area under current climate conditions, and as a result of increases in mean annual air temperature of 1 to 5°C.

Mean annual air temperature	Probability of permafrost presence		
	Mean	Minimum	Maximum
Current	0.6	0.5	0.8
+1°C	0.5	0.4	0.7
+2°C	0.4	0.3	0.5
+3°C	0.3	0.3	0.4
+4°C	0.3	0.2	0.3
+5°C	0.2	0.2	0.2

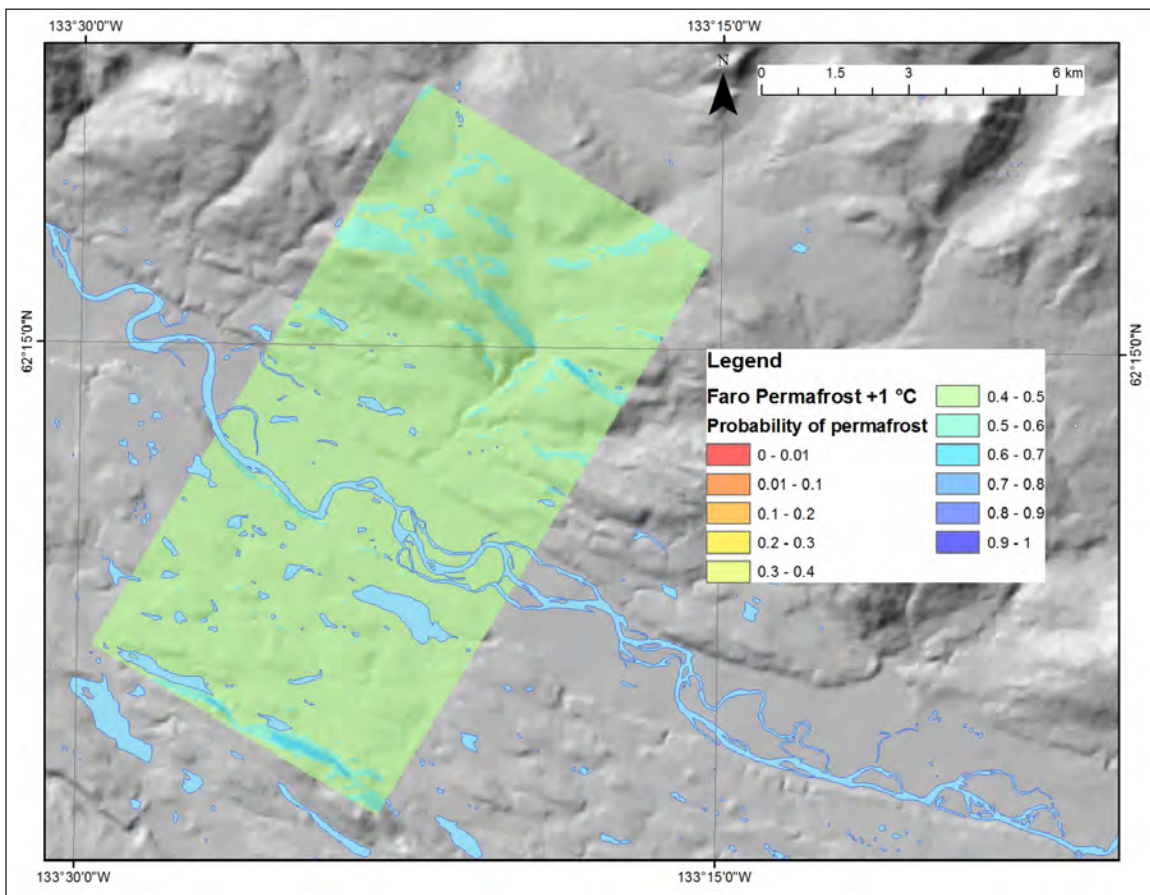


Figure 49. Projected permafrost probability for the Faro region under an increase in mean annual air temperature of 1°C.

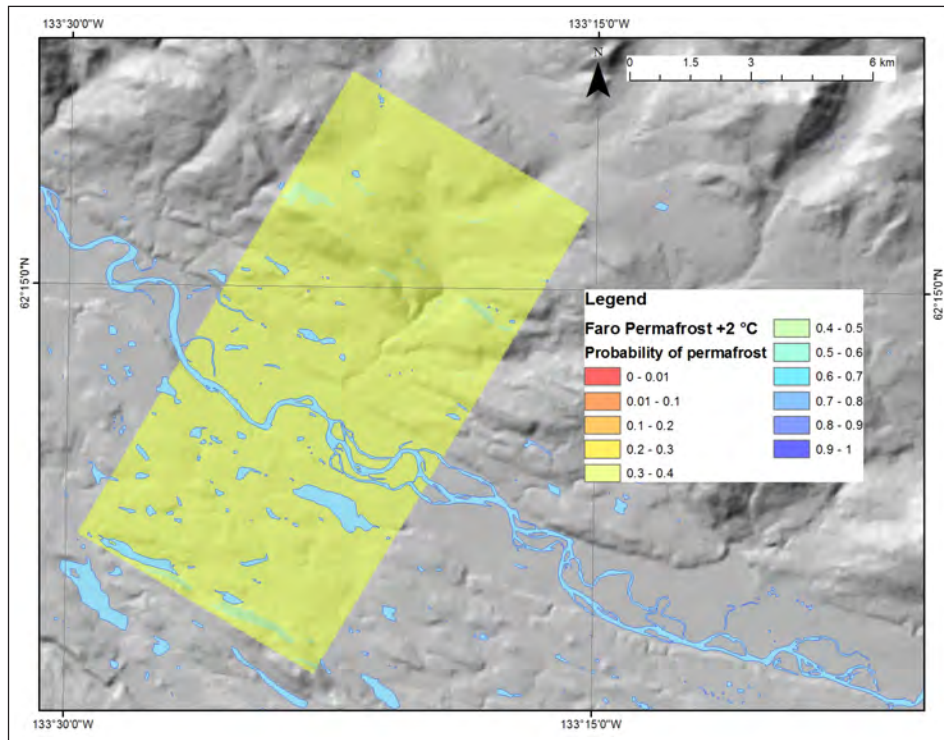


Figure 50. Projected permafrost probability for the Faro region under an increase in mean annual air temperature of 2°C.

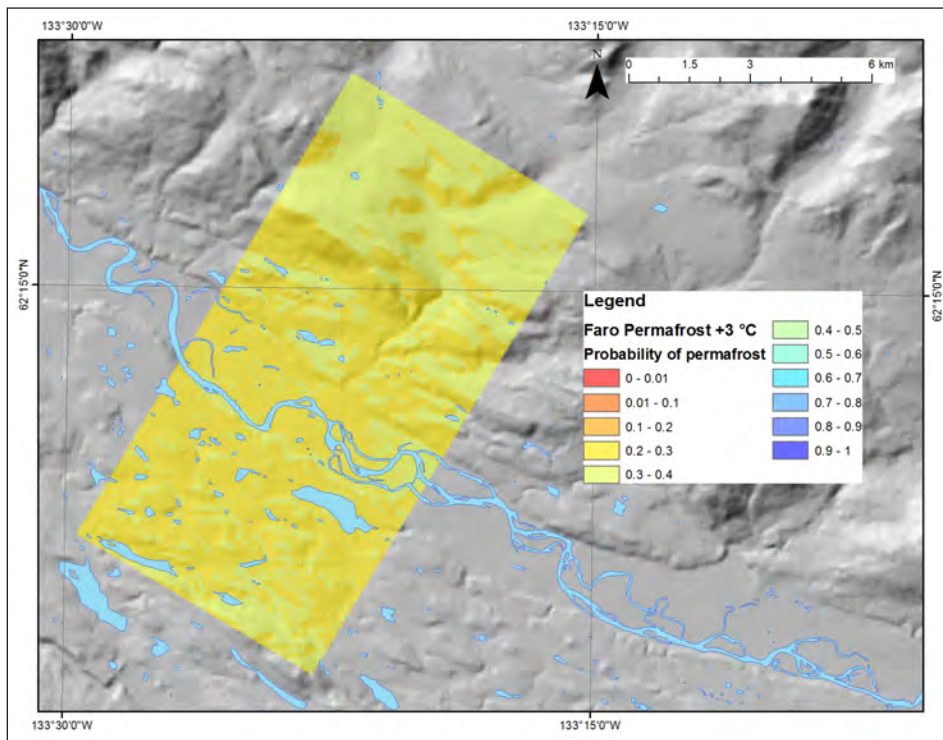


Figure 51. Projected permafrost probability for the Faro region under an increase in mean annual air temperature of 3°C.

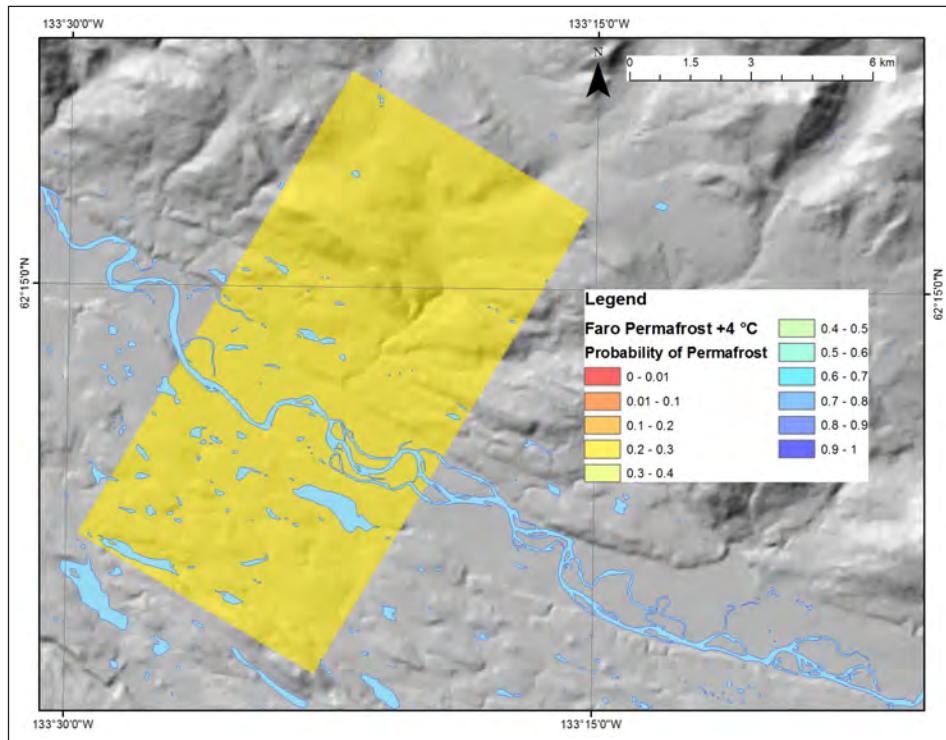


Figure 52. Projected permafrost probability for the Faro region under an increase in mean annual air temperature of 4°C.

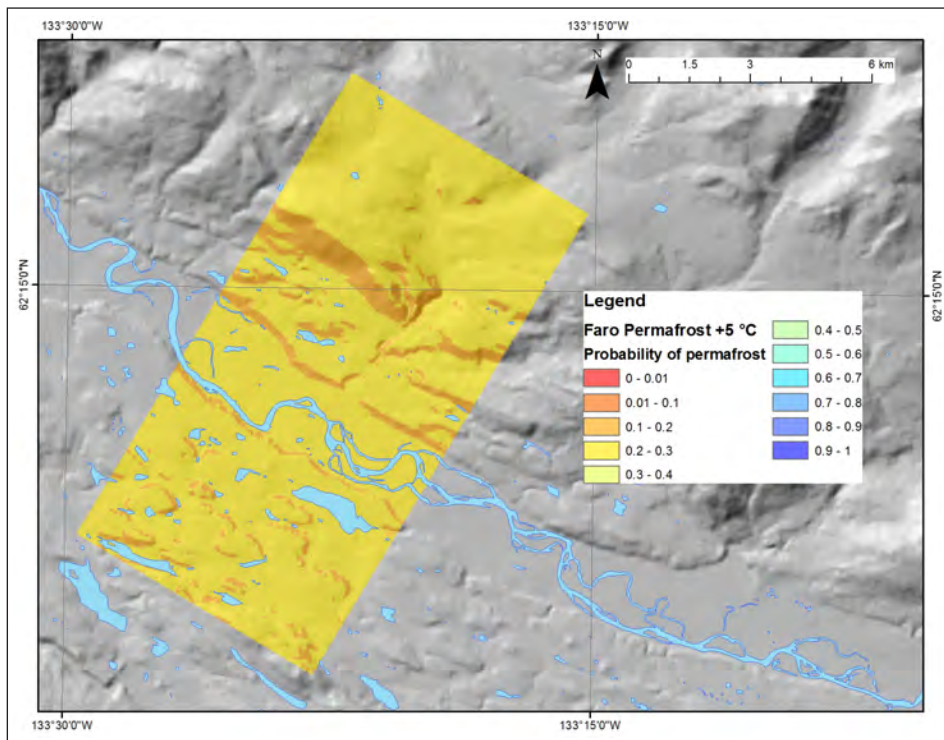





Figure 53. Projected permafrost probability for the Faro region under an increase in mean annual air temperature of 5°C.

INTEGRATING RISK IN A LANDSCAPE HAZARDS MAP FOR THE FARO REGION

To develop a landscape hazards map for the Faro region that integrates current and future hazards risks in a changing climate, results from study region characterization, case study site investigations, laboratory analyses, climate projections, and contemporary and future permafrost probability modelling were integrated. Additional mapping activities were also integrated into the development of the hazard map. These were completed in order to capture nuances in surficial geology features, namely drumlinoid forms in the southwest portion of the map area, because the ridges and slopes of these types of landforms pose a different degree of hazard risk than the depressions between them. All these geoscience parameters were combined to develop a risk-ranking matrix specific to the Faro region, as follows:

-  **Green:** **low** risk of hazards following permafrost degradation, **low** risk of geomorphic hazards.
-  **Yellow:** **moderate** risk of hazards following permafrost degradation (e.g., moderate thaw settlement) **or moderate** risk of geomorphic hazards.
-  **Red:** **high** risk of hazards following permafrost degradation (e.g., high thaw settlement, water ponding, and slow to rapid mass movement on slopes) **and/or high** risk of geomorphic hazards (e.g., gullying, flooding, steep slopes).

This risk matrix was then applied to each of the surficial geology polygons in the hazards map footprint (see Figure 1), and a risk ranking was assigned based on the geoscience characteristics of each polygon. It is important to note that in classifying polygons, we have taken a precautionary approach and applied a category of higher risk where we are not confident in lower categories. However, every polygon will contain zones of lower and higher risk than the overall polygon classification. This is particularly relevant with regards to the drumlinoid features in the southwest part of the map area. Because of the scale of the hazard map, only the most significant ridges and depressions associated with these large drumlins were mapped (e.g., polygons 16, 22, 53, 128, 129, 143, 151). In yellow polygons surrounding drumlinoid forms (e.g., polygons 134, 136, 139, 141), other smaller drumlin features may be present, resulting in inherent heterogeneity in risk within each polygon. It is for this reason that this map should serve only as an initial guide for planning purposes. Any development will still require detailed site investigations. It is also important to note that hazard rankings are based on general observations of surface materials, drainage, slope angle, vegetation and the presence of permafrost landforms, as well as subsurface information provided by ERT and GPR profiles, drilling and probing of permafrost, and textural analyses of surficial and borehole samples. This has resulted in a *projected* risk ranking that will require geotechnical and/or engineering analyses to quantify.

The hazards map for the Faro region encompasses an area of 90.3 km², and is presented in Figure 54, as well as in a larger print version in the back pocket of this report. As described earlier, the hazards map area is a subset of the surficial geology map completed as part of this project (Turner et al., 2014; included in back pocket of this report), and each of the surficial geology polygons within the hazards map area has been assigned a hazard risk ranking. Appendix E details the hazard classification assigned to each numbered polygon in the map area, and outlines its associated hazard(s).

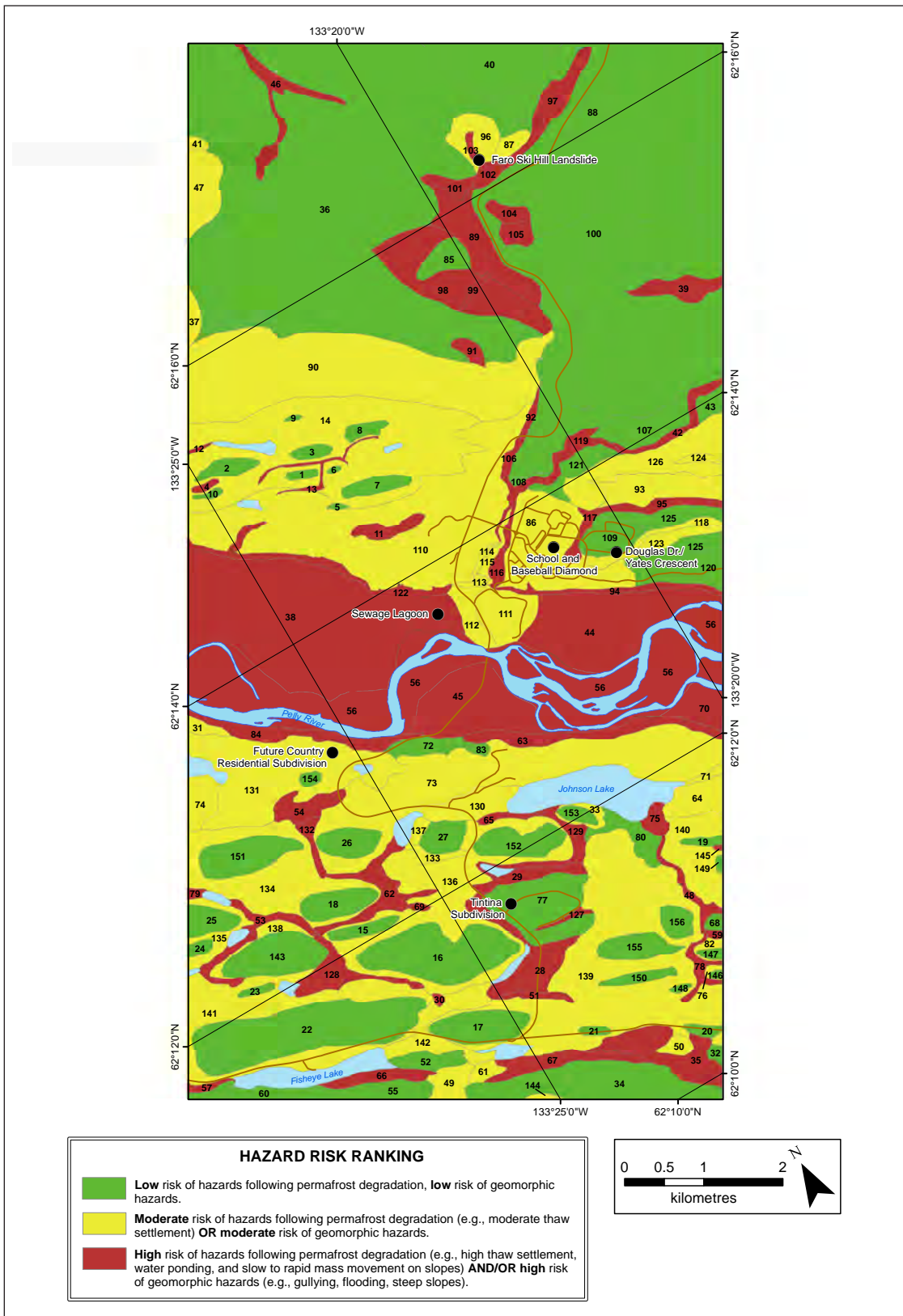


Figure 54. Map depicting hazard risk ranking for the Faro area (see Figure 1 for location of the map boundary). Specific hazards associated with each numbered polygon are listed in Appendix E. A larger fold-out version of this map is included in the map pocket in the back of this report.

A total of 156 polygons fall within the map area and were ranked based on current and perceived hazard risks. Of these, 57 polygons (representing 36.0 km² of the map area) were assigned a low hazard risk ranking, 43 polygons (30.9 km² of the map area) were assigned a moderate hazard risk ranking, and 56 polygons (19.9 km² of the map area) were assigned a high hazard risk ranking. (Water bodies make up an additional 3.5 km² of the map area.)

Most of the southwestern region of the map area, located south of the Pelly River, is composed of morainal (till) deposits. Numerous drumlinoid forms, originating from past glacial flows, are easily recognizable on the landscape. These elongated features are oriented northwest-southeast and vary in size, ranging from a few tens of metres to hundreds of metres long. As a result, the landscape is scattered with ridges (20-60 m high) and their associated depressions. The ridges, which form the upper portion of the drumlins, were classified as having low hazard risk because they are thaw stable and well drained (e.g., polygons 16, 18, 22, 155). In contrast, the depressions located between these landforms (e.g., polygons 29, 53, 62, 127) were classified as having high hazard risk because of the presence of poorly drained accumulations of organic matter which, in some areas, contains significant amounts of ice. As a result, there is a high risk of hazards associated with permafrost degradation. Between the ridges and the depressions, the lower slopes of the drumlins usually exhibit an increase moisture (e.g., more humid soils, potential presence of ice), and as a result, these zones were classified as having moderate hazard risk (e.g., polygons 82, 133, 138).

As stated above, the scale of the hazards map was limiting in terms of mapping every single drumlin feature present on the landscape, and therefore some polygons in the region are mapped as having moderate hazard risk due to the likely presence of within-polygon heterogeneity not captured in the hazard map (e.g., polygons 131, 134, 139). Another set of drumlin features is located north of the Pelly River, and these are mapped using the same principles as those described above (e.g., polygons 1-3, and 5-10).

Investigations at case study sites in the Faro area allow for a more detailed assessment of hazard risk at each location. The Tintina Subdivision case study site is located in the drumlin field described above (south of the Pelly River), and its hazard ranking therefore reflects low hazard risk associated with drumlin ridges (polygon 77) and high hazard risk associated with drumlin depressions (polygons 29 and 127). As described above, drumlin ridges are relatively stable with low risk of settlement in response to permafrost degradation, although there is also a low risk of slow mass movement on slopes due to the high content of fine-grained material in local deposits. The depressions between the drumlins are highly sensitive to hazard risks in response to permafrost degradation, because the peat that has developed and accumulated in the depressions can contain a notable amount of ice and is highly compressible when thawed. Till deposits underlie the peat, and could pose an additional hazard risk in response to permafrost degradation, depending on its water content and plasticity.

The future country residential subdivision is also located in the drumlin-associated area of the map. As described above, this area has been ranked as having moderate hazard risk, because there is potential for local-scale, permafrost-related hazards that were not captured at the scale of the hazards map. For example, in local depressions, a thick moss cover insulates underlying, thick, ice-rich peat that poses a notable hazard risk should permafrost degradation occur (as a result of disturbance or an increase in mean annual air temperature). On the contrary, ridges at this site have a thin organic layer overlying glaciofluvial deposits and no shallow permafrost present, and are therefore likely stable and may be suitable development sites. (Note that additional geotechnical or engineering site-scale investigations should be conducted prior to development.)

The sewage lagoon case study site is located on the floodplain of the Pelly River, and is therefore classified as having high hazard risk due to the potential for flooding in the area. There is also a risk of erosion along river banks. Permafrost distribution at this site was variable and reflects patterns of landscape disturbance. For example, where vegetative cover has been removed (e.g., northwest of the largest lagoon), the ground was unfrozen to at least 25 m. In contrast, permafrost 15-20 m thick was present in the forest between the lagoons and the river. No risk of hazards in response to permafrost degradation is expected in disturbed areas, but in areas where permafrost is present, there is a moderate risk of settlement due to permafrost degradation in response to disturbance. Notably, because the material used to construct the sewage lagoons is fine-grained till with low hydraulic conductivity, the risk of lagoon leak in response to permafrost degradation is low. Regardless, this site has been ranked as having high hazard risk due to the risk of flooding by the Pelly River.

In the Douglas Drive/Yates Crescent area, local polygons were ranked as having either low or moderate hazard risk. Deforested areas (e.g., polygon 109) did not contain permafrost, and are therefore at low risk for hazards associated with permafrost degradation. In forested areas (e.g., polygon 123), ice-poor permafrost with a low to moderate settlement potential was detected. No notable geological hazards were detected in the area, although community members reported seepage south of Douglas Drive in the spring. It is possible that groundwater flow in the area could affect permafrost by heat advection, contributing to accelerated degradation in response to disturbance. Local water movement could also increase erosion potential and risk of mass movement. As a result, deforested areas with no permafrost were given a low risk ranking, while forested areas with permafrost and groundwater movement and/or seepage were given a moderate hazard risk ranking.

The area around Del Van Gorder School and the baseball diamond has been ranked as having moderate hazard risk. Glaciofluvial and glaciolacustrine sediments in the area include interbedded sand and silt, which can be vulnerable to settlement as a result of permafrost thaw. In addition, low-lying areas (like the baseball diamond) contain deposits that are fine-grained, wet, and organic-rich, which likely contributed to the growth of ice-rich permafrost in the past. Notably, permafrost at this site is deeper than previously published values (30-40 m, rather than 10 m, as reported by EBA (1981)). Considerable permafrost degradation has already occurred in this area (e.g., visible as taliks in geophysical profiles, noted in the relatively shallow depth to the top of permafrost, and the observed settlement-induced damage in the school and parking lot), likely in response to the removal of vegetation as part of development. Given the amount of frozen ground still present at this site, it is likely that permafrost degradation at this location will continue for decades.

North of the Pelly River, a few notable areas have been given a high hazard risk ranking. Polygon 11 contained two lakes that have receded over time, and ice accumulation is probable in the paleo shorelines, resulting in a high risk of hazards associated with permafrost degradation. Polygons in the vicinity of the slope failure near the former ski hill (e.g., polygons 89, 97-99, 101-105) have also been ranked as having high hazard risk due to slope movement, debris flows, landslides, ice-rich permafrost, and thermokarst. Risk is particularly high on south-facing, till-blanketed slopes where ice is present, and can be compounded by the presence of moving water (e.g., springs). Sinuous polygons such as 42, 92, 106 and 119 represent depressions between drumlins, where risk of permafrost degradation and poor drainage are notable.

Large swaths of the northern part of the map area are ranked as having low risk of hazards. These are composed mainly of morainal material (e.g., polygons 36 and 40) or glaciofluvial deposits (polygons 88 and 100), which do not present notable permafrost degradation, geological or flood-related hazards.

It is important to note that no matter the classification, all future development projects must be preceded by thorough engineering investigations prior to construction. The higher the hazard-risk ranking, the more notable and potentially problematic hazard risks at this site will likely be. Nonetheless, a moderate or high hazard risk ranking does not preclude the possibility of development, should suitable engineering and mitigation techniques be employed. Appendix F describes the types of foundation techniques that may be suitable for buildings in permafrost environments similar to those found in Faro, and may assist in mitigating permafrost thaw.

GENERATING ACTION FROM SCIENCE

The knowledge and data generated by the Faro hazards mapping project can be used to inform planning and policy development and establish a baseline from which future science can be generated. It is the hope of the authors that the information contained herein informs planning and decision-making processes in the Faro area.

This project has contributed to the assessment of vulnerability for the Faro area. In particular, this project has characterized the local landscape and assessed local hazards, while advancing our understanding of potential climate change impacts in the region. This information may serve as a basis for evaluating how community infrastructure, security and well-being may be influenced by climate variability, and how the community might take action to respond. By integrating variability into decision-making through multiple scenarios, robust and responsive adaptation strategies can be developed. In this way, the science of hazard assessment is an important foundation from which to build action.

REFERENCES

- Beierle, B. and Bond, J.D., 2002. Density-induced settling of tephra through organic lake sediments. *Journal of Paleolimnology*, vol. 28, p. 433-440.
- Bond, J.D., 1999a. McConnell ice-flow map of the Anvil District (105K), central Yukon (1:250 000). Exploration and Geological Services Division, Yukon Region, Indian and Northern Affairs, Canada, Open File 1999-14.
- Bond, J.D., 1999b. The Quaternary history and till geochemistry of the Anvil District, east-central Yukon. *In: Yukon Exploration and Geology 1998*, C.F. Roots and D.S. Emond (eds.), Exploration and Geological Services Division, Yukon, Indian and Northern Affairs Canada, p. 105-116.
- Bond, J.D., 2001. Quaternary geology and till geochemistry of the Anvil district (parts of 105K/2, 3, 5, 6 and 7), central Yukon Territory. Exploration and Geological Services Division, Yukon, Indian and Northern Affairs Canada, Bulletin 11, 39 p.
- Bond, J.D. and Kennedy, K.E., 2005. Late Wisconsinan McConnell ice-flow and sediment distribution patterns in the Pelly Mountains, Yukon. *In: Yukon Exploration and Geology 2004*, D.S. Emond, L.L. Lewis and G.D. Bradshaw (eds.), Yukon Geological Survey, p. 65-82.
- Bonnaventure, P.P., Lewkowicz, A.G., Kremer, M. and Sawada, M., 2012. A regional permafrost probability model for the southern Yukon and northern British Columbia, Canada. *Permafrost and Periglacial Processes*, vol. 23, p. 52-68, doi:10.1002/ppp.1733.
- Brown, R.J.E., 1963. Influence of vegetation on permafrost. First International Conference on Permafrost, Lafayette, PA, November 1963.
- Brown, R.J.E. and Péwé, T.L., 1973. Distribution of permafrost in North America and its relationship to the environment: A review, 1963-1973. Second International Conference on Permafrost, Yakutsk, USSR, July 1973.
- Burn, C.R., 1994. Permafrost, tectonics, and past and future regional climate change, Yukon and adjacent Northwest Territories. *Canadian Journal of Earth Sciences*, vol. 31, p. 182-191.
- Clague, J.J., Evans, S.G., Rampton, V.N. and Woodsworth, G.J., 1995. Improved age estimates for the White River and Bridge River tephtras, western Canada. *Canadian Journal of Earth Sciences*, vol. 32, p. 1172-1179.
- Colpron, M. (compiler), 2015. Update of the Yukon bedrock geology map. Yukon Geological Survey, January 16, 2015 version. [http://www.geology.gov.yk.ca/update_yukon_bedrock_geology_map.html]. Accessed February, 2015.
- Consortium for Climate Risk in the Urban Northeast (CCRUN), 2011. What methods do scientists use to make projections about future climate change and its impacts? CCRUN, Fact Sheet #4, Columbia University, New York, NY, 3 p. [http://ccrun.org/ccrun_files/attached_files/FactSheet4.pdf]. Accessed September, 2014.
- Darrow, M.M., Huang, S.L., Shur, Y. and Akagawa, S., 2008. Improvements in frost heave laboratory testing of fine-grained soils. *Journal of Cold Regions Engineering*, vol. 22, p. 65-78.

- Duk-Rodkin, A., Barendregt, R.W. and White, J.M., 2010. An extensive late Cenozoic terrestrial record of multiple glaciations preserved in the Tintina Trench of west-central Yukon: Stratigraphy, paleomagnetism, paleosols, and pollen. *Canadian Journal of Earth Sciences*, vol. 47, p. 1003-1028.
- EBA Engineering Consultants Ltd., 1981. Geotechnical evaluation, proposed 1981 trailer park, Faro, Yukon. Report to Department of Municipal and Community Affairs, Yukon Territorial Government, 12 p.
- Environment Canada, 2014a. Historical Climate Data. Environment Canada, Ottawa, Ontario. [http://climate.weather.gc.ca/index_e.html]. Accessed January, 2015.
- Environment Canada, 2014b. Climate Trends and Variations. Environment Canada, Ottawa, Ontario. [<http://ec.gc.ca/adsc-cmda/default.asp?lang=En&n=F3D25729-1>]. Accessed January, 2015.
- Environmental Mining Council of British Columbia, 2001. Mining in Remote Areas: Issues and Impacts. A Community Primer. MiningWatch Canada, Victoria, BC, 34 p.
- Environment Yukon, 1976. Groundwater Information Network water well 211030018. [<http://gw-info.net/>; http://ngwd-bdnes.cits.nrcan.gc.ca/service/gin/wfs/gin?REQUEST=GetFeature&INFO_FORMAT=text/html&FID=yk.ww.211030018]. Accessed February, 2015.
- Environment Yukon, 1990. Groundwater Information Network water well 211030017. [<http://gw-info.net/>; http://ngwd-bdnes.cits.nrcan.gc.ca/service/gin/wfs/gin?REQUEST=GetFeature&INFO_FORMAT=text/html&FID=yk.ww.211030017]. Accessed February, 2015.
- Faro Mine Remediation Project, 2011a. A Detailed History of the Faro Mine Complex. [<http://www.faromine.ca/assets/files/history.pdf>]. Accessed December, 2014.
- Faro Mine Remediation Project, 2011b. Faro Mine: General Information. [<http://www.faromine.ca/mine/general.html>]. Accessed December, 2014.
- French, H., 2007. *The Periglacial Environment*, 3rd edition. John Wiley and Sons, West Sussex, England, 478 p.
- French, H. and Shur, Y., 2010. The principles of cryostratigraphy. *Earth Science Reviews*, vol. 101, p. 190-206.
- Froese, D.G., Barendregt, R.W., Enkin, R.J. and Baker, J., 2000. Paleomagnetic evidence for multiple Late Pliocene – Early Pleistocene glaciations in the Klondike area, Yukon Territory. *Canadian Journal of Earth Sciences*, vol. 37, p. 863-877.
- Gabrielse, H., Murphy, D.C. and Mortensen, J.K., 2006. Cretaceous and Cenozoic dextral orogen-parallel displacements, magmatism and paleogeography, north-central Canadian Cordillera. *In*: J.W. Haggart, J.W.H. Monger and R. Enkin (eds.), *Paleogeography of the North American Cordillera: Evidence for and against large-scale displacements*, Geological Association of Canada, Special Paper 46, p. 255-276.
- Gartner Lee Limited, 2003. Yukon Groundwater and Ground Source Heat Potential Inventory. Prepared for Energy Solutions Centre Inc., Report #GLL 22-680, 258 p.
- Gordey, S.P. and Irwin, S.E.B., 1987. Geology, Sheldon Lake and Tay River map areas, Yukon Territory. Geological Survey of Canada, Map 19-1987 (3 sheets) (1:250 000 scale).

- Gordey, S.P., 2013a. Geology, Selwyn Basin (Tay River), Yukon. Geological Survey of Canada, Map 2149A, Sheet 2, scale 1:250 000.
- Gordey, S.P., 2013b. Geology, Selwyn Basin, Yukon. Geological Survey of Canada, Bulletin 599, 5 sheets and 190 p.
- Hauck, C., Isaksen, K., Vonder Mühll, D. and Sollid, J.L., 2004. Geophysical surveys designed to delineate the altitudinal limit of mountain permafrost: An example from Jotunheimen, Norway. *Permafrost and Periglacial Processes*, vol. 15, p. 191-205, doi:10.1002/ppp.493.
- Hidy, A., Gosse, J.C., Froese, D.G., Bond, J.D. and Rood, D.H., 2013. A latest Pliocene age for the earliest and most extensive Cordilleran Ice Sheet in northwestern Canada. *Quaternary Science Reviews*, vol. 61, p. 77-84.
- Hilbich, C., Hauck, C., Hoelzle, M., Scherler, M., Schudel, L., Voelksch, I., Vonder Muehll, D. and Mausbacher, R., 2008. Monitoring mountain permafrost evolution using electrical resistivity tomography: A 7-year study of seasonal, annual, and long-term variations at Schilthorn, Swiss Alps. *Journal of Geophysical Research-Earth Surface*, vol. 113, F01S90, doi:10.1029/2007JF000799.
- Hilbich, C., Maescot, L., Hauck, C., Loke, M.H. and Mausbacher, R., 2009. Applicability of electrical resistivity tomography monitoring to coarse blocky and ice-rich permafrost landforms. *Permafrost and Periglacial Processes*, vol. 20, p. 269-284, doi:10.1002/ppp.652.
- Hoggan Engineering and Testing (1980), 1989. Geotechnical investigation, Ross River roads and sanitary sewer development, Ross River, Yukon Territory. Report to Department of Community and Transportation Services, Yukon Territorial Government, Whitehorse, Yukon, 11 p.
- Huntington, H. and Weller, G., 2005. Chapter 1: An Introduction to the Arctic Climate Impact Assessment. *In: Arctic Climate Impact Assessment Scientific Report*, C. Symo, L. Arris and B. Heal (eds.), Cambridge University Press, p. 1-20.
- Instanes, A., 2003. Climate change and possible impacts on Arctic infrastructure. *Proceedings of the Eighth International Conference on Permafrost*, Zurich, Switzerland, June 2003, p. 461-466.
- Intergovernmental Panel on Climate Change (IPCC), 2015. Fifth Assessment Report. IPCC, Geneva, Switzerland. [<https://www.ipcc.ch/index.htm>]. Accessed January, 2015.
- Jackson, L.E., Jr., 1989. Paleogeology of the Selwyn Lobe of the Cordilleran Ice Sheet and Quaternary stratigraphy of east-central Yukon. *In: Late Cenozoic History of the Interior basins of Alaska and the Yukon*, L.D. Carter, T.D. Hamilton and J.P. Galloway (eds.), U.S. Geological Survey, Circular 1026, p. 60-65.
- Jackson, L.E., Jr., 1994. Terrain inventory and Quaternary history of the Pelly River area (105 F, G, J, K), Yukon Territory. Geological Survey of Canada, Memoir 437, 41 p.
- Jackson, L.E., Jr. and Harington, C.R., 1991. Pleistocene mammals, stratigraphy, and sedimentology at the Ketza River site, Yukon Territory. *Géographie Physique et Quaternaire*, vol. 45, p. 69-77.
- Jackson, L.E., Jr., Ward, B., Duk-Rodkin, A. and Hughes, O., 1991. The latest Cordilleran ice sheet in southern Yukon Territory. *Géographie Physique et Quaternaire*, vol. 45, p. 341-354.

- Janke, J.R., 2005. Modelling past and future alpine permafrost distribution in the Colorado Front Range. *Earth Surface Processes and Landforms*, vol. 30, p. 1495-1508, doi: 10.1002/esp.1205.
- Janowicz, R., 2008. Apparent recent trends in hydrologic response in permafrost regions of northwest Canada. *Hydrology Research*, vol. 39, p. 267-275.
- Jensen, B.J., Pyne-O'Donnell, S., Plunkett, G., Froese, D.G., Hughes, P.D., Sigl, M., McConnell, J.R., Amesbury, M.J., Blackwell, P.G., van den Bogaard, C., Buck, C.E., Charman, D.J., Clague, J.J., Hall, V.A., Koch, J., Mackay, H., Mallon, G., McColl, L. and Pilcher, J.R., 2014. Transatlantic distribution of the Alaskan White River Ash. *Geology*, vol. 42, no. 10, p. 875-878.
- Jorgenson, M.T. and Osterkamp, T.E., 2005. Response of boreal ecosystems to varying modes of permafrost degradation. *Canadian Journal of Forest Research*, vol. 35, p. 2100-2111.
- Kneisel, C., Hauck, C. and Vonder Mühl, D., 2000. Permafrost below the timberline confirmed and characterized by geoelectrical resistivity measurements, Bever Valley, eastern Swiss Alps. *Permafrost and Periglacial Processes*, vol. 11, p. 295-304, doi:10.1002/1099-1530(200012)11:4<295::AID-PPP353>3.0.CO;2-L.
- Kneisel, C., Hauck, C., Fortier, R. and Moorman, B., 2008. Advances in geophysical methods for permafrost investigations. *Permafrost and Periglacial Processes*, vol. 19, p. 157-178.
- Lerbekmo, J.F., 2008. The White River Ash: Largest Holocene Plinian tephra. *Canadian Journal of Earth Sciences*, vol. 45, p. 693-700.
- Lerbekmo, J.F. and Campbell, F.A., 1969. Distribution, composition and source of the White River Ash, Yukon Territory. *Canadian Journal of Earth Sciences*, vol. 6, p. 109-116.
- Lewkowicz, A.G. and Bonnaventure, P.P., 2011. Equivalent elevation: A method to incorporate variable lapse rates into mountain permafrost modeling. *Permafrost and Periglacial Processes*, vol. 22, p. 153-162, doi: 10.1002/ppp.720, 2011.
- Lewkowicz, A.G. and Ednie, M., 2004. Probability mapping of mountain permafrost using the BTS method, Wolf Creek, Yukon Territory, Canada. *Permafrost and Periglacial Processes*, vol. 15, p. 67-80.
- Lewkowicz, A.G., Etzelmüller, B. and Smith, S.L., 2011. Characteristics of discontinuous permafrost from ground temperature measurements and electrical resistivity tomography, southern Yukon, Canada. *Permafrost and Periglacial Processes*, vol. 22, p. 320-342, doi: 10.1002/ppp.703, 2011.
- Lipovsky, P.S., 2015. Summary of Yukon Geological Survey permafrost monitoring network results, 2008-2013. *In: Yukon Exploration and Geology 2014*, K.E. MacFarlane, M.G. Nordling and P.J. Sack (eds.), Yukon Geological Survey, p. 113-122.
- Lipovsky, P.S. and Huscroft, C., 2007. A reconnaissance inventory of permafrost-related landslides in the Pelly River watershed, central Yukon. *In: Yukon Exploration and Geology 2006*, D.S. Emond, L.L. Lewis and L.H. Weston (eds.), Yukon Geological Survey, p. 181-195.
- Lipovsky, P.S. and Yoshikawa, K., 2009. Initial results from the first year of the Permafrost Outreach Program, Yukon, Canada. *In: Yukon Exploration and Geology 2008*, L.H. Weston, L.R. Blackburn and L.L. Lewis (eds.), Yukon Geological Survey, p. 161-172.

- Lipovsky, P.S., Coates, J., Lewkowicz, A.G. and Trochim, E., 2006. Active-layer detachments following the summer 2004 forest fires near Dawson City, Yukon. *In: Yukon Exploration and Geology 2005*, D.S. Emond, G.D. Bradshaw, L.L. Lewis and L.H. Weston (eds.), Yukon Geological Survey, p. 175-194.
- Lunardini, V.J., 1994. Heterogenetic and syngenetic growth of permafrost. Ground Freezing '94, Proceedings of the Seventh International Symposium on Ground Freezing, Nancy, France, p. 361-373.
- Mathews, W.H., 1986. Physiographic map of the Canadian Cordillera. Geological Survey of Canada, Map 1701A, scale 1:5 000 000.
- MiningWatch Canada, 2001. Mining in Remote Areas: Issues and Impacts. Produced by Environmental Mining Council of British Columbia. [http://www.miningwatch.ca/files/mine_impacts_kit_0.pdf]. Accessed December, 2014.
- Murton, J.B. and French, H.M., 1994. Cryostructures in permafrost, Tuktoyaktuk coastlands, western arctic Canada. *Canadian Journal of Earth Sciences*, vol. 31, no. 4, p. 737-747.
- Natural Resources Canada, 2010. Simplified seismic hazard map for Canada. [<http://www.earthquakescanada.nrcan.gc.ca/hazard-alea/simphaz-eng.php>]. Accessed December, 2014.
- Nebojša, N., Davidson, O., Davis, G., Grübler, A., Kram, T., La Rovere, E.L., Metz, B., Morita, T., Pepper, W., Pitcher, H., Sankovski, A., Shukla, P., Swart, R., Watson, R. and Dadi, Z., 2000. Emissions Scenarios: A Special Report of Working Group III of Intergovernmental Panel on Climate Change. Intergovernmental Panel on Climate Change, Geneva, Switzerland, 27 p.
- Nelson, F.E., Anisimov, O.A. and Shiklomanov, N.I., 2002. Climate change and hazard zonation in the circum-Arctic permafrost regions. *Natural Hazards*, vol. 26, p. 203-225.
- Northern Climate ExChange (NCE), 2011. Mayo Landscape Hazards: Geological Mapping for Climate Change Adaptation Planning. Yukon Research Centre, Yukon College, Whitehorse, YT, 64 p.
- Noson, L., 2002. Hazard Mapping and Risk Assessment. *In: Regional Workshop on Best Practices in Disaster Mitigation*, Bali, Indonesia, September 24-26, 2002; Asian Disaster Preparedness Center (ADPAC), p. 69-94.
- O'Donnell, J.A., Jorgenson, M.T., Harden, J.W., McGuire, A.D., Kanevskiy, M.Z. and Wickland, K.P., 2012. The effects of permafrost thaw on soil hydrologic, thermal and carbon dynamics in an Alaskan peatland. *Ecosystems*, vol. 15, p. 213-229.
- Pigage, L.C., 2004a. Geological Map of Anvil District, Yukon (1:100 000 scale). Yukon Geological Survey, Geoscience Map 2004-2.
- Pigage, L., 2004b. Bedrock geology compilation of the Anvil District (parts of NTS 105K/2, 3, 5, 6, 7 and 11), central Yukon. Yukon Geological Survey, Bulletin 15, 103 p.
- Plouffe, A., 1989. Drift prospecting and till geochemistry in Tintina Trench, southeastern Yukon. MSc thesis, Department of Earth Sciences, Carleton University, 81 p.
- Roddick, J.A., 1967. Tintina Trench. *Journal of Geology*, vol. 75, p. 23-32.
- Scenarios Network for Alaska and Arctic Planning (SNAP), 2013. [<http://www.snap.uaf.edu/about.php>]. Accessed September, 2014.

- Shur, Y.L. and Jorgenson, M.T., 2007. Patterns of permafrost formation and degradation in relation to climate and ecosystems. *Permafrost Periglacial Processes*, vol. 18, doi:10.1002/lppp. 582.
- Smith, M.W. and Riseborough, D.W., 2002. Climate and the limits of permafrost: A zonal analysis. *Permafrost and Periglacial Processes*, vol. 13, p. 1-15.
- Smith, C.A.S., Meikle, J.C. and Roots, C.F. (editors), 2004. *Ecoregions of the Yukon Territory: Biophysical properties of Yukon landscapes*. Agriculture and Agri-Food Canada, PARC Technical Bulletin No. 04-01, Summerland, British Columbia, 313 p.
- Stephani, E., Fortier, D. and Shur, Y., 2010. Applications of cryofacies approach to frozen ground engineering – Case study of a road test site along the Alaska Highway (Beaver Creek, Yukon, Canada). *GEO2010: 63rd Canadian Geotechnical Conference and 6th Canadian Permafrost Conference*, Calgary, Canada.
- Stephani, E., Fortier, D., Shur, Y., Fortier, R., Doré, G. and Walsh, R., 2014. A geosystems approach to permafrost investigations for engineering applications, an example from a road stabilization experiment, Beaver Creek, Yukon, Canada. *Cold Region Science and Technology*, vol. 100, p. 20-35.
- Tempelman-Kluit, D., 1980. Evolution of physiography and drainage in southern Yukon. *Canadian Journal of Earth Sciences*, vol. 17, no. 9, p. 1189-1203.
- Town of Faro, 2014. History of Faro. [<http://www.faroyukon.ca/about-faro/history-of-faro/history-of-faro.cfm>]. Accessed December, 2014.
- Turner, D.G., Bond, J.D. and Lipovsky, P.S., 2014. Surficial geology, Faro region, Yukon, parts of NTS 105K/3, 4, 5 & 6 (1:25 000 scale). Yukon Geological Survey, Energy, Mines and Resources, Government of Yukon, Open File 2014-14.
- Wahl, H.E., Fraser, D.B., Harvey, R.C. and Maxwell, J.B., 1987. *Climate of Yukon*. Climatological Studies Number 40. Ottawa, Ontario: Atmospheric Environment Service, Environment Canada, 233 p.
- Ward, B.C., 1989. Quaternary stratigraphy along Pelly River in Glenlyon and Carmacks map areas, Yukon Territory. *In: Current Research, Part E*. Geological Survey of Canada, Paper 89-1E, p. 257-264.
- Ward, B.C. and Jackson, L.E., Jr., 2000. Surficial geology of the Glenlyon map area, Yukon Territory. Geological Survey of Canada, Bulletin 559, 60 p.
- Warren, F.J. and Lemmen, D.S. (eds.), 2014. *Canada in a Changing Climate: Sector Perspectives on Impacts and Adaptation*. Government of Canada, Ottawa, ON, 286 p.
- Water Resources Branch, 2010. Yukon Water Well Registry. Yukon Department of Environment, Government of Yukon, Water Resources Branch. [<http://www.environmentyukon.gov.yk.ca/pdf/YukonWaterWellsSummary.pdf>]. Accessed January, 2015.
- Water Survey of Canada, 2015. National Water Quantity Survey Program. Environment Canada, [<https://wateroffice.ec.gc.ca>]. Accessed January, 2015.
- Weinstein, M.S., 1992. Just Like People Get Lost: A Retrospective Assessment of the Impacts of the Faro Mining Development on the Land Use of the Ross River Indian People. Report prepared for the Ross River Dena Council, Ross River, YT, 193 p.

- Yoshikawa, K., Bolton, W.R., Romanovsky, V.E., Fukuda, M. and Hinzman, L.D., 2003. Impacts of wildfire on the permafrost in the boreal forests of Interior Alaska. *Journal of Geophysics*, vol. 108, doi:10.1029.2001JD000438.
- Yukon Bureau of Statistics (YBS), 2010. Government of Yukon Socio-Economic and Web Portal – Faro: Housing Tenure, Condition, Period of Construction and Structural Type Census 2006. [http://www.sewp.gov.yk.ca/data?regionId=YK.RR&subjectId=POPCOM&groupId=POPCOM.DWELL&dataId=CENSUS_2006_DWELLINGS&tab=region]. Accessed December, 2014.
- Yukon Bureau of Statistics (YBS), 2011. Government of Yukon Socio-Economic Web Portal. [http://sewp.gov.yk.ca/data?regionId=YK.FO&subjectId=POPCOM&groupId=POPCOM.POP&dataId=NHS_2011_VIS_MINORITY&tab=region]. Accessed December, 2014.
- Yukon Environment Geomatics, 2012. Traditional Territories of Yukon First Nations and Settlement Areas of Inuvialuit and Tetlit Gwich'in. [http://www.env.gov.yk.ca/animals-habitat/documents/traditional_territories_map.pdf]. Accessed December, 2014.

APPENDIX A - APPROACH AND METHODS

SURFICIAL GEOLOGY

Surficial geology is the study of unconsolidated material (i.e., the surficial material that overlies bedrock) on the Earth's surface, including all sediments and soils. These sediments may be deposited through a variety of different processes including glacial (deposited directly out of glacial ice); glaciofluvial (formed by glacial rivers and streams); colluvial (deposited on or at the base of hillslopes by gravity); fluvial (river and stream deposits); lacustrine (lake deposits); and eolian (wind deposits). Additionally, organic deposits can accumulate either over bedrock or over unconsolidated material, particularly in low-lying areas.

Surficial geology mapping involves a combination of aerial photograph interpretation and field work. The maps provide information on the physical properties and characteristics (e.g., texture or grain size) of the surface sediments, the morphology (shape) of the landforms produced, the genesis or origin of the landforms (the past environment in which the landform was produced), and identifies any geomorphological processes that may have significantly modified those materials (e.g. landslides, gulying, or permafrost). In the process of mapping the surficial geology, the distribution of permafrost is also captured, making these maps an essential part of the hazards assessment process.

Previous mapping of surficial geology within the study area was completed by Jackson (1993) at a scale of 1:100 000, and Bond (1999a,b) north of the Pelly River, at a scale of 1:25 000. The focus of the new 1:25 000-scale mapping conducted for this project was to provide more detailed unit descriptions of the surficial geology south of the Pelly River, and surrounding the town of Faro. An open file map displaying the results of this new work was released by Yukon Geological Survey in 2014 (Turner, 2014) and accompanies this report.

Map units were interpreted using remote predictive mapping following the Yukon Terrain Classification System, a variation of the British Columbia Terrain Classification System (Howes and Kenk, 1997). Remote predictive mapping was completed by viewing 1:40 000 and 1:50 000-scale digital monochrome aerial photographs from 1989 and 2004 with PurVIEW v2.0 3D stereo viewing software in ArcGIS 10.1.

Surficial geological mapping fieldwork was completed in September 2013 and 2014. Mapped polygons were field checked at 79 locations by foot, truck and helicopter traverses. Some of these sites corresponded to areas targeted for subsequent permafrost investigation. Field checking of units was completed by documenting road and stream-cut exposures of surficial materials, and by digging soil pits (up to ~1 m depth) in a broad range of materials and landforms. Stratigraphic relationships were also examined at four sites in areas that had not previously been described by Jackson (1993).

Other new data incorporated in the surficial mapping includes geophysical profiles of the subsurface (using Ground Penetrating Radar (GPR) and Electrical Resistivity Tomography (ERT)) and shallow boreholes. Previously acquired subsurface geological data was made available from borehole, test pits, and water well logs provided by EBA Engineering Consultants Ltd. (R. Trimble, Tetra Tech EBA, pers. comm., 2010).

PERMAFROST

GROUND-PENETRATING RADAR

Ground-penetrating radar (GPR) is a non-invasive method used to identify subsurface features such as stratigraphic boundaries, permafrost, and other anomalies using electromagnetic fields. For this project, GPR was used to gain a two dimensional image below the ground surface. Two GPR systems were used for field investigations. A TerraSIRch Subsurface Interface Radar (SIR) System 3000® with a shielded 200-MHz antenna (Geophysical Survey Systems, Inc. (GSSI)) was employed for shallow profiles (maximum 3 m penetration depth). The collection parameters for the SIR-3000 control unit were set to record at 64 scans per second, with a dielectric constant set at 13, which corresponds to a penetration speed of 0.0914 m/ns to 0.1 m/ns, depending on the ground type. The GPR antenna was hand-towed along the survey line. For deeper profiles (maximum 8 m penetration depth) and for sites located in rough terrain, a Pulse Ekko Pro system with 50 MHz antennas was used. The antennas were moved manually with a separation of 2 m and a step size of 0.5 m. The penetration speed used for this system was between 0.1 and 0.11 m/ns, depending on the ground type.

Where possible, the GPR transects were situated adjacent to sections of the electrical resistivity tomographic profiles and boreholes; site conditions were described in detail. This enabled a comparison of the results from the three techniques and to verify the findings.

Post collection data processing was conducted using RADAN™ (Version 7, GSSI) and Ekko_Project 2 software and applied to all of the profiles. Processing of the GPR data included the following: the correction of the initial pulse to time-zero to ensure that the first reflection is from the ground surface and the subsequent reflections are from deeper below the ground surface; correction of the penetration depth with a common midpoint method or with borehole information; topographic correction where required; the application of a FIR boxcar filter to remove background horizontal noise where required; and the use of range gain adjustments to recover lower-amplitude waves from reflections deeper in the ground (Conyers, 2004). Overall, the processing procedures were employed to reduce signal attenuation with depth, as well as improve the continuity of stratigraphic reflections and the signal-to-noise ratio.

ELECTRICAL RESISTIVITY

Electrical Resistivity Tomography (ERT) profiling is a geophysical technique that measures variations in the ability of the ground to conduct electricity along a transect, producing a two-dimensional image of changes in electrical conductance. In permafrost areas, variations in conductance relate mainly to the changes in frozen versus thawed ground, because water and ice serve as good and poor conductors of electricity, respectively.

ERT profiling has been used extensively to investigate mountain permafrost in Europe (e.g., Kneisel et al., 2000, 2008; Hauck et al., 2004; Hilbich et al., 2008, 2009) and is growing in importance in North America as a technique for permafrost investigations in both mountains and lowlands (e.g., Lewkowicz et al., 2011; Miceli, 2012). ERT is regarded as one of the best methods to examine changes in frozen ground conditions over short distances, such as in areas underlain by discontinuous permafrost.

Many ERT profiles show very clear distinctions relating to frozen ground conditions which can be correlated to surface changes in drainage, vegetation cover, or land use (Lewkowicz et al., 2011). However, like all geophysical techniques, confidence in the interpretation increases where complementary information is available; this may include data from borehole logs, observations

of natural exposures, ground temperature measurements, probing of the active layer, or other geophysical techniques such as ground penetrating radar.

There is a major difference in the resistivity of water and ice, but there is not always a sharp line between the phase of water in soil pores (frozen or unfrozen) at temperatures above and below 0°C. Instead, percentages of unfrozen moisture gradually increase in the pores of frozen soils (especially in fine-grained soils such as silts and clays) as their temperatures approach 0°C. Consequently, the difference in the electrical resistivity of frozen and unfrozen soils can be gradational rather than sharp (Lewkowicz et al., 2011). In addition, because there can be differences in the porewater salinity and in the conductance of the soil minerals it is not possible to identify a single universal threshold resistivity value below which soils are definitely unfrozen and above which soils are definitely frozen. However, given the scale of the case study sites examined in this project, a threshold value unique to each case study site was determined based on site characteristics and other ground-truthing approaches (e.g., permafrost drilling).

The ERT profiling included in this report was undertaken in September 2013 and 2014, when the active layer (i.e., depth from ground surface to the top of permafrost) was at its thickest. The equipment used was an ABEM Terrameter LS profiling system with the electrode array (stainless steel pins) inserted into the ground in a Wenner configuration. The electricity entering the ground builds up an image of its resistivity along a profile whose depth depends on the spread of the array of electrodes (25 m for an array 160 m in length and 8 m for a 40-m array). The penetration depth remains at 25 m, even if surveys longer than 160 m are created using a roll-along technique. Eight ERT profiles were completed.

Each ERT site was described in terms of vegetation and other salient features. UTM co-ordinates (relative to the WGS 84 datum) were taken using a hand-held Garmin Etrex Vista GPS. Relative variations in elevation along the individual profiles were measured in the field using an abney level and are expected to have accuracies of ± 1 m.

Resistivity profiles were topographically corrected using the abney level surveys. The actual elevations shown on the surveys are approximate. Measured resistivity data were processed with RES2DINV software (Loke and Barker, 1996) using a robust inversion that can respond to the rapid transitions and high contrasts in resistivity (Loke et al., 2003) that occur between frozen and unfrozen ground. A reversed colour scheme was used to portray the profiles so that blue represents high resistivities (generally indicative of frozen soils) and red represents low resistivities (ice-poor or unfrozen soils). All the resistivity profiles use the same scale to allow for inter-site comparison.

There is no single model that fits the observed resistivities. Instead, the modelled results converge by iteration with the measured values. The choice of when to stop iteration in the RES2DINV software is made by the operator. Too few iterations leads to large Root Mean Square (RMS) errors (i.e., the model does not fit the measurements). Too many iterations can result in model 'over-fit' in which the broad patterns are lost. Analyses for this study were stopped after the 4th iteration as RMS errors were all very low (less than 5%) by that point. The profiles are presented with a linear depth scale and no vertical exaggeration. ERT profiles were interpreted in conjunction with the results of frost probing along the profiles, field descriptions of vegetation cover at the site, GPR surveys, borehole and laboratory analyses undertaken by the research team, and surficial mapping.

DRILLING AND SAMPLE COLLECTION

The drilling program was carried out in September 2013 and August 2014. The objective was to core and collect permafrost samples from predetermined study sites. These sites were selected in advance through a desktop interpretation based on available maps, aerial photos, satellite images

and consultation with community members. The drilling and coring operations required the use of four different drills to account for changes in subsurface conditions: two core-drills (a modified GÖLZ™ portable core-drill system and a modified Winkie core-drill system), one auger drill, and one hand auger.

The GÖLZ™ portable core-drill system (Figure A1) is a light hand core-drill with a high rotation speed (600 rpm) that can be controlled by two people, and is therefore used with minimal impact on the environment. Stainless steel rods measuring 1 m in length and 4.5 cm in diameter, and a core barrel 40 cm long and 10 cm in diameter were used, making it possible to drill up to 5 m into unconsolidated, fine to medium grained material (sand to clay). A core catcher was used to extract the frozen core out of the borehole, which allows for continuous undisturbed permafrost sampling.



Figure A1. Photograph of the GÖLZ™ portable Earth-drill system used for permafrost coring.



Figure A2. Photograph of the Winkie drill, used for permafrost coring.

The Winkie drill is a gas-powered core-drill with a two-speed transmission made for bedrock drilling; this drill has been modified for permafrost drilling in unconsolidated material using a gearbox that lowers the speed to approximately 1200 rpm. Although it is not as mobile as the GÖLZ™ portable core-drill system, it is one of the lightest shift drills on the market (see Figure A2, above) and has the potential to go down to 30 m in ice-rich, fine-grained material. The Winkie drill was used with aluminum rods (0.9 and 1.5 m long; Figure A3) and core barrels 10.8 cm in diameter.

The auger drill is equipped with a Honda GVX160 (144 rpm) motor and flight auger extensions with diameters of 5-46 cm (Figure A4). This drill is destructive and is used to pass through unfrozen sediments of the active layer allowing for bulk ‘grab’ samples. This type of auger is also useful in retrieving deposits of gravel containing clasts that are cobble to boulder sized at the bottom of a borehole.

The hand auger is used to sample the thawed active layer; it has a 10.2 cm-diameter sampling core barrel, and three 1 m-long extension rods (Figure A5). It is ideal for sampling near-surface,

fine-grained, unfrozen soil (e.g., clay, silt, sand and fine gravel containing pebbles with a maximum diameter of 25 mm).



Figure A3. Photograph of aluminum rods used for the Winkie drill for permafrost coring.



Figure A4. Photograph of the Honda drill, used for permafrost coring.



Figure A5. Photograph of the hand auger, used for permafrost coring.

Using a combination of these drills, boreholes were drilled along ERT and GPR profiles in representative areas (e.g., forested areas, open fields) or in an area belonging to a particular surficial geology unit. For each borehole, the same sampling and drilling procedures were followed. The site was first described (e.g., hydrology, vegetation type and density, and topography), photos were taken, and locations were recorded using a handheld GPS. The boreholes were initiated using a hand auger if the ground was soft or an auger drill if the ground was gravelly or compacted. As soon as the permafrost table was reached, the GÖLZ™ portable core-drill system was used. For specific locations where maximum depth was desired, the Winkie core-drill was used.

A sample of every unfrozen layer was collected from each borehole. Each sample was photographed and described in situ (e.g., soil type, soil moisture, presence or absence of organic matter, any particularities). The sample was identified with the borehole name and depth and placed in doubled hermetic Ziploc bags for laboratory analyses. Frozen samples were also collected and described on site (Figure A6). Each core was cleaned to remove the drilling mud and photographed.



Figure A6. Photograph of the setup used for in-field core descriptions.

GEOTECHNICAL ANALYSIS OF PERMAFROST

Laboratory analyses were carried out to measure geotechnical properties of active layer and permafrost samples, and additional tests were conducted to evaluate the mechanical behavior of the permafrost upon thawing. Both soil grain characteristics and ice characteristics were evaluated. To evaluate soil grain characteristics, a grain-size analysis was performed on every sample. Additionally, plasticity index, remolded bulk density, porosity, specific gravity and thaw settlement potential were calculated for representative samples. To evaluate ice characteristics in permafrost samples, the cryostructure, volumetric ice content, gravimetric ice content and settlement potential were quantified. These methods are described below.

GRAIN-SIZE ANALYSIS

Sieve and hydrometer analysis of grain size were performed following a specifically modified American Standard and Testing Method protocol (ASTM D422-63, 2000). The sieves typically used were 4, 2, 1, 0.5, 0.25, 0.125 and 0.063 mm. A hydrometer test was performed on samples with enough fine-grained material, or on specific samples. A 40-g subsample was passed through 0.25 mm openings, and after sedimentation started, readings were taken after 0.25, 0.50, 0.75, 1, 1.5, 2, 5, 15, 30, 60, 120, 180, 300 and 1440 minutes. A total of 16 analyses were completed.

SPECIFIC GRAVITY

Specific gravity (the ratio of a solid's grain density to the density of water) was systematically measured for every sample collected, and followed the American Standard and Testing Method (ASTM D854-10, 2000). The results were used to compute the porosity of the soil (see below) for 3 types of soils.

CRYOSTRUCTURE

Cryostructure (the geometry of the ice in the permafrost) depends on water availability, as well as the soil's ice-segregation potential and the time of freezing, resulting in the development of ice structures in the soil matrix. Information such as soil genesis, climate conditions at the time of freezing, permafrost development history, and ground vulnerability when permafrost degrades can be interpreted from cryostructure, cryofacies analysis, and general cryostratigraphy.

Because field descriptions are based only on a visual interpretation of the core, the samples were re-examined in the laboratory using a standard terminology that would provide a more detailed description (Stephani et al., 2010; Murton and French, 1994). Frozen core samples were warmed to near 0°C and any refrozen mud was scrapped off prior to the description.

CONSOLIDATION TESTING

Compaction and consolidation tests were carried out at Laval University. They were measured by thawing a soil sample and measuring the associated total settlement. A load was then applied vertically (stress) on a confined and drained sample to simulate the influence of weight from an embankment or a building on consolidation. The total settlement was the sum of two distinct processes: 1) the compaction associated with the water phase change, resulting in a significant decrease in volume, especially when excess ice is present; and 2) the consolidation of the soil under the applied stress following the expulsion of water out of the pore structure and the rearrangement of soil particles. In general, compaction is more prevalent for samples with excess ice (e.g., segregated ice lenses), whereas consolidation is common in samples with interstitial ice (e.g., unsaturated to saturated soils).

During testing, an initial vertical stress of 25 kPa (corresponding to the approximate weight of a thawed active layer) was applied to frozen samples. Using two thermal baths to control the upper and lower temperatures, the permafrost samples were thawed from above by applying heat with a temperature of 2°C ± 1°C. Ultimately, the temperature of both thermal baths was increased to ensure complete thawing of the sample. After complete thawing, when there was no more vertical deformation, the stress was increased to 150 kPa for a minimum period of 24 hours in order to simulate the weight of an embankment or a medium-sized building. By proceeding in near oedometric conditions, it was possible to estimate the index of final voids (e_f) when thawing and consolidation of the grains were completed (at a given applied force). By also determining the index of initial voids in the frozen state (e_f - calculated using the frozen density and water content), it was possible to obtain a total settlement value under different forces for the same sample.

To assess the total settlement (s), the sum of the thaw settlement (s_t) and the subsequent consolidation of the soil (s_c) were calculated by using:

$$S = s_t + s_c \quad [1]$$

When the thickness of the original frozen soil layer (H_f) is subject to effective stress (σ'), the components of the total settlement are expressed using:

$$s_t = A_0 H_f \quad [2]$$

$$s_c = m_v \sigma' H_f \quad [3]$$

The thawing compaction parameter (A_0) is expressed as a percentage and represents the relationship between void ratio in frozen (e_f) and thawed (e_t) states which is summarized by using:

$$A_0 = \frac{e_f - e_t}{1 + e_f} \quad [4]$$

The volume change coefficient (m_v) is defined as a volume changing unit added by an effective stress unit. When the effective stress increases from σ' to σ'_0 and the void ratio decreases from e_t to e , this coefficient is expressed using:

$$m_v = \frac{1}{1 + e_t} \cdot \left(\frac{e_t - e}{\sigma' - \sigma'_0} \right) \quad [5]$$

In order to determine the total settlement following the thawing of permafrost under loads imposed by buildings or transportation infrastructure, A_0 and m_v values must be determined from consolidation tests on representative soil samples. Once these values are determined, the total compaction of partially or completely thawed frozen soil layers is determined by using:

$$s = \sum_{i=1}^n A_{0,i} H_i + \sum_{i=1}^n m_{v,i} H_i \sigma'_i \quad [6]$$

BULK DENSITY

Bulk density and voids in aggregate (ρ_b ; the ratio of a dried soil's mass, including its porosity, to its volume (g/cm^3)) were calculated following American Standard and Testing Method protocol (ASTM C29-09, 2000). Values were generated by weighing a 45- cm^3 beaker filled with compacted sediment and subtracting the empty beaker weight. The sediment weight was then divided by the beaker's volume using:

$$\rho_s = \frac{(M_{S+B} - M_B)}{V_B} \quad [7]$$

where M_{S+B} is the weight of the beaker full of compacted sediment, M_B is the weight of the empty beaker, and V_B is the beaker's internal volume.

GRAVIMETRIC ICE CONTENT

Ice content was calculated using:

$$u_I = \frac{(M_I)}{(M_S)} \quad [8]$$

where M_I is the ice weight (measured as weight loss after drying (g)) and M_S is dry soil weight (g). Results are expressed as percentages (dimensionless).

VOLUMETRIC ICE CONTENT

Ice volume was measured using a water displacement method. The frozen sample was weighed and lowered into a four-inch diameter PVC tube filled with 1.5 L of water. Water was then extracted from the tube until the initial water level (1.5 L) was achieved. The amount of water displaced was measured using a 250 mL graduated cylinder with a precision of ± 2 mL. The sample was then removed from the tube, placed in a clean tin tray, and dried completely in a drying oven at 60°C. The dry sample was then weighed, crushed using a mortar and pestle, vacuum sealed in a clear

plastic bag, and labelled according to the borehole and sample increment. The volumes of the vacuum-sealed dry samples were measured using the same methods as the frozen cores, and the volume of the vacuum bags was subtracted from the measurement to obtain a dry sample volume. Assuming the density of ice to be 1.09 cm³/g, volumetric ice content was calculated using:

$$IVC_{(\%)} = \left(\frac{W_c \times 1.09}{V_{tot}} \right) \times 100 \quad [9]$$

where W_c is the water mass content and V_{tot} is the total (frozen) core volume. Results are expressed as percentages.

VOLUMETRIC EXCESS ICE CONTENT

The volume of excess ice content was calculated using:

$$V_{tot} - V_{sed} = V_{ice} \quad [10]$$

where V_{tot} is the total frozen core volume and V_{sed} is the dry soil volume. The volumetric excess ice content (V_{ice}) is then divided by the total frozen core volume (V_{tot}) and expressed as a percentage (fundamentally meaning cm³/cm³). This method is valid for mineral soils only.

PLASTICITY INDEX

The plasticity index (PI ; the range of water content where the soil has a plastic behaviour) was measured according to the American Standard and Testing method (ASTM D4318-00, 2000) using:

$$PI = LL - PL \quad [11]$$

where LL is the liquid limit and PL is the plastic limit.

The LL was calculated using the multipoint liquid limit (ASTM D4318-00, 2000) which requires one of the trials to be between 25 to 35 blows, one closure between 20 and 30 blows, and one trial with a closure requiring 15 to 25 blows. The PL was calculated using the *Hand Method* which consists of rolling the mass between the palm or fingers and the ground-glass plate with sufficient pressure to roll the mass into a thread of uniform diameter throughout its length. The thread is further deformed on each stroke so that its diameter reaches 3.2 mm (1/8 in).

BOREHOLE LOGS

A log for each permafrost borehole was created using the *Rockware Log Plot* software. Borehole logs include GPS coordinates; a description of the surrounding environment; the stratigraphy of the sediment; the depth to the water table, to the frozen table in the active layer, and to the permafrost table; the ice structure (cryostructure); the grain size ratio; the specific gravity; the bulk density; the porosity; the volumetric ice content; and the thaw-settlement potential (see Appendix B for all borehole log descriptions and data).

REFERENCES

- ASTM Standard C29-09, 2000. Standard Test Method Bulk Density (“Unit Weight”) and Voids in Aggregate. West Conshohocken, PA, ASTM International.
- ASTM Standard D422-63, 2000. Standard Test Method for Particle-Size Analysis of Soils. West Conshohocken, PA, ASTM International.

- ASTM Standard D854-10, 2000. Standard Test Methods for Specific Gravity of Soil Solids by Water Pycnometer. West Conshohocken, PA, ASTM International.
- ASTM Standard D4318-00, 2000. Standard Test Methods for Liquid Limit, Plastic Limit, and Plasticity Index of Soils. West Conshohocken, PA, ASTM International.
- Bond, J.D., 1999a. Surficial geology map of Mount Mye and Faro (105K 3&6 E), central Yukon (1:25 000). Exploration and Geological Services Division, Yukon Region, Indian and Northern Affairs, Canada, Open File 1999-7.
- Bond, J.D., 1999b. Surficial geology map of Mount Mye and Faro (105K 3&6 W), central Yukon (1:25 000). Exploration and Geological Services Division, Yukon Region, Indian and Northern Affairs, Canada, Open File 1999-8.
- Conyers, L., 2004. Ground-penetrating radar for Archaeology. AltaMira Press, Walnut Creek, California, 209 p.
- Hauck, C., Isaksen, K., Vonder Mühll, D. and Sollid, J.L., 2004. Geophysical surveys designed to delineate the altitudinal limit of mountain permafrost: An example from Jotunheimen, Norway. *Permafrost and Periglacial Processes*, vol. 15, p. 191-205, doi:10.1002/ppp.493.
- Hilbich, C., Hauck, C., Hoelzle, M., Scherler, M., Schudel, L., Voelksch, I., Vonder Muehll, D. and Mausbacher, R., 2008. Monitoring mountain permafrost evolution using electrical resistivity tomography: A 7-year study of seasonal, annual, and long-term variations at Schilthorn, Swiss Alps. *Journal of Geophysical Research-Earth Surface*, vol. 113, doi:10.1029/2007JF000799.
- Hilbich, C., Marescot, L., Hauck, C., Loke, M.H. and Mausbacher, R., 2009. Applicability of electrical resistivity tomography monitoring to coarse blocky and ice-rich permafrost landforms. *Permafrost and Periglacial Processes*, vol. 20, p. 269-284, doi:10.1002/ppp.652.
- Howes, D.E. and Kenk, E., 1997. Terrain Classification System for British Columbia (Version 2). Province of British Columbia, Resource Inventory Branch, Ministry of Environment, Lands and Parks; Recreational Fisheries Branch, Ministry of Environment; and Surveys and Resources Mapping Branch, Ministry of Crown Lands, 102 p.
- Jackson, L.E., Jr., 1993. Surficial geology, Magundy River, Yukon Territory. Geological Survey of Canada, Map 1821A, scale 1:100 000.
- Kneisel, C., Hauck, C. and Vonder Mühll, D., 2000. Permafrost below the timberline confirmed and characterized by geoelectrical resistivity measurements, Bever Valley, eastern Swiss Alps. *Permafrost and Periglacial Processes*, vol. 11, p. 295-304, doi:10.1002/1099-1530(200012)11:4<295::AID-PPP353>3.0.CO;2-L.
- Kneisel, C., Hauck, C., Fortier, R. and Moorman, B., 2008. Advances in geophysical methods for permafrost investigations. *Permafrost and Periglacial Processes*, vol. 19, p. 157-178.
- Lewkowicz, A.G., Etzelmüller, B.E. and Smith, S.L., 2011. Characteristics of discontinuous permafrost from ground temperature measurements and electrical resistivity tomography, southern Yukon, Canada. *Permafrost and Periglacial Processes*, vol. 22, p. 320-342.
- Loke, M.H. and Barker, R.D., 1996. Rapid leastsquares inversion of apparent resistivity pseudosections using a quasi-Newton method. *Geophysical Prospecting*, vol. 44, p. 131-152, doi:10.1111/j.1365-2478.1996.tb00142.x
- Loke, M.H., Acworth, I. and Dahlin, T., 2003. A comparison of smooth and blocky inversion methods in 2D electrical imaging surveys. *Exploration Geophysics*, vol. 34, p. 182-187.

- Miceli, C., 2012. Seasonal cycling in electrical resistivities at ten thin permafrost sites, southern Yukon and northern British Columbia. Unpublished MSc thesis, Department of Geography, University of Ottawa, ON, 201 p.
- Murton, J.B. and French, H.M., 1994. Cryostructures in permafrost, Tuktoyaktuk coastlands, western arctic Canada. *Canadian Journal of Earth Sciences*, vol. 31, no. 4, p. 737-747.
- Stephani, E., Fortier, D. and Shur, Y., 2010. Applications of cryofacies approach to frozen ground engineering – Case study of a road test site along the Alaska Highway (Beaver Creek, Yukon, Canada). GEO2010: 63rd Canadian Geotechnical Conference and 6th Canadian Permafrost Conference, Calgary, Canada.
- Turner, D.G., 2014. Surficial geology, Ross River region, Yukon, parts of N TS 105K /1 & 2 and 105F /15 & 16 (1:25 000 scale). Yukon Geological Survey, Energy, Mines and Resources, Government of Yukon, Open File 2014-13.

APPENDIX B - BOREHOLE LOGS

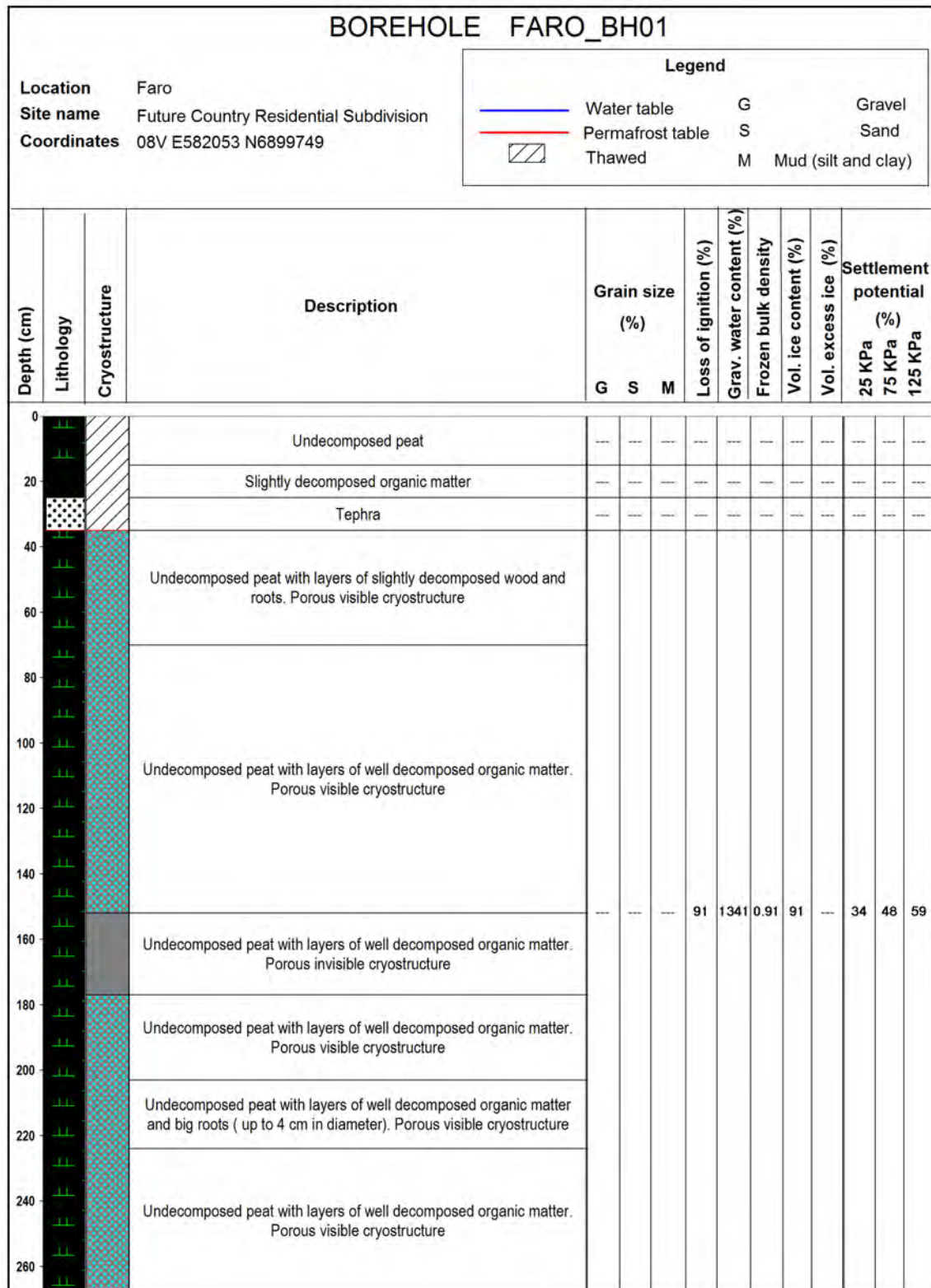


Figure B1. Borehole log for borehole FARO_BH01, from the future country residential case study site (see Figure 26 in the main body of this report for location).

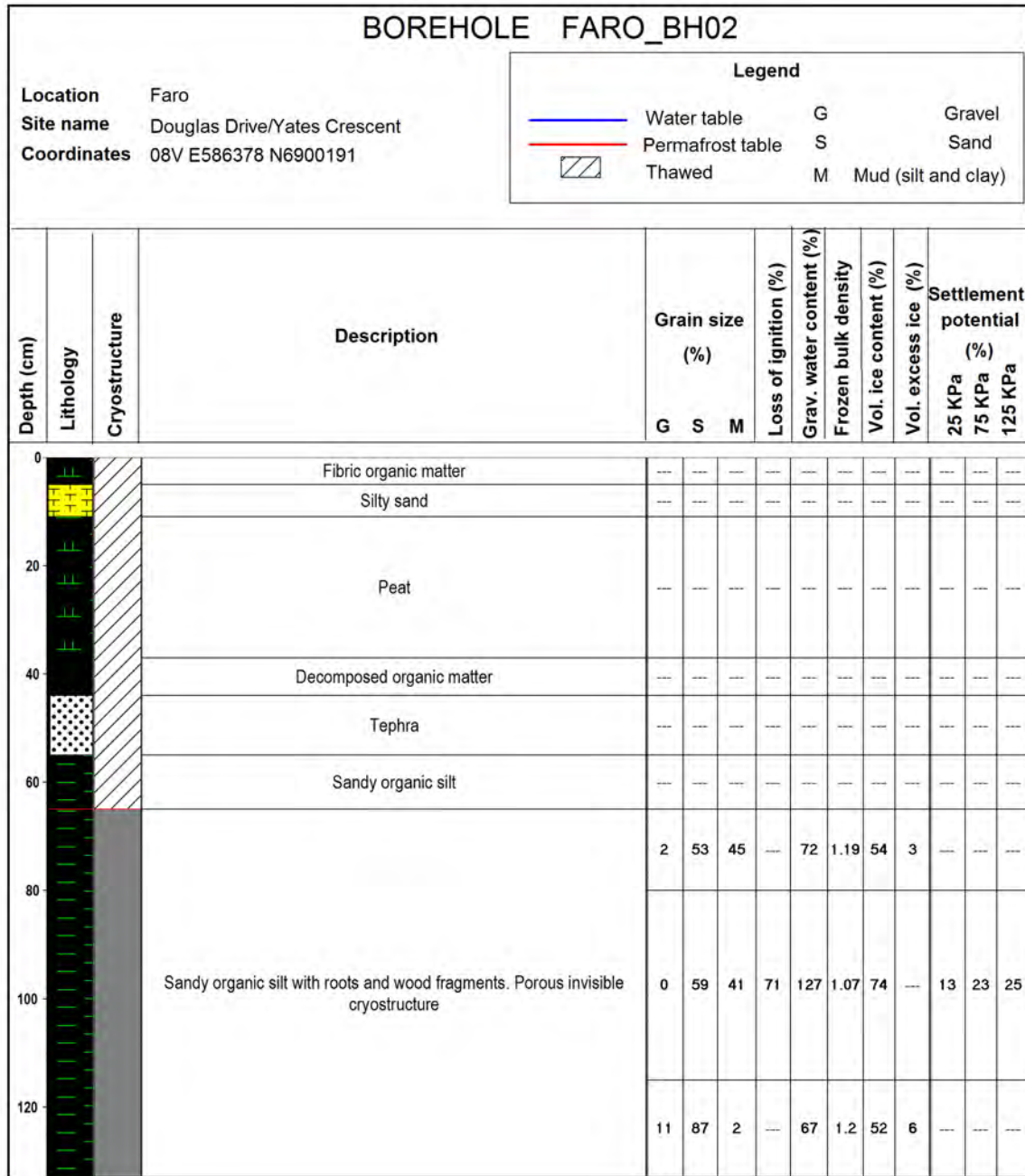


Figure B2. Borehole log for borehole FARO_BH02, from the Douglas Drive/Yates Crescent case study site (see Figure 34 in the main body of this report for location).

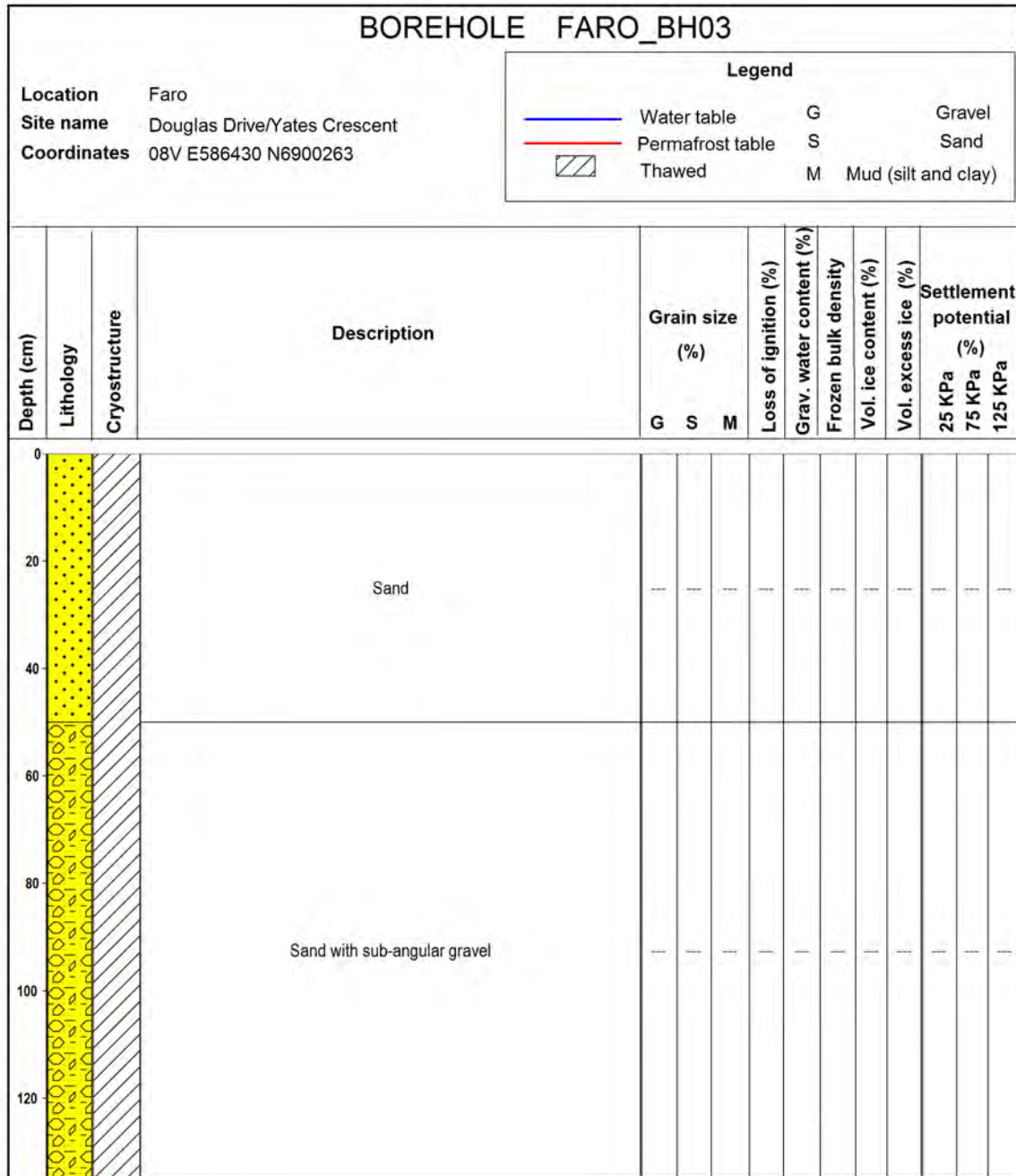


Figure B3. Borehole log for borehole Faro_BH03, from the Douglas Drive/Yates Crescent case study site (see Figure 34 in the main body of this report for location).

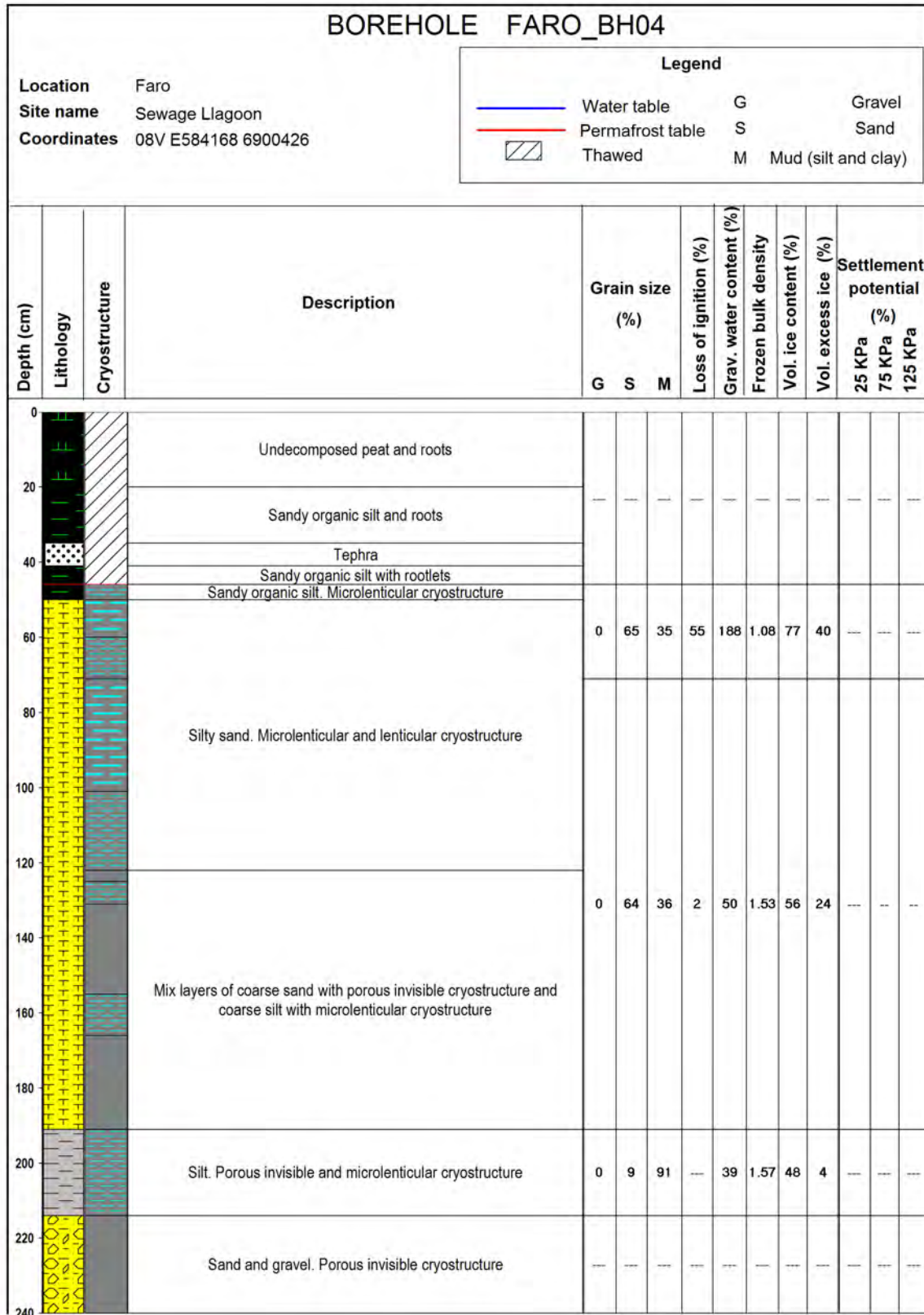


Figure B4. Borehole log for borehole Faro_BH04, from the Sewage Lagoon case study site (see Figure 29 in the main body of this report for location).

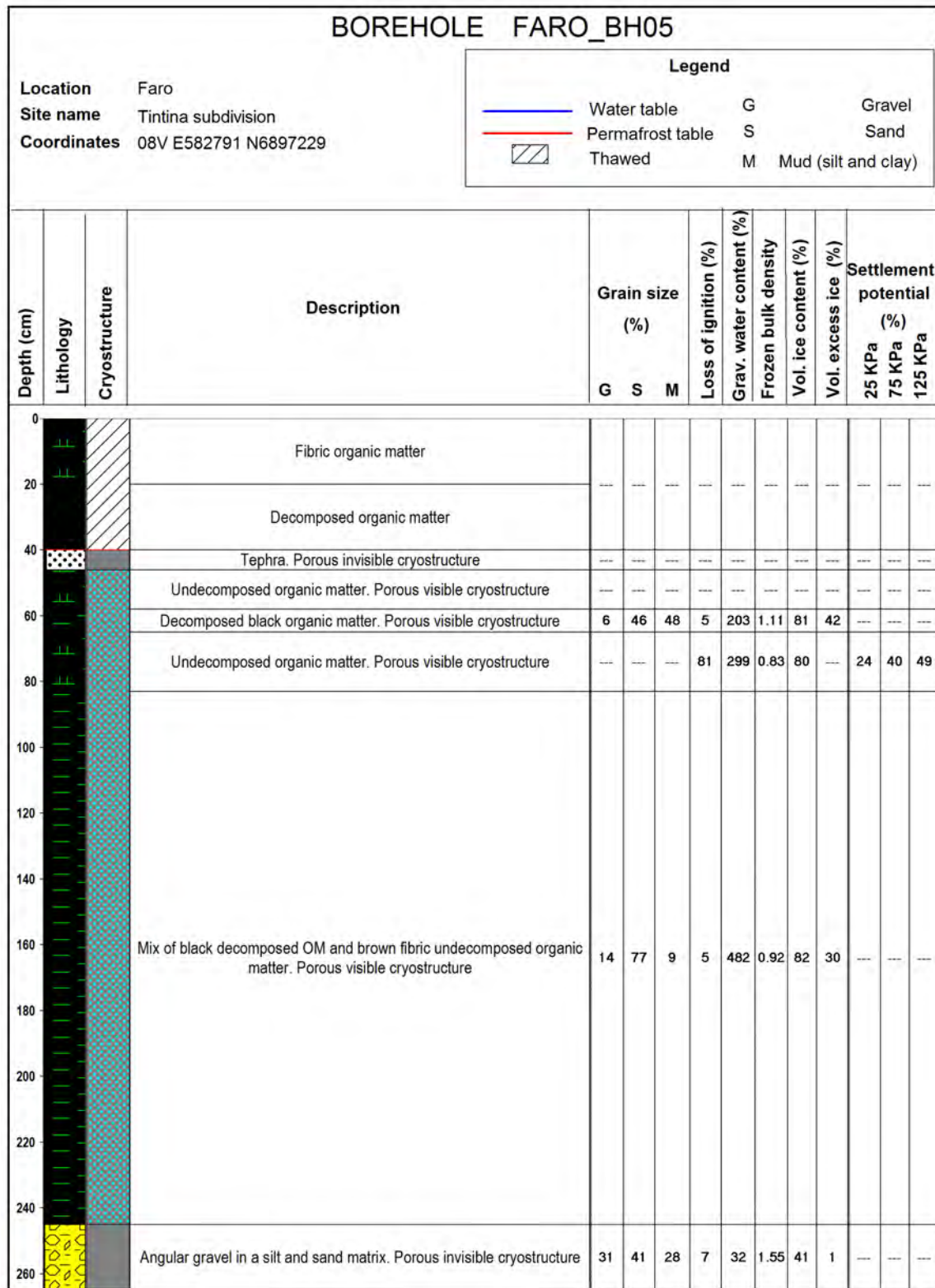


Figure B5. Borehole log for borehole Faro_BH05, from the Tintina Subdivision case study site (see Figure 23 in the main body of this report for location).

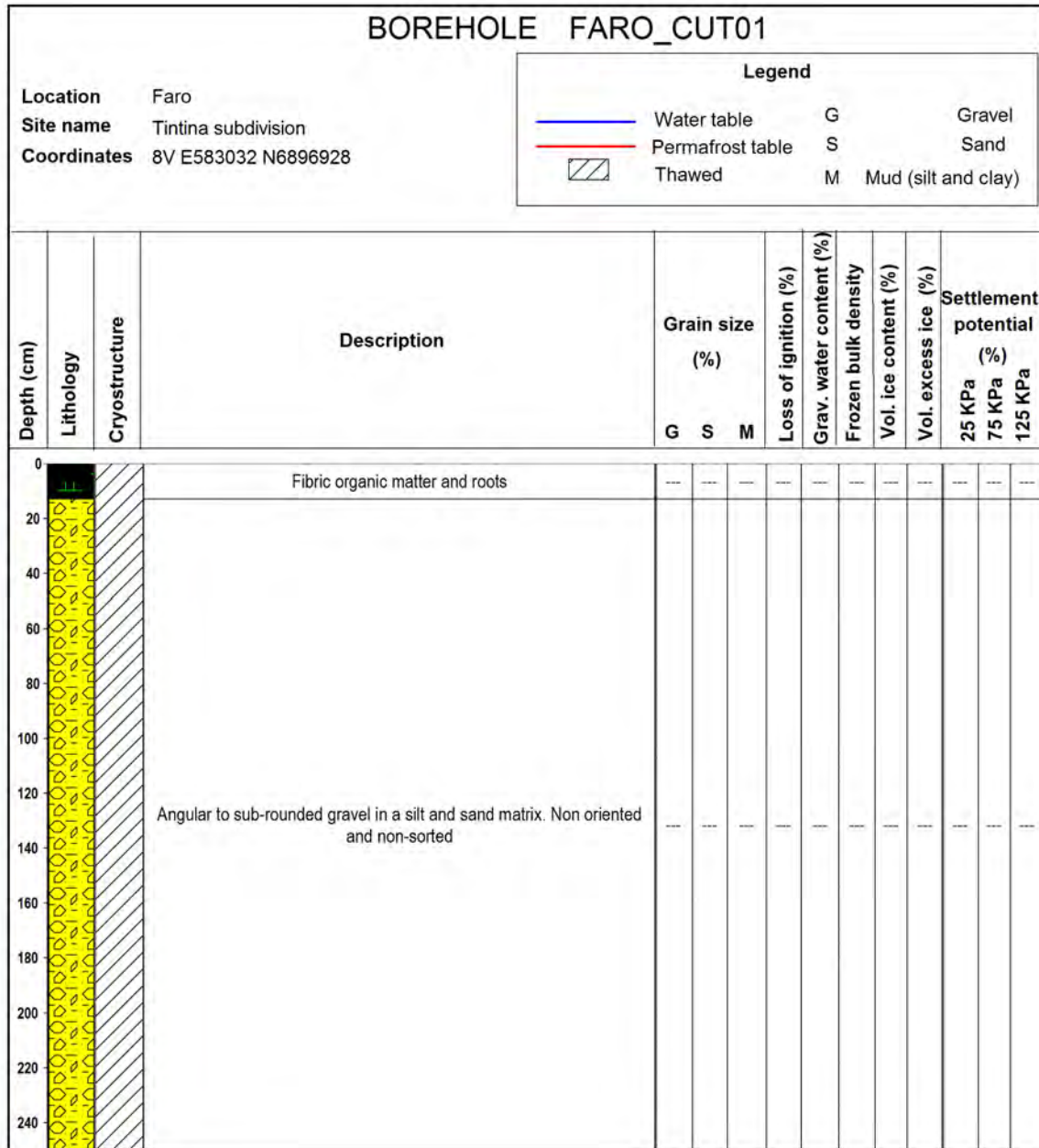


Figure B6. Borehole log for borehole Faro_CUT01, from the Tintina Subdivision case study site (see Figure 23 in the main body of this report for location).

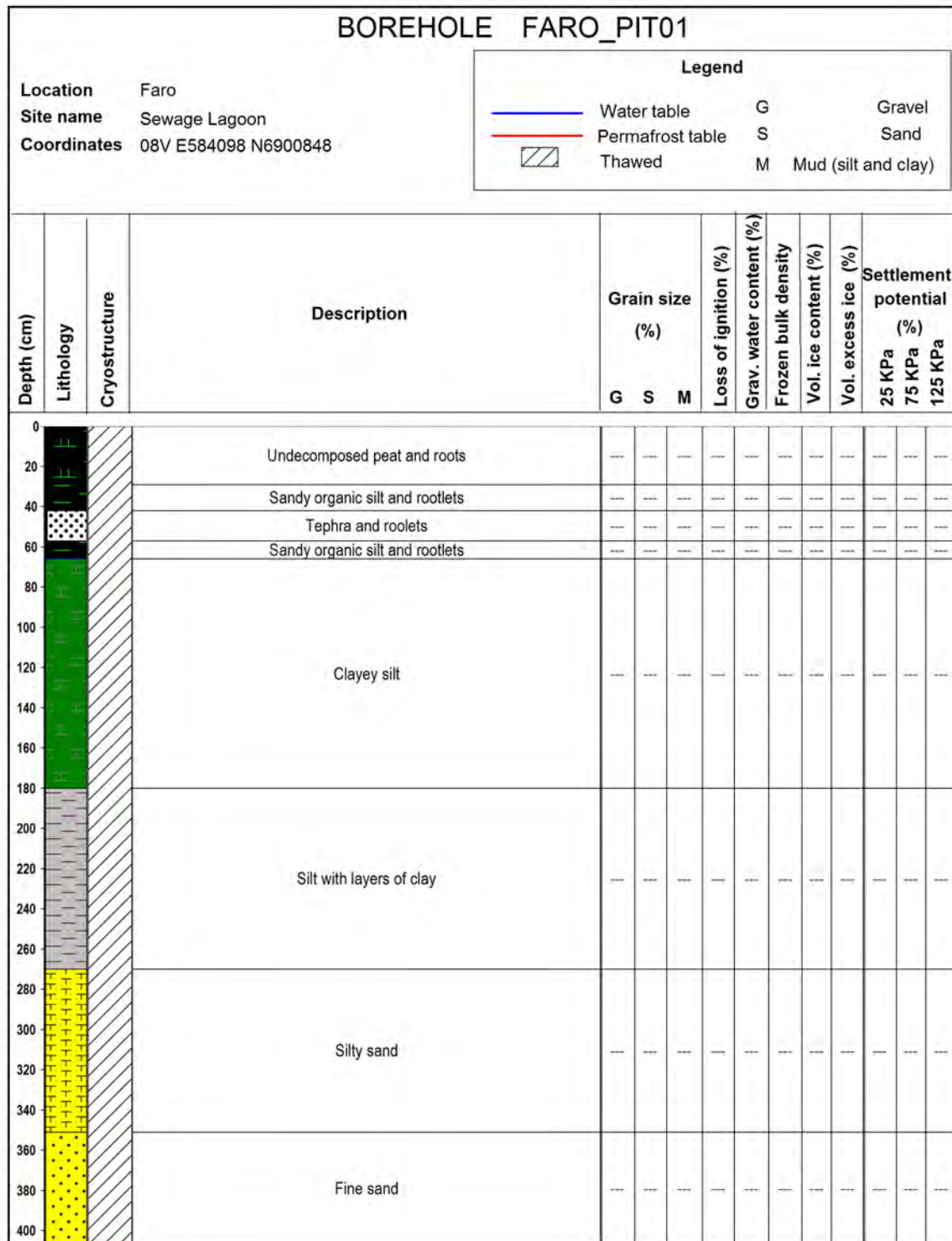


Figure B7. Borehole log for borehole Faro_PIT01, from the Sewage Lagoon case study site (see Figure 29 in the main body of this report for location).

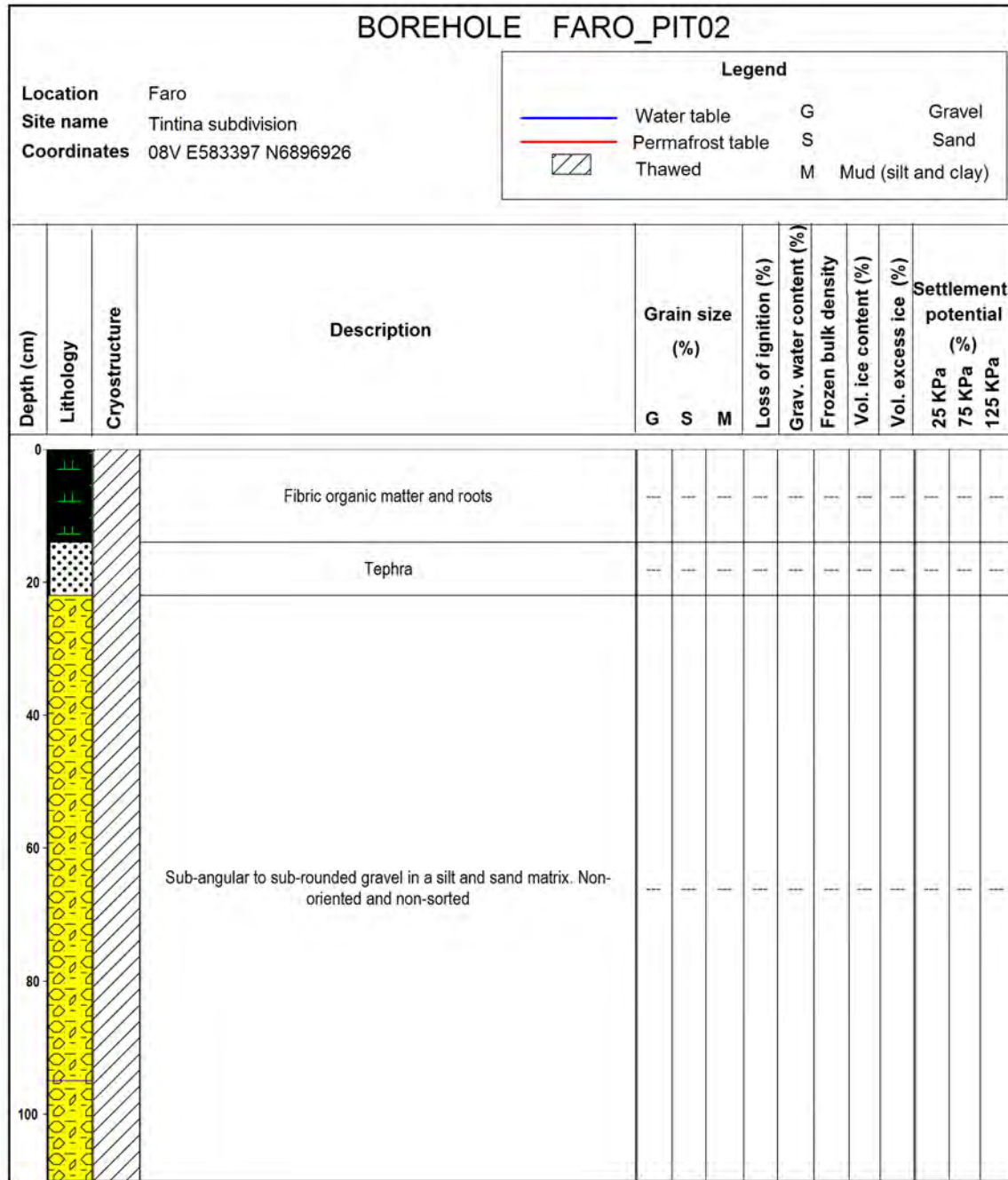


Figure B8. Borehole log for borehole Faro_PIT02, from the Tintina Subdivision case study site (see Figure 23 in the main body of this report for location).

APPENDIX C - GRAIN SIZE ANALYSIS

Table C1. Grain size analysis results for samples collected from boreholes drilled at case study sites in the Faro area. See Figures 23, 26, 29 and 34 in the main body of this report for location of case study sites and boreholes, and Appendix A for methodology.

Sample Name:	FARO_BH02_73	FARO_BH02_88 (2)	FARO_BH02_133
Analyst and Date	LPR, 1/13/2015	LPR, 1/14/2015	LPR, 1/15/2015
Sieving Error	0.0%	0.0%	0.0%
Sample Type	Bimodal, Poorly Sorted	Trimodal, Poorly Sorted	Polymodal, Poorly Sorted
Textural Group	Slightly Gravelly Muddy Sand	Slightly Gravelly Muddy Sand	Gravelly Sand
Sediment Name	Slightly Very Fine Gravelly Very Coarse Silty Very Fine Sand	Slightly Very Fine Gravelly Very Coarse Silty Coarse Sand	Very Fine Gravelly Fine Sand
% Gravel	2.0%	0.2%	11.3%
% Sand	52.8%	58.5%	87.0%
% Silt & Clay	45.2%	41.3%	1.6%
% Very Coarse Gravel	0.0%	0.0%	0.0%
% Coarse Gravel	0.0%	0.0%	0.0%
% Medium Gravel	0.0%	0.0%	0.0%
% Fine Gravel	0.1%	0.0%	0.9%
% Very Fine Gravel	1.9%	0.1%	10.5%
% Very Coarse Sand	0.0%	0.0%	0.0%
% Coarse Sand	9.2%	25.2%	27.6%
% Medium Sand	9.9%	13.7%	21.3%
% Fine Sand	12.9%	9.9%	30.4%
% Very Fine Sand	20.8%	9.8%	7.7%
% Very Coarse Silt	45.2%	41.3%	1.6%
% Coarse Silt	0.0%	0.0%	0.0%
% Medium Silt	0.0%	0.0%	0.0%
% Fine Silt	0.0%	0.0%	0.0%
% Very Fine Silt	0.0%	0.0%	0.0%
% Clay	0.0%	0.0%	0.0%

Table C2. Grain size analysis results for samples collected from boreholes drilled at case study sites in the Faro area. See Figures 23, 26, 29 and 34 in the main body of this report for location of case study sites and boreholes, and Appendix A for methodology.

Sample Name:	FARO_BH05_66	FARO_BH05_103	FARO_BH05_124
Analyst and Date	LPR, 1/16/2015	LPR, 1/17/2015	LPR, 1/18/2015
Sieving Error	0.0%	0.0%	0.0%
Sample Type	Trimodal, Poorly Sorted	Polymodal, Poorly Sorted	Polymodal, Poorly Sorted
Textural Group	Gravelly Mud	Gravelly Sand	Gravelly Sand
Sediment Name	Very Fine Gravelly Very Coarse Silt	Very Fine Gravelly Coarse Sand	Very Fine Gravelly Coarse Sand
% Gravel	5.8%	14.6%	7.3%
% Sand	45.9%	78.7%	85.4%
% Silt & Clay	48.4%	6.7%	7.3%
% Very Coarse Gravel	0.0%	0.0%	0.0%
% Coarse Gravel	0.0%	0.0%	0.0%
% Medium Gravel	0.0%	0.0%	0.0%
% Fine Gravel	1.1%	3.3%	1.2%
% Very Fine Gravel	4.7%	11.3%	6.1%
% Very Coarse Sand	0.0%	0.0%	0.0%
% Coarse Sand	10.3%	37.4%	27.4%
% Medium Sand	0.0%	20.8%	23.9%
% Fine Sand	20.8%	13.0%	21.6%
% Very Fine Sand	14.8%	7.4%	12.4%
% Very Coarse Silt	48.4%	6.7%	7.3%
% Coarse Silt	0.0%	0.0%	0.0%
% Medium Silt	0.0%	0.0%	0.0%
% Fine Silt	0.0%	0.0%	0.0%
% Very Fine Silt	0.0%	0.0%	0.0%
% Clay	0.0%	0.0%	0.0%

Table C3. Grain size analysis results for samples collected from boreholes drilled at case study sites in the Faro area. See Figures 23, 26, 29 and 34 in the main body of this report for location of case study sites and boreholes, and Appendix A for methodology.

Sample Name:	FARO_BH05_148	FARO_BH05_183	FARO_BH05_204
Analyst and Date	LPR, 1/19/2015	LPR, 1/20/2015	LPR, 1/21/2015
Sieving Error	0.0%	0.0%	0.0%
Sample Type	Polymodal, Poorly Sorted	Polymodal, Poorly Sorted	Polymodal, Poorly Sorted
Textural Group	Gravelly Sand	Gravelly Sand	Gravelly Sand
Sediment Name	Very Fine Gravelly Coarse Sand	Very Fine Gravelly Coarse Sand	Very Fine Gravelly Coarse Sand
% Gravel	10.7%	20.9%	9.7%
% Sand	84.1%	74.9%	82.7%
% Silt & Clay	5.2%	4.3%	7.6%
% Very Coarse Gravel	0.0%	0.0%	0.0%
% Coarse Gravel	0.0%	0.0%	0.0%
% Medium Gravel	0.0%	0.0%	0.0%
% Fine Gravel	0.1%	5.8%	1.5%
% Very Fine Gravel	10.6%	15.1%	8.3%
% Very Coarse Sand	0.0%	0.0%	0.0%
% Coarse Sand	33.9%	34.4%	31.7%
% Medium Sand	25.7%	18.4%	21.0%
% Fine Sand	16.7%	15.1%	19.3%
% Very Fine Sand	7.8%	7.0%	10.7%
% Very Coarse Silt	5.2%	4.3%	7.6%
% Coarse Silt	0.0%	0.0%	0.0%
% Medium Silt	0.0%	0.0%	0.0%
% Fine Silt	0.0%	0.0%	0.0%
% Very Fine Silt	0.0%	0.0%	0.0%
% Clay	0.0%	0.0%	0.0%

Table C4. Grain size analysis results for samples collected from boreholes drilled at case study sites in the Faro area. See Figures 23, 26, 29 and 34 in the main body of this report for location of case study sites and boreholes, and Appendix A for methodology.

Sample Name:	FARO_BH05_240	FARO_BH05_265	FARO_BH04_71
Analyst and Date	LPR, 1/22/2015	LPR, 1/23/2015	LPR, 1/24/2015
Sieving Error	0.0%	0.0%	0.0%
Sample Type	Polymodal, Very Poorly Sorted	Polymodal, Very Poorly Sorted	Trimodal, Poorly Sorted
Textural Group	Gravelly Muddy Sand	Muddy Sandy Gravel	Slightly Gravelly Muddy Sand
Sediment Name	Very Fine Gravelly Very Coarse Silty Coarse Sand	Very Coarse Silty Sandy Fine Gravel	Slightly Fine Gravelly Very Coarse Silty Fine Sand
% Gravel	17.8%	31.4%	0.0%
% Sand	56.9%	41.1%	64.6%
% Silt & Clay	25.3%	27.5%	35.3%
% Very Coarse Gravel	0.0%	0.0%	0.0%
% Coarse Gravel	0.0%	0.0%	0.0%
% Medium Gravel	0.0%	0.0%	0.0%
% Fine Gravel	7.0%	22.6%	0.0%
% Very Fine Gravel	10.8%	8.8%	0.0%
% Very Coarse Sand	0.0%	0.0%	0.0%
% Coarse Sand	21.5%	14.4%	0.0%
% Medium Sand	12.4%	7.4%	18.2%
% Fine Sand	12.0%	9.6%	24.9%
% Very Fine Sand	11.0%	9.8%	21.4%
% Very Coarse Silt	25.3%	27.5%	35.3%
% Coarse Silt	0.0%	0.0%	0.0%
% Medium Silt	0.0%	0.0%	0.0%
% Fine Silt	0.0%	0.0%	0.0%
% Very Fine Silt	0.0%	0.0%	0.0%
% Clay	0.0%	0.0%	0.0%

Table C5. Grain size analysis results for samples collected from boreholes drilled at case study sites in the Faro area. See Figures 23, 26, 29 and 34 in the main body of this report for location of case study sites and boreholes, and Appendix A for methodology.

Sample Name:	FARO_BH04_110	FARO_BH04_148	FARO_BH04_182	FARO_BH04_214
Analyst and Date	LPR, 1/25/2015	LPR, 1/26/2015	LPR, 1/27/2015	LPR, 1/28/2015
Sieving Error	0.0%	0.0%	0.0%	0.0%
Sample Type	Bimodal, Moderately Sorted	Trimodal, Moderately Sorted	Trimodal, Poorly Sorted	Unimodal, Very Well Sorted
Textural Group	Slightly Gravelly Muddy Sand	Slightly Gravelly Muddy Sand	Slightly Gravelly Muddy Sand	Slightly Gravelly Mud
Sediment Name	Slightly Very Fine Gravelly Very Coarse Silty Very Fine Sand	Slightly Very Fine Gravelly Very Coarse Silty Fine Sand	Slightly Very Fine Gravelly Very Coarse Silty Very Fine Sand	Slightly Very Fine Gravelly Very Coarse Silt
% Gravel	0.2%	0.3%	0.8%	0.1%
% Sand	59.5%	75.3%	56.1%	8.6%
% Silt & Clay	40.3%	24.4%	43.1%	91.3%
% Very Coarse Gravel	0.0%	0.0%	0.0%	0.0%
% Coarse Gravel	0.0%	0.0%	0.0%	0.0%
% Medium Gravel	0.0%	0.0%	0.0%	0.0%
% Fine Gravel	0.0%	0.0%	0.0%	0.0%
% Very Fine Gravel	0.2%	0.3%	0.8%	0.1%
% Very Coarse Sand	0.4%	0.1%	2.3%	0.0%
% Coarse Sand	0.4%	0.2%	3.8%	0.0%
% Medium Sand	2.1%	8.4%	5.4%	0.0%
% Fine Sand	18.1%	34.9%	17.4%	1.2%
% Very Fine Sand	38.5%	31.8%	27.3%	7.4%
% Very Coarse Silt	40.3%	24.4%	43.1%	91.3%
% Coarse Silt	0.0%	0.0%	0.0%	0.0%
% Medium Silt	0.0%	0.0%	0.0%	0.0%
% Fine Silt	0.0%	0.0%	0.0%	0.0%
% Very Fine Silt	0.0%	0.0%	0.0%	0.0%
% Clay	0.0%	0.0%	0.0%	0.0%

APPENDIX D - CLIMATE PROJECTIONS

Projections of changes in mean annual air temperature (MAAT) were prepared for this report based on annual air temperature modelling, and were enhanced to reflect heterogeneity in the local landscape (specifically, mountainous terrain). This represents a significant increase in the understanding of MAAT. This approach incorporated specific topographical features in the study region (e.g., mountains) and knowledge about related area-specific surface lapse rates (SLRs) at fine resolution (30 x 30 m). To develop these enhanced air temperature models and predictions, current MAAT modeling was conducted. Work drew on data from clusters of previously established air temperature monitoring stations in Yukon. Each monitoring station consisted of a radiation shield mounted at 1.5-1.6 m on a metal pole. An Onset Hobo Pro data-logger (accuracy $\pm 0.2^{\circ}\text{C}$), equipped with an external thermistor, was used to monitor air temperature inside the screen. In order to predict MAAT across the region, a 3rd order polynomial trend surface of annual SLR values below treeline was generated (Lewkowicz and Bonnaventure, 2011). This surface was then combined with a 4th order polynomial trend surface of treeline elevations, which was separately developed from sampling topographic maps and Google Earth images to limit the application of the SLR values to terrain below treeline. Above this level, it was assumed that standard environmental lapse rates of $-6.5^{\circ}\text{C}/\text{km}$ prevail. In addition, a 3rd order polynomial trend surface of projected sea level temperature was generated from the long-term records of 18 climate stations in the region (Environment Canada, 2013), which had been reduced to sea level (e.g., Etmuller et al., 2007) by applying the projected SLR value for each station based on its continentality (Lewkowicz and Bonnaventure, 2011). The projected sea level temperature surface was then readjusted using a digital elevation model at 30 x 30 m resolution, the SLR grid for elevations up to treeline, and the standard environmental lapse rate from treeline upwards. The result was a gridded model of MAAT for the region based on elevation with the measured variability in SLR taken into account but not including aspect or localized topographic effects on cold-air pooling.

The basis for developing projections of MAAT incorporating the SLRs (also called perturbed MAAT models) involved using statistically downscaled Global Climate Model (GCM) data obtained from the Scenarios Network for Arctic and Alaska Planning at the University of Alaska Fairbanks (SNAP, 2012; www.snap.uaf.edu). The SNAP dataset contains multiple GCM scenarios for mean annual air temperatures, as well as modelled average temperature surfaces for past climate normals (e.g., 1980-2009). The data used to obtain the perturbed MAAT models included the 2 km-resolution projection surfaces provided by SNAP for the IPCC scenarios of A1B, A2 and B1. These particular scenarios were chosen for this application because they represent the most commonly used scenarios in GCM modelling and represent a broad range of potential climate conditions. To develop each scenario, SNAP drew on data from five separate models, thereby ensuring the greatest range of predictions within each scenario. Perturbed MAAT models were developed by examining difference (and thus change) between what the SNAP model predicted for the current climate (i.e., the 1980-2009 climate normal) and each of the three scenarios for the years 2020, 2050 and 2080. In addition, a backcasted model was also produced which examined the difference between current climate (1980-2009) and the climate normal from 1950-1979. Hence, modelling efforts examined the predicted difference between each time slice for each scenario and adjusted the previously created MAAT model accordingly. In order to incorporate the data from the 2 x 2 km grid cells for each SNAP model, the cell size was resampled to 30 x 30 m. This effectively provided a broad geographic basis for sample change at a territorial scale (macroclimate), which could then be topographically corrected to site specific SLRs in the Faro study area. The differences between the predicted SNAP models were then added (forecasting) or subtracted (backcasting) to the current MAAT model using raster calculator in ArcGIS[®] 10.1 (ESRI, USA). The results of

these models provide significantly more information about the variable nature of spatial climate in geographically mountainous areas than the raw GCM data itself, which typically displays high levels of inaccuracies in the mountainous regions of Yukon.

Results are presented in Figures D1 to D10, below. Current (i.e., 1980-2009) MAAT results in the area of Faro fall within the range of -2.6 to -3.1°C, and temperatures were found to be colder in the backcasted (1950-1979) model for the area by about 1°C. A summary of temperature results for each model for the study region are presented below in Table D1.

Note that additional climate projections, based on data provided by SNAP (2012), are available by contacting the Northern Climate ExChange (Yukon Research Centre, Yukon College). Projections are available for mean annual and seasonal temperature and precipitation, as well as freeze and thaw dates and growing degree days, for the A1B and B1 scenarios, for the 2020s and 2050s, as well as the 1960-1990 time period.

Table D1. Statistics generated for the B1, A1B and A2 climate scenarios, showing mean, minimum and maximum air temperature in the 2020s, 2050s and 2080s.

Projection	Air Temperature (°C)		
	Mean	Minimum	Maximum
Current MAAT	-2.8	-3.5	-2.5
1950 - 1979	-4.0	-4.6	-3.7
B1 2020s	-2.7	-3.4	-2.4
B1 2050s	-2.1	-2.8	-1.8
B1 2080s	-1.1	-1.8	-0.8
A1B 2020s	-2.7	-3.4	-2.4
A1B 2050s	-1.5	-2.2	-1.2
A1B 2080s	-0.1	-0.8	0.2
A2 2020s	-2.8	-3.5	-2.5
A2 2050s	-1.8	-2.5	-1.5
A2 2080s	0.2	-0.5	0.5

REFERENCES

- Environment Canada, 2013. Canadian Climate Normals 1971-2000. Ottawa, Ontario: Environment Canada. [http://www.climate.weatheroffice.gc.ca/climate_normals/index_e.html]. Accessed January, 2013.
- Etzelmüller, B., Farbrot, H., Guomundsson, A. and Humlum, O., 2007. The regional distribution of mountain permafrost in Iceland. *Permafrost and Periglacial Processes*, vol. 18, p. 185-199.
- Intergovernmental Panel on Climate Change (IPCC), 2015. Fifth Assessment Report. IPCC, Geneva, Switzerland. [<https://www.ipcc.ch/index.htm>]. Accessed January, 2015.
- Lewkowicz, A.G. and Bonnaventure, P.P., 2011. Equivalent elevation: a method to incorporate variable lapse rates into mountain permafrost modeling. *Permafrost and Periglacial Processes*, vol. 22, p. 153-162.
- SNAP (Scenarios Network for Alaska and Arctic Planning), 2012. www.snap.uaf.edu.

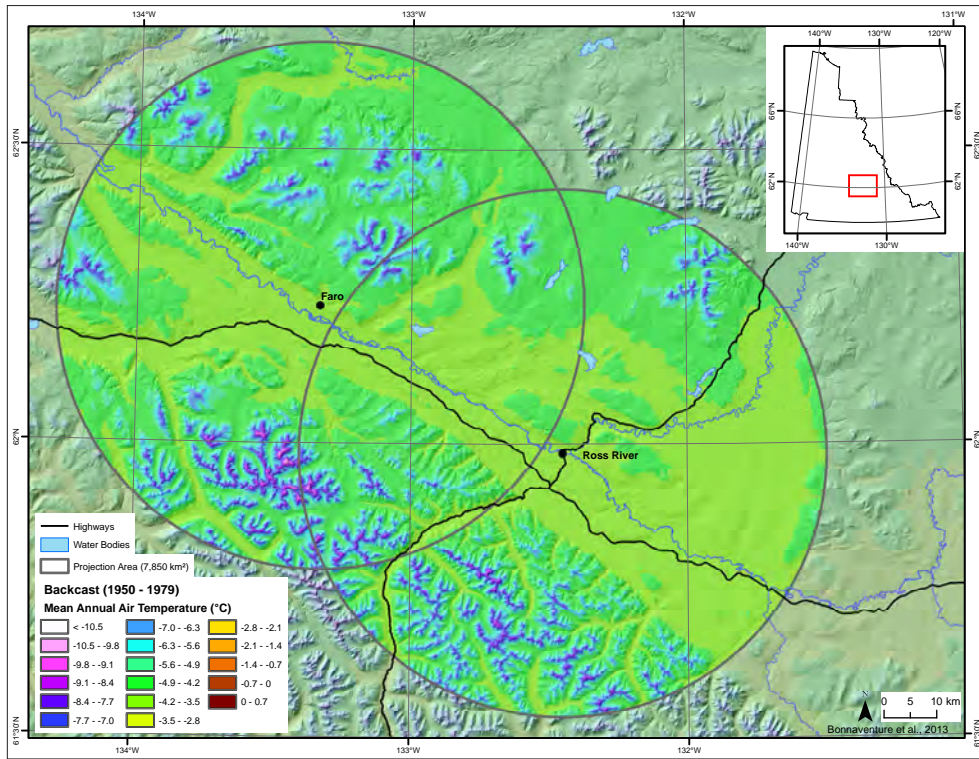


Figure D1. Mean annual air temperature for the Faro area, backcasted for the 1950-1979 period.

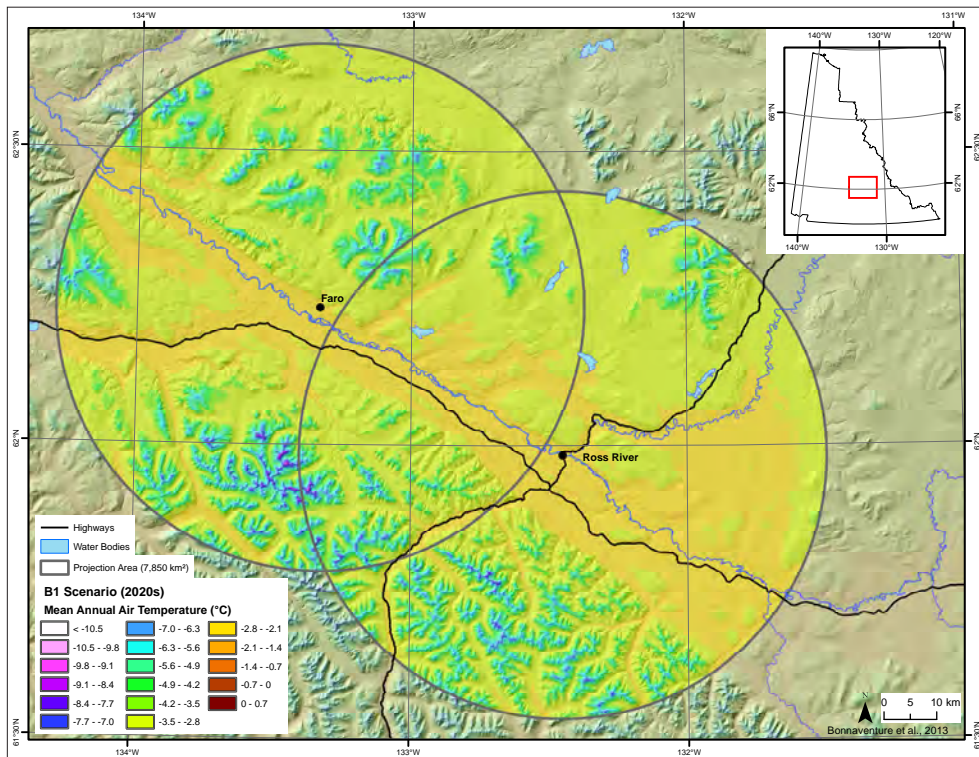


Figure D2. Mean annual air temperature for the Faro area for 2020, projected using the B1 scenario.

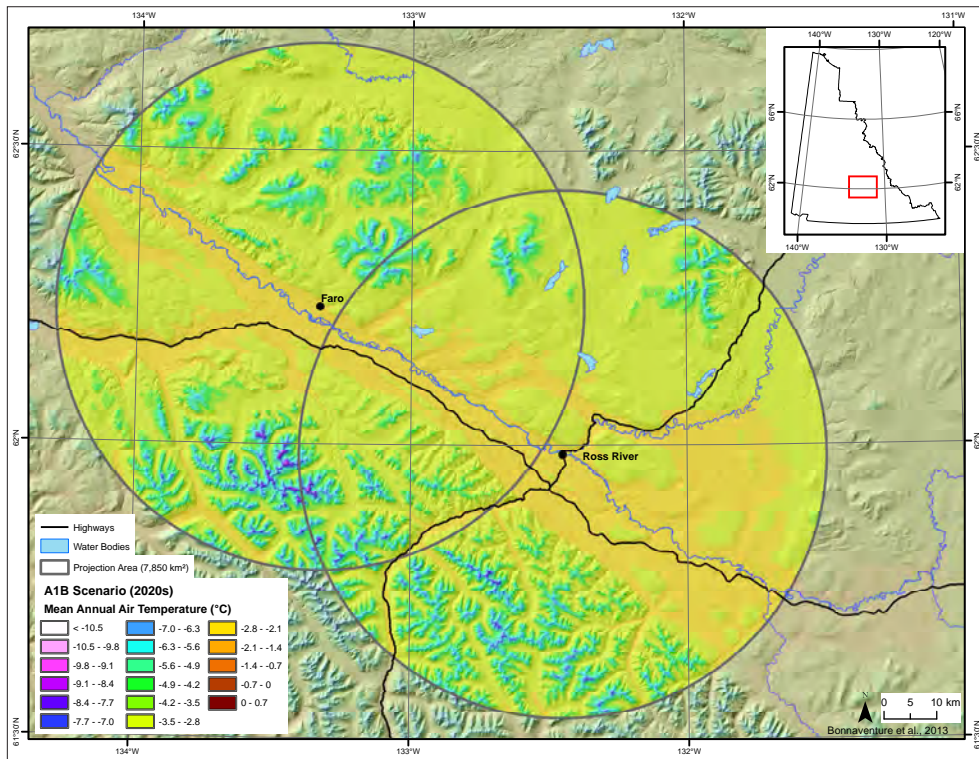


Figure D3. Mean annual air temperature for the Faro area for 2020, projected using the A1B scenario.

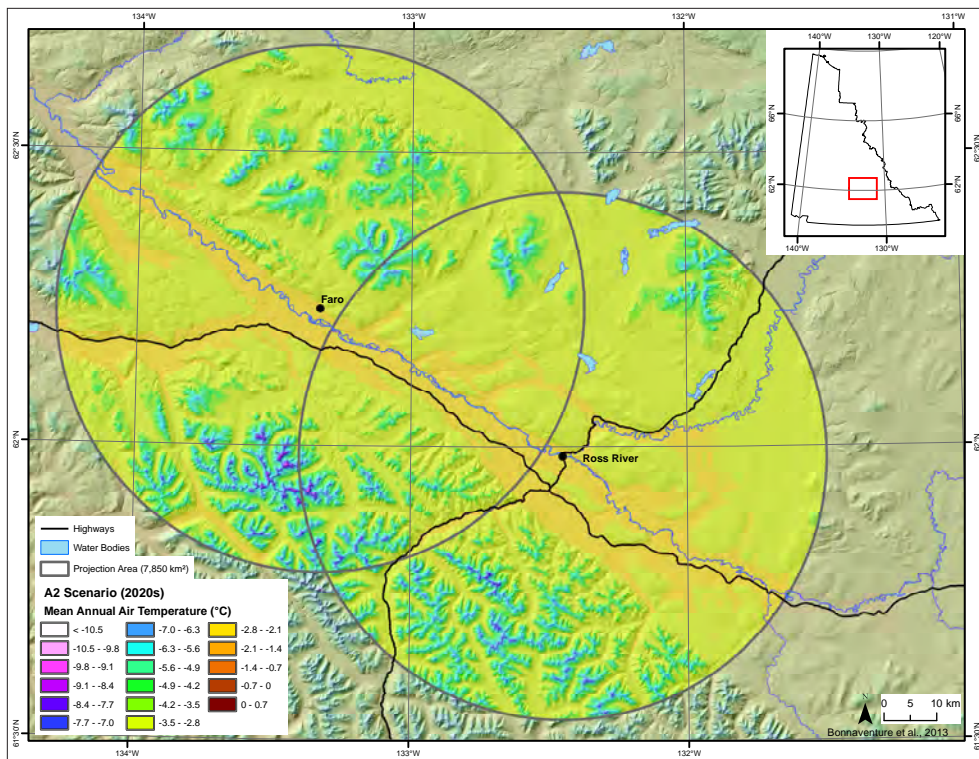


Figure D4. Mean annual air temperature for the Faro area for 2020, projected using the A2 scenario.

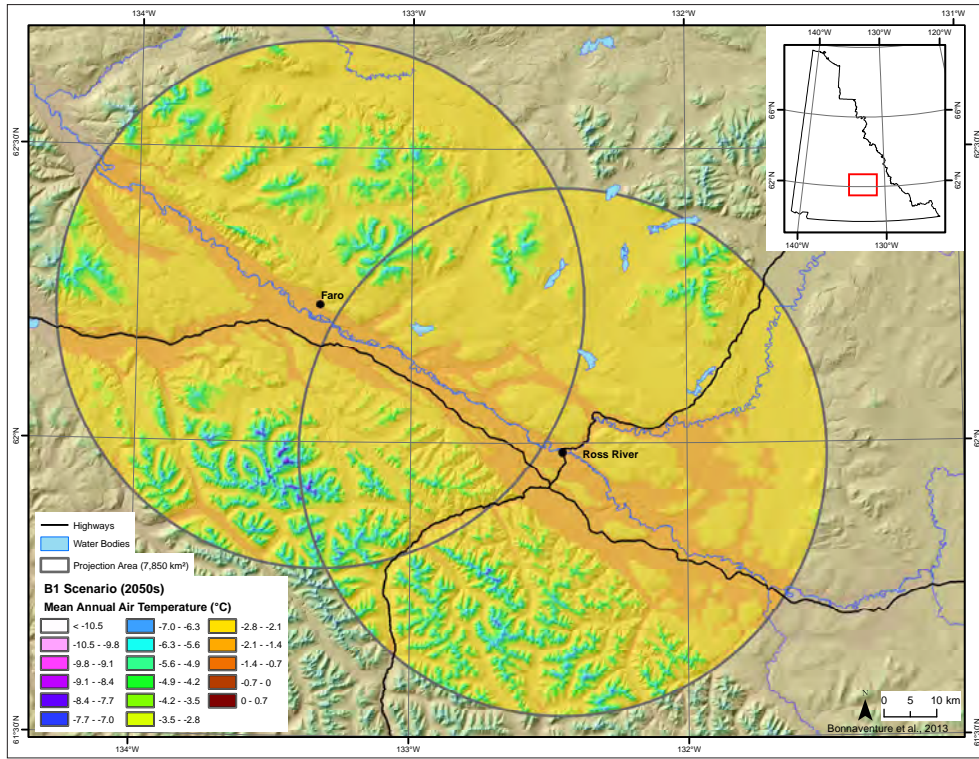


Figure D5. Mean annual air temperature for the Faro area for 2050, projected using the B1 scenario.

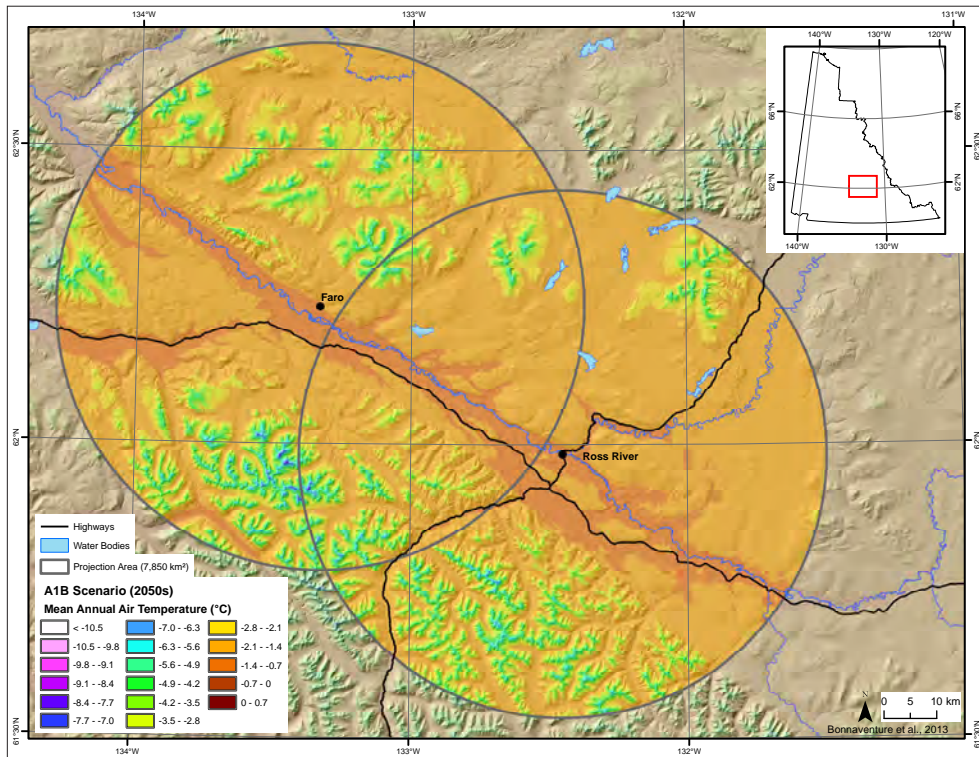


Figure D6. Mean annual air temperature for the Faro area for 2050, projected using the A1B scenario.

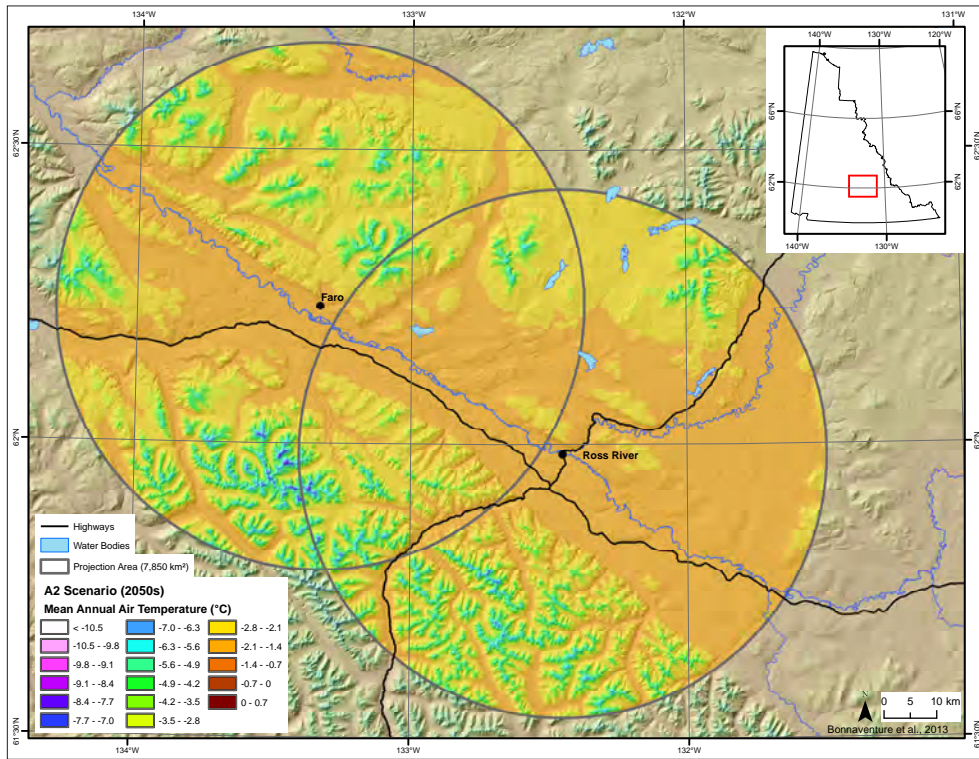


Figure D7. Mean annual air temperature for the Faro area for 2050, projected using the A2 scenario.

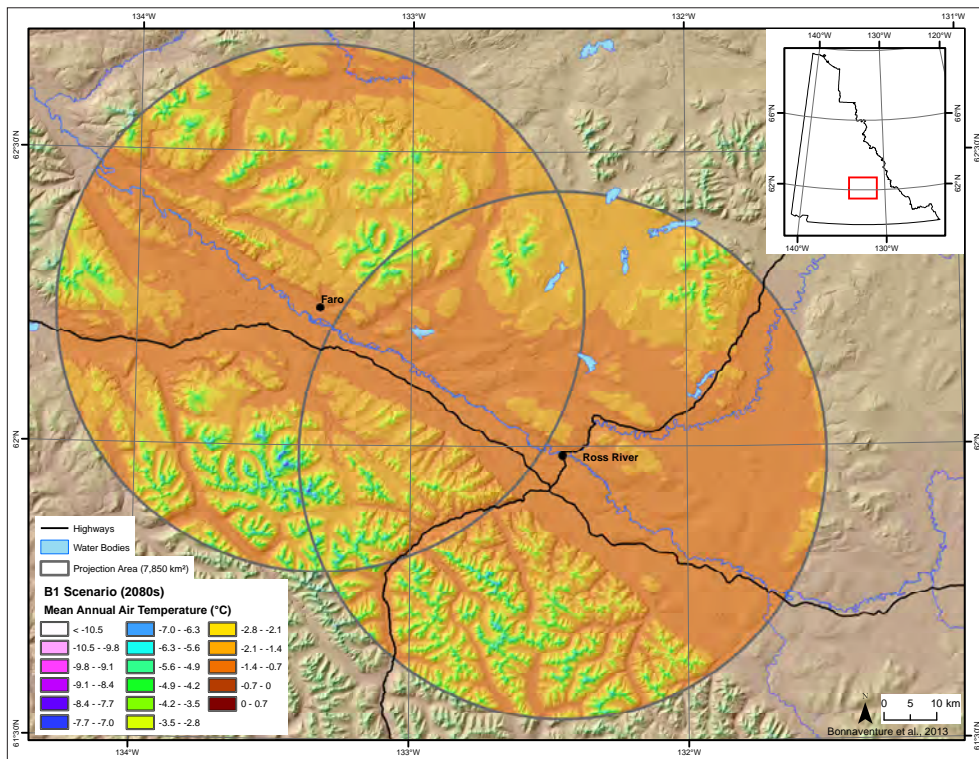


Figure D8. Mean annual air temperature for the Faro area for 2080, projected using the B1 scenario.

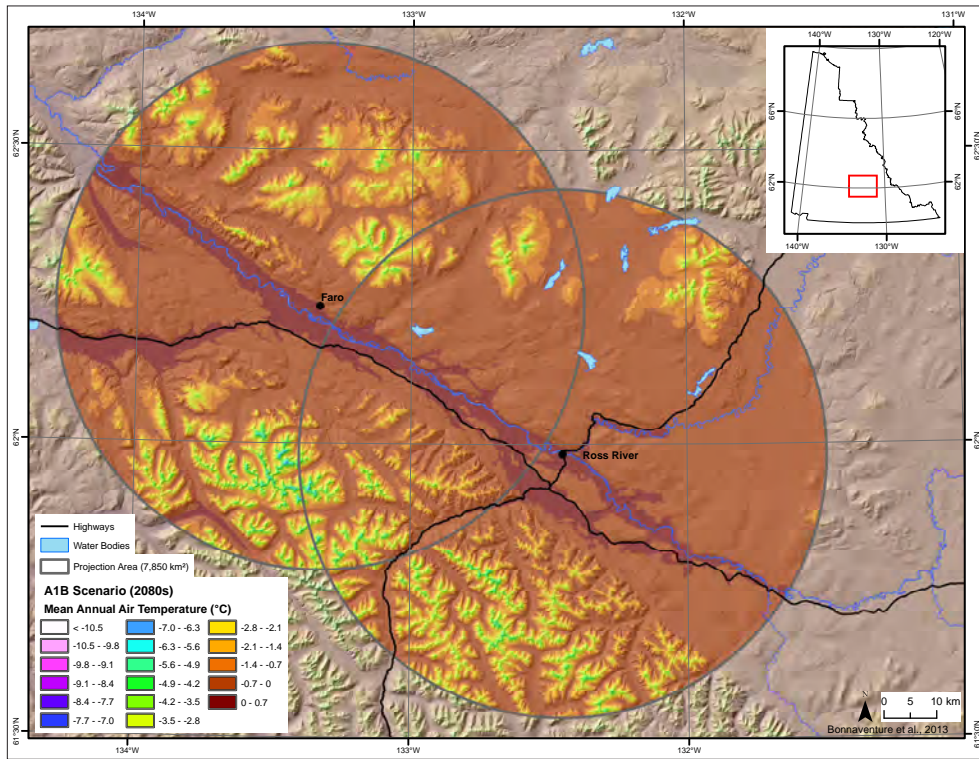


Figure D9. Mean annual air temperature for the Faro area for 2080, projected using the A1B scenario.

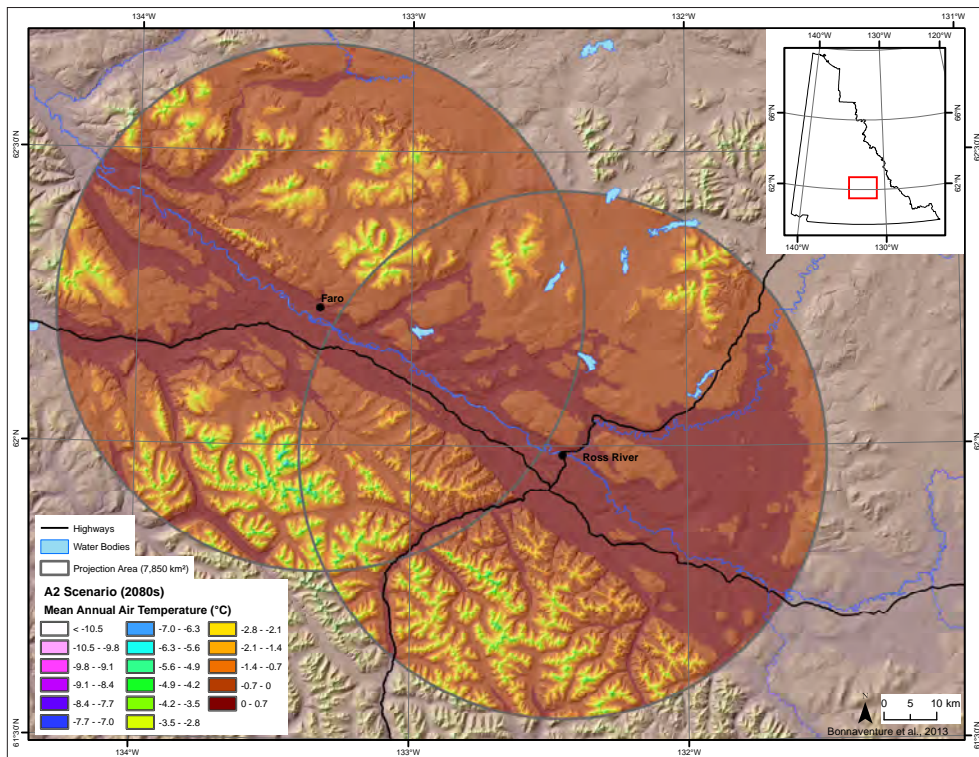


Figure D10. Mean annual air temperature for the Faro area for 2080, projected using the A2 scenario.

APPENDIX E - HAZARD RANKINGS

Table E1. Hazard classification results for polygons labeled on Figure 54 in the main body of this report (see larger print version of the map in back pocket). Asterisk (*) denotes polygons that are associated with drumlinoid ridges; see *'Integrating risk in a landscape hazards map for the Faro region'* on p. 64 in the main body of this report for more details.

Polygon Number	Surficial Geology	Hazard Ranking	Hazard Description
1-3*	Morainal (till) (M)	1	
4	Morainal (till) (M)	3	ice-rich permafrost potential; poor drainage
5-10*	Morainal (till) (M)	1	
11	Glaciofluvial (FG)	3	ice-rich permafrost potential; wetland
12-13	Morainal (till) (M)	3	ice-rich permafrost potential; poor drainage
14	Morainal (till) (M)	2	drumlin sideslope and/or unmapped drumlins
15-27*	Morainal (till) (M)	1	
28-29	Morainal (till) (M)	3	ice-rich permafrost potential; poor drainage
30	Organic (O)	3	permafrost; thermokarst
31	Glaciolacustrine (LG)	2	ice-rich permafrost potential
32	Morainal (till) (M)	1	
33	Morainal (till) (M)	2	drumlin sideslope and/or unmapped drumlins
34	Bedrock (R)	1	
35	Colluvium (C)	3	landslides, debris flows, permafrost
36	Morainal (till) (M)	1	
37	Colluvium (C)	2	slope movement
38	Fluvial (F)	3	flooding
39	Colluvium (C)	3	gullying
40	Morainal (till) (M)	1	
41	Colluvium (C)	2	slope movement
42	Fluvial (F)	3	flooding
43	Glaciofluvial (FG)	1	
44-46	Fluvial (F)	3	flooding
47	Bedrock (R)	2	moderate-steep slopes
48	Fluvial Active (FA)	3	flooding
49	Morainal (till) (M)	2	drumlin sideslope and/or unmapped drumlins
50	Bedrock (R)	2	moderate-steep slopes
51	Organic (O)	3	ice-rich permafrost potential; poor drainage
52	Bedrock (R)	1	
53	Morainal (till) (M)	3	ice-rich permafrost potential; poor drainage
54	Organic (O)	3	permafrost; thermokarst
55	Morainal (till) (M)	1	
56	Fluvial Active (FA)	3	flooding
57	Organic (O)	3	permafrost; thermokarst
58	Morainal (till) (M)	1	
59	Morainal (till) (M)	3	ice-rich permafrost potential; poor drainage

Table E1, continued. Hazard classification results for polygons labeled on Figure 54 in the main body of this report (see larger print version of the map in back pocket). Asterisk (*) denotes polygons that are associated with drumlinoid ridges; see ‘Integrating risk in a landscape hazards map for the Faro region’ on p. 64 in the main body of this report for more details.

Polygon Number	Surficial Geology	Hazard Ranking	Hazard Description
60	Morainal (till) (M)	1	
61	Colluvium (C)	2	slope movement
62	Morainal (till) (M)	3	ice-rich permafrost potential; poor drainage
63	Morainal (till) (M)	3	permafrost; thaw flows
64	Morainal (till) (M)	2	drumlin sideslope and/or unmapped drumlins
65	Morainal (till) (M)	3	ice-rich permafrost potential; poor drainage
66	Bedrock (R)	3	landslides
67	Bedrock (R)	3	rockfall
68	Morainal (till) (M)	1	
69	Organic (O)	3	permafrost; thermokarst
70	Fluvial (F)	3	flooding
71	Colluvium (C)	2	slope movement
72	Morainal (till) (M)	1	
73	Morainal (till) (M)	2	drumlin sideslope and/or unmapped drumlins
74	Glaciolacustrine (LG)	2	ice-rich permafrost potential
75	Fluvial Active (FA)	3	flooding
76	Morainal (till) (M)	2	drumlin sideslope and/or unmapped drumlins
77*	Morainal (till) (M)	1	
78	Fluvial Active (FA)	3	flooding
79	Morainal (till) (M)	3	permafrost; thermokarst
80	Morainal (till) (M)	1	
81	Morainal (till) (M)	3	ice-rich permafrost potential; poor drainage
82	Morainal (till) (M)	2	drumlin sideslope and/or unmapped drumlins
83	Glaciofluvial (FG)	1	
84	Glaciolacustrine (LG)	3	gulying; ice-rich permafrost at depth
85	Morainal (till) (M)	1	
86	Glaciofluvial (FG)	2	potential permafrost at depth
87	Colluvium (C)	2	slope movement
88	Glaciofluvial (FG)	1	
89	Fluvial (F)	3	permafrost; thermokarst
90	Bedrock (R)	2	moderate-steep slopes
91	Colluvium (C)	3	gulying
92	Fluvial (F)	3	flooding
93	Colluvium (C)	2	slope movement
94	Colluvium (C)	3	gulying
95	Morainal (till) (M)	3	permafrost; poor drainage
96	Colluvium (C)	2	slope movement
97	Colluvium (C)	3	slope movement

Table E1, continued. Hazard classification results for polygons labeled on Figure 54 in the main body of this report (see larger print version of the map in back pocket). Asterisk (*) denotes polygons that are associated with drumlinoid ridges; see 'Integrating risk in a landscape hazards map for the Faro region' on p. 64 in the main body of this report for more details.

Polygon Number	Surficial Geology	Hazard Ranking	Hazard Description
98	Colluvium (C)	3	permafrost; debris flows
99	Colluvium (C)	3	landslides, permafrost
100	Glaciofluvial (FG)	1	
101-102	Colluvium (C)	3	slope movement
103	Morainal (till) (M)	3	landslides, permafrost
104	Colluvium (C)	3	debris flows, tension cracks
105	Morainal (till) (M)	3	permafrost; thermokarst
106	Colluvium (C)	3	gullying
107	Glaciofluvial (FG)	1	
108	Glaciofluvial (FG)	1	
109	Morainal (till) (M)	1	
110	Glaciofluvial (FG)	2	potential permafrost at depth
111	Fluvial (F)	2	fluvial fan
112	Glaciofluvial (FG)	2	ice-rich permafrost potential
113-114	Colluvium (C)	2	slope movement
115	Fluvial (F)	2	flooding
116	Colluvium (C)	3	landslide, slumping
117	Organic (O)	3	permafrost thaw settlement
118	Organic (O)	2	permafrost
119	Colluvium (C)	3	gullying
120	Glaciofluvial (FG)	1	
121	Glaciofluvial (FG)	1	
122	Colluvium (C)	3	gullying
123	Morainal (till) (M)	2	permafrost
124	Organic (O)	2	permafrost
125	Morainal (till) (M)	1	
126	Morainal (till) (M)	2	permafrost
127	Morainal (till) (M)	3	ice-rich permafrost potential; poor drainage
128	Morainal (till) (M)	3	permafrost; thermokarst
129	Fluvial Active (FA)	3	flooding; permafrost
130	Glaciofluvial (FG)	2	drumlin sideslope and/or unmapped drumlins
131	Glaciofluvial (FG)	2	drumlin sideslope and/or unmapped drumlins
132	Fluvial Active (FA)	3	permafrost; thermokarst
133-142	Morainal (till) (M)	2	drumlin sideslope and/or unmapped drumlins
143*	Morainal (till) (M)	1	
144	Bedrock (R)	2	moderate-steep slopes
145	Morainal (till) (M)	3	ice-rich permafrost potential; poor drainage
146-156*	Morainal (till) (M)	1	

APPENDIX F - SAFE HOME CONSTRUCTION ON PERMAFROST

Prepared by

Julie Malenfant-Lepage (M.A., Eng.) and Benoit Loranger (Jr. Eng.)

Northern Climate ExChange, Yukon Research Centre, Yukon College

TABLE OF CONTENTS

INTRODUCTION	111
CONSTRUCTION ON PERMAFROST	111
Problems Related to House Construction on Permafrost.....	112
Types of Surface Materials and the Thawing Processes.....	113
SITE INVESTIGATION	114
Preliminary Observations.....	115
Frost Probing.....	115
Drilling.....	115
Geophysics.....	115
FOUNDATIONS IN PERMAFROST	116
Construction Data Requirements.....	116
Foundation Types.....	117
<i>Surface gravel pads</i>	117
<i>Insulation</i>	118
<i>Screw-jack foundations</i>	119
<i>Timber-block foundations</i>	120
<i>Space-frame foundations</i>	120
<i>Pile foundations</i>	120
<i>Foundations with heat exchangers</i>	122
BASIC PRINCIPLES TO MAINTAIN PERMAFROST	123
Drainage.....	123
Ventilation.....	124
Shading.....	124
Heat Extraction.....	124
Monitoring.....	124
CONCLUSIONS AND RECOMMENDATIONS	124
REFERENCES	125

INTRODUCTION

Construction in permafrost environments requires a good understanding of the nature of permafrost as well as the surficial geology. There are several principles and techniques for building on permafrost that have been proven efficient in various parts of northern Canada and Alaska. This report aims to briefly present the different approaches applied in construction of new buildings. In some ways, it can be considered as an introductory guide for basic principles, design and construction on permafrost. It is important to note, however, that this report is not prepared as an engineering design text and should not be used as such.

This report on safe home construction in permafrost environments will provide an overview of building construction on permafrost including issues related to house construction on permafrost, types of surface materials and thawing processes, preliminary investigation procedures, construction data requirements, types of foundations built in northern regions, basic principles to maintain permafrost under existent structures, and finally, recommendations that should be followed throughout the construction process.

CONSTRUCTION ON PERMAFROST

The best advice that could be given to an individual or to a contractor is to avoid building on permafrost terrain. If possible, it is always better to find a new site than to face the extra expense and maintenance involved in construction on permafrost. However, in many regions where permafrost is extensive (e.g., in northern Canada, including the Yukon) or where other factors preclude construction on non-permafrost terrain, this advice is sometimes impossible to follow. Building directly on bedrock is a good practice and should be done whenever possible (Figure F1).



Figure F1. Houses in Ilulissat, western Greenland, built directly on bedrock.

In areas underlain by continuous permafrost, permafrost is one of the major controlling factors in design parameters. As a result, it is important to design and build in a way that will preserve the underlying permafrost. Stability and lifetime of the infrastructure depend directly on the success of this endeavour.

Areas that are underlain by discontinuous permafrost offer the greatest engineering challenge since it is very difficult to determine exactly where there is underlying permafrost as it may change on a very local scale. Despite the high costs associated with the analysis of a potential construction site by drilling, these analyses will never confidently ensure the presence or absence of permafrost. If the site is located in a thaw-stable area, more conventional and less expensive construction techniques can be used without risk of destabilizing the ground. However, if the site is located in an area of ice-rich soil, which is considered thaw-unstable, standard structural foundations may thaw the underlying permafrost and potentially lead to an eventual failure of the structure. It is sometimes possible to remove or thaw permafrost on a site before starting construction, but this is a process that is rarely performed. The choice of a good structural foundation design and good mitigation techniques will help preserve permafrost, as well as respect a budget, which is the main challenge in regions underlain by discontinuous permafrost (Permafrost Technology Foundation, 2000).

PROBLEMS RELATED TO HOUSE CONSTRUCTION ON PERMAFROST

The most significant impact to permafrost usually occurs immediately beneath the house as heat is conducted downwards into the soil foundation. If a heated building is directly placed on permafrost, it will warm the ground throughout the entire year (Figure F2). However, if the building is not in contact with the ground surface, as is commonly found in northern communities, thawing is still possible due to the following: obstructed water drainage, insulation of ground by snow piling, and wind obstruction beneath the house. Furthermore, impacts from site preparation and infrastructure construction such as vegetation clearance, surface grading, and removal or compression of the organic layer, can increase heat intake by the ground surface. These ground disturbances usually result in an increase of ground temperatures, deepening of the thaw depth, and subsequent thaw settlement. In most cases, it will take several years for permafrost temperatures to reach a new equilibrium following construction.

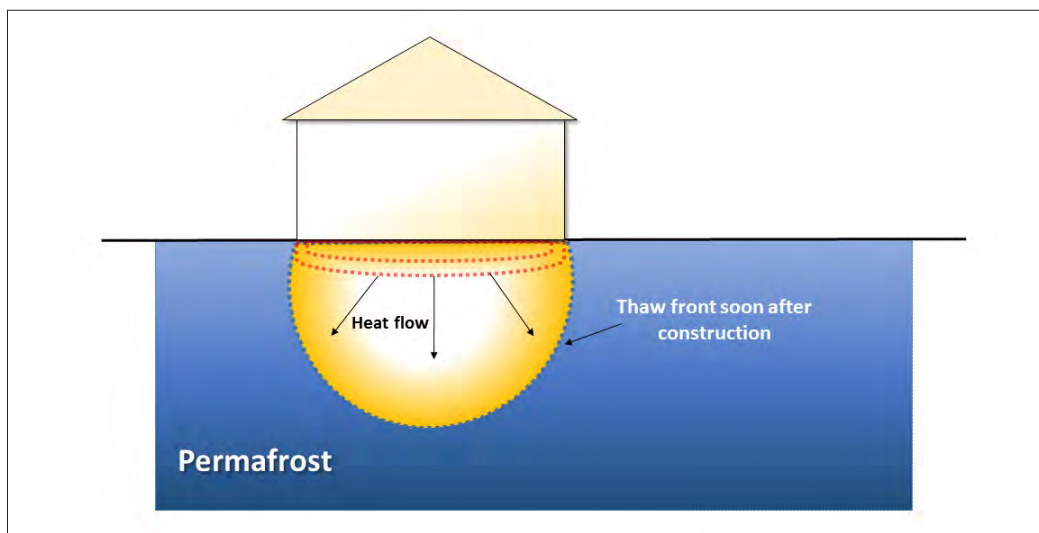


Figure F2. Cross section displaying the evolution of permafrost degradation under house construction. Based on Barriault (2012).

Foundation failure does not normally occur in a short period of time. Sudden collapse is extremely rare in the context of permafrost and is more likely associated with thermal erosion by water. The

time it takes for heat generated by a building to diffuse into the underlying permafrost depends on permafrost type, as well as factors such as the thickness of the active layer (i.e., layer of soil that thaws and freezes annually), the soil type, the temperature of the permafrost, the presence of water in the soil, and the amplitude of temperature change at the surface. However, once the process of warming is initiated, thawing of the soil is irreversible.

If buildings are left unattended, soil degradation can end up affecting the structure and will lead to the formation of cracks and bindings on doors, walls and ceilings (Figure F3). Tilted floors can also be associated with permafrost-related problems. Eventually, a building can become non-functional and even condemned. Damage associated with permafrost degradation should therefore be monitored and repaired as soon as possible to ensure viability of the structure. Monitoring can also be used to collect relevant data that would be useful in assessing permafrost-related damage. It is by far more cost effective to initiate repairs at the first signs of permafrost-related failures.



Figure F3. Examples of unmaintained buildings in Pyramiden, Svalbard, displaying cracks and uneven settlement in response to permafrost thaw.

TYPES OF SURFACE MATERIALS AND THE THAWING PROCESSES

In permafrost regions, coarse, granular surface material (sand and gravel) and rocks without ice inclusions are typically the best material on which to construct a foundation. Upon thawing, these materials are stable and have good bearing capacity. Bearing capacity refers to the load a surface material can safely withstand, without significant compaction or settlement. Foundation design in such materials should follow the current practice of moderate temperature regions.

Conversely, fine-grained surface materials, which are often ice-rich, have low permeability and tend to be oversaturated after thawing. Pore-pressure generated during thawing may result in a significant loss of stiffness (bearing capacity) and volume (Figure F4). For fine-grained deposits, foundation design in permafrost poses several challenges when attempting to control differential settlement of the materials that leads to the deformation of structures. The bearing capacity of fine-grained materials is largely a function of the amount and temperature of ground ice present.

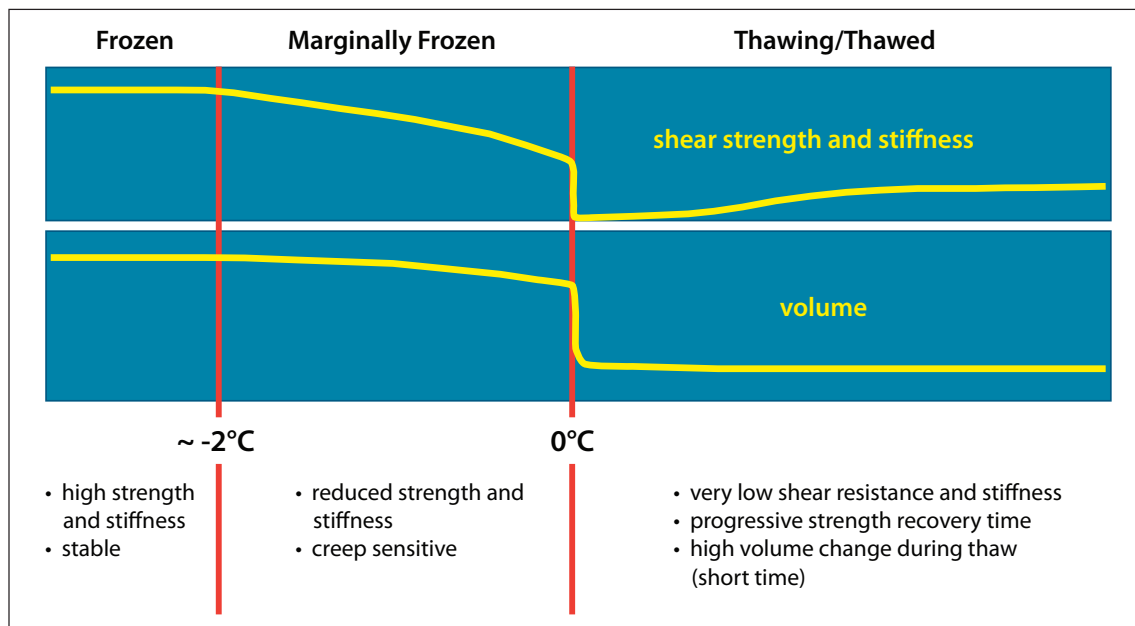


Figure F4. Mechanical properties of frozen ground undergoing thaw (Doré, 2011).

As the amount of ground ice commonly varies across a construction site in zones of discontinuous permafrost, bearing capacity may differ within a foundation, causing different portions of the structure to experience settlement at different rates. Furthermore, since ice-rich deposits consolidate and discharge excess water as they thaw, variably distributed ground ice can result in the settlement of specific areas of the ground, causing distortion in the structure above. Therefore, these types of surface materials do not offer good support for construction of buildings (Canadian Standard Association (CSA), 2010).

It is also important to note that permafrost with a temperature between -2°C and 0°C is marginally frozen (i.e., considered to be ‘warm permafrost’) and may not appear to be warming rapidly. At this temperature, a significant amount of heat transfer is mainly used to melt ground ice instead of warming the surface materials. Consequently, the strength of permafrost under the structure will be reduced significantly as the ground ice melts even if the temperature of the sediments remains below 0°C (see Figure F4). Moreover, several problems of creeping related to thick gravel pads and heavy structures are commonly associated with warm permafrost. Creep is related to slow ice deformation within the ground under a constant load. Ice then reacts as a malleable material and tends to flow laterally, away from the load source.

In summary, fine deposits of silt and clay are more likely to be problematic because of their frost susceptibility. Well-drained materials such as sand and gravel will be more stable; however, it is important to note that many sandy and gravelly deposits may contain a significant amount of fines that could pose a threat to the integrity of a structure. Frost susceptibility appears when approximately 10% of the mass of the surface deposit is composed of material with a fine grain size, i.e., $80\ \mu\text{m}$. If in doubt, it is best to seek advice from a geotechnical engineer.

SITE INVESTIGATION

The objectives of the site investigation are to identify terrain units, determine relevant surface material properties, and identify areas of thaw-sensitive or unstable deposits. The type of building

and its lifespan define the quantity and complexity of information necessary. The following section provides the current practices used during the site investigation.

PRELIMINARY OBSERVATIONS

The first step is an attentive observation of all permafrost-related features that could be present at the site. Features such as frost mounds, cracks, depressions and uneven terrain are typical characteristics of a permafrost landscape. Therefore, it is important to pay close attention to terrain morphology and topography since these are indicators of underlying permafrost conditions.

FROST PROBING

When the top of the permafrost is shallow and the active layer is relatively soft, frost probing is an effective method for locating depth to permafrost (Figure F5). This technique uses a steel rod with a handle, which is pushed into the ground manually until the top of the permafrost is reached. With this method, shallow permafrost can easily be detected, and its depth measured. Frost probing is inexpensive, fast and very useful for preliminary site investigations.



Figure F5. Frost-probing to determine depth to permafrost.



Figure F6. Example of ice-rich permafrost core from the Beaver Creek area, Yukon.

DRILLING

The most effective way to determine ground ice conditions at a potential site is to drill boreholes and collect samples of permafrost for geotechnical analysis (Figure F6). This provides specific information about soil characteristics and conditions at the subsurface at a particular location. A good borehole log will provide information at varying depths, including the thickness of the active layer, the soil or rock types, the ice content, the depth and characteristics of permafrost, the presence of massive ice bodies, and in some cases, the depth to bedrock.

The information derived from multiple boreholes in a given area can be extrapolated to obtain a spatial representation of subsurface conditions. It is very important to drill deep enough to obtain the appropriate information for each project. Generally speaking, the larger the building, the deeper the drilling must be. Permafrost drilling requires trained personnel with proper equipment adapted to site conditions.

GEOPHYSICS

If a larger area is being surveyed, complementary geophysical approaches like electrical resistivity tomography (ERT) and ground penetrating radar (GPR) surveys should be considered. Both applications work by sending signals into the ground and measuring the rate or strength of their return, and using those results to map subsurface conditions.

Geophysical surveys can be applied to help extrapolate information between boreholes. It is particularly useful for determining the thickness and extent of permafrost bodies, and zones of unfrozen ground within permafrost (Figure F7 a,b). ERT and GPR are applied for different detection purposes and professional geophysicists will select the most appropriate technique for the site. Geophysical surveys have the advantage of covering a relatively large area in a short period of time. Furthermore, ERT and/or GPR surveys are a cost-effective way to minimize the number of boreholes that need to be completed at any given site. The results obtained by drilling, coupled with geophysical surveys allow for a more comprehensive analysis of the subsurface conditions of the entire site.

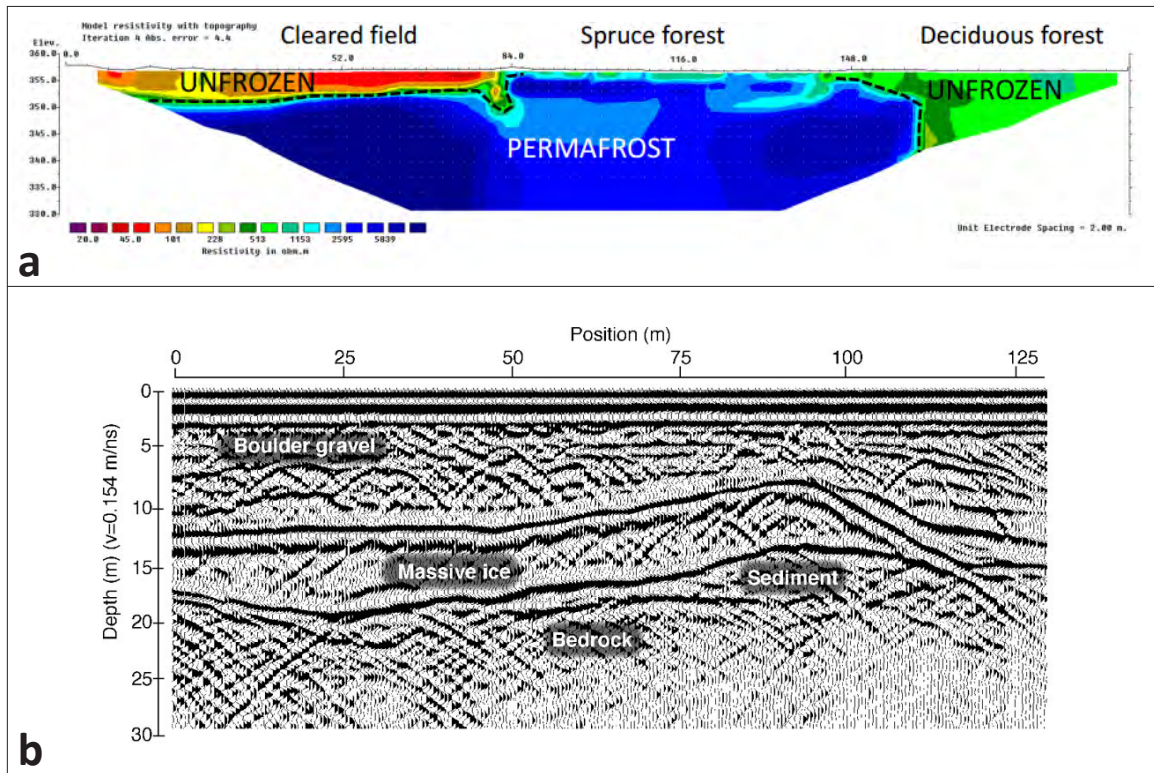


Figure F7. (a) ERT profile from the Klondike Valley, Yukon (Lewkowicz et al., 2014). **(b)** GPR profile along an ice-cored esker near Carat Lake, Northwest Territories (Moorman et al., 2007).

FOUNDATIONS IN PERMAFROST

Robust foundations for infrastructure in permafrost areas are critical for long-term building stability. General data requirements and the most common types of foundations are presented below.

CONSTRUCTION DATA REQUIREMENTS

The following list indicates principal information requirements related to construction and foundation design (Andersland and Ladanyi, 2004). This list is for large-scale projects and only needs to be fully applied in those cases. However, some elements are essential in the selection of the right type of foundation, such as the amount and temperature of ground ice, as well as the active layer thickness. It is good practice to gather as much information as possible about a site prior to construction.

1. Site data:
 - a. location
 - b. climate
 - c. physiography and geology
 - d. subsurface materials and their characteristics
 - e. thermal regime
 - f. hydrology and drainage
 - g. materials and construction
 - h. transportation facilities and access
 - i. construction cost factors
 - j. Availability of :
 - i. labor, skills, and knowledge
 - ii. construction equipment
 - iii. support facilities and equipment
2. Design policies, general criteria, and cost limitations
3. Technology (state of the art)
4. Facility technical data
 - a. size and design life (e.g., permanent versus temporary)
 - b. foundation loading
 - c. thermal conditions
 - d. movement and distortion

FOUNDATION TYPES

Good foundation construction in the North is essential to assure a full service life of a structure. Proper foundation design will be the difference between a safe, stable structure with relatively low maintenance costs, and one with constant stability problems leading to a shorter lifespan. The selection of a foundation type will generally depend on the soil behaviour upon thawing. Foundations built on permafrost can be divided into three main categories: 1) surface pads; 2) deep foundations, and; 3) foundations with heat exchangers.

SURFACE GRAVEL PADS

Construction on a surface pad to preserve the temperature of the underlying permafrost is common in northern Canada. According to Allard et al. (2010), houses built on properly designed, compacted, granular foundations should not undergo significant thaw settlement because the adjustment of the thermal profile to the new geometry leads to a rise of the permafrost into the gravel pad (Figure F8 a,b). The active layer then becomes limited to the non-frost sensitive foundation, which ensures stability over cycles of freezing and thawing. Gravel pads are frequently used with insulant panels and techniques that allow airflow beneath the building.

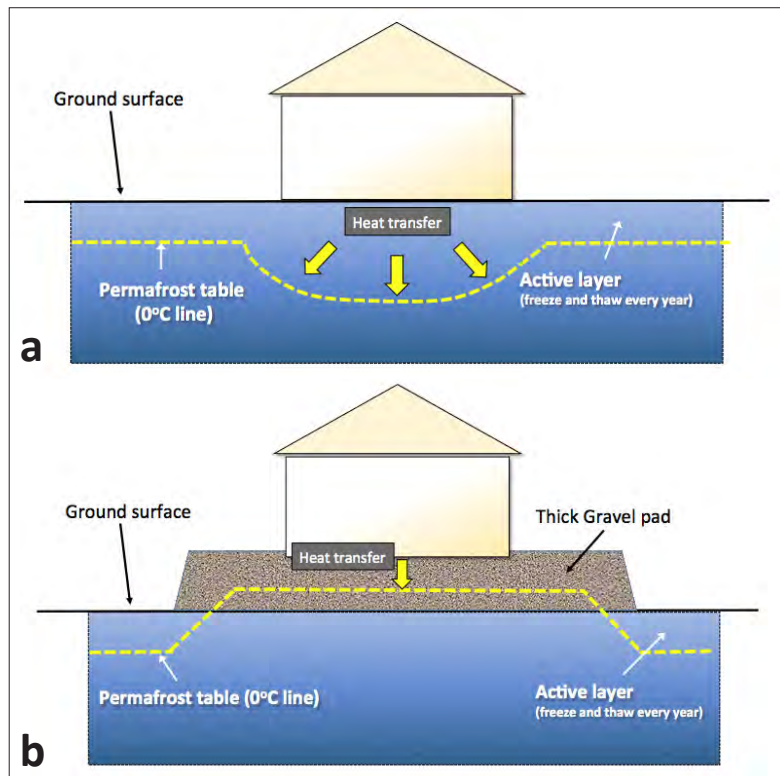


Figure F8. Schematics demonstrating the theoretical position of the permafrost table underneath (a) a building built directly on the ground, and (b) a building built on a gravel pad.

INSULATION

Structures may be built directly on insulating material (Figure F9). Insulation will slow the rate at which heat enters the ground, but it does not eliminate heat exchange. It is possible to add enough layers of insulation to establish a new thermal balance between heat input from the area around the building and winter cooling, but this procedure is almost never performed due to the high cost. Insulation is commonly applied along with a gravel pad.

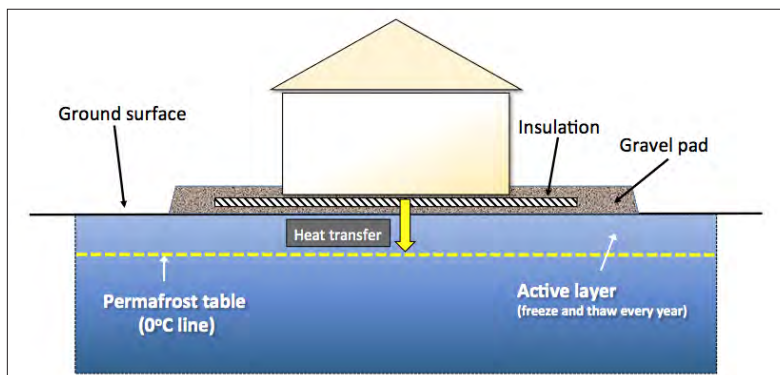


Figure F9. Basic insulation-pad foundation design (modified from CSA, 2010).

Several types of insulation can be considered in the construction of an unheated foundation. An insulated layer that is intended to be in contact with the soil must be able to withstand deterioration of its thermal properties and physical shape in the presence of soil moisture, soil chemicals, physical loading and other outside forces (Permafrost Technology Foundation, 2000).

SCREW-JACK FOUNDATIONS

In the 1980s, the Société d'Habitation du Québec developed a concept for house foundations to preserve permafrost. It involved buildings that are constructed on adjustable metal jacks over a compacted granular foundation (Figure F10). The granular foundation is laid directly on the ground surface without the removal of the vegetation cover. To date, this construction technique has been proven very effective for preserving permafrost (Gravel, 2012). The foundation must raise the building high enough to promote uninhibited air circulation beneath the building. It allows the wind to flow freely under the building, mainly to avoid snow accumulation that could increase the soil temperature (by insulation) under the foundation. Under these conditions, a snow bank will form approximately six metres away from the dwelling's foundation. It is important that nothing be stored in the space between the floor and the ground surface so as to not interfere with the free air circulation during the winter months. The winter airflow allows for the extraction of heat from the ground beneath the building, and helps preserve permafrost. Sufficient insulation should be placed under the floor of the structure so the energy loss from the bottom of the building is minimized and the floor inside the building is comfortable for residents.

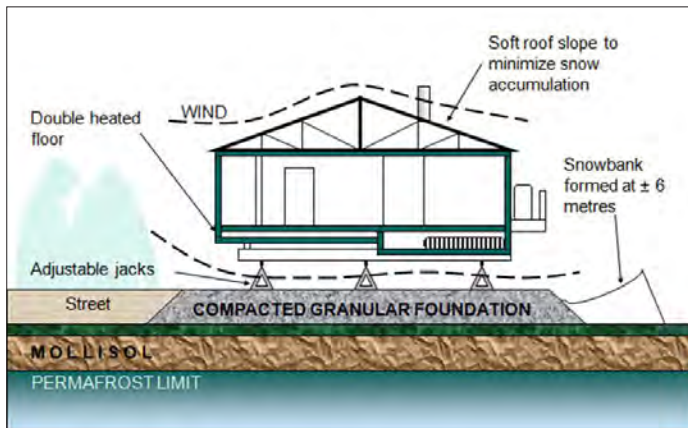


Figure F10. Conceptual design of a screw-jack foundation on a compact granular foundation (Gravel, 2012).

Once or twice a year, maintenance of a building on jacks needs to be performed in order to preserve the building's stability. During the maintenance process, screws in the middle of the jacks are used to raise or lower the height of the building (Figure F11). For a small, single-family house, it is common to use about nine adjustable jacks which can withstand nearly 35 000 kg each (Gravel, 2012). It is important to ensure that the slope of the terrain around the building allows for adequate drainage of surface water away from the structure.



Figure F11. Examples of adjustable-jack foundations from Gravel (2012) and CSA (2010).

TIMBER-BLOCK FOUNDATIONS

Timber-block foundations (Figure F12) work on the same principle as the screw-jack technique. However, screw jacks are not always easily obtainable and it can be more convenient to use timber blocks. Timber blocks are normally screwed together to ensure lateral stability. Timber blocks are commonly sited directly on natural ground (without a gravel pad).



Figure F12. Example of a timber-block foundation used in Nunavut (Government of Nunavut, 2013).

Maintenance operations are almost the same as for screw-jack foundations, described above; however, the operator must use a hydraulic jack to lift the load of the building before shimming the timber blocks. Maintenance for this style of foundation is therefore more labour intensive than for screw-jack foundations.

SPACE-FRAME FOUNDATIONS

Another surface foundation that has proven successful in permafrost regions is the rigid, three-dimensional, truss-type foundation (Figure F13). This is a commercially available, pre-manufactured foundation that consists of metal tube members flattened on each end and connected by metal node pieces at the top and bottom to form approximately one metre-square cells. It is custom-made to fit the building, and is assembled directly on-site on a compacted, granular foundation.

A screw at each structural node is used to level the building in the event of permafrost thaw underneath the building. These types of foundations are quite expensive, and are used mainly for service buildings and large, public infrastructure.



Figure F13. Examples of space-frame foundations in Nunavut (Barriault, 2012).

PILE FOUNDATIONS

In the far North, the majority of public and private dwellings, as well as commercial buildings, are built on steel piles. Piles are long steel pipes driven into the ground to stabilize buildings into the permafrost or bedrock (Figure F14). This type of foundation requires little to no gravel,

which can be a very expensive resource to procure and transport to northern communities. The use of steel piles also allows for construction on harsher and steeper terrain compared with conventional foundations. The steel piles are also more resilient to climate change compared to other foundation types when they are placed directly on bedrock.



Figure F14. Example a steel-pile foundation in Nunavik (Gravel, 2012).

There are two principal pile types currently in use in the Canadian North: 1) adfreeze piles (driven and slurry), and 2) rock-socketed piles. Their design and applications are fundamentally different. Adfreeze piles are commonly installed where permafrost extends to substantial depths without encountering bedrock. These piles rely on the bond with the surrounding ground for their load-bearing capacity. They can be driven directly into the ground, or a drill hole can be fixed to accommodate the pile. Slurry is then used to fill the empty space between the soil and the pile. For this application, the ground can be ice-rich, but should be below -3°C , or colder if the soil is saline (CSA, 2010).

Rock-socketed piles are used where bedrock occurs within a practical depth below the surface. These piles are designed to transfer the full load of a structure to the underlying bedrock. In Nunavut, rock-socketed piles are commonly used. Adfreeze piles have been either discontinued or are being driven deeper due to a deepening of the active layer (Barriault, 2012).

In response to ground warming, if the active layer deepens, foundation systems that rely on piles may experience increased frost heaving (Figure F15 a,b,c). This frost heaving occurs when a small part of each pile's surface is frozen to the surrounding soil year-round, while a larger part of the pile's surface is exposed to the lifting force exerted through soil expansion when the water in the active layer re-freezes in the autumn and winter (CSA, 2010). If piles are used in a frost-sensitive soil and cannot be placed directly on bedrock, the piles must be equipped with anti-lift shafts to prevent the exertion of a vertical force by seasonal frost, which can distort the building's structure. Various methods can prevent frost heaving when using pile jacking and a competent engineer should be consulted if this method is being considered.



Figure F15. Examples of pile jacking in Nunavut (Barriault, 2012).



Figure F16. Example of thermosyphons, a foundation system that requires a significant amount of expertise to design, install, maintain and monitor (CSA, 2014).

FOUNDATIONS WITH HEAT EXCHANGERS

Foundations enhanced with heat exchangers are now widespread in Canada's North. They are generally used where heated crawl spaces and warm first floors at finished grade are required. For such structures, systems are built to intercept heat that would otherwise flow into the ground and affect the underlying permafrost. Thermosyphons are the most widely used heat exchangers (Figure F16). Two-phase thermosyphons work passively during the winter to extract heat from the ground and preserve permafrost (Figure F17 a,b,c). When designs using thermosyphons are being considered, detailed geothermal analyses are required. The inclusion of climate warming in the design process requires careful consideration of the conditions of the site chosen for the design, particularly in winter when low temperatures drive heat removal (CSA, 2010). Due to their high cost, thermosyphons are mainly placed in strategic locations next to high-risk service buildings, bridges or pipelines.

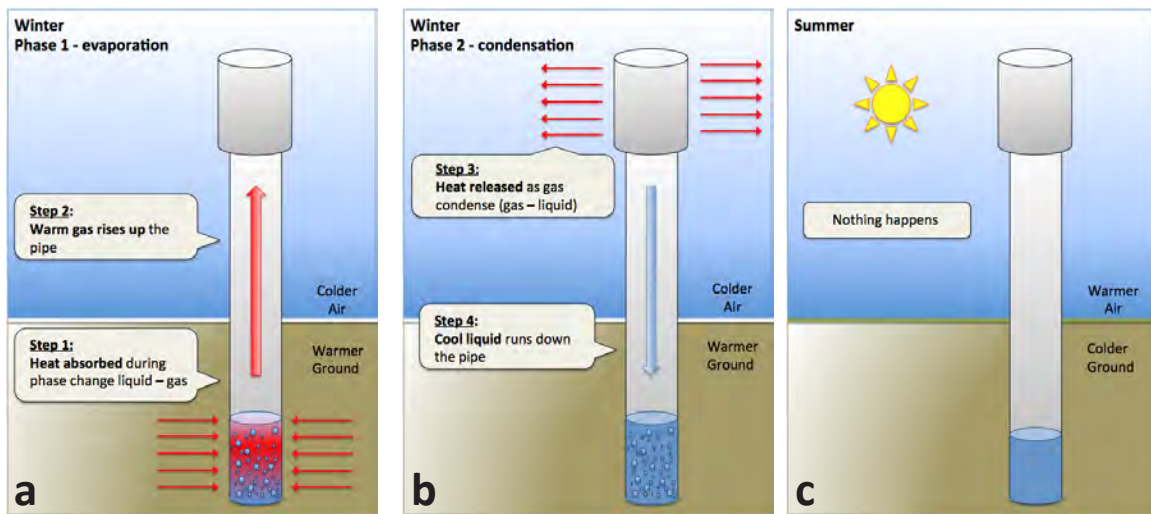


Figure F17. Schematic demonstrating (a) and (b) a winter two-phase thermosyphon cycle, as well as (c) the non-operative state during summer.

BASIC PRINCIPLES TO MAINTAIN PERMAFROST

Once construction of a building is finished, it is essential to maintain the permafrost beneath and around it. Basic elements to consider are outlined below. For more detail, please refer to the Canadian Standards Council (CSA, 2014 and 2013).

DRAINAGE

Because water transfers heat to the ground and can negatively impact permafrost, ditches should not be excavated in permafrost. Proper surface drainage to avoid water ponding beneath or next to the building is very important (Figure F18), especially with regards to spring meltwater (which can result in a high volume of flow during a short period of time). Slopes of approximately 4% are considered sufficient to drain any water at least 4 m (and preferably 6 m) from a building. Any terrain modification that could alter water paths should be carefully considered.



Figure F18. Example of water ponding around a foundation built on permafrost (Government of Nunavut, 2013). Water ponding can have a negative impact on permafrost thermal regimes.

VENTILATION

Winter airflow under buildings extracts considerable heat from the ground and thereby keeps the ground frozen. Air space should be at minimum 0.5-1 m to allow free circulation. Nothing should be stored beneath the building, in order to avoid restricting ventilation. Furthermore, snow should be managed such that it does not reduce ventilation and insulate the ground near the building. Frequent snow clearing may be required.

SHADING

In some cases, vegetation cover or a sun shade may be put in place to shade the ground surface. As mentioned above, it is important to not interfere with airflow or to enhance snow accumulation near the building. Natural vegetation and trees that exist prior to construction should not be disturbed in order to promote shading.

HEAT EXTRACTION

Active heat extraction systems like thermosyphons may be installed if required. These are described in more detail above.

MONITORING

The effectiveness of measures used to preserve permafrost should be monitored to ensure performance is maintained. Ground temperature should also be monitored to detect changes to the ground thermal regime that may affect permafrost – the temperature regime can be a powerful forecasting tool. For example, thermistor cables may be inserted along a pile if drilling is used during the construction phase.

CONCLUSIONS AND RECOMMENDATIONS

Construction in regions underlain by permafrost is a process that requires many steps, including preliminary site investigation, drilling, data analysis, as well as the appropriate choice of foundation design, construction and maintenance. In summary, several recommendations related to building on permafrost can be made:

- Foundations need to be adapted to local permafrost and landscape conditions.
- The organic layer should not be removed before construction.
- The best available geotechnical measures and techniques should be applied for all construction.
- A geotechnical investigation should be completed before construction.
- Compacted granular foundations should be built at least two years in advance of construction to allow the rise of the permafrost table and the stabilization of the soil (Allard et al., 2010).

The permafrost thermal regime should be considered in the design-phase of construction while at the same time integrating the anticipated effects of climate warming in northern Canada.

It may also be appropriate, in some areas, to develop a municipal program with appropriate regulations to ensure yearly maintenance of houses and infrastructure (Allard et al., 2010).

It must be reiterated that this guide does not replace the necessary engineering design needed for building on permafrost. It is important to consult permafrost experts in order to get appropriate advice at the preliminary investigation stages, as well as through the construction and maintenance phases. Additionally, for detailed guidance with respect to roads and permafrost, the *“Guidelines for Development and Management of Transportation Infrastructure in Permafrost Regions”* should be consulted (McGregor et al., 2010).

REFERENCES

- Allard, M., L’Hérault, E., Gybérien, T. and Barrette, C., 2010. Impact des changements climatiques sur la problématique de la fonte du pergélisol au village de Salluit (Nunavik). Rapport final, Centre for Northern Studies, Université Laval, Quebec City, QC, 69 p.
- Andersland, O.B. and Ladanyi, B., 2004. Frozen Ground Engineering, 2nd Edition. Wiley, Hoboken, NJ, 384 p.
- Barriault, A., 2012. Climatic Adaptations to Construction in Nunavut. Nunavut Housing Corporation, Northern Forum, April 18 2012, Quebec City, QC.
- Canadian Standards Association (CSA), 2014. Standards Council of Canada Approves New National Standard to Help Address the Effect of Climate Change on Canada’s North. [<https://www.scc.ca/en/news-events/news/2014/standards-council-canada-approves-new-national-standard-help-address-effects-climate-change-canadas>]. Accessed February, 2015.
- Canadian Standards Association (CSA), 2010. Technical guide: Infrastructure in permafrost: A guideline for climate change adaptation, 1st edition. Canadian Standards Association Publication, 112 p.
- Canadian Standards Association (CSA), 2013. Moderating the Effects of Permafrost Degradation on Building Foundations. Document S501 Draft Standard No. 3, 42 p.
- Doré, G. 2011, Advanced Seminar on Permafrost Engineering Applied to Transportation Infrastructure, lecture notes, Yukon College, Whitehorse.
- Government of Nunavut, 2013. A Homeowner’s Guide to Permafrost in Nunavut: Keep Your House on Solid Ground. Government of Nunavut, 28 p.
- Gravel, J.-F., 2012. Impact of climate change on habitat development in Nunavik (Société d’habitation du Québec). Northern Forum, Quebec City, QC.
- Lewkowicz, A., Miceli, M., Duguay, M., Bevington, A., 2014. Electrical Resistivity Tomography (ERT) as an Essential Tool to Investigate Sites in Discontinuous Permafrost. University of Ottawa. EUCOP, June 18-21 2014.
- Moorman, B.J., Robinson, S.D. and Burgess, M.M., 2007. Imaging Periglacial Conditions with Ground-Penetrating Radar. University of Calgary, Alberta, Canada. 17 p.
- Permafrost Technology Foundation, 2000. Design Manual for New Foundations on Permafrost. Permafrost Technology Foundation publications, 94 p.
- McGregor, R., Hayley, D., Wilkins, D., Hoeve, E., Grozic, E., Roujanski, V., Jansen, A. and Doré, G., 2010. Guidelines for Development and Management of Transportation Infrastructure in Permafrost Regions. Transportation Association of Canada, Ottawa, ON, 177 p.